OIPE JC73
APR 29 2003
PATENT & TRADEMARK OFFICE

#12 Suppl. Appeal Brief
J. Robinson
8/7/03

OLD DOCKET NO: DB3
NEW DOCKET NO: OSEM-DB3

IN RE APPLICATION OF: Braddock Examiner: KANG

SERIAL NO: 09/636,484 GROUP ART UNIT: 2811

FILED: 08/10/00

TITLE: INTEGRATED TRANSISTOR DEVICES

TO: ASSISTANT COMMISSIONER OF PATENTS

37 CFR 1.192(b)(2)(ii) REQUEST TO REINSTATE THE APPEAL AND SUPPLEMENTAL APPEAL BRIEF

Sir: Responsive to the non-final office action dated 1/30/2003, the applicant maintains the appeal and the traversal of the restriction requirement. The applicant also concurrently submits a 37 CFR 1.116 amendment after appeal and declaration.

RECEIVED
MAY - 2 2003
TECHNOLOGY CENTER 2800

Table of Contents

TRAVERSAL OF THE ELECTION REQUIREMENT - CLAIMS 53-55

The board should note that the applicant maintains the traversal of the restriction requirement of claims 53-55 and that a petition requesting withdrawal of that requirement is pending. The applicant presumes for this appeal that the petition has been granted and that claims 53-55 are not withdrawn in order to expedite prosecution. In that regard, claim 53 should be allowable over the prior art applied to rejected claims 36 and 38 for the reasons presented for claim 36. Claims 54 and 55 recite limitations not addressed by the examiner and therefore should be allowable over the art applied by the examiner for that additional reason.

37 CFR 1.193(b)(ii) SUPPLEMENTAL APPEAL BRIEF

I. **37 CFR 1.192(a)**

This supplemental brief is being filed within 3 months from the examiner's 37 CFR 1.193(b)(2) reopening or prosecution after appeal. The notice of appeal and fee for the notice of appeal were filed with the original brief. The supplemental brief is filed in triplicate. The supplemental brief sets forth the authorities and argument the applicant will rely upon in the appeal.

II. **37 CFR 1.192(b)**

The appeal is timely and should not be dismissed.

III. **37 CFR 1.192(c)**

A. **Real Party in Interest**

The real party in interest is Osemi, Inc., which is wholly owned by David Braddock, the named inventor.

B. **Related Appeals and Interferences**

There are no related appeals or interferences.

C. **Status of Claims**

Claims 1-26 and 36-55 are pending. Claims 53-55 stand withdrawn. The applicant is disputing the withdrawal of claims 53-55 via a petition previously filed. Claims 1-26, 37, and 39-52 stand allowed. Claims 36 and 38 stand rejected.[1] New claims 56 and 57 are presented in a 37 CFR 1.116 amendment filed herewith.

While the office action is not final, the applicant exercises the right to maintain the appeal pursuant to 37 CFR 1.193(b)(ii), and 37 CFR 1.116 expressly applies to "Amendments after final action or appeal". Accordingly, the examiner has the right to not enter the amendment. However, the amendment and associated evidence show clearly and convincingly that the rejections of claims 36 and 38 are improper. Accordingly, I strongly urge the examiner to enter the amendment and allow claims 36 and 38 as well as the newly presented dependent claims 56 and 57.

Clean copies (1) of claims as they now stand and (2) as they will stand if the examiner

---

[1]If the examiner withdraws the restriction requirement prior to decision on appeal, then claims 53-55 will be pending and not withdrawn, and either allowed or rejected. This brief addresses the contingency in which those claims are rejected on the same grounds as claims 36 and 38.

enters the amendment are attached as an appendix in case the examiner decides to exercise his discretion to enter the amendment instead of or in addition to filing an Examiner's Answer. See 37 CFR 1.193(1) and (b)(2).

D. **Status of amendments**

An amendment filed pursuant to 37 CFR 1.116/37 CFR 1.193(a)(2) is filed herewith and stands un-entered.

E. **Summary of the Rejected Inventions Under Appeal with Reference to Page and Line Numbers and Drawings**

The rejected inventions provide (claim 36) an enhancement mode metal-oxide-compound semiconductor field effect transistor (Fig. 1 element 10) comprising:

a compound semiconductor wafer structure (Fig. 1 element 13 and page 6 line 8) having an upper surface;

a gate insulator structure (Fig. 1 element 30 and page 6 line 13) positioned on upper surface of said compound semiconductor wafer structure;

a gate electrode (Fig. 1 element 17 and page 6 line 20) positioned on upper surface of said gate insulator structure layer;

source and drain ion implants self-aligned to the gate electrode (Fig. 1 elements 21, 22; specification page 6 fourth line from bottom) ; and

source and drain ohmic contacts (Fig. 1 elements 19, 20 and page 6 fifth line from bottom) positioned on ion implanted source and drain areas;

wherein said compound semiconductor wafer structure comprises a Al_xGa_{1-x} As, $In_yGa_{1-y}As$, InP, or $In_zGa_{1-z}P$ layer (Fig. 1 element 15 and page 5 lines 19-20), said layer being positioned on said upper surface;

a substrate (Fig. 1 element 11 and page 6 line 12) on which resides said compound semiconductor wafer structure; and

wherein said substrate includes a InP based semiconductor wafer (page 5 third line from bottom).

If the after appeal amendment is entered, then claim 36 defines "a Al_xIn_{1-x} As, $In_yGa_{1-y}As$, or InP layer" instead of an Al_xGa_{1-x} As, $In_yGa_{1-y}As$, InP, or $In_zGa_{1-z}P$ layer.

The claim 38 invention also provides that "said transistor is integrated together with similar and complementary transistor devices to form complementary metal-oxide compound semiconductor integrated circuit."

F. **Issues**

I. Whether the rejections of claim 36 as obvious in view of USP 5,945,718 to Passlack and the USP to Kikkawa should be reversed.

II. Whether the rejections of claim 38 as obvious in view of USP 5,945,718 to Passlack should be reversed.

G. **Groupings of Claims**

The claims do not stand or fall together.
Group 1 - Claim 36
Group 2 - Claim 38
In entered prior to decision on appeal, each one of claims 53-57 define a separate group, groups 3-8, respectively.
The claims do not stand or fall together.

H. **Argument (Reasoning)**

1. **Why Claims 36 and 38 Comply with 35 USC 103**

In rejecting claims 36 as obvious over Passlack in view of Kikkawa, the examiner now states that:

> Passlack et al. teach an enhancement mode metal-oxide-compound semiconductor field effect transistor comprising (Fig. 1):
> A compound semiconductor wafer structure (12) having an upper surface' [sic] a gate insulator structure (14) positioned on upper surface of said compound semiconductor wafer structure; a gate electrode (17) positioned on upper surface of said gate insulator structure layer; source (21) and drain (22) ion implants self-aligned to the gate electrode; and source and drain ohmic contacts (19 & 20) positioned on ion implanted source and drain areas, wherein said compound semiconductor wafer structure comprises a AlGaAs (23) and InGaAs (24) layers positioned on said upper surfaces; and a substrate (11) on which resides said compound semiconductor wafer structure. See also Col. 2, line 65 - Col. 4, line 4.
> Passlack teaches a GaAs substrate instead of [an] InP substrate. However, Kikkawa teaches that one may use InP for the substrate in place of GaAs (Col. 16, lines 5-9). Therefore, it would have been obvious in the art at the time the invention was made to substitute [the] GaAs substrate of Passlack with InP substrate as taught by Kikkawa, since both GaAs and InP exhibits faster and more optimized speed/power performance.
> Furthermore, one of ordinary skill in the art would have recognized that GaAs and InP would have worked equally as well as a substrate material for various high speed devices, such as MISFET, HEMPT or HBT. [Office action mailed 1/30/3003 page 5 lines 3-22.]

In rejecting claims 38 as obvious over Passlack, the examiner now states that:

> Passlack teaches an enhancement mode metal-oxide-compound semiconductor field effect tranasistor comprising (Fig. 1):
> a compound semiconductor wafer structure (12) having an upper surface; a

gate insulator structure (14) positioned on said upper surface; a gate electrode (17) positioned on upper surface of said gate insulator structure layer; source (21) and drain (22) ion implants (19 and 20) positioned on ion implanted source and drain areas wherein the compound semiconductor wafer structure comprises a wider band gap spacer layer and a narrower band gap channel layer (InGaAs, 24). See also Col. 2, line 65 - Col. 4 line 4.

Passlack does not show in Fig. 1 that transistor is integrated together with similar and complementary devices to form complementary metal-oxide compound semiconductor integrated circuit. However, it is well known to form MOS transistors (CMOS) which are used generally in various devices of LSI constitution including memory LSIs and logic LSIs since they have advantageous features of low power and high speed operation. The advantageous [sic] of complementary metal oxide semiconductor devices are well known in the art. Note that Passlack also teaches complementary GaAs devices exhibit optimum speed/power performance and efficiency at low supply voltage of 1 V and below (Col. 1 lines 18-24.) .. that complementary GaAs exhibits optimum speed/power performance and efficiency at a low supply voltage of 1 V and below (see Col. 1, lines 22-24).

Therefore, it would have been obvious to one of ordinary skill in the art at the time the invention was made to integrate transistor together with complementary metal-oxide semiconductor integrated circuit because of the well known advantages of CMOS configurations. [Office action page 6 line 15 to page 7 line 17.]

In reply, the applicant disagrees with the examiner's statements of fact and conclusions of law. Specifically, the applicant submits for the reasons presented below (1) that Passlack does not disclose a gate insulator structure and (2) there is no motivation to modify Passlack in view of Kikkawa by substituting Passlack's substrate with Kikkawa's substrate.

As factual matters, Passlack's Ga2O3 is not insulating and the structure of layers above Passlack's GaAs substrate could not be grown on Kikkawa's InP substrate. These facts are inconsistent with the obviousness conclusions reached by the examiner. Therefore, the examiner's conclusions are not supported by substantial evidence.

Moreover, the examiner's conclusion that Kikkawa teaches the equivalency of InP and GaAs substrates is inconsistent with additional facts noted herein and also contrary to an interpretation of Kikkawa that is consistent with all facts of record and additional facts supported by evidence filed herewith.

a. **Additional Facts**

The following additional facts and conclusions are supported by the second 37 CFR 1.132 declaration of the inventor, David Braddock, and attachments 1-3, all filed with this substitute appeal brief.

1. There is no AlGaAs composition for which lattice matching exists with InP. The

lattice constants of InP and AlGaAs, at any composition of AlGaAs, are so far apart that epitaxially growth of the AlGaAs in InP is impossible. Therefore, AlGaAs can not be grown epitaxially on InP. These facts are well known in the art. Non-epitaxially grown AlGaAs on InP has no device potential and therefore no utility of which David Braddock is aware.

2. Even for a composition of $In_xGa_{1-x}P$ containing as low as one percent GaP, $In_xGa_{1-x}P$ does not lattice match to an InP substrate. Therefore, InGaP cannot be grown epitaxially on InP with low defect densities. These facts are well known in the art. Compositions of less then one percent GaP in $In_xGa_{1-x}P$, wherein lattice matching may be possible, on InP, have no device potential and therefore no utility of which David Braddock is aware . InGaP grown non-epitaxially on InP has no device potential and therefore no utility of which David Braddock is aware. Therefore, $In_xGa_{1-x}P$ on InP has no utility of which David Braddock is aware.

3. The applied Passlack patent teaches using only AlGaAs or InGaP lattice matched to GaAs. The applied Passlack patent does not mention InP substrates. Dr. Braddock presumes that Passlack's failure to mention InP substrates is at least because Dr. Passlack knew that his AlGaAs and InGaP devices grown on an InP substrate would not grow epitaxially on InP and therefore could not produce a useful device.

3a. In a telephone conference with counsel on April 18, 2003, Dr. Braddock reviewed the office action and the outstanding rejections against this application. During that review Dr. Braddock recognized that his claim 36, as amended, claimed some inoperative embodiments, in that claim 36 claimed alternatives of an AlGaAs heterostructure or an InGaP heterostructure grown on InP. Dr. Braddock's specification for this application, in the summary of the invention, states the following for the InP substrate inventions:

> In another preferred embodiment, the compound semiconductor heterostructure comprises an $In_yGa_{1-y}As$, $Al_xIn_{1-x}As$, and InP compound semiconductor heterostructure and n-type and/or p-type charge supplying layers which are grown on an InP substrate, and a refractory metal gate of W, WN, or WSi, self aligned donor (n-channel FET) or acceptor (p-channel FET) implants, and source and drain ohmic contacts.

That passage defines $Al_x\underline{In}_{1-x}As$, not $Al_x\underline{Ga}_{1-x}As$, as an alternative composition of the heterostructure on an InP substrate. That passage does not define InGaP as an alternative composition of the heterostructure on an InP substrate. Nevertheless, the rejection of claim 36 as unpatentable for obviousness is still improper because the subject matter defined by claim 36 is in fact not obvious. The 37 CFR 1.116 amendment submitted with this supplemental appeal brief proposes changes to claim 36, which, if entered, would correct the defects noted above.

4. It is now known that stoichiometric Ga2O3 is an *n type semiconductor*, not an insulator. It has room temperature residual n type conductivity on the order of 10^{16} per cubic centimeter. That conductivity is much larger than the conductivity of insulating materials used as gate insulators. Materials used as gate insulators generally must have conductivities of *less than* 10^{12} per cubic centimeter. Accordingly, stoichiometric Ga2O3, which is what the Passlack patent teaches, is not useful for performing the function of a gate insulator.

5-5a. At the time Passlack filed for the applied Passlack patent, Dr. Braddock believes

that Passlack did not know that stoichiometric Ga2O3 had a relatively large residual conductivity. Dr. Braddock speculates that Passlack filed for the Passlack patent assuming that residual conductivity of Ga2O3 was caused by defects, vacancies, or impurities and therefore Passlack thought that conductivity could potentially be reduced to a level at which his Ga2O3 would be commercially useful as a gate insulator.

5b. Dr. Passlack has recently first authored a book chapter regarding Gallium Oxide on GaAs, co-authored with Dr. Braddock and others.[2] In that chapter, Dr. Passlack admits that, even though stoichiometry of Ga2O3 can be maintained, Ga2O3's inherently conductive nature cannot be eliminated. Dr. Passlack's own book chapter discusses that conductivity of Ga2O3 is as high as 10E18, and that the specific resistivity is always low relative to an insulator. See section 4.3, page 347. Moreover, Passlack also has another patent, 6,094,295, wherein he identified Ga2O3 as a UV transparent conducting material.[3] For example, see the abstract of 6,094,295. Thus, the implication that the examiner draws from the applied Passlack patent, which is that Ga2O3 can form an insulating layer, and therefore that it can form a gate insulating layer, is clearly incorrect.

6. Moreover, the devices disclosed in the applied Passlack patent are not commercially useful and have no practical utility due to their reliance on Ga2O3. As Dr. Braddock states it, "the Passlack device is not commercially useful and would not have any practical utility. I state this because the Ga2O3 oxide leaks just as badly or worse than a standard compound semiconductor HEMT (or PHEMT) that utilizes gate metal directly on top of an AlGaAs top layer. The metal on the AlGaAs layer forms a Schottky-barrier to current flow at the gate of the transistor. In the case of Passlack, the Ga2O3 can be so highly conducting (e.g. 10E18cm-3 conductivity) that the gate metal on Passlack's MOSFETs will form Ohmic contacts at the gate (and thus have huge gate leakage). Thus, Passlack's MOSFET devices that utilize Ga2O3-on-GaAs would have no practical utility over the prior art (i.e. standard HEMTS and PHEMTs) over which Passlack has obtained a patent."

7. The Passlack patent does not disclose a gate insulator. Instead, the Passlack patent discloses:

> The FET includes a *stoichiometric Ga2O3 gate oxide layer* positioned on upper surface of a compound semiconductor wafer structure. [Col. 2 lines 45-47; emphasis supplied.]

b. **Reasoning**

Obviousness requires both a specific teaching suggesting the proposed motivation and a

---

[2]A copy of chapter 12, entitled "Gallium Oxide on Gallium Arsenide: Atomic Structure, Materials, and Devices", is attachment 1. Chapter 12 is either published or scheduled for publication in "Gallium Oxide on Gallium Arsenide: Atomic Structure, Materials, and Devices" in III-V Semiconductor Heterostructures: Physics and Devices, edited by W.Z. Cai, Transworld Research Publisher, Kerala, India (2003).

[3]A copy of 6,094,295 to Passlack is attachment 2.

reasonable expectation of success. In re Rouffet, 149 F.3d 1350, 1359, 47 USPQ2d 1453, 1459 (Fed. Cir. 1998) ("even when the level of skill in the art is high, the Board must identify specifically the principle, known to one of ordinary skill, that suggests the claimed combination. In other words, the Board must explain the reasons one of ordinary skill in the art would have been motivated to select the references and to combine them to render the claimed invention obvious."); In re Fritch, 972 F.2d 1260, 1265, 23 USPQ2d 1780, 1783 (Fed. Cir. 1992) (the examiner can satisfy the burden of showing obviousness of the combination "only by showing some objective teaching in the prior art or that knowledge generally available to one of ordinary skill in the art would lead that individual to combine the relevant teachings of the references").

"Where claimed subject matter has been rejected as obvious in view of a combination of prior art references, a proper analysis under § 103 requires, inter alia, consideration of two factors: (1) whether the prior art would have suggested to those of ordinary skill in the art that they should make the claimed composition or device, or carry out the claimed process; and (2) whether the prior art would also have revealed that in so making or carrying out, those of ordinary skill would have a reasonable expectation of success. See In re Dow Chemical Co., 837 F.2d 469, 473, 5 USPQ2d 1529, 1531 (Fed. Cir. 1988). Both the suggestion and the reasonable expectation of success must be founded in the prior art, not in the applicant's disclosure. Id." In re Vaeck, ___ F.3d ___, 20 USPQ2d 1438 (Fed. Cir. 1991).

Neither is present in this case.

i. **No motivation to combine**

8. There is no motivation in the art to substitute InP for the GaAs substrate used by Passlack, for two reasons. First, there is no specific teaching or suggestion of such a modification of Passlack's teachings. Second, it is well known that such a substitution would prevent epitaxial growth of either one of the AlGaAs and InGaP materials that Passlack discloses are epitaxially grown in his structure on GaAs.

8a. The lattice constants of InP and AlGaAs, at any composition, are so far apart that epitaxially growth of the AlGaAs is impossible.

8b. The lattice constants of InP and GaP are so far apart that only less than a one percent solid solution in GaP in InP can be grown epitaxially on InP, and there are no known uses for such a low concentration solid solution of InGaP grown epitaxially on an InP substrate.

8c. The examiner asserts now that Kikkawa provides a teaching to substitute an InP substrate for the GaAs substrate of Passlack. Not so!

8d. Kikkawa describes a method and device structure for improving the contact resistance of p-type MISFET devices fabricated in GaAs-compatible materials systems. The materials of the layers that Kikkawa describes possess lattice constants similar to or slightly strained from GaAs. These materials all have lattice constants close enough to GaAs so that they can be grown epitaxially on a GaAs substrate.

8e. Kikkawa does not describe a compound semiconductor structure or transistor that would have any possibility of being grown epitaxially on an InP substrate. Depositing any of the structures described in the embodiments of Kikkawa on an InP substrate will result in the deposited layers being amorphous. This collection of amorphous layers would result in a

transistor-like structure, in the sense that its macroscopic shape would look like a transistor, but that transistor-like structure would not function as a transistor. Thus, InP could not be substituted for the GaAs substrate for any embodiment disclosed in Kikkawa.

8f. Kikkawa does not facially suggest use of an InP substrate. Instead, he states that:

> In the present embodiment, the material of the channel layer 54 acting also as the etching stopper is not limited to InGaAs but other materials such as InGaAsP or InGaP may also be used. Further, one may use InP for the substrate 51 in place of GaAs. The barrier layer 55, in turn, may be formed of GaAsSb or AlGaAsSb. [Column 16 lines 5-10; emphasis added.]

8g. However, it appears that, in context, and based upon that fact that neither AlGaAs nor InGaP lattice matches to InP, Kikkawa is suggesting a completely alternative structure to the GaAs substrate structure of the embodiment discussed up to column 16 line 5. That is, it appears that Kikkawa is suggesting using Sb based layers on InP as opposed to AlGaAs or InGaP layers. This is (1) because certain compositions of the Sb based quaternary's noted by Kikkawa, which are GaAsSb or AlGaAsSb, do lattice matched to InP because they have similar enough lattice constant to InP and (2) because no substantial composition of Sb in GaAsSb can lattice match to a GaAs substrate. The fact that a GaAsSb composition can lattice match to InP is confirmed by Fig. 2 of Vurgaftman et al, "Band Parameters for III-V Semiconductors and Their Alloys", J. Appl. Phys. PP 5816-5875 (June 1, 2001).[4] Figure 2 shows a line connecting GaAs to GaSb indicating the existence of GaAsSb solid solution. That solid solution contains compositions having the same lattice constant as InP, as indicated by the fact that the line crosses on the x axis the lattice constant value for InP and therefore enabling lattice matching to InP. The fact that no substantial composition of Sb in a layer of GaAsSb will lattice match to GaAs is apparent from the relatively large lattice constant differences of GaAs and GaSb. Therefore, the only reasonable inference to draw from Kikkawa's reference to InP in combination with Sb based semiconductors is that a total replacement of all layers with InP and Sb based materials instead of merely replacing the GaAs substrate with InP. For all of these reasons, the examiner's interpretation of the teachings of Kikkawa are incorrect. Kikkawa does not suggest that GaAs and InP are equivalent or that they can be substituted for one another.

8h. Neither Passlack nor Kikkawa suggest substituting an InP substrate for the GaAs substrate of Passlack. Moreover, such a substitution would result in a non-functional device since (1) AlGaAs cannot be grown epitaxially on InP and (2) InGaP cannot (to an extent that could provide any useful properties) be grown epitaxially on InP. Since the teachings of Passlack and Kikkawa do not suggest combination, the rejection of claim 36 is improper and should be reversed.

---

[4]A copy of Vurgaftman et al, "Band Parameters for III-V Semiconductors and Their Alloys", J. Appl. Phys. PP 5816-5875 (June 1, 2001) is attachment 3.

ii. **The Proposed Combination is Not Subject Matter Defined by Any Claim**

The examiner's construction of the claims is improper since the examiner has not construed the meaning to one of ordinary skill in the art the of the claimed "gate insulator structure" based upon what is stated in the specification, as required by law.

> The written description must be examined in every case, because it is relevant not only to aid in the claim construction analysis, but also to determine if the presumption of ordinary and customary meaning is rebutted. See Renishaw PLC v. Marposs Societa' per Azioni, 158 F.3d 1243, 1250, 48 USPQ2d 1117, 1122 (Fed. Cir. 1988). The presumption will be overcome where the patentee, acting as his or her own lexicographer, has clearly set forth a definition of the term different from its ordinary and customary meaning. See In re Paulsen, 30 F.3d 1475, 1480, 31 USPQ2d 1671, 1674 (Fed. Cir. 1994); Intellicall, Inc. v. Phonometrics, Inc., 952 F.2d 1384, 1387-88, 21 USPQ2d 1383, 1386 (Fed. Cir. 1992). The presumption also will be rebutted if the inventor has disavowed or disclaimed scope of coverage, by using words or expressions of manifest exclusion or restriction, representing a clear disavowal of claim scope. See Teleflex, 299 F.3d at 1324, 63 USPQ2d at 1380. [Brookhill-Wilk 1, LLC v. Intuitive Surgical, Inc., ___ F.3d ___, ___, ___ USPQ2d ___, ___ (Fed. Cir. Docket No. 02-1145, 4/11/03).]

9. Second, Passlack's stoichiometric Ga2O3 does not respond to the limitation defined in claims 36 and 38 of "a gate insulator structure." The first paragraph of the section of the specification of this application describing the invention defined the "gate insulator structure" recited in claims 36 and 38 as both electrically insulating and comprising at least two layers. That paragraph states in part:

> The present invention provides, among other things, a self-aligned enhancement mode metal-oxide-compound semiconductor FET. The FET includes *a gallium oxygen insulating structure that is composed of at least two distinct layers*. The *first layer is* most preferably more that 10 angstroms thick but less that 25 angstroms in thickness and *composed substantially of gallium oxygen compounds including but not limited to stoichiometric Ga_2O_3 and Ga_2O, and possibly a lesser fraction of other gallium oxygen compounds.* The *upper insulating layer in the gallium oxide insulating structure* is composed of an insulator that does not intermix with the underlying gallium oxygen insulating structure. This upper layer must possess excellent insulating qualities, and is most typically composed of gallium oxygen and a third rare earth element that together form a ternary insulating material. *Therefore the entire gallium oxide rare earth gate insulator structure is composed of at least two layers* and may contain a third intermediate graded layers that consists of a mixture of the upper insulating

material and the gallium oxygen compounds that compose the initial layer.

10. Please note that the specification was written by Dr. Braddock, the inventor, without advise of counsel, which explains in part the reference to two layers as "first layer" and an "upper insulating layer" to the extent that that lack of clarity and any other descriptions that lack complete clarity cause the panel any confusion.

11. The specification contains specific references to "gate insulator structure" or the equivalent "gate insulating structure" all of which are consistent with a multi layer structure that is insulating to the extent necessary to form a useful gate insulator. See the recitations:

> A refractory metal gate electrode is preferably positioned on the upper surface of the gate insulator structure layer. [Page 5 lines 10-12.]
>
> Together the lower gallium oxide compound layer and the second insulating layer form a gallium oxide gate insulating structure. [Abstract.]
>
> The gallium oxide gate insulating structure and underlying compound semiconductor gallium arsenide layer (15) meet at an atomically abrupt interface at the surface of with the compound semiconductor wafer structure (14). [Abstract.]

Therefore, the proposed combination does not result in subject matter defined by claim 36. Therefore, the rejection of claim 36 should be reversed.

12. Third, Passlack does not disclose a gate insulator. The teachings of Passlack do not enable one skilled in the art to form a structure containing a commercially useful device because the conductivity of the *stoichiometric Ga2O3 gate oxide layer* taught by Passlack is too high to be useful. Passlack does not teach one or ordinary skill in the art that the conductivity of the *stoichiometric Ga2O3 gate oxide layer* taught by Passlack is too high to be useful. Moreover, Passlack does not teach one of ordinary skill in the art how to make a gate insulating structure having low enough conductivity to be useful.

Therefore, the proposed combination does not result in subject matter defined by claim 36. Therefore, the rejection of claim 36 should be reversed.

IV. Claim Groups

A. Group 1 - Claim 36

The obviousness rejection of claim 36 should be reversed because Passlack and Kikkawa patent do not suggest any modification of Passlack to define a "substrate includes a InP based semiconductor wafer" and because the proposed combination does not define the "gate insulator structure."

B. Group 2 - Claim 38

The obviousness rejection of claim 38 should be reversed because the Passlack patent does suggest a "gate insulator structure," as claimed.

C. **Claims 53-55**

If considered on appeal, claim 53-55 are non-obvious over the applied Passlack patent for the reasons presented for claim 36.

D. **Claim 54**

If considered on appeal, claim 54 is non-obvious over all applied prior art for the additional reason that it recites "rapid thermal annealing said structure in UHV."

E. **Claim 55**

If considered on appeal, claim 55 is non-obvious over all applied prior art for the additional reason that it recites "rapid thermal annealing comprising annealing at between 700 and 900 degrees Centigrade."

F. **Claim 56**

If considered on appeal, claim 56 is non-obvious over all applied prior art for the additional reason that it recites "an InP upper spacer layer."

G. **Claim 57**

If considered on appeal, claim 57 is non-obvious over all applied prior art for the additional reason that it recites "said compound semiconductor wafer structure is formed from a layer comprising InGaP."

Respectfully Submitted,

31518
PATENT TRADEMARK
OFFICE

4/28/03
Date

Richard A. Neifeld, Ph.D.
Registration No. 35,299
Attorney of Record

Neifeld IP Law, PC
Crystal Plaza 1
2001 Jefferson Davis
Highway
Suite 1001
Arlington, VA 22202

Tel: 703-415-0012
Fax: 703-415-0013
Email: rneifeld@Neifeld.com

Y:\Clients\Osemi\OSEM_DB3\OSEM-DB3-US\Drafts\AppealBrief_030419.wpd

APPENDIX 1 - CLAIMS REJECTED AND UNDER APPEAL WITHOUT ENTRY OF 37 CFR 1.116 AMENDMENT FILED WITH THIS SUPPLEMENTAL APPEAL BRIEF

Claims 36 and 38 read as follows:

36. (Previously Amended) An enhancement mode metal-oxide-compound semiconductor field effect transistor comprising:

a compound semiconductor wafer structure having an upper surface;

a gate insulator structure positioned on upper surface of said compound semiconductor wafer structure;

a gate electrode positioned on upper surface of said gate insulator structure layer;

source and drain ion implants self-aligned to the gate electrode; and

source and drain ohmic contacts positioned on ion implanted source and drain areas;

wherein said compound semiconductor wafer structure comprises a Al_xGa_{1-x} As, $In_yGa_{1-y}As$, InP, or $In_zGa_{1-z}P$ layer, said layer being positioned on said upper surface;

a substrate on which resides said compound semiconductor wafer structure; and

wherein said substrate includes a InP based semiconductor wafer.

38. A complementary metal-oxide compound semiconductor integrated circuit comprising an enhancement mode metal-oxide-compound semiconductor field effect transistor, said transistor comprising:

a compound semiconductor wafer structure having an upper surface;

a gate insulator structure positioned on said upper surface;

a gate electrode positioned on said upper surface;

source and drain ion implants self-aligned to the gate electrode; and

source and drain ohmic contacts positioned on ion implanted source and drain areas,

wherein the compound semiconductor wafer structure comprises a wider band gap spacer layer and a narrower band gap channel layer;

wherein the narrower band gap channel layer comprises $In_yGa_{1-y}As$; and

and wherein said transistor is integrated together with similar and complementary transistor devices to form complementary metal-oxide compound semiconductor integrated circuit.

53. A method for forming an enhancement mode metal-oxide-compound semiconductor field effect transistor structure, comprising:

providing a compound semiconductor wafer structure having an upper surface;

depositing a gate insulator structure comprising depositing a first layer and depositing a second layer, said gate insulator on said upper surface;

said first layer substantially comprising compounds of gallium and oxygen;

said second layer comprising at least one compound of gallium, oxygen and at least one rare earth element; and

depositing a gate electrode positioned on said gate insulator structure.

54. The method of claim 53 comprising rapid thermal annealing said structure in UHV.

55. The method of claim 54 wherein said rapid thermal annealing comprising annealing at between 700 and 900 degrees Centigrade.

APPENDIX 2 - CLAIMS REJECTED AND UNDER APPEAL WITH ENTRY OF 37 CFR 1.116 AMENDMENT FILED WITH THIS SUPPLEMENTAL APPEAL BRIEF

Claims 36 and 38 read as follows:

36. (Twice Amended) An enhancement mode metal-oxide-compound semiconductor field effect transistor comprising:

a compound semiconductor wafer structure having an upper surface;

a gate insulator structure positioned on upper surface of said compound semiconductor wafer structure;

a gate electrode positioned on upper surface of said gate insulator structure layer;

source and drain ion implants self-aligned to the gate electrode; and

source and drain ohmic contacts positioned on ion implanted source and drain areas;

wherein said compound semiconductor wafer structure comprises a Al_xIn_{1-x} As, $In_yGa_{1-y}As$, or InP, said layer being positioned on said upper surface;

a substrate on which resides said compound semiconductor wafer structure; and

wherein said substrate includes a InP based semiconductor wafer.

38. A complementary metal-oxide compound semiconductor integrated circuit comprising an enhancement mode metal-oxide-compound semiconductor field effect transistor, said transistor comprising:

a compound semiconductor wafer structure having an upper surface;

a gate insulator structure positioned on said upper surface;

a gate electrode positioned on said upper surface;

source and drain ion implants self-aligned to the gate electrode; and

source and drain ohmic contacts positioned on ion implanted source and drain areas,

wherein the compound semiconductor wafer structure comprises a wider band gap spacer layer and a narrower band gap channel layer;

wherein the narrower band gap channel layer comprises $In_yGa_{1-y}As$; and

and wherein said transistor is integrated together with similar and complementary transistor devices to form complementary metal-oxide compound semiconductor integrated circuit.

53. A method for forming an enhancement mode metal-oxide-compound semiconductor field effect transistor structure, comprising:

providing a compound semiconductor wafer structure having an upper surface;

depositing a gate insulator structure comprising depositing a first layer and depositing a second layer, said gate insulator on said upper surface;

said first layer substantially comprising compounds of gallium and oxygen;

said second layer comprising at least one compound of gallium, oxygen and at least one rare earth element; and

depositing a gate electrode positioned on said gate insulator structure.

54. The method of claim 53 comprising rapid thermal annealing said structure in UHV.

55. The method of claim 54 wherein said rapid thermal annealing comprising annealing at between 700 and 900 degrees Centigrade.

56. (New) The transistor of claim 36 wherein said compound semiconductor wafer structure comprises an InP upper spacer layer.

57. (New) The transistor of claim 14 wherein said upper surface of said compound semiconductor wafer structure is formed from a layer comprising InGaP.

APPENDIX 3 - ALL PENDING CLAIMS AS THEY STAND AND ALTERNATIVELY SHOWING THEM IF THE 37 CFR 1.116 AMENDMENT IS ENTERED

The claims as amended appear below. All claims are reproduced for convenience.

1. (Amended) An enhancement mode metal-oxide-compound semiconductor field effect transistor comprising:

a compound semiconductor wafer structure having an upper surface;

a gate insulator structure comprising a first layer and a second layer;

said first layer substantially comprising compounds of gallium and oxygen;

said second layer comprising compounds of gallium and oxygen and at least one rare earth element;

a gate electrode positioned on said gate insulator structure;

source and drain ion implants self-aligned to said gate electrode; and

source and drain ohmic contacts positioned on ion implanted source and drain areas;

wherein gate electrode comprises a metal selected from the group consisting of W, WN, WSi , and combinations thereof.

2. (Amended) The transistor of claim 1 wherein said first layer forms an atomically abrupt interface with said upper surface.

3. (Amended) The transistor of claim 1 wherein said gate insulator structure is composed of at least three layers, including a graded layer that contains varying compositions of gallium oxygen and at least one rare-earth element.

4. (Amended) The transistor of claim 3 wherein said gate insulator structure further comprises at a third layer containing gallium and oxygen.

5. (Amended) The transistor of claim 1 said first layer has a thickness of more than 10 angstroms and less than 25 angstroms.

6. (Amended) The transistor of claim 1 wherein said gate insulator structure has a thickness of 20-300 angstroms.

7. (Amended) The transistor of claim 1 wherein said first layer forms an interface with said upper surface that extend less than four atomic layers in depth of structural interface modulation.

8. (Amended) The transistor of claim 1 wherein said first layer and said gate insulator structure protects said upper surface.

9. (Amended) The transistor of claim 1 wherein said gate electrode comprises a refractory metal which is stable in presence of the top layer of the gate insulator structure at 700°C.

10. (Amended) The transistor of claim 1 wherein said source and drain ion implants provide one of an n-channel or p-channel.

11. (Amended) The transistor of claim 1 wherein said source and drain ion implants comprise at least one of Be/F and C/F.

12. (Amended) The transistor of claim 1 wherein said upper surface comprises GaAs.

13. (Amended) The transistor of claim 1 wherein said upper surface comprises $In_xGa_{1-x}As$.

14. (Amended) An enhancement mode metal-oxide-compound semiconductor field effect transistor comprising:

a compound semiconductor wafer structure having an upper surface;

gate insulator structure on said upper surface, said gate insulator structure comprising a first layer, a second layer, and a third layer;

said first layer substantially comprising compounds of gallium and oxygen;

said second layer substantially comprising compounds of gallium and oxygen and at least one rare earth element such that the normalized relative composition of at least one of gallium, oxygen, and said at least one rare earth element in said second layer varies in a monotonic manner as a function of depth within said second insulating layer;

said third layer above said second layer, said third layer substantially comprising gallium oxygen and at least one rare earth element, said third layer being insulating;

a gate electrode positioned on said gate insulator structure;

source and drain ion implants self-aligned to said gate electrode; and

source and drain ohmic contacts positioned on ion implanted source and drain areas;

wherein said gate electrode comprises a metal selected from the group consisting of W, WN, WSi , and combinations thereof.

15. (Amended) The transistor of claim 14 wherein said first layer forms an atomically abrupt interface with said upper surface.

16. (Amended) The transistor of claim 14 wherein the gate insulator structure comprises a varying layer that substantially comprises gallium, oxygen, and at least one rare-earth element in which relative concentration of at least one of gallium, oxygen, and said at least one rare earth in said varying layer monotonically vary with depth in said layer.

17. (Amended) The transistor of claim 14 wherein said first layer has a thickness of more than 10 angstroms and less than 25 angstroms.

18. (Amended) The transistor of claim 14 wherein the gate insulator structure has a thickness of 20-300 angstroms.

19. (Amended) The transistor of claim 14 wherein said first layer forms an interface with the compound semiconductor wafer structure that extend less than four atomic layers in depth of modulation of said interface.

20. (Amended) The transistor of claim 14 wherein said first layer and said gate insulator structure protects said upper surface.

21. (Amended) The transistor of claim 14 wherein said gate electrode comprises a metal which is stable in presence of the top layer of the gate insulator structure at 700°C.

22. (Amended) The transistor of claim 14 wherein said source and drain ion implants define an n-channel.

23. (Amended) The transistor of claim 14 wherein said source and drain ion implants comprise and Be/F and C/F, and define a p-channel.

24. (Amended) The transistor of claim 14 wherein said upper surface comprises GaAs.

25. (Amended) The transistor of claim 14 wherein said upper surface comprises $In_xGa_{1-x}As$.

26. An enhancement mode metal-oxide-compound semiconductor field effect transistor comprising:

a compound semiconductor wafer structure having an upper surface;

a multilayer gate insulator structure positioned on said upper surface, said multilayer gate insulator structure substantially comprising alternating layers each of which comprises gallium, oxygen, and at least one rare-earth element;

a gate electrode positioned on said multilayer gate insulator structure;

source and drain ion implants self-aligned to the gate electrode; and

source and drain ohmic contacts positioned on ion implanted source and drain areas;

and dielectric spacers positioned on sidewalls of said gate electrode.

27-35. - Canceled by this amendment.

If the 37 CFR 1.116 amendment is not entered by the examiner claim 36 reads as follows:

36. (Amended) An enhancement mode metal-oxide-compound semiconductor field effect transistor comprising:

a compound semiconductor wafer structure having an upper surface;

a gate insulator structure positioned on upper surface of said compound semiconductor wafer structure;

a gate electrode positioned on upper surface of said gate insulator structure layer;

source and drain ion implants self-aligned to the gate electrode; and

source and drain ohmic contacts positioned on ion implanted source and drain areas;

wherein said compound semiconductor wafer structure comprises a Al_xGa_{1-x} As, In_yGa_{1-y}As, InP, or $In_zGa_{1-z}P$ layer, said layer being positioned on said upper surface;

a substrate on which resides said compound semiconductor wafer structure; and

wherein said substrate includes a InP based semiconductor wafer.

If the 37 CFR 1.116 amendment has been entered by the examiner then claim 36 reads as follows:

36. (Twice Amended) An enhancement mode metal-oxide-compound semiconductor field effect transistor comprising:

a compound semiconductor wafer structure having an upper surface;

a gate insulator structure positioned on upper surface of said compound semiconductor wafer structure;

a gate electrode positioned on upper surface of said gate insulator structure layer;

source and drain ion implants self-aligned to the gate electrode; and

source and drain ohmic contacts positioned on ion implanted source and drain areas;

wherein said compound semiconductor wafer structure comprises a Al_xIn_{1-x} As, In_yGa_{1-y}As, or InP, said layer being positioned on said upper surface;

a substrate on which resides said compound semiconductor wafer structure; and

wherein said substrate includes a InP based semiconductor wafer.

37. (Amended) A complementary metal-oxide compound semiconductor integrated circuit comprising the transistor of claim 1, 13, or 26 integrated together with similar and

complementary transistor devices to form said complementary metal-oxide compound semiconductor integrated circuit.

38. A complementary metal-oxide compound semiconductor integrated circuit comprising an enhancement mode metal-oxide-compound semiconductor field effect transistor, said transistor comprising:

a compound semiconductor wafer structure having an upper surface;

a gate insulator structure positioned on said upper surface;

a gate electrode positioned on said upper surface;

source and drain ion implants self-aligned to the gate electrode; and

source and drain ohmic contacts positioned on ion implanted source and drain areas,

wherein the compound semiconductor wafer structure comprises a wider band gap spacer layer and a narrower band gap channel layer;

wherein the narrower band gap channel layer comprises $In_yGa_{1-y}As$; and

and wherein said transistor is integrated together with similar and complementary transistor devices to form complementary metal-oxide compound semiconductor integrated circuit.

39. An enhancement mode metal-oxide-compound semiconductor field effect transistor structure, comprising:

a compound semiconductor wafer structure having an upper surface;

a gate insulator structure comprising a first layer and a second layer, said gate insulator on said upper surface;

said first layer substantially comprising compounds of gallium and oxygen;

said second layer comprising at least one compound of gallium, oxygen and at least one rare earth element; and

a gate electrode positioned on said gate insulator structure.

40. The structure of claim 39 wherein said gate electrode comprises a refractory metal.

41. The structure of claim 39 wherein said gate electrode comprises a member of the group consisting of W, WN, WSi , and combinations thereof.

42. The structure of claim 39 wherein said gate insulator structure further comprises a third layer.

43. The structure of claim 42 wherein said third layer comprises compounds comprising gallium and oxygen.

44. The structure of claim 43 wherein compounds of said third layer comprising gallium and oxygen further comprise a rare earth element.

45. The structure of claim 44 wherein a composition of said third layer varies monotonically with depth in said third layer.

46. The structure of claim 43 wherein said gate insulator structure further comprises a fourth layer.

47. The structure of claim 43 wherein said fourth layer comprises compounds comprising gallium and oxygen.

48. The structure of claim 47 wherein compounds of said fourth layer comprising gallium and oxygen further comprise a rare earth element.

49. The structure of claim 39 wherein said first layer is adjacent and in contact with said upper surface.

50. The structure of claim 39 further comprising source and drain contacts.

51. The structure of claim 39 wherein said source and drain contacts are rapid thermal annealed in UHV.

52. The structure of claim 39 wherein said gate insulator structure passivates said upper surface.

53. A method for forming an enhancement mode metal-oxide-compound semiconductor field effect transistor structure, comprising:

providing a compound semiconductor wafer structure having an upper surface;

depositing a gate insulator structure comprising depositing a first layer and depositing a second layer, said gate insulator on said upper surface;

said first layer substantially comprising compounds of gallium and oxygen;

said second layer comprising at least one compound of gallium, oxygen and at least one rare earth element; and

depositing a gate electrode positioned on said gate insulator structure.

54. The method of claim 53 comprising rapid thermal annealing said structure in UHV.

55. The method of claim 54 wherein said rapid thermal annealing comprising annealing at between 700 and 900 degrees Centigrade.

If the 37 CFR 1.116 amendment has been entered by the examiner then claims 56 and 57 are entered and reads as follows:

56. (New) The transistor of claim 36 wherein said compound semiconductor wafer structure comprises an InP upper spacer layer.

57. (New) The transistor of claim 14 wherein said upper surface of said compound semiconductor wafer structure is formed from a layer comprising InGaP.

Y:\Clients\Osemi\OSEM_DB3\OSEM-DB3-US\Drafts\AppealBrief_030419.wpd

OLD DOCKET NO: DB3
NEW DOCKET NO: OSEM-DB3

LIST OF ATTACHMENTS

Attachment 1 -	Article "Gallium Oxide on Gallium Arsenide: Atomic Structure, Materials, and Devices", pp. 335 - 357.
Attachment 2 -	Copy of Patent No. 6,094,295 to Passlack et al.
Attachment 3 -	"Band Parameters for III - V Compound Semiconductor and Their Alloys" Journal of Applies Physics, pp. 5815 - 5875.

CHAPTER 12

GALLIUM OXIDE ON GALLIUM ARSENIDE: ATOMIC STRUCTURE, MATERIALS, AND DEVICES

M. PASSLACK*, Z. YU, R. DROOPAD, AND J. K. ABROKWAH
Motorola Inc., 2100 East Elliot Road, Tempe, AZ 85284, USA

D. BRADDOCK
Osemi, Inc., 300 First Street N.E., Rochester, MN 55906, USA

S.-I. YI, M. HALE, J. SEXTON, AND A.C. KUMMEL
University of California - San Diego, Department of Chemistry, La Jolla, CA 92093, USA

ABSTRACT

This study pertains to aspects of deposited gallium oxide films on gallium arsenide including (1) atomic surface and interface structure, (2) deposition technique, (3) film and interface properties, and (4) field effect transistor applications. Ga_2O_3 films are deposited by effusive evaporation from a polycrystalline Ga_2O_3 source onto the GaAs(001)-(2x4) surface in ultra-high vacuum. The first monolayer of Ga_2O forms a charge balanced (2x2) surface order with a crystalline interface that is electronically unpinned. Further deposition proceeds via the formation of amorphous bulk Ga_2O_3. We review the structural and electrical properties of Ga_2O_3 films and Ga_2O_3-GaAs interfaces. Finally, a GaAs based enhancement-mode heterostructure MOSFET is discussed and a performance comparison to prior art is presented.

1 INTRODUCTION

The quest for III-V gate oxides has been fueled by scientific curiosity and commercial opportunity for almost four decades. More recently, the demand for III-V semiconductors in high volume applications such as wireless and fiber optic communications has sparked even stronger interest in III-V based metal-oxide-semiconductor (MOS) field effect transistors (FET); the past and present lack of III-V MOSFET devices has limited functionality, scalability, performance, and market acceptance of III-V technologies.

Excellent reviews of early gate insulator research on III-V semiconductors were published by W.F. Croydon and E.H.C. Parker [1] and C.W. Wilmsen [2] in 1982 and 1985, respectively. The conclusions of almost 20 years of effort in the field were not encouraging: attempts at adopting the wildly successful thermal oxidation technique of silicon had failed and insulator deposition techniques did not look more promising [1]-[10]. Consequently, the field had been

* Electronic mail: m.passlack@motorola.com

Attachment 1

nearly abandoned. However, the pioneering work by Spicer [11], Pianetta [12] and others had greatly advanced the understanding of III-V semiconductor surface reactivity and would later support the foundation of modern III-V MOS technology concerning the requirement of surface preparation under ultra-high vacuum conditions.

When Callegari et al. reported on the first deposition of gallium oxide thin films on GaAs in 1988 [13], the evidence of Fermi level unpinning was spotty at best and the deposition technique was questionable; the oxide film was prepared by gallium metal deposition in an oxygen plasma. In fact, the authors attributed the suggested Fermi level unpinning to hydrogen and nitrogen plasma treatments rather than to the formation of a gallium oxide-GaAs interface. This was in agreement with conventional wisdom at the time: it was speculated that any material containing oxygen causes Fermi level pinning (pp. 197-198 in [2]), a hypothesis apparently substantiated by Spicer's earlier observation of Fermi level pinning at an oxygen exposed GaAs surface [11].

Work on gallium oxide deposition on GaAs was accelerated at AT&T Bell Laboratories in early 1993. The motivation for this effort is intuitive--it was thought that an interface comprising similar materials is more likely to exhibit an unpinned Fermi level compared to an interface consisting of more dissimilar materials. Since existing gallium oxide deposition techniques [13]- [15] were considered to be incompatible with the requirements of oxide deposition onto a GaAs surface, electron beam evaporation from a high purity, single crystal gadolinium gallium garnet ($Gd_3Ga_5O_{12}$) was introduced [16], [17]. Initially, G. Zydzik deposited gallium oxide films onto GaAs substrates. However, Fermi level unpinning was only observed later when M. Hong and J.P. Mannaerts deposited oxide films on freshly grown GaAs(001) surfaces using in-situ molecular beam epitaxy (MBE) [18]-[23]. Most important, accumulation and inversion in n- and p-type capacitors were demonstrated [18]. This unequivocally established the requirement of ultra-high vacuum for Fermi level unpinning at the oxide-GaAs interface. Early applications included mirror passivation of high power 980 nm pump laser [24], [25].

Although the demonstration of inversion/accumulation at oxide-GaAs interfaces [18] represented an impressive engineering feat, the underlying fundamental mechanism of Fermi level unpinning remained elusive. The matter was further complicated by the presence of Gd in the oxide films manufactured at AT&T Bell Laboratories [18], [22]. In addition, it was found that in-situ MBE of other oxides such as aluminum oxide, silicon oxide, and magnesium oxide resulted in Fermi level pinning [20]. Obviously, the atomic level structure of the oxide-GaAs interface and its associated electrical properties had to move to center stage: to reveal the interface's fundamental properties became imperative for further technology advancement.

This paper represents a first comprehensive, seminal work on unpinned oxide-GaAs interfaces commencing with fundamental atomic level interface studies and concluding with the demonstration of an enhancement mode heterostructure MOSFET. The foundation of this work is the unique property of gallium oxide to unpin the interface Fermi level on GaAs. All aspects of Ga_2O_3 deposition are discussed: atomic structure, physics, chemistry, materials, characterization, manufacturing, and device processing. Significant progress in experimental and theoretical methods, equipment, and manufacturing techniques have led to fundamental advancements and discoveries as further discussed below.

The introduction of effusive evaporation from a crystalline Ga_2O_3 source provides a high purity molecular gallium oxide beam and enables the reproducible manufacture of smooth, amorphous Ga_2O_3 films forming atomically abrupt interfaces with GaAs(001) [26] (Section 3). Scanning tunneling microscopy, scanning tunneling spectroscopy, low energy electron diffraction, and Auger electron spectroscopy supported by density functional calculations reveal that a monolayer of Ga_2O molecules forms a charge balanced (2x2) surface order on GaAs(001) that is electronically unpinned [27] (Section 2). The amorphous oxide films are stoichiometric

(Ga_2O_3) and of high volume density. The atomically abrupt interface is thermally stable [28] and characterized by low interface recombination velocity and interface state density [29]. In analogy to the SiO_2-Si, system, hydrogen atoms are found to passivate defects at as-deposited Ga_2O_3-GaAs interfaces [30]. A photoluminescence intensity technique enables interface optimization [31] and, in combination with standard capacitance-voltage (C-V) measurements, virtually eliminates common pitfalls in insulator-III-V semiconductor interface characterization (Section 4). The effort culminates in the first demonstration of a functional enhancement mode GaAs based MOSFET. The 0.6 μm self-aligned p-channel heterostructure MOSFET exhibits a maximum dc transconductance g_m of 51 mS/mm, an improvement of more than two orders of magnitude over previously reported results. A complete and manufacturable process flow and 66% of theoretical performance are demonstrated [32] (Section 5).

The authors believe that the discussed technology constitutes a milestone in the development of commercially viable III-V MOSFETs. The presented technology has its deficiencies and challenges remain.

2 ATOMIC SURFACE AND INTERFACE STRUCTURE

We first discuss the basic chemistry and physics of the oxide-semiconductor interface. To ensure an unpinned Fermi level, the atomic structure of the interface must be controlled. Through the aid of scanning tunneling microscopy (STM), scanning tunneling spectroscopy (STS), low energy electron diffraction (LEED), and Auger electron spectroscopy (AES), we are able to directly show which adsorption sites provide an unpinned interface Fermi level.

A clean GaAs(001)-(2x4) surface reconstruction is obtained by thermally desorbing an arsenic capping layer from a GaAs wafer grown by molecular beam epitaxy (MBE) in an ultra-high vacuum (UHV) chamber. The clean surface is confirmed by AES, LEED, and STM. A filled-state STM image of the clean surface taken with a bias of -3 V and a constant tunneling current of 0.2 nA is shown in Fig. 1. In STM, the electronegative arsenic atoms image as bright features and the electropositive gallium atoms image as dark features. As seen in the ball-and-stick diagram in Fig. 1, the bright rows along the [$\bar{1}$10] azimuth consist of two arsenic dimers that bond in the same direction as the row [33], [34]. An additional arsenic dimer resides in the

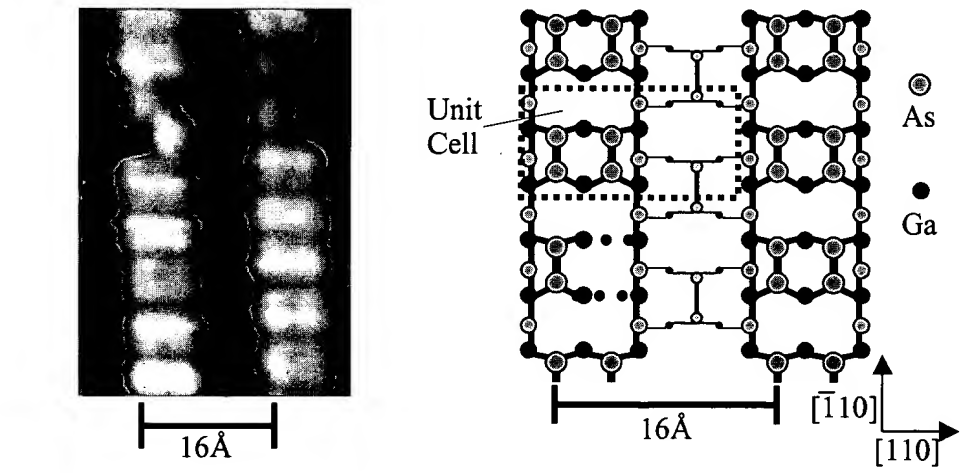

Fig. 1 A filled state STM image (left) of a clean GaAs(001) (2x4) surface reconstruction taken at V = -3 V and I = 0.2 nA. The clean surface is comprised of three arsenic dimers per unit cell as seen in the unit cell specified in the ball-and-stick diagram (right). The legend in the lower right corresponds to both the STM image and the ball-and-stick diagram.

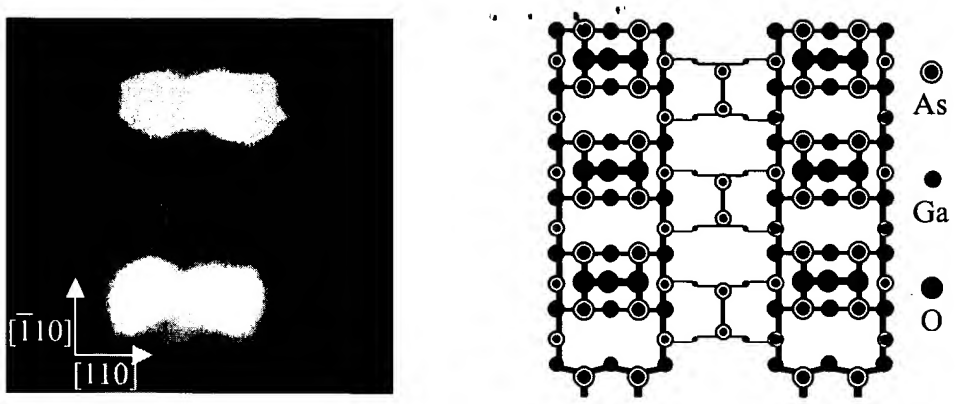

Fig. 2 Filled state STM image of two Ga_2O molecules inserted into the As dimer row taken at V = -1.5 V and I = 0.2 nA (left). The brightest features in the image are the Ga_2O molecules inserted into the As dimers, and the black region is the trough. The legend in the lower left describes both the STM image and the ball-and-stick diagram (right).

trough of each unit cell, but this dimer is not imaged in STM due to the exponential tunneling dependence on the tip-sample separation. Also present in the STM image in Fig. 1, and represented in the ball-and-stick diagram, are arsenic dimer vacancies. These sites are formed during the thermal decapping procedure.

After the confirmation of a clean GaAs(001)-(2x4) surface reconstruction, the surface is dosed in-situ at an elevated surface temperature with $Ga_2O_{(g)}$. The $Ga_2O_{(g)}$ molecules are produced from the sublimation of polycrystalline Ga_2O_3 (see also Section 3). The polycrystalline Ga_2O_3 sublimates as $Ga_2O_{(g)} + O_{2(g)}$ [35]-[37]. The sticking probability of $O_{2(g)}$ is about six orders of magnitude lower than that of $Ga_2O_{(g)}$ at 25 °C [38]; therefore, it can be assumed that only $Ga_2O_{(g)}$ sticks to the clean surface. A filled state STM image at submonolayer coverage of Ga_2O/GaAs(001) taken with a sample bias of -1.5 V and a tunneling current of 0.2 nA is shown in Fig. 2. In this image, the gallium atoms in the Ga_2O molecule image as the brightest features, despite gallium being an electropositive atom, due to their height above the arsenic atoms in the original arsenic dimer row. The oxygen atoms are not imaged because the electronic states associated with them reside well below the valence band maximum (VBM) [38]. From this image, it can be seen that Ga_2O molecules insert into two arsenic dimers on top of the original arsenic dimer row. The ball-and-stick diagram in Fig. 2 shows the atomic placement of the Ga_2O insertions. Ga_2O bonding is not observed in the trough due to the lack of arsenic dimer pairs.

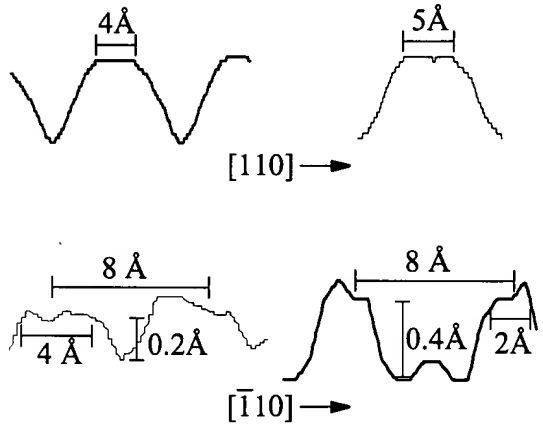

Fig. 3 Line scans of the As dimer rows of clean GaAs(001)-(2x4) (left) and Ga_2O inserted into the dimers (right). The top line scans run across the As dimer row direction ([110]), and the bottom two line scans are along the rows ([$\bar{1}$10]).

Line scan analysis from both the clean GaAs(001)-(2x4) surface and from the same surface with Ga_2O inserted into the row arsenic dimers can be seen in Fig. 3. From the top half of Fig. 3, line scans are taken along the [110] direction (across the dimer row). The clean surface shows the row width to be 4

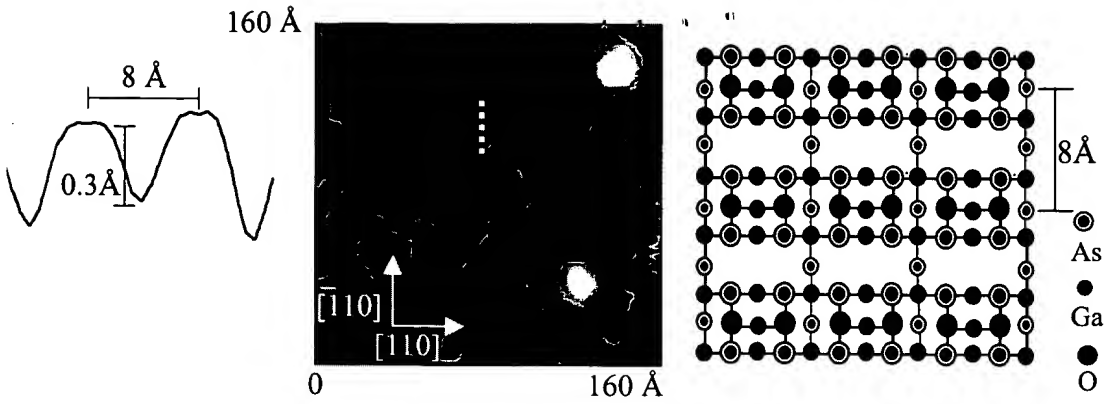

Fig. 4 The center filled state STM image of monolayer coverage of Ga_2O adsorbed on the clean GaAs(001)-(2x4) surface at elevated temperature as taken at V = -1.5 V and I = 0.2 nA (center). Line scan analysis (left) taken along the dotted line drawn on the STM image corresponds well to the proposed atomic placement in the ball-and-stick diagram (right).

Å, whereas the row width on Ga_2O/GaAs is measured to be 5 Å along the Ga_2O molecule. Line scans along the arsenic dimer row ([$\bar{1}$10]) show an even more pronounced difference between the clean surface and the surface formed upon deposition of Ga_2O. The first major difference is the apparent depth between the two peaks that are spaced 8 Å apart. The clean surface has an apparent depth of 0.2 Å, whereas the Ga_2O inserted site has an apparent depth of 0.4 Å. This difference is attributed to the height difference between the gallium and arsenic atoms and the ability of the arsenic atoms' electrons to more readily tunnel into the tip. The other major difference between the two line scans is the 4 Å spacing along the dimer row of the clean surface showing the two arsenic dimer atoms versus the 2 Å spacing along the Ga_2O inserted site showing only the single gallium atom. This line scan clearly shows the difference between the two sites.

A simple extension of the bonding structure proposed for the low coverage Ga_2O insertion site is used to explain the bonding structure for monolayer coverage of Ga_2O deposited on the GaAs(001)-(2x4) surface at an elevated surface temperature. Fig. 4 shows a filled state STM image of a monolayer of Ga_2O/GaAs(001) taken with a bias of -1.5 V and a tunneling current of 0.2 nA. At monolayer coverage of Ga_2O, the surface has rows that run perpendicular to the original arsenic dimer rows. We find good agreement between the Tersoff-Hamman STM simulations [39] using the plane wave/pseudo-potential DFT code VASP [40], [41] and our proposed monolayer structure [27]. The initial (2x4) surface has an intrinsic arsenic deficiency compared to that of the proposed (2x2) surface structure. The proposed (2x2) surface structure contains a single monolayer of arsenic whereas the initial (2x4) surface only contains 0.75 monolayers of arsenic. It is proposed that the surface reconstructs to form steps as a result of the ar-

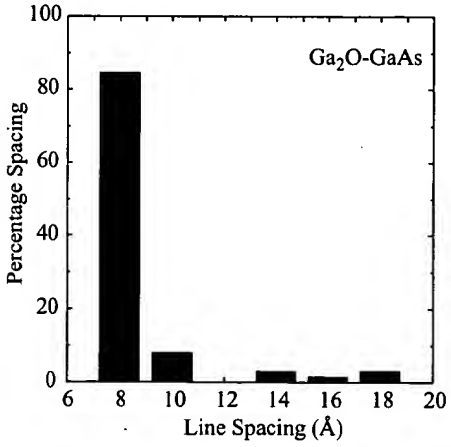

Fig. 5 Percentage spacing as a function of consecutive line spacing shows that Ga_2O fully saturates at a line spacing of 8 Å. The near uniform spacing is a result of a surface reconstruction that liberates As to reduce strain.

senic deficiency. By taking numerous line scans across the newly formed Ga_2O rows (along the [$\bar{1}$10] azimuth), a line spacing distribution is obtained as shown in Fig. 5. The graph shows that Ga_2O fully saturates the surface at a line spacing of 8 Å and our STM images at monolayer coverage are very near full saturation. The surface reconstruction allows for the formation of a uniform monolayer.

The electronic structure of the surface at monolayer coverage is studied by STS. The spectroscopic technique holds the tip within a few angstroms from the surface and a bias is swept through the sample while the differential conductivity is measured using a lock-in amplifier. The differential conductivity is then divided by a broadened I/V curve, $(\overline{I/V})$, to arrive at a unitless quantity which is a good approximation of the density of states in the near surface region. In Fig. 6, the measured STS spectra of monolayer coverage of Ga_2O on both p- and n-type GaAs(001) is shown. Both materials show a bandgap of ~1.5eV, very close to the GaAs bulk value of 1.43 eV [42], [43]. The small discrepancy in the surface bandgap compared with that of bulk GaAs is due to the low doping levels of both materials. The samples were doped with $2x10^{16}$ cm^{-3} Be and $2x10^{16}$ cm^{-3} Si for the p and n-type material, respectively. The density of states and the Fermi level position for both p and n-type material are indicative of unpinned surfaces with no measurable states in the bandgap.

Density functional theory calculations are performed on the GaAs-β2(2x4) surface to model the energetics of surface reactions, different bonding configurations and corresponding electronic structures. A plane-wave pseudopotential approach is implemented along with the PW91 GGA-DFT method using the VASP code [40], [41]. The clean GaAs-β2(2x4) surface is modeled with an 8-layer slab consisting of 32 gallium and 28 arsenic atoms, terminated with pseudo-hydrogen (H with 1.25 valence electrons to mimic bulk arsenic bonding), and utilizing periodic boundary conditions. All structures shown are allowed to fully relax and are rigorously checked with respect to plane-wave and k-point sampling convergence. Adequate values are determined to be 500 eV plane-wave cut-off with a 4x2x1 Monkhorst-Pack k-point sampling in the 1st Brillouin zone.

Fig. 7 shows two side-on models of the GaAs-β2(2x4) surface. Model (a) shows the clean unit cell. Model (b) shows a Ga_2O molecule inserted into two arsenic dimers (gallium atoms from Ga_2O molecule are marked with an asterisk). Model (c) shows a top-down view of the

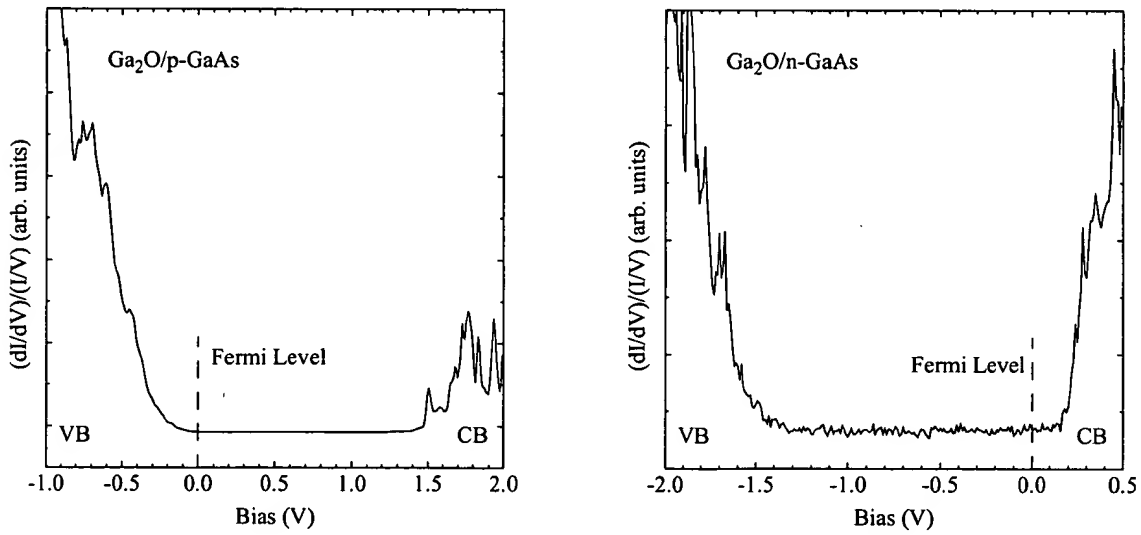

Fig. 6 Scanning tunneling spectroscopy spectra of monolayer coverage of Ga_2O adsorbed onto both p- and n-type GaAs(001)-(2x4). The Fermi level position is near the valence band edge and conduction band edge for p and n-type material, respectively.

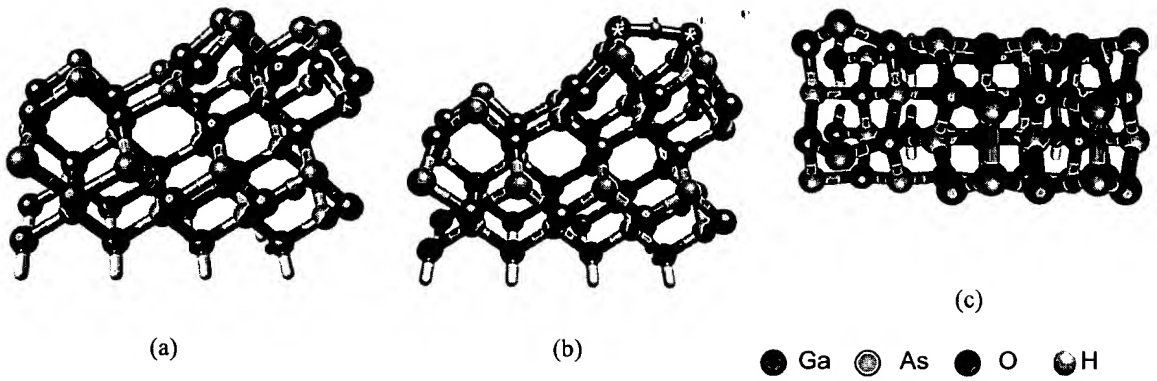

Fig. 7 Model (a) shows a side view of a clean GaAs-β2(2x4) surface, (b) shows a side view of the same surface with Ga_2O inserted into the arsenic dimer pair, and (c) shows a top view of the clean surface.

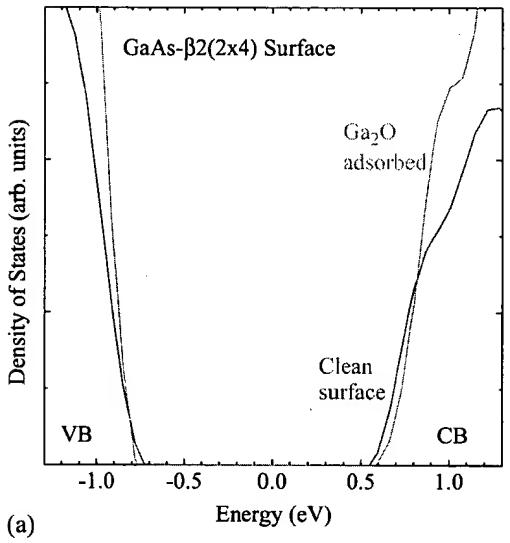

Fig. 8 Calculated DOS for both clean and Ga_2O adsorbed surfaces shown in Fig. 7.

clean GaAs-β2(2x4) surface. Tersoff-Hamman STM simulations confirm that these are the correct surface structures [27], [39].

Fig. 8 shows the electronic structure of the bonding model depicted in Fig. 7. The density of states (DOS) is calculated as a function of energy and is shown in the bandgap region for both discussed structures. The solid blue line in Fig. 8 shows the clean GaAs-β2(2x4) surface DOS; it exhibits a band-gap region free of electronic states. The green line in Fig. 8 shows the DOS of the clean GaAs-β2(2x4) surface with a Ga_2O molecule inserted into the arsenic dimer pair. This calculation confirms that the adsorption of Ga_2O onto the clean surface does not induce states within the bandgap. Using the surface Ga_2O monolayer as a template, further oxide deposition proceeds via the formation of Ga_2O_3 with an amorphous microstructure as discussed in the next section.

3 DEPOSITION TECHNIQUE

An effusive evaporation technique has been developed to deposit Ga_2O_3 thin films on GaAs(001) substrates in a production-type molecular beam epitaxy (MBE) system [26]. A polycrystalline Ga_2O_3 charge heated in a high-temperature effusion cell is used as the evaporation source. In this section, atomic force microscopy (AFM), ellipsometry, electron diffraction, and transmission electron microscopy (TEM) is used to characterize the Ga_2O_3-GaAs structures. Under optimal deposition conditions, the Ga_2O_3 film surface is atomically smooth as revealed by AFM, while the Ga_2O_3-GaAs interface is atomically abrupt as confirmed by cross-sectional TEM.

Preferentially, Ga_2O_3 deposition runs are carried out in a production-type V100 dual-chamber multiwafer MBE system (VG Semicon). One chamber is dedicated for the growth of GaAs-based III-V semiconductor device structures while the second chamber is configured for

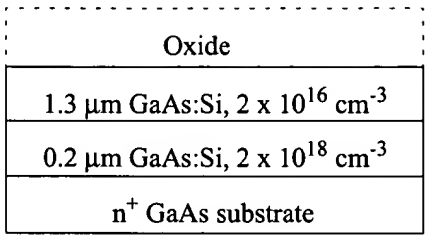

Fig. 9 Epitaxial layer structure optimized for photoluminescence (PL) and capacitance-voltage (CV) measurements. The gate oxide to be deposited is indicated by a dashed line.

oxide deposition. Both chambers are equipped with reflection high energy electron diffraction (RHEED) for in-situ monitoring of the surface during GaAs epilayer growth and during the initial stage of oxide deposition. The base pressure in both chambers is below mid-10^{-10} Torr. For oxide deposition, a polycrystalline Ga_2O_3 charge thermally heated in a high-temperature effusion cell and a rf plasma oxygen source are used for providing the oxide molecular flux and activated oxygen, respectively. An Ir crucible is used in the high-temperature cell. The chamber pressure during oxide deposition typically ranges from about $5x10^{-7}$ Torr to about $7x10^{-6}$ Torr and the oxygen plasma operation power is varied from 350 W to 550 W.

Commercial GaAs(001) substrates up to 6-inch in diameter are employed in this study. GaAs epitaxial layer are grown under standard growth conditions after the thermal desorption of the native oxide in the III-V chamber. A sharp and streaky As-stabilized GaAs(001)-(2x4) RHEED pattern is obtained after the epilayer growth, indicating an atomically ordered and flat GaAs(001) surface. The epitaxial GaAs substrates are either covered by an arsenic cap layer or transferred directly from the III-V chamber to the oxide growth chamber via a UHV buffer chamber. Fig. 9 shows a typical GaAs epitaxial layer structures utilized in this study. After the epitaxial GaAs substrate has been loaded into the oxide chamber, the substrate temperature is ramped up to the deposition temperature in the range of 350-550 °C until a sharp and streaky (2x4) RHEED pattern is obtained. The polycrystalline Ga_2O_3 charge in the high-temperature cell is then heated to its setpoint to produce a molecular oxide flux (see Section 2). A background oxygen in the order of $7x10^{-8}$ Torr is typically observed upon heating from the charge oxide decomposition. Once the substrate and high-temperature cell temperatures reach their equilibrium, the oxide cell and oxygen source shutters are opened such that the GaAs-(2x4) surface is exposed to the molecular oxide flux to commence the oxide deposition. Optionally, low levels of additional molecular oxygen can be provided at the initial stage of the oxide deposition and rf plasma activated oxygen for the remainder of the Ga_2O_3 film deposition. In some cases, only background oxygen from Ga_2O_3 sublimation is used throughout the deposition. In general, rf plasma activated oxygen enhances the deposition rate by up to a factor of 3.

The following reactions may occur on the substrate surface during oxide deposition wherein the Gibbs free energy of formation ΔG_f is given at 700 K:

$$Ga_2O_{(s)} + 2O_{(g)} \rightarrow Ga_2O_{3(s)},\ \Delta G_f = -245 \text{ kcal/mol, and} \quad (1)$$

$$Ga_2O_{(s)} + O_{2(g)} \rightarrow Ga_2O_{3(s)},\ \Delta G_f = -145 \text{ kcal/mol.} \quad (2)$$

Since ΔG_f is a large negative number in both cases, the reaction rates will be determined by the sticking probabilities of atomic and molecular oxygen, respectively. O_2 has a very low sticking probability on oxides since the O_2 bond is strong. The sticking probability is likely to be especially low on a surface that is, for example, already 99% Ga_2O_3 and 1% Ga_2O. The reaction with atomic oxygen is thus favored based on a lower activation barrier and the oxide formation is kinetically and not thermodynamically controlled.

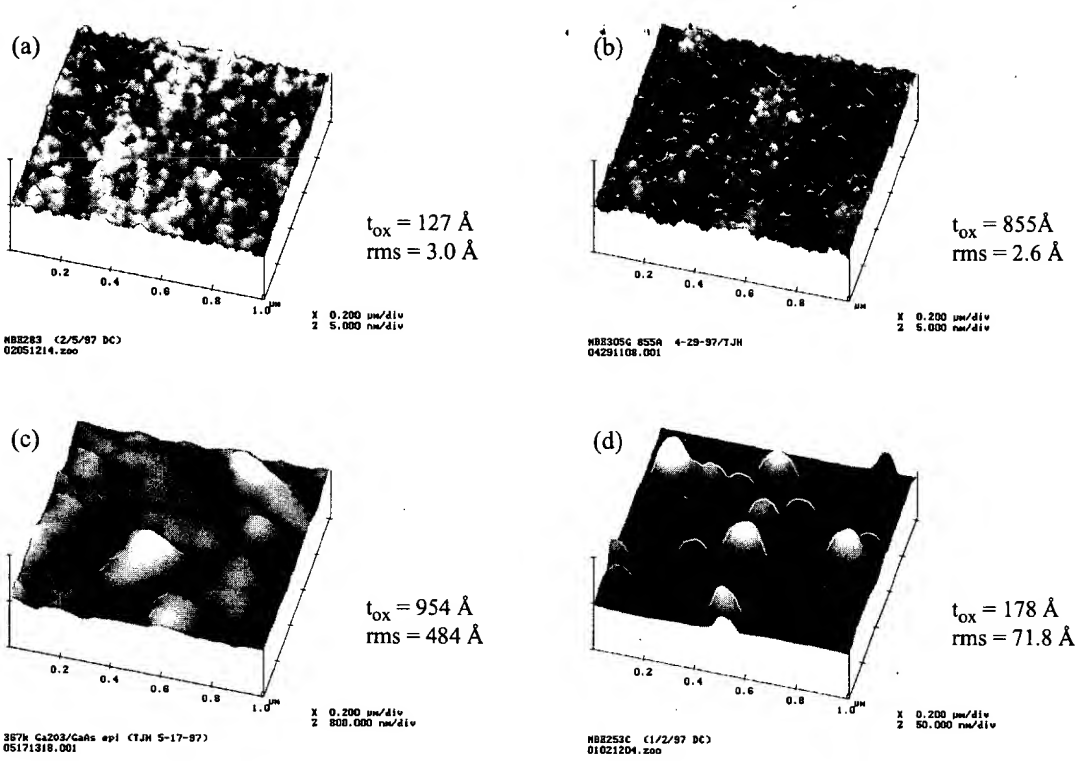

Fig. 10 AFM images of a Ga_2O_3 oxide films (a) deposited at T_s = 450 °C using molecular oxygen (4-6x10^{-6} Torr); (b) deposited at T_s = 440 °C using rf plasma activated oxygen (10^{-5} Torr). Plasma power = 400 W; (c) deposited at T_s = 350 °C using rf plasma activated oxygen (10^{-5} Torr). Plasma power = 450 W; (d) deposited at T_s = 500 °C using molecular oxygen (2-3x10^{-5} Torr). The starting GaAs surface had a sharp (4x6) reconstruction.

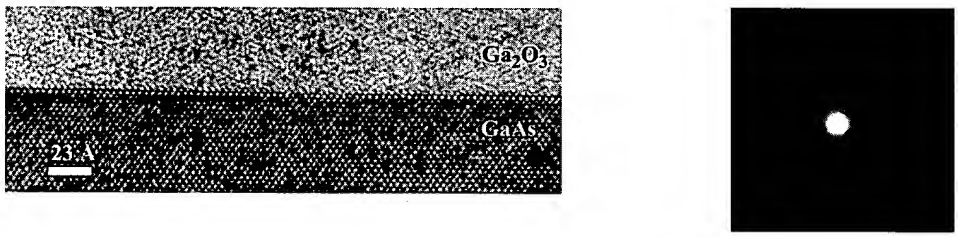

Fig. 11 Cross sectional high resolution TEM of a Ga_2O_3-GaAs interface (left) and corresponding electron diffraction pattern of the oxide film (right). This oxide film was deposited at T_s = 420 °C.

The surface morphology of Ga_2O_3 oxide films has been studied in detail by AFM. A typical root-mean-square (rms) roughness of the order of 1.0-1.5 monolayer (2.5-3.5 Å) is observed for Ga_2O_3 oxide films deposited at substrate temperatures T_s = 440-450 °C. A roughness as small as 1.6 Å is measured on some films. Fig. 10 shows that monolayer roughness is obtained when using either molecular O_2 (a) or rf plasma activated oxygen (b). The films are deposited at T_s = 450 °C and 440 °C and their thicknesses are 127 Å and 855 Å, respectively, as measured by ellipsometry at 632.8 nm. In general, no correlation between film thickness and rms roughness is observed. However, the surface roughness rapidly increases for a substrate temperature beyond the range of about 420-450 °C. This is illustrated in Fig. 10 for T_s = 350 °C (c) and for T_s = 500 °C (d). The onset and extent of surface roughness also depends on the deposition rate and the supply of rf plasma activated oxygen.

It is worthwhile to note that oxide surface morphology and interface quality are strongly correlated. Fig. 11 is a high resolution cross-sectional TEM image of the Ga_2O_3-GaAs interface

including a transmission electron diffraction image of the oxide film. It is clearly evident that the interface is atomically flat and the oxide film completely amorphous.This oxide film was deposited at T_s = 420 °C. However, beyond the optimal substrate temperature range of T_s = 420-450 °C, crystalline oxide growth is observed and the oxide crystallinity extends to the substrate as evident from high resolution cross sectional TEM images (not shown). This crystalline oxide growth is accompanied by high surface roughness and a pinned Fermi level at the Ga_2O_3-GaAs interface.

4 FILM AND INTERFACE PROPERTIES

4.1 Structural Film Properties

Some film properties related to oxide morphology and microstructure have been presented in Section 3 using techniques such as TEM, AFM, and electron diffraction. In this section, further oxide film properties are discussed. Ga_2O_3 films are characterized by Rutherford backscattering (RBS), Auger electron spectroscopy (AES), high resolution x-ray reflectivity, secondary ion mass spectroscopy (SIMS), and ellipsometry. RBS, AES, SIMS, x-ray reflectivity, and ellipsometry provide atomic composition and volume density, atomic composition and depth uniformity, trace impurities, volume density, and film thickness, respectively.

Fig. 12 shows the AES depth profile of a 855 Å thick Ga_2O_3 film deposited at a substrate temperature T_s = 420 °C using polycrystalline Ga_2O_3 as evaporation source and providing additional oxygen flux from a plasma source (wafer MBE305G). The depth uniformity of the oxide film is apparent. The acquired oxygen-to-gallium ratio is compared against a polycrystalline Ga_2O_3 standard. Within the limits of Auger spectroscopy, the oxide films are found to be stoichiometric (60 at.% oxygen, 40 at.% gallium) irrespective of substrate temperature T_s, evaporation source, and supply of additional oxygen. This is further discussed in the next paragraph in the context of RBS measurements. Note that e-beam deposited gallium oxide films were only stoichiometric when the substrate was held at room temperature during deposition and additional oxygen was supplied [17]. The standard deviation of oxide thickness is typically less than 1% over a two inch wafer as determined by ellipsometry (not shown).

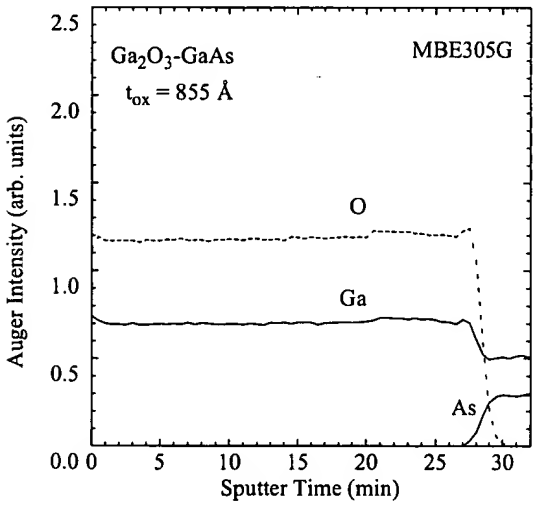

Fig. 12 AES depth profile of a 855 Å thick Ga_2O_3 film using polycrystalline Ga_2O_3 as evaporation source and oxygen plasma at T_s = 420 °C.

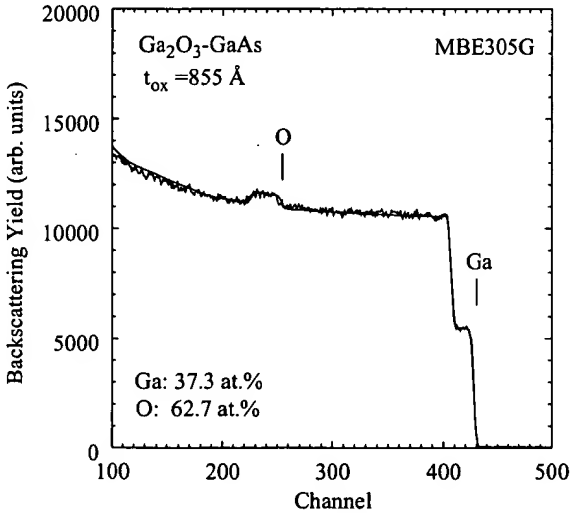

Fig. 13 RBS spectrum for a 855 Å thick Ga_2O_3 film using polycrystalline Ga_2O_3 as evaporation source at T_s = 420 °C and oxygen plasma.

Fig. 13 shows a RBS spectrum obtained from the oxide film of the same wafer MBE305G. For this film, RBS provides a composition of 62.7 at.% O and 37.3 at% Ga. Thus, within the limits of RBS, the oxide stoichiometry is confirmed. This is further supported by RBS analysis of 19 oxide films of different thickness and deposited under different conditions: the average oxygen content as determined by RBS is 59.6±1.7 at.%. RBS is further used to measure the volume density ρ of Ga_2O_3 films. Fig. 14 shows the volume density as a function of deposition rate. Note that data from both RBS and x-ray reflectivity measurements are shown and that the density appears to be independent of deposition rate: the average density is 5.50 ± 0.20 g/cm^3 as determined from a total of 22 measurement points. This volume density is significantly higher than the volume density of 3.9 - 4.8 g/cm^3 of e-beam deposited gallium oxide films [17]. To our knowledge, no other reports on the volume density of amorphous Ga_2O_3 exist; however, the bulk density of crystalline Ga_2O_3 is well known: 6.4 and 5.9 g/cm^3 for α– and β-Ga_2O_3, respectively [44].

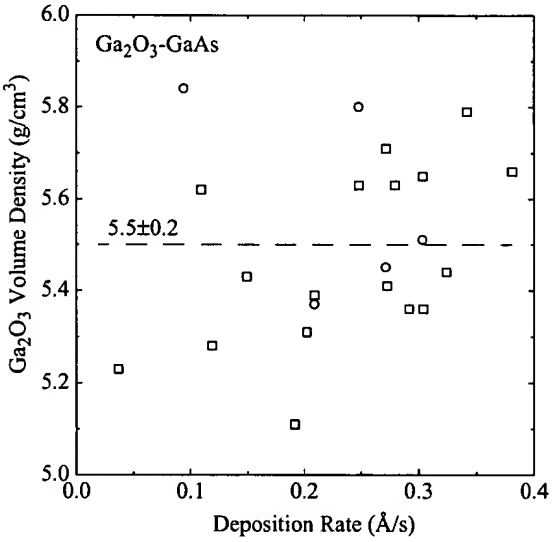

Fig. 14 Ga_2O_3 volume density measured by RBS (squares) and x-ray reflectivity (circles) as a function of deposition rate.

Table 1 shows trace impurities of Ga_2O_3 films deposited on GaAs. The Si, Mg, Al, As, and C concentrations are measured by Quadropole SIMS (PHI Model 6600). The Mo, La, Ta, and W concentrations are acquired by magnetic sector SIMS (Cameca IMS-4f) with the respective detection limits of 1x10^{16}, 1x10^{16}, 5x10^{16}, and 1x10^{16}. Since Ga_2O_3 SIMS standards were unavailable at the time, SiO_2 SIMS standards are used. Hence, the absolute concentration may be in error by a factor of 2-4, however, the comparisons between

Table 1 Trace Impurities in Ga_2O_3 films on GaAs. The pressure in the leftmost column reads as follows: Pressure from Ga_2O_3 source only (10^{-6} Torr)/Pressure with additional oxygen from plasma source (10^{-6} Torr).

Sample #	Trace Impurity concentration (cm^{-3})								
	Si	Mg	Al	As	C	La	W	Ta	Mo
98-23, t_{ox} = 188 Å pressure = 1.6	6x10^{18}	1x10^{18}	4x10^{16}	1x10^{19}	6x10^{19}	Oxide film not thick enough for reliable quantification			
98-25, t_{ox} = 640 Å pressure = 1.6/5.4	1x10^{18}	2x10^{17}	1x10^{16}	<1x10^{18}	6x10^{18}	6x10^{16}	< 1x10^{16}	7x10^{17}	6x10^{16}
98-27, t_{ox} = 1140 Å, pressure = 1.1/27	7x10^{17}	1x10^{17}	1x10^{16}	<5x10^{17}	6x10^{18}	6x10^{16}	< 1x10^{16}	6x10^{17}	6x10^{16}
98-34, t_{ox} = 590 Å, pressure= 0.2/21	1.5x10^{18}	1.5x10^{17}	1.5x10^{16}	<3x10^{18}	3x10^{19}	3x10^{16}	not measured		
98-63, t_{ox} = 558 Å, pressure = 1.3/13 + annealing	3x10^{18}	1x10^{17}	8x10^{15}	1x10^{18}	2x10^{19}	4x10^{16}	not measured		

samples are accurate to within 5%. The impurity concentrations are typically lower when the film deposition is assisted by an oxygen plasma source. When O plasma is on, the Si, Mg, and Al levels are typically below 10 ppm. Carbon may originate from the chamber background. The As concentration is typically higher for thinner films and is attributed to As release during As cap desorption. The La, W, and Mo impurity concentrations are very low.

4.2 Optical Film Properties

The oxide thickness t_{ox}, refractive index n, and extinction coefficient k are determined by spectroscopic ellipsometry (SE) over the wavelength range λ from 180 - 800 nm. The optical bandgap of the amorphous Ga_2O_3 films is estimated from the dependence of the absorption coefficient on photon energy (Tauc plots).

Fig. 15 shows the refractive index of Ga_2O_3 films with different thickness at $\lambda = 632.8$ nm as determined by spectroscopic ellipsometry. The refractive index is 1.896 ± 0.010 and independent of film thickness which indicates an excellent depth uniformity. The refractive index is also not altered when deposition conditions such as substrate temperature T_s, evaporation source, and supply of additional oxygen are varied. Previously, a refractive index n of 1.916 (λ = 632.8 nm) was reported for e-beam deposited Ga_2O_3 [17] and n = 1.92 (no wavelength specified) was given in [44] for crystalline Ga_2O_3. Fig. 16 shows the estimated optical bandgap as a function of chamber pressure. When oxygen is supplied from the Ga_2O_3 source only, an optical bandgap in between 3.1 and 3.8 eV (circles) is measured. In this case, the chamber pressure is $\cong 10^{-6}$ Torr. The supply of additional oxygen raises the chamber pressure and increases the optical bandgap; in particular the use of the oxygen plasma source widens the optical bandgap to as high as 4.7 eV (diamonds and triangles). This is well within previously reported bandgap for crystalline Ga_2O_3; an optical bandgap of 4.52 and 4.79 eV was reported along the b and c axis of single crystal β-Ga_2O_3, respectively [45]. For comparison purposes, the bandgaps of single crystal β-Ga_2O_3 are also shown in Fig. 16.

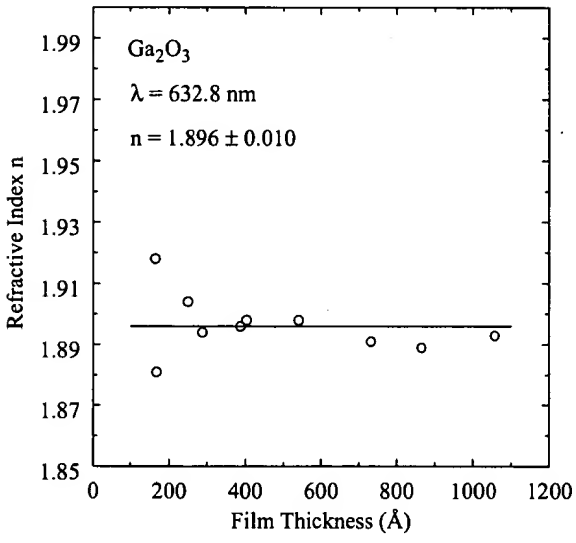

Fig. 15 Refractive index of various Ga_2O_3 films at 632.8 nm wavelength as determined by spectroscopic ellipsometry.

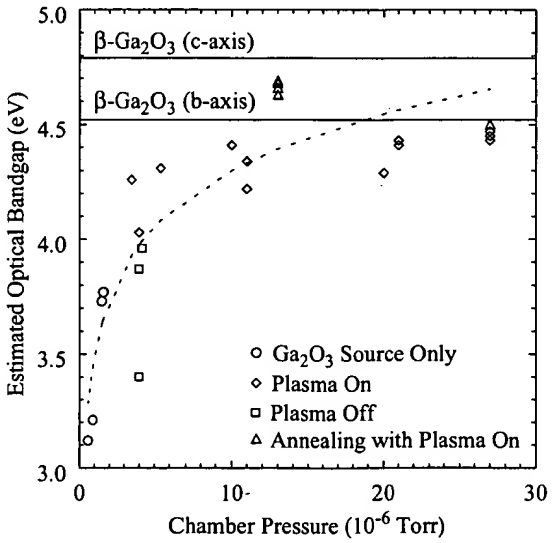

Fig. 16 Bandgap of amorphous (symbols) Ga_2O_3 as a function of chamber pressure during deposition. The dashed line is a guide to the eye.

4.3 Electrical Interface and Film Properties

Electrical film and interface properties are measured using current voltage (I-V), capacitance-voltage (C-V), and photoluminescence intensity (PLI) measurements. All measurements are done at room temperature.The photoluminescence intensity technique enables interface optimization without sample processing and, in combination with standard capacitance-voltage measurements, virtually eliminates common pitfalls in insulator-III-V semiconductor interface characterization. All data discussed in this section are obtained from the test structure shown in Fig. 9. The epitaxial layers of this test structure are optimized for PLI and C-V measurement and analysis. For C-V and I-V measurements, circular metal dots (Ti/Au) with diameters d of 50, 250, and 500 μm are deposited on top of the oxide and a blanket metal deposit (Ge/Ni/Au) is done on the substrate backside.

Fig. 17 shows typical I-V curves obtained from Ga_2O_3-GaAs structures. Large leakage currents are observed for low voltage for both negative and positive polarity. Here, the polarity is defined with respect to the metal dot deposited on top of the oxide. A Ga_2O_3 specific resistivity ρ of the order of 400 - 700 Ω cm is estimated from the slope of the I-V characteristics. At a first glance, these large currents may appear to be inconsistent with the observation of a stoichiometric oxide and an optical bandgap as high as 4.7 eV. However, strong electrical conduction only requires defect densities of the order of 10^{18} cm^{-3} within the oxide bandgap, levels which are far below the detection limit of structural analysis techniques such as RBS and optical techniques such as ellipsometry.

Extensive post-deposition annealing studies were performed to address the issue of high oxide conductivity. Different plasma source designs provided partial pressures of active oxygen of about 0.1 - 0.2 Torr (mostly O) and of about 5 Torr (O_3). Samples were treated in a range of substrate temperature from room temperature to 500 °C for periods of 30, 60, and 120 min. The maximum specific resistivity obtained is estimated to 10^4 Ω cm. Thus, electrical Ga_2O_3 bulk properties could only be marginally improved. The lack of response to active oxygen exposure suggests that the defects responsible for conduction are not related to oxygen vacancies or the defect nature of the amorphous network is complex and defects cannot be removed by exposure to active oxygen under the above discussed conditions.

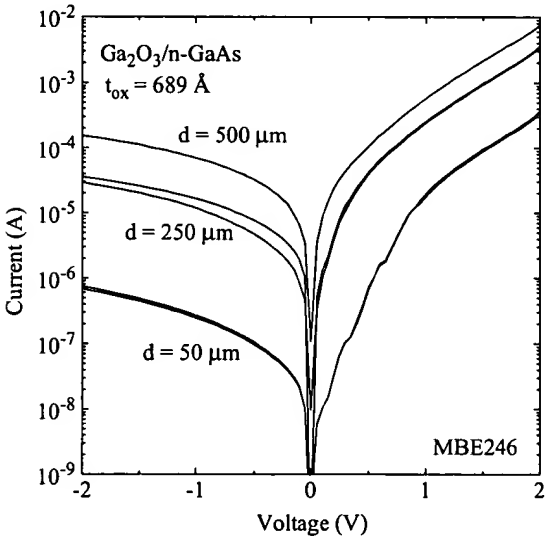

Fig. 17 Measured room temperature I-V curves of Ga_2O_3/n-GaAs test samples with different metal dot diameter d. The current scales approximately with area.

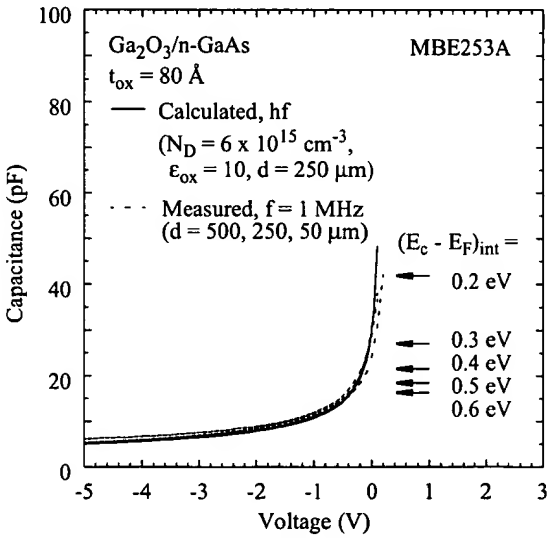

Fig. 18 1 MHz C-V measurements (dashed lines) and high frequency (hf) C-V simulation assuming $D_{it} = 0$ (solid line).

Fig. 18 shows a typical result of a 1 MHz C-V measurement (dashed lines). For comparison purposes, a high frequency (hf) capacitance-voltage simulation is shown assuming that the interface state density D_{it} equals zero (solid line). Note that quasistatic C-V curves cannot be acquired due to high leakage current. Dot sizes of 500, 250, and 50 μm diameter are measured. Measured data are normalized to the metal dot diameter of 250 μm used in the simulations. Hysteresis is not observed in the measurement and the calculated curves fit the measured data well. The horizontal lines included in Fig. 18 indicate the distance between the GaAs conduction band edge E_c and the Fermi energy level E_F at the Ga_2O_3-GaAs interface $(E_c\text{-}E_F)_{int}$. Note that C-V measurements fail towards accumulation for $E_F \geq E_c$ - 0.2 eV due to excessive leakage currents (positive bias). Further, steady-state deep depletion is observed under negative bias when E_F falls below the intrinsic energy level E_i (E_c - E_i = 0.67 eV for GaAs). Since C-V data do not contain information about interface states D_{it} in steady-state deep depletion [46], the measured C-V data may be applied to D_{it} analysis within the range of $E_i \leq E_F \leq E_c$ - 0.2 eV only. Considering standard techniques for D_{it} analysis such as the quasistatic- high frequency technique (qs/hf) [47] and the Terman method [48], the serious limitations of the acquired data become apparent: The qs/hf method is not applicable since quasistatic data are unavailable and the Terman method fails since the difference between measured and calculated hf C-V curves is below the detection limit of Terman's method. Hence, quantitative interface characterization has been mainly accomplished by a photoluminescence intensity technique as described in the following section.

The photoluminescence intensity technique has been introduced as a standard tool to monitor the interface and surface quality during device fabrication [23]. This technique is based on the radiative intensity I_{PL} of the spontaneous emission (photoluminescence, PL) of a direct-gap semiconductor [49] as a function of incident light density on the sample surface P_0 ($10^{-1} \leq P_0 \leq 10^4$ W/cm^2) wherein the measured steady-state I_{PL}-P_0 dependence is analyzed using an advanced self-consistent drift-diffusion model [46]. The efficacy of the PLI technique strongly depends on the range of excitation power, the laser spot size, and the design of the test structure. Some basics of the experimental and analysis techniques are discussed in the following; the reader is referred to Refs. [29] and [31] for further details.

Fig. 19 shows a block diagram including the essential components of the optical measurement system. Excitation is provided by a Spectra Physics argon ion laser with a nominal maximum power output of 5 watts emitting at λ_0 = 514.5 nm. A first Oriel motorized filter wheel system equipped with one set of Oriel absorptive neutral density filters with optical densities of 1, 2, 3, and 4, and a second Oriel motorized filter wheel system equipped with another set of Oriel absorptive neutral density filters with optical densities of 0.3, 0.5, and 0.8 provide a maximum combined attenuation of 6.9 x 10^4. A telescope comprising two lenses with a focal length of 120 and 80 mm, respectively, is used to adjust the focal plane of the incoming laser beam which enters through the microscope illumination port at the microscope's backside. The microscope is equipped with a customized stage comprising a Newport 406 dual axis translation stage having two DM-13 differential micrometers with 0.07 μm resolution, and a 488 Newport rotary platform with 10 μm vertical resolution. A full-width-at-half-maximum (FWHM) of 35 μm is measured for the laser spot on the sample surface. The collimated luminescence beam emitted from a test sample positioned on the stage of the microscope exits on the microscope's top where a 514.5 nm laser line filter is used to filter out laser light reflected by the test sample's surface. The collimated luminescence beam is attenuated as required using Oriel glass metallic neutral density filters with optical densities of 1, 2, 3 and 4 providing a maximum attenuation of 3.97 x 10^3. Subsequently, the PL signal is coupled into a spectrometer manufactured by Acton Research Corporation using various mirrors and a lens with a focal length of 100 mm. Finally, the PL spectra are acquired by a model ST-6 CCD camera.

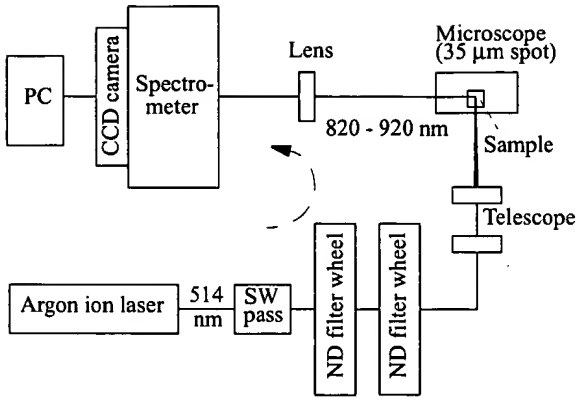

Fig. 19 Experimental setup for photoluminescence intensity measurements to characterize oxide/III-V semiconductor interfaces.

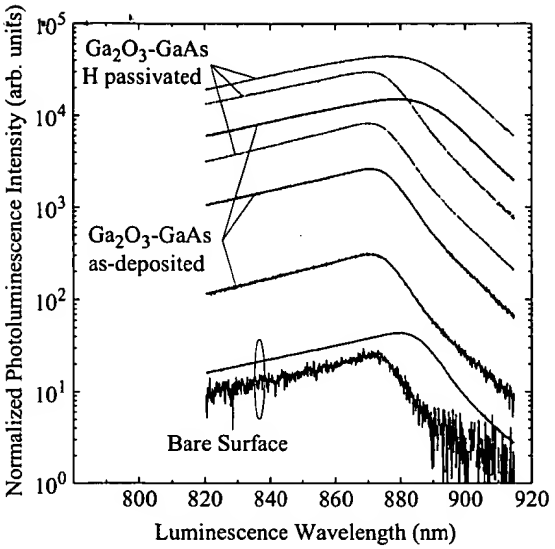

Fig. 20 Selected normalized measured PL spectra of Ga_2O_3-GaAs interfaces and bare GaAs substrate with the light density P_0' as a parameter (see text for further details).

Fig. 20 shows measured normalized PL spectra for selected test structures at various excitation densities $P_0' = T P_0$ where P_0' and T are the light density entering the semiconductor surface and the optical transmissivity of the sample surface at the excitation wavelength λ_0, respectively. Starting at the highest curve for each test structure, $P_0' = 6.6x10^3, 7.1x10^1, 5.6x10^{-1}$ W/cm^2 for hydrogen passivated Ga_2O_3-GaAs, $6.9x10^3, 7.4x10^1, 5.8x10^{-1}$ W/cm^2 for as-deposited Ga_2O_3-GaAs, and $6.5x10^3, 5.5x10^{-1}$ W/cm^2 for the bare surface, respectively. The spectra shown in Fig. 20 are normalized to the excitation density P_0' and the optical transmissivity of the sample surface at the PL wavelength of 870 nm is also taken into account. The Ga_2O_3 film thickness is 74 Å. We will discuss next some basics of our modeling approach.

A calculated energy-band diagram of the investigated structure (see Fig. 9) is depicted in Fig. 21 for an excitation density P_0' of 0.1 W/cm^2 ($\lambda_0 = 514.5$ nm) entering the semiconductor surface. The band diagram is calculated based on an extended self-consistent drift-diffusion model [46] including defect-mediated Shockley-Read-Hall recombination occurring at interfaces via a continuum of interface states D_{it} (r_{SRH}) [49] and due to trapping centers of density N_t located at discrete energy levels E_t [50] in the semiconductor bulk (R_{SRH}). Here, E_v, E_{Fn}, E_{Fp}, S_n, S_p, σ_n, σ_p, h, and ν are the valence band edge, the quasi Fermi level for electrons and holes, the interface recombination velocity for electrons and holes, the capture cross section for electrons and holes, Planck's constant, and the photon frequency of the incident light, respectively.

The test structure shown in Fig. 9 is optimized such that the PL signal I_{PL} is emitted primarily from a lightly doped n-type (donor concentration $N_D = 2 \times 10^{16}$ cm^{-3}) GaAs active layer (see Fig. 22). This is accomplished by inserting a highly doped GaAs buffer layer ($N_D = 2 \times 10^{18}$ cm^{-3}) between the GaAs substrate ($N_D \cong 2 \times 10^{18}$ cm^{-3}) and the lightly doped active layer. As demonstrated in Ref. [29] and [46], the only resulting unknown parameters which effectively determine I_{PL} in such a test structure are the state density D_{it} and the capture cross sections σ at the interface or surface to be investigated.

Fig. 23 shows measured (symbols) and calculated (lines) internal quantum efficiencies η as a function of excitation power density P_0' for as-deposited Ga_2O_3-GaAs structures (triangles), hydrogen plasma exposed Ga_2O_3-GaAs structures indicated by diamonds (further dis-

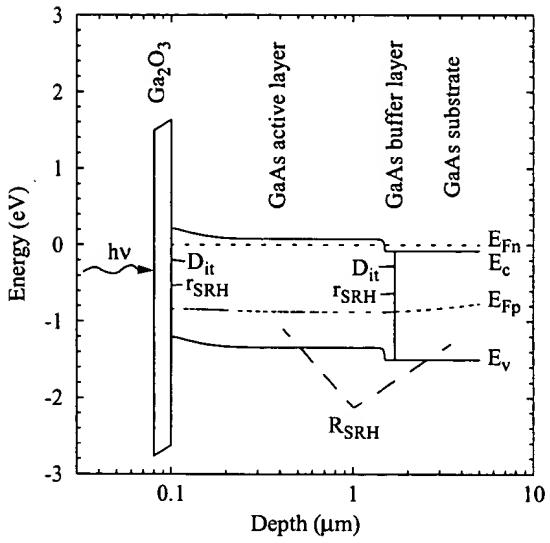

Fig. 21 Calculated energy-band diagram of the investigated Ga_2O_3-GaAs structure. The active layer (1.4 μm) and the buffer layer (0.2 μm) were grown on GaAs substrate by molecular beam epitaxy. The energy-band diagram is calculated using the following oxide-GaAs interface parameters: $D_{it} = 1.6 \times 10^{11}$ cm^{-2} eV^{-1}, $\sigma_n = \sigma_p = 2.2 \times 10^{-14}$ cm^2, and $S_n = S_p = 3.2 \times 10^4$ cm/s. The energy is shown relative to the bulk Fermi level in equilibrium.

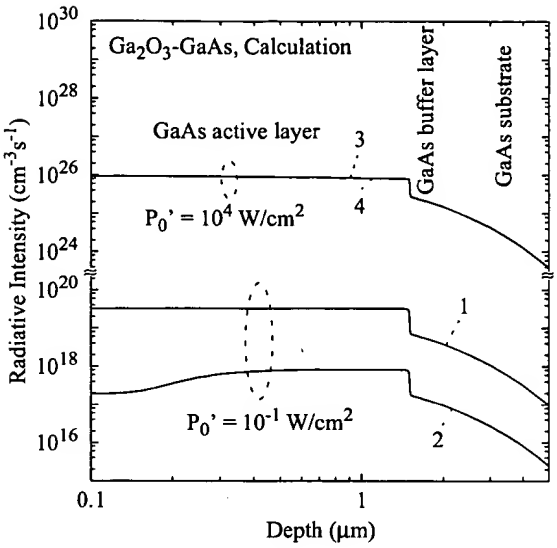

Fig. 22 Calculated depth profiles of the radiative GaAs emission (PL) of the investigated Ga_2O_3-GaAs structure. The following oxide-GaAs interface parameters are used: $S_n = S_p = 3.2 \times 10^4$ cm/s and $D_{it} = 0$ (curve 1 and 3) and $D_{it} = 1.6 \times 10^{11}$ cm^{-2} eV^{-1} (curve 2 and 4). 88.6%, 87.5%, 84.0%, and 83.9% of the total spontaneous emission originates from the active layer for curve 1, 2, 3,and 4, respectively.

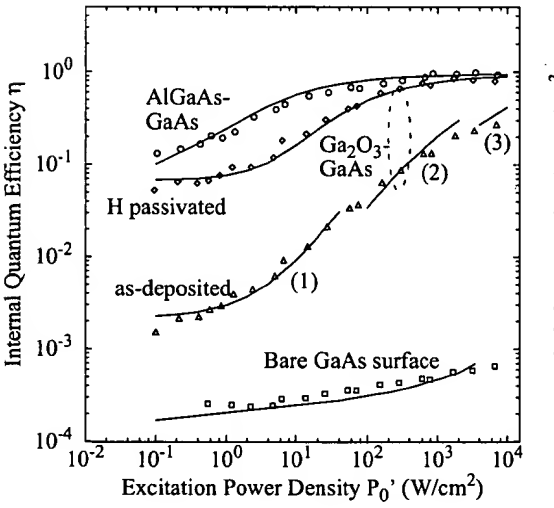

Fig. 23 Measured (symbols) and calculated (lines) internal quantum efficiencies η as a function of excitation power density P_0'. The excitation wavelength is 514.5 nm. $S_n = 2 \times 10^4$, 3.2×10^4, and 5×10^4 cm/s for curves labeled (1), (2), and (3), respectively.

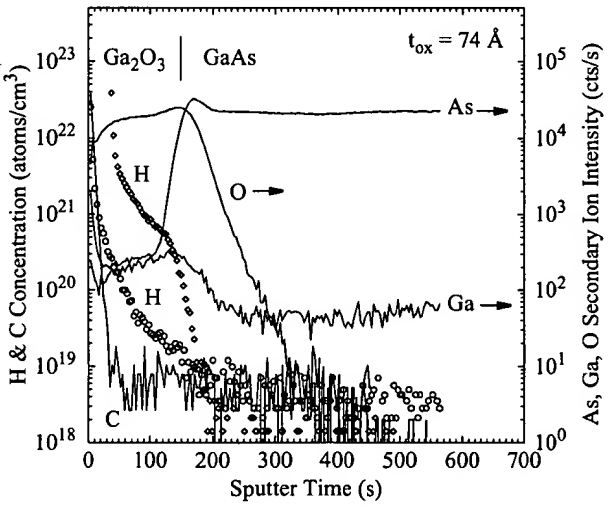

Fig. 24 Concentration (H, C) and secondary ion intensity (As, Ga, O) depth profiles of the Ga_2O_3-GaAs structure as measured by SIMS. The hydrogen concentration profiles are shown before (circles) and after (diamonds) hydrogen plasma exposure.

cussed below) and baseline samples (circles and squares). The experimental results have been obtained as follows: Measured PL intensities I_{PL} are attained by integrating the normalized GaAs PL spectra from 820 to 910 nm wavelength (Fig. 20) for each excitation power density P_0'; the thus acquired I_{PL}/I_0' curves are shifted along the vertical η axis to the position of the calculated curves obtained from integrating the depth profile of radiative intensity (Fig. 22) using one normalization factor for all measured curves. Here, $I_0' = P_0' / h\nu$ where ν is the photon frequency of the incident light. In order to unequivocally map the measured characteristics onto the calculated curves, a range for P_0' of five orders of magnitude including very high injection ($P_0' \geq 10^3$ W/cm^2), high injection (10^3 W/cm$^2 > P_0' \geq 10$ W/cm^2), and low injection ($P_0' < 10$ W/cm^2) is required, and both baseline structures with low D_{it} ($\eta \cong 1$, AlGaAs-GaAs interface) and very high D_{it} ($\eta \cong 0$, bare GaAs surface) must be provided. Before we summarize the interface properties, we discuss hydrogen plasma exposure of the as-deposited Ga_2O_3-GaAs interface structure in the following.

In striking analogy to the SiO_2-Si, system, hydrogen atoms are found to passivate defects at as-deposited Ga_2O_3-GaAs interfaces [30] as indicated by the significant improvement of quantum efficiency after hydrogen exposure (Fig. 23). Hydrogen exposure of as-deposited Ga_2O_3-GaAs structures with varying oxide thickness is conducted in a Tegal 6000 etching tool where the atomic hydrogen is provided by an RF plasma discharge device with a frequency of 13.56 MHz. The following parameter range is explored: RF power 5 - 500 W, pressure 2 - 75 mTorr, hydrogen flow 10 sccm, and exposure time 5 - 300 s. The efficiency of interface passivation is found to depend only slightly on plasma parameters; however, no interface passivation could be observed when the RF source was turned off. The substrate is not intentionally heated but we estimate that the sample surface temperature reaches up to about 150 °C during plasma treatment.

The quantum efficiency data shown in Fig. 23 are correlated to the presence or absence of hydrogen at the Ga_2O_3-GaAs interface as determined by SIMS. Fig. 24 shows the corresponding hydrogen concentration depth profiles of the above discussed Ga_2O_3-GaAs structure with a 74 Å thin Ga_2O_3 layer as-deposited (circles) and after hydrogen plasma exposure (diamonds) as measured by SIMS. Conversion of ion counts to concentrations was accomplished by using relative sensitivity factors derived from ion-implanted Ga_2O_3 standards which were analyzed along with our test samples. Whereas the interfacial hydrogen signal is at or below the detection limit of the instrumentation ($\cong 5\text{x}10^{18}$ cm^{-3}) for the as-deposited structure, a clear shoulder with

Table 2 Ga_2O_3-GaAs, AlGaAs-GaAs interface and GaAs surface properties.

Structure	Interface State Density D_{it} (cm^{-2} eV^{-1})	Capture Cross Section σ (cm^2)	Interface Recombination Velocity S (cm/s)	Interface Hydrogen Concentration (cm^{-3})
Ga_2O_3-GaAs H plasma	$\leq 3.5 \times 10^{10}$	$9.7\text{x}10^{-15}$	$4\text{x}10^3$	$> 10^{20}$
Ga_2O_3-GaAs as-deposited	10^{11} (midgap) $\geq 10^{12}$ (close to E_c, E_v)	$2.0\text{x}10^{-14}$	$2\text{x}10^4$ (low injection) $5\text{x}10^4$ (very high inj.)	below detection limit ($\cong 5\text{x}10^{18}$)
AlGaAs-GaAs	not determined		$1.2\text{x}10^3$	not applicable
GaAs Surface	$> 10^{13}$	5×10^{-14}	10^7	not applicable

an interfacial hydrogen concentration above 10^{20}·cm^{-3} is observed after hydrogen plasma exposure. The increase of hydrogen and carbon concentration towards the surface for both as-deposited and hydrogen plasma exposed samples is due to surface hydrocarbons. Table 2 summarizes Ga_2O_3-GaAs, AlGaAs-GaAs interface and GaAs surface properties.The electrical interface parameters in Table 2 comprise the parameter set used to obtain the best fit (lines) to the measured data (symbols) in Fig. 23; the interface hydrogen concentration is taken from the SIMS data shown in Fig. 24.

4.4 Thermal Stability

In this section, we investigate the correlation between structural and electrical properties at the Ga_2O_3-GaAs interface under thermal stress and we determine the mechanism of interface destruction which occurs above a critical temperature T_c. As outlined in Section 3, as-deposited Ga_2O_3 films are found to be amorphous forming an atomically abrupt interface of low interface state density D_{it} with GaAs. Rapid thermal annealing (RTA) above a critical temperature T_c = 720 °C induces Ga_2O_3 bulk crystallization, resulting in structural deformation of the Ga_2O_3-GaAs interface and complete destruction of its low D_{it} character for thicker oxide films ($t_{ox} \geq$ 127 Å). Further, preliminary data suggest that the critical temperature T_c may increase in the limit of very thin Ga_2O_3 films.

Prior to RTA, the Ga_2O_3-GaAs structures are capped by a silicon nitride layer using a standard chemical vapor deposition technique. Thermal annealing is done in a standard RTA tool by subjecting test samples to a target temperature in between 300 and 800 °C for 6 s in nitrogen gas. Subsequent to RTA, the silicon nitride film is removed using a dry etch process. Cross sectional transmission electron microscopy images, electron diffraction patterns, and PL intensity data are acquired and analyzed before and after RTA.

Fig. 25 shows high resolution cross sectional TEM micrographs of (a) a 700 °C and (b) a 780 °C rapid thermal annealed Ga_2O_3-GaAs test sample. The TEM micrograph of the as-deposited film is shown in Fig. 11. The oxide thickness for all three samples is 689 Å. The inter-

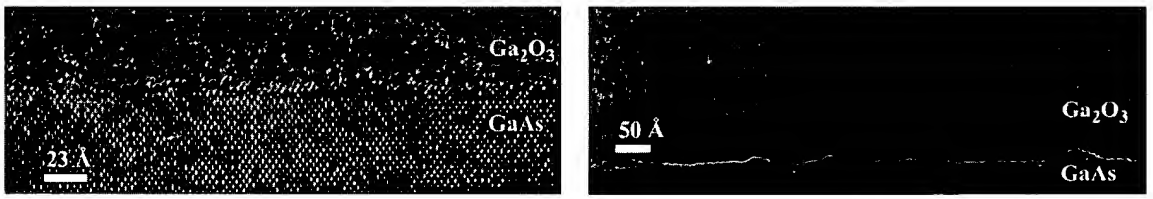

Fig. 25 High resolution cross sectional TEM micrographs of (a) a 700 °C and (b) a 780 °C rapid thermal annealed Ga_2O_3-GaAs test sample. Note the crystallinity in the oxide and the interface deformation in (b).

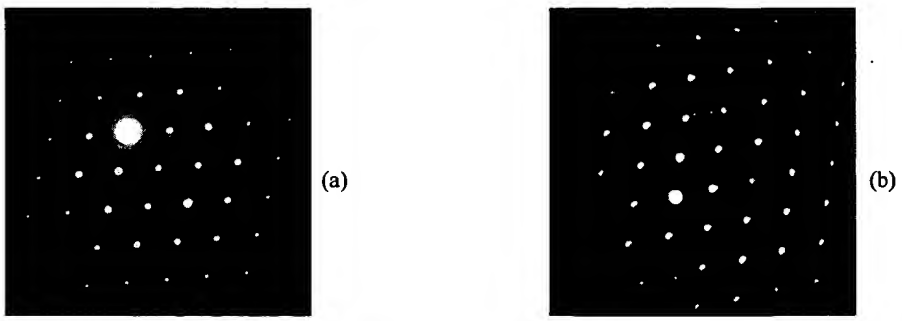

Fig. 26 Corresponding electron diffraction patterns after (a) RTA at 700 °C and (b) RTA at 780 °C. The diffraction patterns also include the substrate which is near the (110) zone. The additional spots in (b) are due to the polycrystalline oxide.

face is atomically abrupt for the as-deposited and 700 °C annealed test sample. However, crystallinity is observed in the oxide and structural deformation occurs at the Ga_2O_3-GaAs interface after RTA at 780 °C (Fig. 25b). Crystalline "hillock" type spots with a typical lateral size and spacing of 70 - 100 Å form in some areas at the Ga_2O_3-GaAs interface. The light and dark contrast in the oxide show oxide grains of different orientation. The dark grains are oriented close to a diffraction condition and the lighter grains are not close to a diffraction condition. Fig. 26 shows the corresponding electron diffraction patterns after (a) RTA at 700 °C and (b) RTA at 780 °C. Again, the electron diffraction pattern for the as-deposited Ga_2O_3 film is shown earlier (Fig. 11). The diffraction patterns in Fig. 26 also include the (110) single crystal diffraction pattern from the GaAs substrate. For the as-deposited and 700 °C annealed films, a diffuse halo surrounded by weak halos with rapidly decreasing intensity is indicative of an amorphous oxide microstructure. However, the broad amorphous ring disappears after 780 °C RTA and additional spots are observed originating from the polycrystalline oxide (Fig. 26b). Clearly, oxide crystallinity is thermally induced by annealing at 780 °C.

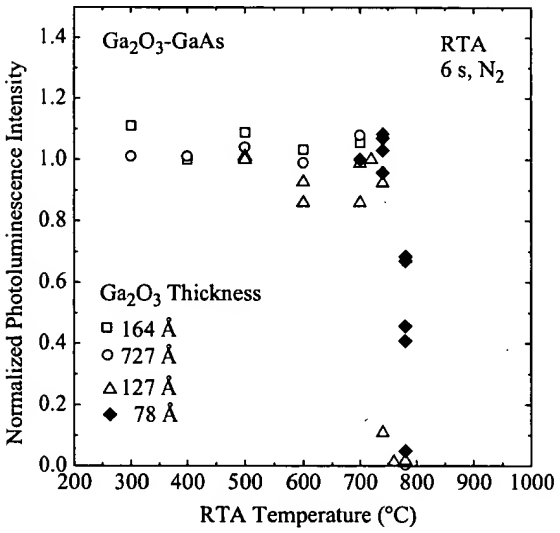

Fig. 27 Normalized PL intensity of Ga_2O_3-GaAs test samples as a function of RTA temperature from 300 to 780 °C. Note that the data point for t_{ox} = 164 Å and RTA temperature of 780 °C (open square) is hidden behind the other data points for t_{ox} = 727 Å and 127 Å and RTA temperature of 780 °C (open circle and open triangle).

Fig. 27 shows the normalized PL intensity of Ga_2O_3-GaAs test samples as a function of RTA temperature from 300 to 780 °C. Normalization is done in reference to the corresponding as-deposited samples. Data are shown for a large range of Ga_2O_3 film thickness from 78 - 727 Å. A normalized PL intensity around one indicates an electrically intact interface with low recombination velocity S of the order of 2 x 10^4 cm/s in low injection (compare to Table 2). In contrast, a normalized PL intensity approaching zero characterizes an electrically destroyed interface with an interface recombination velocity exceeding 10^7 cm/s. PL intensities measured for electrically destroyed interfaces are typically lower by a factor of 400 (see also Fig. 23). As shown in Fig. 27, low S interfaces are preserved for RTA temperatures ≤ 720 °C for all Ga_2O_3 thicknesses considered in this study. Therefore, we define here the temperature of 720 °C as the critical temperature T_c. Note that with the exception of the thinnest Ga_2O_3 film (78 Å), all Ga_2O_3-GaAs interfaces are electrically destroyed after RTA at 780 °C. This electrical interface destruction coincides with the appearance of crystallinity in the Ga_2O_3 bulk film and structural deformation of the Ga_2O_3-GaAs interface as evident in the cross sectional TEM micrograph of Fig. 25(b) and the diffraction pattern of Fig. 26(b). Further, the data shown in Fig. 27 for the thinnest oxide film with t_{ox} =78 Å (filled diamonds) indicate that some interface degradation but no complete interface destruction has yet occurred for the thinnest film investigated in this study. This provides preliminary evidence that the critical temperature T_c may increase with decreasing film thickness in the limit of very thin Ga_2O_3 films.

5 FIELD EFFECT TRANSISTOR APPLICATIONS

Self-aligned GaAs enhancement mode metal-oxide-semiconductor (MOS) heterostructure FETs (HFET) employing a Ga_2O_3 gate oxide have been successfully manufactured. We chose to use the term *enhancement-mode* rather than *inversion-* or *accumulation-type* since the latter terms become meaningless in the strict sense of inverting a surface from one conduction type to the other or accumulating majority carriers at the surface when semi-insulating substrates and undoped epitaxial layers are used. The p-channel devices with a gate length of 0.6 μm exhibit a maximum dc transconductance g_m of 51 mS/mm which is an improvement of more than two orders of magnitude over previously reported results. With the demonstration of a complete process flow and 66% of theoretical performance, GaAs MOS technology has moved into the realm of reality.

Fig. 28 shows the cross section of a self-aligned p-channel enhancement mode MOS-HFET. The epitaxial layer structure is grown by molecular beam epitaxy on 3" semi-insulating GaAs substrates and consists of a 0.2 μm undoped GaAs buffer layer, a 15 nm undoped $In_{0.2}Ga_{0.8}As$ channel layer, a 15 nm undoped $Al_{0.75}Ga_{0.25}As$ barrier layer, and a 2 monolayer thick GaAs cap layer. A silicon δ-doping with an areal density of $3.3x10^{11}$ cm^{-2} is positioned 3 nm below the channel. The epitaxial layer structure is derived from Motorola's standard CGaAs^{TM} technology [51]. Subsequent to completion of epitaxial layer growth, the wafer platen is transferred under ultra-high vacuum to a second oxide deposition chamber. Finally, the 9 nm thick Ga_2O_3 gate oxide layer is deposited by thermal evaporation of Ga_2O_3 from an effusion cell. Fig. 29 shows a high resolution TEM cross-sectional micrograph of the completed device layer structure including the electron diffraction pattern of the oxide film. As evident from Fig. 29, the interface between the single crystal semiconductor surface and the amorphous Ga_2O_3 layer is atomically abrupt.

Device fabrication is again built on Motorola's standard CGaAs^{TM} process [51]. A refractory gate metal (TiWN) is used with a 20 nm W diffusion barrier. The source/drain implants are implemented self-aligned to the gate and activated by RTA at 700 °C for 10 sec. The implant

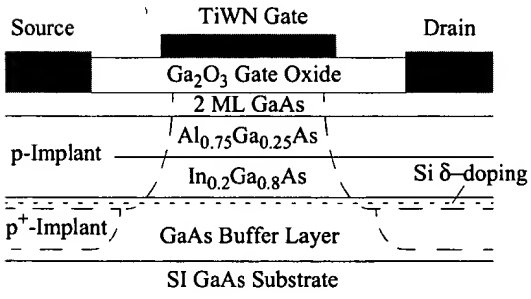

Fig. 28 Cross section of a p-channel self-aligned GaAs enhancement mode MOS heterostructure field effect transistors.

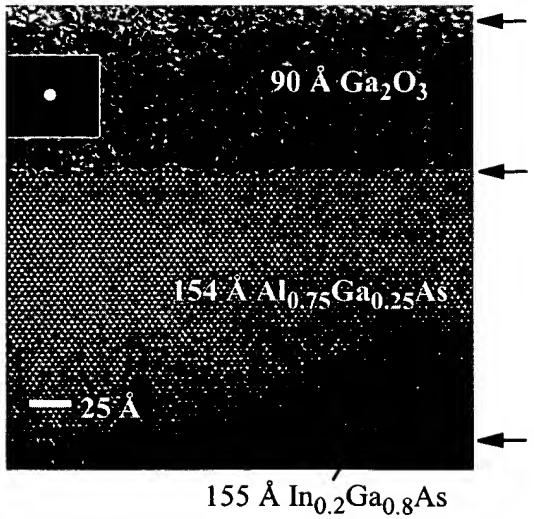

Fig. 29 High resolution TEM cross-sectional micrograph of the completed device layer structure. The inset shows the electron diffraction pattern of the oxide film.

sheet resistance ρ_s = 1234 Ω/sq. and the contact resistance R_c = 1.05 Ω mm were determined using a transmission line model (TLM). The device dimensions L_G (gate length), L_{GS} (gate-source-spacing), and L_{GD} (gate-drain-spacing) are 0.6 μm, 1.2 μm, and 1.2 μm, respectively.

Fig. 30 shows the measured dc output characteristics of the fabricated 0.6 μm GaAs p-channel MOS-HFET. The transistor characteristics have been measured using a HP4145 semiconductor parameter analyzer; repeated curve scanning has always exactly reproduced the previously measured data. Simulated data (not shown) have been obtained using the two-dimensional simulator PISCES [52] under the assumption of D_{it} = 0. The parameters of the steady-state field velocity relationship have been calibrated based on Motorola's established CGaAs^{TM} technology [53]. The measured and simulated maximum dc transconductance g_m and threshold voltage V_{th} are 51 and 77 mS/mm, and -0.93 V and - 0.76 V, respectively. Although reduced g_m and shifted V_{th} indicate that interface states still affect the devices to a certain extent, the demonstrated performance of 66% of theoretical dc transconductance is a clear breakthrough. The device uniformity across a 3" wafer is g_m = 46.7 ± 3.9 mS/mm and V_{th} = - 0.93 ± 0.1 V.

Fig. 31 shows a comparison of published dc transconductance data of enhancement mode GaAs MOSFETs. The comparison to previously reported data will be restricted to enhancement mode FETs which are defined by a threshold voltage $V_{th} > 0$ (n-channel) and $V_{th} < 0$ (p-channel) for the following reasons: (1) enhancement mode is technologically the most important device type and (2), the operation of depletion mode devices does not necessarily require Fermi level unpinning and thus, is not a conclusive indicator of interface quality [46]. For p-channel devices, the highest dc g_m previously reported was 0.3 mS/mm. The dc g_m of our MOS-HFETs is higher by a factor of 170. All previously reported dc g_m data for both n- and p-channel GaAs enhancement mode MOSFETs were at least two orders of magnitude lower than those of competing GaAs technologies such as PHEMT and CGaAs^{TM}. A further comparison of previously published data for GaAs n-channel enhancement mode MOSFETs reveals that essentially no progress had been made since 1978 when a dc g_m of 3.3 mS/mm was reported for a 2 μm GaAs MOSFET.

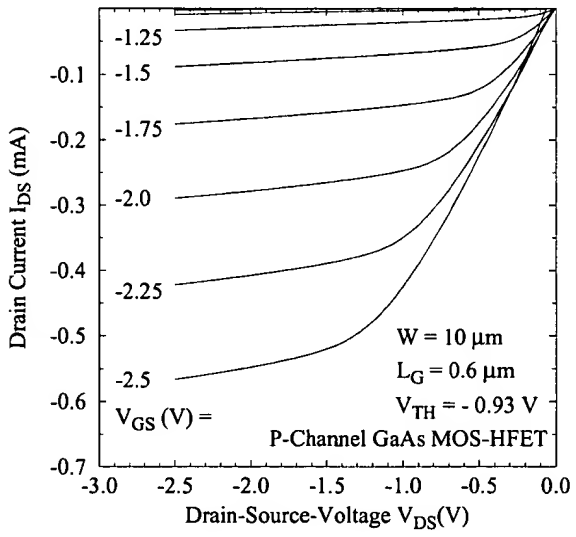

Fig. 30 Measured dc output characteristics of a 0.6 μm GaAs p-channel MOS-HFET.

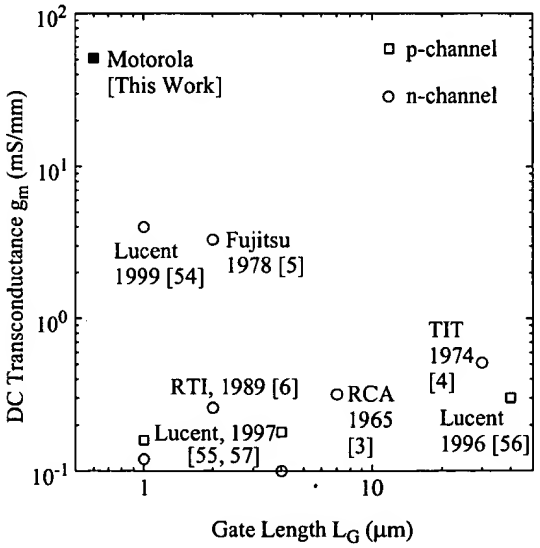

Fig. 31 Comparison of dc transconductance data of p-channel (squares) and n-channel (circles) enhancement mode GaAs MOSFETs.

ACKNOWLEDGMENT

We would like to acknowledge the contributions of all engineers and technicians of Motorola's Physical Science Research Laboratories (PSRL) who contributed to the success of this project. We would like to thank Evans East (T. Büyüklimanli), Charles Evans & Associates, J.A. Woolam Co., Advanced Materials Engineering Research, Inc. (H. Kawayoshi), and Bede Scientific (K. Matney) for SIMS, RBS, SE, TEM, and x-ray reflectivity analysis, respectively. We would like to thank Effusion Science, Inc. and SVT Associates for their contributions towards the development of a thermal evaporation technique for Ga_2O_3 and the supplier of the polycrystalline Ga_2O_3 for many valuable discussions. We also would like to thank N. Medendorp for his contributions to the success of this project. Finally, we would like to thank K. Johnson and P. Maniar for their encouragement and support.

References

[1] Croydon, W.F. and Parker, E.H.C. 1981, *Dielectric Films on Gallium Arsenide*, Gordon and Breach Scientific Publishers, New York.

[2] Wilmsen, C.W. 1985, *Physics and Chemistry of III-V Compound Semiconductor Interfaces*, Plenum Press, New York.

[3] Becke, H., Hall, R., and White, J. 1965, *Solid-State Electron.*, **8**, 813-823.

[4] Ito, T. and Sakai, Y. 1974, *Solid-State Electron.*, **17**, 751-759.

[5] Mimura, T., Odani, K., Yokoyama, N., Nakayama, Y., and Fukuta, M. 1978, *IEEE Trans. Electron Devices*, **25**, 573-579.

[6] Fountain, G.G., Rudder, R.A., Hattangady, S.V., Markunas, R.J., and Hutchby, J.A. 1989, *IEDM Tech. Dig.*, 887-889.

[7] Colquhoun, A., Kohn, E., and Hartnagel, H.L. 1978, *IEEE Trans. Electron Devices*, **25**, 375-376.

[8] Mimura, T., Odani, K., Yokoyama, N., and Fukuta, M. 1978, *Electron. Lett.*, **14**, 500-502.

[9] Kamimura, K. and Sakai, Y. 1979, *Thin Solid Films*, **56**, 215-223.

[10] Bayraktaroglu, B., Kohn, E., and Hartnagel, H.L. 1976, *Electron. Lett.*, **12**, 53-54.

[11] Spicer, W.E., Lindau, I., Skeath, P., Su, C.Y., and Chye, P. 1980, *J. Vac. Sci. Technol.*, **17**, 1019-1027.

[12] Pianetta, P., Lindau, I., Garner, C.M., and Spicer, W.E. 1979, *Surf. Sci.*, **88**, 439-460.

[13] Callegari, A., Hoh, P.D., Buchanan, D.A., and Lacey, D. 1989, *Appl. Phys. Lett.*, **54**, 332-334.

[14] Hoeneisen, B., Mead, C.A., and Nicolet, M.-A. 1971, *Solid-State Electron.*, **14**, 1057-1059.

[15] Fleischer, M., Hanrieder, W., and Meixner, H. 1990, *Thin Solid Films*, **190**, 93-102.

[16] Passlack, M., Hunt, N.E.J., Schubert, E.F., Zydzik, G.J., Hong, M., Mannaerts, J.P., Opila, R.L., and Fischer, R.J. 1994, *Appl. Phys. Lett.*, **64**, 2715-2717.

[17] Passlack, M., Schubert, E.F., Hobson, W.S., Hong, M., Moriya, N., Chu, S.N.G., Konstadinidis, K., Mannaerts, J.P., Schnoes, M.L., and Zydzik, G.J. 1995, *J. Appl. Phys.*, **77**, 686-693.

[18] Passlack, M., Hong, M., and Mannaerts, J.P. 1996, *Appl. Phys. Lett.*, **68**, 1099-1101.

[19] Passlack, M., Hong, M., Schubert, E.F., Kwo, J.R., Mannaerts, J.P., Chu, S.N.G., Moriya, N., and Thiel, F.A. 1995, *Appl. Phys. Lett.*, **66**, 625-627.

[20] Passlack, M., Hong, M., Mannaerts, J.P., Kwo, J.R., and Tu, L.W. 1996, *Appl. Phys. Lett.*, **68**, 3605-3607.

[21] Passlack, M., Hong, M., Mannaerts, J.P., Opila, R.L., and Ren, F. 1996, *Appl. Phys. Lett.*, **69**, 302-304.

[22] Hong, M., Passlack, M., Mannaerts, J.P., Kwo, J., Chu, S.N.G., Moriya, N., Hou, S.Y., and Fratello, V.J. 1996, *J.Vac.Sci.Technol.*, **B14**, 2297-2300.

[23] Passlack, M., Hong, M., Mannaerts, J.P., Opila, R.L., Chu, S.N.G., Moriya, N., Ren, F., and Kwo, J.R. 1997, *IEEE Trans. Electr. Dev.*, **44**, 214-225.

[24] Passlack, M., Bethea, C.G., Hobson, W.S., Lopata, J., Schubert, E.F., Zydzik, G.J., Nichols, D.T., de Jong, J.F., Chakrabarti, U.K., and Dutta, N.K. 1995, *J. Selec. Topics Quantum Electron.* **1**, 110-116.

[25] Dutta, N.K., Hobson, W.S., Zydzik, G.J., de Jong, J.F., Parayanthal, P., Passlack, M., and Chakrabarti, U.K. 1997, *Electron. Lett.*, **33**, 213-214.

[26] Yu, Z., Droopad, R., Overgaard, C.D., Abrokwah, J. K., and Passlack, M., submitted to *Appl. Phys. Lett.*

[27] Yi, S.-I., Hale, M., Sexton, J., Kummel, A.C., and Passlack, M., in preparation.

[28] Passlack, M., Abrokwah, J.K., Yu, Z., Droopad, R., Overgaard, C.D., and Kawayoshi, H., submitted to *Appl. Phys. Lett.*

[29] Passlack, M., Yu, Z., Droopad, R., Bowers, B., Overgaard, C.D., Abrokwah, J.K., and Kummel, A.C. 1999,

J. Vac. Sci. Technol., **B17**, 49-52.
[30] Passlack, M., Clemens, S.B., Yu, Z., Droopad, R., Overgaard, C.D., Abrokwah, J.K., and Büyüklimanli, T., submitted to *Appl. Phys. Lett.*
[31] Passlack, M., Legge, R.N., Convey, D., Yu, Z., and Abrokwah, J.K. 1998, *IEEE Trans. Instrumentation and Measurement*, **47**, 1362-1366.
[32] Passlack, M., Abrokwah, J.K., Droopad, R., Yu, Z., Overgaard, C.D., Yi, S.-I., Hale, M., Sexton, J., and Kummel, A.C. 2002, *IEEE Electr. Dev. Lett.*, **23**, 508-510.
[33] Schmidt, W.G. and Bechstedt, F. 1996, *Phys. Rev. B*, **54**, 16742.
[34] Moll, N., Kley, A., Pehlke, E., and Scheffler, M. 1996, *Phys. Rev. B*, **54**, 8844.
[35] Burns, R.P. 1965, *J. Chem. Phys.*, **44**, 3307.
[36] Carruthers, J.R., Kokta, M., Barns, R.L., and Grasso, M. 1973, *J. Cryst. Growth*, **19**, 204.
[37] Piekarczyk, W. and Pahaczkowska, A. 1979, *J. Crst. Growth*, **46**, 483.
[38] Kruse, P., McLean, J., and Kummel, A. 2000, *J. Chem. Phys.*, **113**, 9225.
[39] Tersoff, J. and Hamman, D.R. 1985, *Phys. Rev. B*, **31**, 805.
[40] Kresse, G. and Furthmuller, J. 1996, *Phys. Rev. B*, **54**, 11169.
[41] Kresse, G. and Hafner, J. 1993, *Phys. Rev. B*, **47**, RC558.
[42] Wassermeier, M., Bressler-Hill, V., Maboudian, R., Pond, K., Wang, X.S., Weinberg, W.H., and Petroff, P.M. 1992, *Surf. Sci.*, **178**, L147.
[43] Bressler-Hill, V., Wassermeier, M., Pond, K., Maboudian, R., Briggs, G.A.D., Petroff, P.M., and Weinberg, W.H.1992, *J. Vac. Sci. Technol. B*, **10**, 1881.
[44] *CRC Handbook of Chemistry and Physics 70th Edition*, 1989-1990, CRC Press, Boca Raton, p B92.
[45] Ueda, N., Hosono, H., Waseda, R., and Kawazoe H. 1997, *Appl. Phys. Lett.*, **71**, 933-935.
[46] Passlack, M., Hong, M., Schubert, E.F., Zydzik, G.J., Mannaerts, J.P., Hobson, W.S., and Harris, T.D. 1997, *J. Appl. Phys.*, **81**, 7647-7661.
[47] Nicollian, E.H. and Brews, J.R. 1982, *MOS Physics and Technology*, John Wiley and Sons, New York.
[48] Terman, L.M. 1962, *Solid-State Electron.*, **5**, 285.
[49] For an introduction to recombination processes see, e.g., Ahrenkiel, R.K. and Lundstrom, M.S. 1993, *Minority Carriers in III-V Semiconductors: Physics and Applications*, Academic, Boston MA.
[50] See, for example, Grove, A.S. 1967, *Physics and Technology of Semiconductor Devices*, John Wiley and Sons, New York.
[51] Abrokwah, J.K., Huang, J.H., Ooms, W., Shurboff, C., Hallmark, J.A., Lucero, R., Gilbert, J., Bernhardt, B., and Hansell, G. 1993, *Proc. IEEE GaAs IC Symp.*, 127.
[52] G-PISCES-IIB Manual, 1998, Gateway Modeling Inc.
[53] Abrokwah J.K., Luceron R., Hallmark J.A., and Bernhardt B. 1997, *IEEE Trans. Electr. Dev.*, **44**, 1040-1045.
[54] Wang, Y.C., Hong, M., Kuo, J.M., Mannaerts, J.P., Kwo, J., Tsai, H.S., Krajewski, J.J., Weiner, J.S., Chen, Y.K., and Cho, A.Y. 1999, *Proc. Mat. Res. Soc. Symp.*, **573**, 219-225.
[55] Ren, F., Hong, M., Hobson, W.S., Kuo, J.M., Lothian, J.R., Mannaerts, J.P., Kwo, J., Chu, S.N.G., Chen, Y.K., and Cho, A. Y. 1997, *Solid-State Electron.*, **41**, 1751-1753.
[56] Ren, F., Hong, M.W., Hobson, W.S., Kuo, J.M., Lothian, J.R., Mannaerts, J.P., Kwo, J., Chen, Y.K., and Cho, A.Y. 1996, *IEDM Tech. Dig.*, 943-945.
[57] Ren, F., Hong, M., Kuo, J.M., Hobson, W.S., Lothian, J.R., Tsai, H.S., Lin, J., Mannaerts, J.P., Kwo, J., Chu, S.N.G., Chen, Y.K., and Cho, A.Y. 1997, *Proc. IEEE GaAs IC Symp.*, 18-21.

APPLIED PHYSICS REVIEW

Band parameters for III–V compound semiconductors and their alloys

I. Vurgaftman[a] and J. R. Meyer
Code 5613, Naval Research Laboratory, Washington, DC 20375

L. R. Ram-Mohan
Worcester Polytechnic Institute, Worcester, Massachusetts 01609

(Received 4 October 2000; accepted for publication 14 February 2001)

We present a comprehensive, up-to-date compilation of band parameters for the technologically important III–V zinc blende and wurtzite compound semiconductors: GaAs, GaSb, GaP, GaN, AlAs, AlSb, AlP, AlN, InAs, InSb, InP, and InN, along with their ternary and quaternary alloys. Based on a review of the existing literature, complete and consistent parameter sets are given for all materials. Emphasizing the quantities required for band structure calculations, we tabulate the direct and indirect energy gaps, spin-orbit, and crystal-field splittings, alloy bowing parameters, effective masses for electrons, heavy, light, and split-off holes, Luttinger parameters, interband momentum matrix elements, and deformation potentials, including temperature and alloy-composition dependences where available. Heterostructure band offsets are also given, on an absolute scale that allows any material to be aligned relative to any other. © *2001 American Institute of Physics.*
[DOI: 10.1063/1.1368156]

TABLE OF CONTENTS

 © 2001 American Institute of Physics

Downloaded 26 Aug 2001 to 128.42.12.177. Redistribution subject to AIP license or copyright, see http://ojps.aip.org/japo/japcr.jsp

I. INTRODUCTION

At present, III–V compound semiconductors provide the materials basis for a number of well-established commercial technologies, as well as new cutting-edge classes of electronic and optoelectronic devices. Just a few examples include high-electron-mobility and heterostructure bipolar transistors, diode lasers, light-emitting diodes, photodetectors, electro-optic modulators, and frequency-mixing components. The operating characteristics of these devices depend critically on the physical properties of the constituent materials, which are often combined in quantum heterostructures containing carriers confined to dimensions on the order of a nanometer. Because ternary and quaternary alloys may be included in addition to the binary compounds, and the materials may be layered in an almost endless variety of configurations, a seemingly limitless flexibility is now available to the quantum heterostructure device designer.

a)Author to whom correspondence should be addressed; electronic mail: vurgaftman@nrl.navy.mil

To fully exploit this flexibility, one clearly needs a reliable and up-to-date band parameter database for input to the electronic structure calculations and device simulations. However, after many years Volume 17 of the Landolt–Bornstein series[1] remains the most frequently quoted source of III–V band parameters. Although that work contains much of the required data for a broad range of materials, it is nearly 20 yr old, lacks detailed descriptions of many of the important III–V alloys, and contains no information at all on the crucial band offset alignments for heterostructures. A popular compilation by Casey and Panish[2] covers the band gaps for all III–V non-nitride binary materials and 12 ternary alloys, but the rapid progress in growth and characterization of many of those materials taking place since its publication in 1978 has decreased its usefulness. While a number of recent books and reviews on individual material systems are available,[3–10] they are not necessarily complete or mutually consistent. A useful recent compilation of band structure parameters by Levinshtein *et al.*[11] does not contain in-depth information on aluminum-containing elemental semiconductors, is often based on a limited number of original sources, and considers only six ternary and two quaternary alloys.

The objective of the present work is to fill the gap in the existing literature by providing a comprehensive and mutually consistent source of the latest band parameters for all of the common III–V zinc blende and wurtzite semiconductors (GaAs, AlAs, InAs, GaP, AlP, InP, GaSb, AlSb, InSb, GaN, AlN, and InN) and their ternary and quaternary alloys. The reviewed parameters are the most critical for band structure calculations, the most commonly measured and calculated, and often the most controversial. They include: (1) direct and indirect energy gaps and their temperature dependences; (2) spin-orbit splitting; (3) crystal-field splitting for nitrides; (4) electron effective mass; (5) Luttinger parameters and split-off hole mass; (6) interband matrix element E_P and the associated F parameter which accounts for remote-band effects in eight-band $\mathbf{k}\cdot\mathbf{P}$ theory; (7) conduction and valence band deformation potentials that account for strain effects in pseudomorphic thin layers; and (8) band offsets on an absolute scale which allows the band alignments between any combination of materials to be determined. All parameter sets are fully consistent with each other and are intended to reproduce the most reliable data from the literature. For completeness, lattice constants and elastic moduli for each material will also be listed in the tables, but in most cases will not receive separate discussion in the text because they are generally well known and noncontroversial.

As a complement to the band parameter compilations, which are the main focus of this work, we also provide an overview of band structure computations. The $\mathbf{k}\cdot\mathbf{P}$ method is outlined, followed by brief summaries of the tight-binding and pseudopotential approaches. The theoretical discussions provide a context for defining the various band parameters, and also illustrate their significance within each computational method. The tables provide all of the input parameters that are normally required for an eight-band $\mathbf{k}\cdot\mathbf{P}$ calculation. While we have not attempted to cover every parameter that may potentially be useful, most of those excluded (e.g., the κ and q parameters necessary for structures in a magnetic field

Downloaded 26 Aug 2001 to 128.42.12.177. Redistribution subject to AIP license or copyright, see http://ojps.aip.org/japo/japcr.jsp

and the inversion asymmetry parameter) are either poorly characterized or have well-known best values that have not changed much over time and are easily obtained from other sources such as Landolt–Bornstein.

To the extent possible, we have fully treated the 12 major III–V binaries and their alloys. Other nominal III–V materials that are not covered include BN and other boron-containing compounds (which are commonly considered to be insulators rather than semiconductors), as well as the narrow-gap InSbBi, InTlSb, InTlAs, and InTlP alloys, which up to now have not achieved technological importance. None of these materials has been integrated appreciably into any of the mainline systems, and in most cases a paucity of band structure information precludes the recommendation of definite parameter values. On the other hand, we attempt to provide a complete and up-to-date description of the nitride family of materials, including those with a wurtzite crystal lattice, in light of its increasing prominence and the numerous intense investigations currently being conducted.

It is naturally impossible for us to universally cite every article that has ever provided information or given values for the relevant band parameters. The reference list for such a review would number in the 10's of thousands, which would be impractical even for a book-length treatment. We have therefore judiciously selected those results that are most central to the purpose of the compilation. In some cases, wide agreement on the value of a given parameter already exists, and/or previous works have critically and comprehensively reviewed the available information. Under those circumstances, we have limited the discussion to a summary of the final conclusions, along with references to the earlier reviews where additional information may be found. In other cases, we discuss more recent data that have modified or altered the earlier findings. The most difficult topics are those for which there is substantial disagreement in the literature. In those instances, we summarize the divergent views, but nonetheless choose a particular result that is either judged to be the most reliable, or represents a composite combining a variety of experimental and/or theoretical findings. Although such selections are inevitably subjective, since they require an assessment of the relative merits and reliabilities, in each case we inform the reader of the basis for our judgment.

A guiding principle has been the maintenance of full internal consistency, both in terms of temperature dependences of the parameters for a given material and with regard to variations with alloy composition. For example, composition-dependent parameter values for the $Al_xGa_{1-x}As$ alloy employ the best information at those intermediate compositions for which data are available, but also invariably agree with the results for GaAs and AlAs when evaluated at $x=0$ and $x=1$. In a few cases, this has required the introduction of additional bowing parameters in contexts where they are not usually applied. We have also been as complete as possible in gathering all available information on the less common ternary and quaternary alloy systems.

The review is organized as follows. Discussions of the **k·P**, tight-binding, and pseudopotential band structure calculations are presented in Sec. II, along with some general considerations regarding the major band parameters. The main results for individual binary compounds, ternary alloys, and quaternary alloys are reviewed in Secs. III, IV, and V, respectively. A table summarizes the parameters recommended for each material, while the text provides justification for the choices. Section VI then reviews the band offsets that are needed to calculate energy bands in quantum heterostructure. Those results are presented in a format that references all offsets to the valence band maximum of InSb, which allows a determination of the relative band alignment for any possible combination of the materials covered in this work.

II. RELATION TO BAND STRUCTURE THEORY AND GENERAL CONSIDERATIONS

A number of excellent books and review articles have summarized the methods for calculating bulk[12–14] and heterostructure[15–20] band structures. Since the present review is intended to focus on band-parameter compilation rather than theoretical underpinnings, this survey is aimed primarily at providing a context for the definitions of the various parameters. The section is limited to a discussion of the bare essentials for treating heterostructures and a brief description of the practical approaches. A more detailed description of the theory will be presented elsewhere.

A. Multiband k·P method

The most economical description of the energy bands in semiconductors is the effective mass approximation, which is also known as the envelope function approximation or multiband **k·P** method. It uses a minimal set of parameters that are determined empirically from experiments. By means of a perturbative approach, it provides a continuation in the wave vector k of the energy bands in the vicinity of some special point in the Brillouin zone (BZ).

The electronic wave functions that satisfy the Schrödinger equation with a periodic lattice potential in a bulk crystal are given by Bloch's theorem:

$$\psi(r)=e^{ikr}u_{nk}(r). \tag{2.1}$$

The cell-periodic Bloch functions $u_{nk}(r)$ depend on the band index n and the envelope function wave vector k. The wave functions $\psi(r)$ form a complete set of states as do the wave functions based on Bloch functions at any other wave vector, including the wave vectors at special points in the BZ.[21] In treating the optical and electronic properties of direct gap semiconductors, it is natural to consider the zone-center Γ-point Bloch functions $u_{n0}(r)$ for our wave function expansions, and we drop the reference to the $k=0$ index for these functions.

For our purposes here, the general form of the wave functions may be considered to be a linear combination of a finite number of band wave functions of the form

$$\psi(r)=f_n(z)e^{ik_xx}e^{ik_yy}u_n(r)\equiv F_n(r)u_n(r). \tag{2.2}$$

The envelope functions $F_n(r)$ are typically considered to be slowly varying, whereas the cell periodic and more oscillatory Bloch functions satisfy Schrödinger's equation with band-edge energies. We distinguish envelope functions cor-

Downloaded 26 Aug 2001 to 128.42.12.177. Redistribution subject to AIP license or copyright, see http://ojps.aip.org/japo/japcr.jsp

responding to the Γ_1 conduction c, Γ_{15} valence v, and the energetically higher remote bands with an index r: $F_n = \{F_c, F_v, F_r\}$. The remote bands are assumed to have band-edge energies $|E_r - E_{cv}| \gg |E_c - E_v| = E_g$, where E_g is the direct energy gap.

Next, Lowdin's perturbation theory[22] is applied in order to eliminate the functions F_r in favor of perturbation terms in the equations for the conduction and valence bands. In the bulk $\mathbf{k}\cdot\mathbf{P}$ theory, these terms correspond to the Kane model[23,24] for the band structure, with quadratic $[\mathbf{O}(k^2)]$ terms within the conduction and the valence bands[24,25] as well as the appropriate interband (conduction-valence) terms.

1. Zinc blende materials

The zinc blende crystal consists of two interpenetrating face-centered-cubic lattices, one having a group-III element atom (e.g., Ga) and the other a group-V element atom (e.g., As). A zinc blende crystal is characterized by a single lattice constant a_{lc}.

The matrix elements of the momentum operator between the conduction and valence bands can be expressed in terms of a single parameter $\mathbf{P}$, originally defined by Kane:

$$\mathbf{P} \equiv \frac{-i\hbar}{m_0}\langle S|p_x|X\rangle, \tag{2.3}$$

where $\langle S|p_x|X\rangle$ is the momentum matrix element between the s-like conduction bands and p-like valence bands. Its value in a given material is usually reported in energy units (eV) as:

$$E_P = \frac{2m_0}{\hbar^2}\mathbf{P}^2. \tag{2.4}$$

The E_P matrix element is one of the band parameters that is extensively reviewed in the subsequent section.

Through second-order perturbation theory, the higher-band contributions to the conduction band are parameterized by the Kane parameter F, whose values are reviewed in the subsequent sections:

$$F = \frac{1}{m_0}\sum_r \frac{|\langle S|p_x|u_r\rangle|^2}{(E_c - E_r)}, \tag{2.5}$$

where $\langle S|p_x|u_r\rangle$ is the momentum matrix element between the s-like conduction bands and remote bands r, and m_0 is the free electron mass.

The second-order valence-band terms include those with possible intermediate r states that belong to energetically higher bands with the symmetry of $s(\Gamma_1)$, $p(\Gamma_{12})$, and $d(\Gamma_{15})$ atomic orbitals.[26] We define the following quantities in terms of matrix elements between p-like valence bands (whose symmetry here and in the following is indicated as X, Y, Z) and remote bands:

$$\sigma = -\left(\frac{1}{3m_0}\right)\sum_r^{\Gamma_1} \frac{|\langle X|p_x|u_r\rangle|^2}{(E_v - E_r)}, \tag{2.6}$$

$$\pi = -\left(\frac{1}{3m_0}\right)\sum_r^{\Gamma_{15}} \frac{|\langle X|p_y|u_r\rangle|^2}{(E_v - E_r)}, \tag{2.7}$$

and

$$\delta = -\left(\frac{1}{6m_0}\right)\sum_r^{\Gamma_{12}} \frac{|\langle X|p_x|u_r\rangle|^2}{(E_v - E_r)}. \tag{2.8}$$

If the conduction-band states were not included into our analysis explicitly, the additional contribution of the nearby c bands would enter the sum over intermediate states in the second-order perturbation theory for the σ parameter. We denote this revised value as σ^L:

$$\sigma^L = \sigma - \left(\frac{1}{3m_0}\right)\sum_c^{\Gamma_1} \frac{|\langle X|p_x|S\rangle|^2}{(E_v - E_c)} = \sigma + \frac{E_P}{6E_g}. \tag{2.9}$$

Now, the σ^L, δ, and π parameter set is simply related to the standard definitions of the Luttinger parameters γ_1, γ_2, and γ_3:

$$\begin{aligned} \gamma_1 &= -1 + 2\sigma^L + 4\pi + 4\delta, \\ \gamma_2 &= \sigma^L - \pi + 2\delta, \\ \gamma_3 &= \sigma^L + \pi - \delta. \end{aligned} \tag{2.10}$$

All of the terms appearing in the valence-band Hamiltonian may be cast in terms of the three quantities σ, δ, and π, or equivalently in terms of the Luttinger parameters.

The inclusion of electron spin and spin-orbit interaction effects are straightforward,[23] and we obtain a 6×6 valence-band Hamiltonian. The matrix elements of the spin-orbit interaction, with $\boldsymbol{\sigma}$ being the Pauli spin matrices here

$$H_{so} = \frac{\hbar}{4m_0^2c^2}\Delta V \times \mathbf{p}\cdot\boldsymbol{\sigma}, \tag{2.11}$$

are parameterized by the quantity called the spin-orbit splitting

$$\Delta_{so} = \frac{3\hbar i}{4m_0^2c^2}\langle X|\frac{\partial V}{\partial x}p_y - \frac{\partial V}{\partial_y}p_x|Y\rangle. \tag{2.12}$$

The atomic potential V appears in the above expressions. The spin-orbit interaction splits the sixfold degeneracy at the zone center into fourfold degenerate heavy-hole (hh) plus light-hole (lh) bands of Γ_8 symmetry with total angular momentum $J = 3/2$, and a doubly degenerate split-off (so) band of Γ_7 symmetry with $J = 1/2$. In practice, the values of the Δ_{so} parameter are determined experimentally.

For a bulk system, the eight-band $\mathbf{k}\cdot\mathbf{P}$ model gives rise to eight coupled differential equations, which define the Schrödinger eigenvalue problem for the energy bands near the center of the BZ. With the envelope functions represented by $e^{\pm ikr}$, we have the usual 8×8 Hamiltonian with terms linear and quadratic in k. In a bulk semiconductor, both direct and indirect energy gaps in semiconductor materials are temperature-dependent quantities, with the functional form often fitted to the empirical Varshni form[27]

$$E_g(T) = E_g(T=0) - \frac{\alpha T^2}{T+\beta}, \tag{2.13}$$

where α and β are adjustable (Varshni) parameters. Although other, more physically justified and possibly quantitatively accurate, functional forms have been proposed,[28,29]

Downloaded 26 Aug 2001 to 128.42.12.177. Redistribution subject to AIP license or copyright, see http://ojps.aip.org/japo/japcr.jsp

they have yet to gain widespread acceptance. In this article, we compile consistent sets of Varshni parameters for all materials.

The effective mass m^* at the conduction and valence band edges can be obtained from the bulk energy dispersion $\Omega(k)$ as[30]

$$\left.\frac{\partial^2}{\partial k^2}\Omega(k)\right|_{\substack{k=0\\E=E_n}} = \frac{\hbar^2}{m^*}. \tag{2.14}$$

Using this procedure, the conduction band effective mass is given in terms of the band parameters

$$\frac{m_0}{m_e^*} = (1+2F) + \frac{E_P(E_g+2\Delta_{so}/3)}{E_g(E_g+\Delta_{so})}. \tag{2.15}$$

Both E_P [defined in Eq. (2.4)] and F [Eq. (2.5)] appearing in Eq. (2.15) are usually taken to be independent of temperature, which means that the temperature variation of the effective mass arises only through the temperature dependences of the energy gaps as in Eq. (2.13). Unfortunately, despite their importance E_P and F are inherently difficult to determine accurately, since the remote-band effects can be calculated but not directly measured. One alternative experimental technique is to rely on measuring the effective g factor, which is not as influenced by remote bands as the effective mass. In this article, we derive consistent sets of F parameters from the best available experimental reports of electron effective masses, energy gaps, spin-orbit splittings, *and* momentum matrix elements. There has been no previous attempt to compile reliable, self-consistent F parameters for such a broad range of materials.

In polar semiconductors such as the III–V compounds, it is the nonresonant polaron[31] mass that is actually measured. That quantity exceeds the bare electron mass by 1%–2%, depending on the strength of the electron–phonon interaction. However, since the band structure is governed by the *bare* electron mass, we attempt to present the latter value and note the approximate magnitude of the polaronic correction whenever the information is available.

At the valence-band edge, the hh effective masses in the different crystallographic directions are given by the relations

$$\begin{aligned}
\left(\frac{m_0}{m_{hh}^*}\right)^{z} &= \gamma_1 - 2\gamma_2;\\
\left(\frac{m_0}{m_{hh}^*}\right)^{[110]} &= \frac{1}{2}(2\gamma_1 - \gamma_2 - 3\gamma_3);\\
\left(\frac{m_0}{m_{hh}^*}\right)^{[111]} &= \gamma_1 - 2\gamma_3.
\end{aligned} \tag{2.16}$$

These expressions show the relationship of the Luttinger parameters, which are not as physically meaningful but more convenient to work with theoretically, to the hh effective masses that can typically be measured in a more direct manner. The lh and so hole effective masses are given by

$$\begin{aligned}
\left(\frac{m_0}{m_{lh}^*}\right)^{z} &= \gamma_1 + 2\gamma_2,\\
\left(\frac{m_0}{m_{lh}^*}\right)^{[110]} &= \frac{1}{2}(2\gamma_1 + \gamma_2 + 3\gamma_3),\\
\left(\frac{m_0}{m_{lh}^*}\right)^{[111]} &= \gamma_1 + 2\gamma_3
\end{aligned} \tag{2.17}$$

and

$$\frac{m_0}{m_{so}^*} = \gamma_1 - \frac{E_P\Delta_{so}}{3E_g(E_g+\Delta_{so})}. \tag{2.18}$$

Equation (2.18), which relates the split-off hole mass to the Luttinger parameters, should in principle contain an additional parameter to account for the effects of remote bands (analogous to F). However, those remote bands are not necessarily the same ones that produce the largest correction to the electron mass. At present, not enough data exist for any of the III–V materials to fix the effect of the interaction with remote bands on the split-off hole mass.

In any theoretical model, being able to reproduce the correct effective masses at the center of the BZ ensures that the curvature of the energy bands is properly reproduced. In the context of heterostructures, using incorrect effective masses could lead to severe deviations from experiment, e.g., in the bound state spectrum of a quantum well. For thin-layer quantum structures, it is also important to have a good model for the nonparabolic dispersion away from the center of the BZ. The eight-band **k·P** model compares well with more rigorous calculations up to about a quarter of the way to the BZ boundary, and extra bands may be included in order to improve the agreement.[32,33] As an illustration, we show in Fig. 1(a) the full-zone band structure in the vicinity of the energy gap obtained for GaAs using the pseudopotential method (see Sec. II B 3). Note the anticrossing of the conduction band with a higher band along the Γ–X direction, which sets one limit on the accuracy of perturbative approaches. A more detailed plot of the band structure near the BZ center in GaAs is given in Fig. 1(b).

The filled points in Fig. 2 show Γ-valley energy gaps as a function of lattice constant for zinc blende forms of the 12 binary III–V semiconductors reviewed in this work. The connecting curves represent band gaps for the random ternary alloys, although in a few cases (e.g., GaAsN and InPN) the extrapolated dependences extend well beyond the regions that are reliably characterized. We also emphasize that the Γ-valley direct gap is not necessarily the smallest, since several of the materials are indirect-gap semiconductors in which the X and L conduction-band valleys lie lower than the Γ minimum. For the non-nitride III–Vs, Fig. 3 shows a similar plot of the *lowest* forbidden gap in each material, with X-valley and L-valley indirect gaps indicated by the dashed and dotted lines, respectively.

2. Nitrides with wurtzite structure

The wurtzite crystal consists of two interpenetrating hexagonal close-packed lattices, one having a group-III element atom (e.g., Ga) and the other a group-V element atom (e.g.,

Downloaded 26 Aug 2001 to 128.42.12.177. Redistribution subject to AIP license or copyright, see http://ojps.aip.org/japo/japcr.jsp

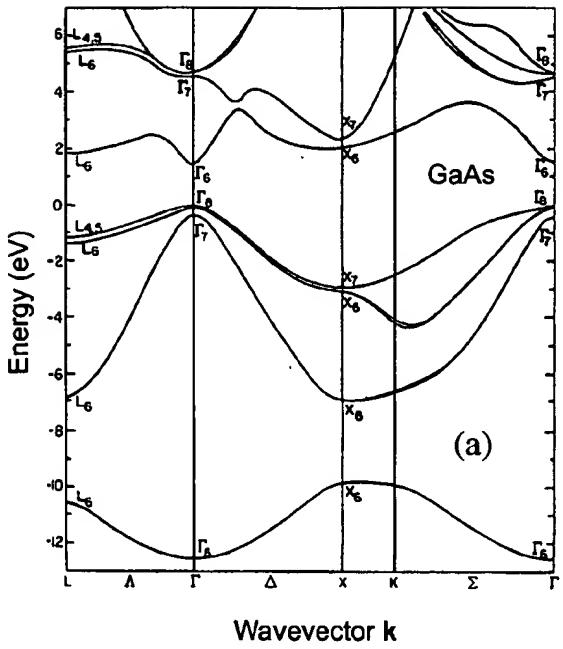

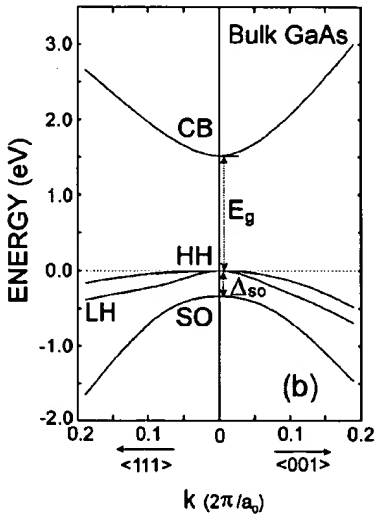

FIG. 1. Diagram of the band structure in the vicinity of the energy gap of GaAs: (a) throughout the first Brillouin zone (reproduced with permission from Ref. 81), (b) a magnified view near the zone center.

N). A wurtzite crystal is characterized by two lattice constants a_{1c} and c_{1c}. A major difference between zinc blende and wurtzite structures is that the in-plane behavior of the bands in a wurtzite crystal is different from the behavior along the [0001] axis (the c axis). The Γ_{1c} conduction bands are s like at the center of the BZ, while the valence bands belong to the $\{\Gamma_{6v}:\{X,Y\}+\Gamma_{1v}:\{Z\}\}$ representations. The nearest higher-order conduction bands belong to the Γ_{6c} states of $\{X,Y\}$ symmetry and the Γ_{3c} states transforming like the $\{Z\}$ representation.

Due to the anisotropy of the crystal, there are two distinct interband matrix elements arising from the $\Gamma_{6v}:\{X,Y\}$ and $\Gamma_{1v}:\{Z\}$ representations, defined by analogy with Eq. (2.3). These are in practice derived from the anisotropic effective mass using expressions similar to Eq. (2.15) (assuming negligible crystal-field and spin-orbit splittings). Although the different conduction-band energy contributions from the higher $\Gamma_{6c}=\{X,Y\}$ and $\Gamma_{3c}=\{Z\}$ intermediate states lead to two distinct F parameters, no experiments that would enable us to establish independent values for the latter have been reported. The compilations in the following sections take the F parameters in the wurtzite nitrides to be zero.

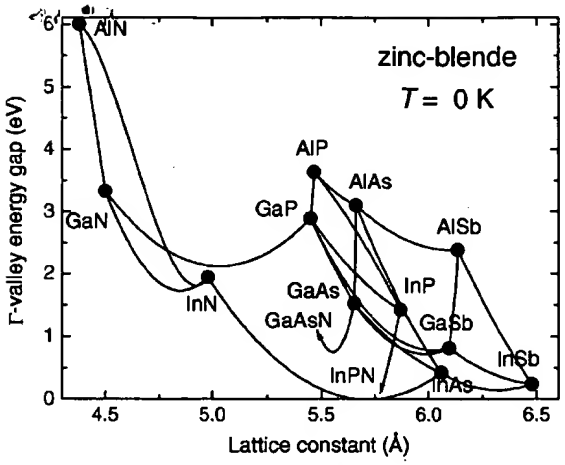

FIG. 2. Direct Γ-valley energy gap as a function of lattice constant for the zinc blende form of 12 III–V binary compound semiconductors (points) and some of their random ternary alloys (curves) at zero temperature. The energy gaps for certain ternaries such as AlAsP, InAsN, GaAsN, InPN, and GaPN are extended into regions where no experimental data have been reported. For GaAsN and InPN, the arrows indicate the boundaries of the regions where the gap dependence on composition may be predicted with any accuracy.

The second-order valence-band terms in the Hamiltonian are evaluated in a manner similar to the earlier discussion for zinc blende structures. The procedure leads to six distinct A parameters, which are to a large extent analogous to the Luttinger parameters in zinc blende materials. The detailed definitions have appeared in the literature.[34–38]

In contrast to the zinc blende materials, the wurtzite structure does not give a triply degenerate valence band

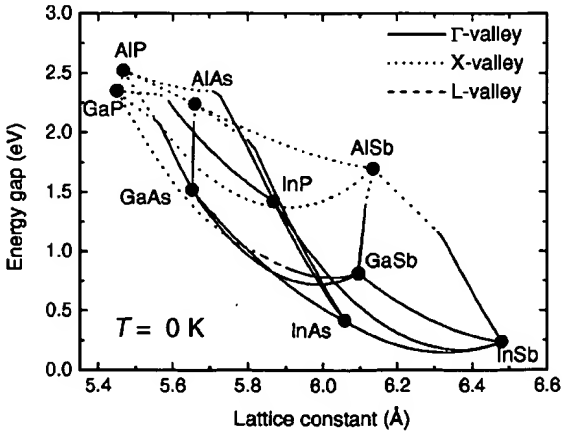

FIG. 3. Lowest forbidden gap as a function of lattice constant for nonnitride III–V compound semiconductors (points) and their random ternary alloys (lines) at zero temperature. The materials with Γ-, X-, and L-valley gaps are indicated by solid, dotted, and dashed lines, respectively.

Downloaded 26 Aug 2001 to 128.42.12.177. Redistribution subject to AIP license or copyright, see http://ojps.aip.org/japo/japcr.jsp

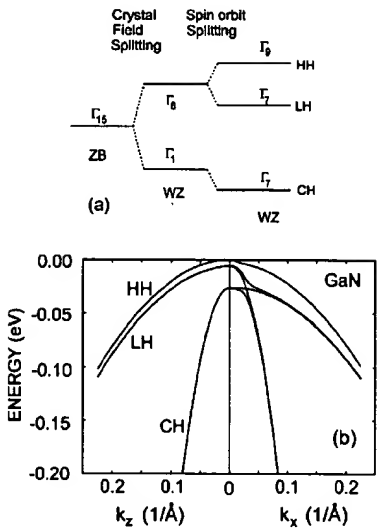

FIG. 4. (a) Schematic illustration of the spin-orbit splitting and crystal-field splitting in wurtzite materials as compared to zinc blende materials. (b) Schematic diagram of the valence band structure of a wurtzite material near the zone center with the heavy-hole (HH), light-hole (LH), and crystal-hole (CH) valence bands explicitly identified.

edge. The crystal-field splitting leads to the band-edge energies:

$$\langle X|H_{\rm cr}|X\rangle=\langle Y|H_{\rm cr}|Y\rangle=E_v+\Delta_1, \tag{2.19}$$

and

$$\langle Z|H_{\rm cr}|Z\rangle=E_v. \tag{2.20}$$

The spin-orbit splitting is parameterized by the relations

$$\langle X|H_{({\rm so})z}|Y\rangle=-i\Delta_2, \tag{2.21}$$

and

$$\langle Y|H_{({\rm so})x}|Z\rangle=\langle Z|H_{({\rm so})y}|X\rangle=-i\Delta_3. \tag{2.22}$$

Although in principle, two different spin-orbit splitting parameters arise, they are commonly assumed equal ($\Delta_2=\Delta_3$). However, the crystal-field splitting (Δ_1) is in general not related to the spin-orbit splitting. The $\Delta_{\rm cr}=\Delta_1$ and $\Delta_{\rm so}=3\Delta_2$ parameters are tabulated for wurtzite materials in the following sections. The definition of the spin-orbit and crystal-field splitting in the wurtzite materials is further illustrated in Fig. 4(a). A typical valence band structure for a wurtzite material is shown in Fig. 4(b).

3. Strain in heterostructures

To model the strain in a pseudomorphically grown heterostructure such as a quantum well, quantum wire, or quantum dot, the elastic continuum theory is usually invoked. In elastic continuum theory, the atomic displacements are represented by a local vector field, $\mathbf{r}'-\mathbf{r}=\mathbf{u}(r)$. Ignoring the quadratic term for small deformations, we define the local strain tensor ε_{ij} via $u_i(r)=\varepsilon_{ij}r_j$.[39,40] The stress tensor σ_{ij} that generates the above strain is given by the relation $\sigma_{ij}=\lambda_{ijkl}\varepsilon_{kl}$. In crystals with cubic symmetry, there are only three linearly independent constants: $\lambda_{xxxx}=C_{11}$, $\lambda_{xxyy}=C_{12}$, $\lambda_{xyxy}=C_{44}$. For the wurtzite structure, there are five linearly independent elastic constants $\lambda_{xxxx}=C_{11}$, $\lambda_{zzzz}=C_{33}$, $\lambda_{xxyy}=C_{12}$, $\lambda_{xxzz}=C_{13}$, $\lambda_{xzxz}=C_{44}$. The values for the elastic constants will be included in our compilation of the band parameters for completeness. Note that, at least for the non-nitride materials, there is little controversy regarding their values, and the datasets given below are widely accepted.

The physical deformation of the crystal leads to a distortion of the atomic locations, which in turn affects the energy levels of the band electrons.[14] The procedure for generating additional terms due to the presence of the strain has been described in detail by Bir and Pikus[14] and Bahder.[41] In the case of hydrostatic compression, the change in the conduction-band-edge energy ΔE_c due to the relative change in volume $\Delta V/V=(\varepsilon_{xx}+\varepsilon_{yy}+\varepsilon_{zz})$ can be parametrized by a linear relation between the change in energy and the hydrostatic strain. The constant of proportionality is the empirical deformation potential constant a_c. Unfortunately, this parameter is difficult to isolate experimentally. Instead it is the deformation potential constant a, associated with the change in band gap E_g due to a hydrostatic deformation, that is measured. Due to the nature of the atomic bonding in III–V materials, the band gap increases for a compressive strain. Under positive hydrostatic pressure, i.e., negative strain, the change in energy $\Delta E_g=a(\varepsilon_{xx}+\varepsilon_{yy}+\varepsilon_{zz})$ must be positive. This implies a negative value for $a\equiv a_c+a_v$. Note that our sign convention for a_v is different from many other works found in the literature. It is generally believed that the conduction band edge moves upward in energy while the valence band moves downward, with most of the change being in the conduction band edge, although Wei and Zunger recently argued that this is not always the case.[42] The distribution of the hydrostatic pressure shift between the conduction and valence bands is generally based from theoretical predictions in this review.

From the Bir–Pikus strain interaction for the valence bands,[14] it may be observed that the single deformation potential a_v, which parameterizes the shift of the valence-band edge $\Delta E_v=a_v(\varepsilon_{xx}+\varepsilon_{xx}+\varepsilon_{xx})$, is insufficient to describe the full effect of strain. Two additional potentials b and d are necessary to describe the shear deformations terms that split the heavy/light-hole degeneracy. For the growth of pseudomorphic layers along the [001] direction, only the value of the potential b is relevant. All of the deformation potentials are tabulated for each material in the sections that follow. For the 6×6 valence-band strain Hamiltonian that is not reproduced here, the reader is referred to the textbooks by Bir and Pikus[14] and by Chuang.[43]

The preceding discussion applies to the zinc blende crystal structure. In a wurtzite material, the crystal anisotropy leads to two distinct conduction-band deformation potentials. Furthermore, six deformation potential constants D_i arise from a full treatment of the effect of strain on the six-band valence-band structure as shown by Bir and Pikus.[14] These D_i are tabulated for each nitride material in the following sections.

4. Piezoelectric effect in III–V semiconductors

Under an externally applied stress, III–V semiconductors develop an electric moment whose magnitude is propor-

Downloaded 26 Aug 2001 to 128.42.12.177. Redistribution subject to AIP license or copyright, see http://ojps.aip.org/japo/japcr.jsp

tional to the stress.[44,45] The strain-induced polarization $\mathbf{P}^s$ can be related to the strain tensor ε_{ij} using piezoelectric coefficients e_{ijk} of the form

$$P_i^s = e_{ijk}\varepsilon_{jk}. \tag{2.23}$$

The symmetry of the strain under interchange of its indices allows us to write e_{ijk} in a more compact form. Converting from the tensor notation to the matrix notation we write

$$\{\varepsilon_{11},\varepsilon_{22},\varepsilon_{33},(\varepsilon_{23},\varepsilon_{32}\},(\varepsilon_{31},\varepsilon_{13}\},(\varepsilon_{12},\varepsilon_{21}\}\} \equiv \{\varepsilon_1,\varepsilon_2,\varepsilon_3,\varepsilon_4,\varepsilon_5,\varepsilon_6\}, \tag{2.24}$$

and

$$e_{ijk} = \begin{cases} e_{im}, & (i=1,2,3; m=1,2,3); \\ \frac{1}{2}e_{im}, & (i=1,2,3; m=4,5,6), \end{cases} \tag{2.25}$$

where it is standard practice to introduce the factor of 1/2 in front of the e_{im} for $m=4,5,6$ in order to obtain the following form without factors of 1/2:

$$P_i^s = e_{i1}\varepsilon_1 + e_{i2}\varepsilon_2 + e_{i3}\varepsilon_3 + e_{i4}\varepsilon_4 + e_{i5}\varepsilon_5 + e_{i6}\varepsilon_6. \tag{2.26}$$

In the zinc blende materials, only off-diagonal terms in the strain give rise to the electric polarization components P_i^s and

$$P_i^s = e_{14}\varepsilon_{jk}, \quad j \neq k, \tag{2.27}$$

where e_{14} is the one independent piezoelectric coefficient that survives due to the zinc blende symmetry. The piezoelectric effect is negligible unless the epitaxial structure is grown along a less common direction such as [111].

On the other hand, in a wurtzite crystal, the three distinct piezoelectric coefficients are $e_{31}=e_{32}$, e_{33}, and $e_{15}=e_{24}$ can be derived from symmetry considerations. The piezoelectric polarization is given in component form by

$$\begin{aligned} P_x^s &= e_{15}\varepsilon_{13}, \\ P_y^s &= e_{15}\varepsilon_{12}, \\ P_z^s &= e_{31}\varepsilon_{11} + e_{31}\varepsilon_{22} + e_{33}\varepsilon_{33}. \end{aligned} \tag{2.28}$$

where we have reverted to the tensor form for the strains ε_{ij}. Thus both diagonal and off-diagonal strain components can generate strong built-in fields in wurtzite materials that must be taken into account in any realistic band structure calculation. The piezoelectric contribution to the total polarization may be specified alternatively in terms of matrix $\mathbf{d}$ related to matrix $\mathbf{e}$ via the elastic constants

$$\begin{aligned} P_i &= \sum_j e_{ij}\varepsilon_j, \\ P_i &= \sum_k d_{ik}\sigma_k = \sum_j \sum_k d_{ik}c_{kj}\varepsilon_j, \end{aligned} \tag{2.29}$$

where ε_j and σ_k are the components of the strain and stress tensors in simplified notation [see Eq. (2.24)], respectively.

The nitrides also exhibit spontaneous polarization, with polarity specified by the terminating anion or cation at the layer surface. Further details are available from recent publications[46,47] and reviews.[48,49] In the sections that follow, we tabulate both piezoelectric coefficients and spontaneous polarizations for the wurtzite nitride materials.

5. Band structure in layered heterostructures

So far we have considered the band parameters of individual materials in the presence of strain. The misalignment of energy band gaps in adjacent layers of a quantum heterostructure is taken into account by specifying a reference layer and defining a band offset function relative to it. In general, this potential energy is given as a function $V_P(z)$ of the coordinate in the growth direction and defines the band edge profile for the top of the valence band. With $V_P(z)=0$ in the reference layer, the conduction band edge profile is $V_S(z) = E_g(z) - E_g(\text{ref}) + V_P(z)$. Valence band offsets have been determined experimentally by optical spectroscopy of quantum well structures, x-ray photoelectron spectroscopy, electrical capacitance measurements, and other techniques. On the theoretical side, this is supplemented by pseudopotential supercell calculations that include atomic layers on either side of a heterointerface. A critical review of valence band offset determinations was given by Yu, McCaldin, and McGill.[50] In Sec. VII we will provide an updated review of the valence band offsets in zinc blende and wurtzite materials, putting the main emphasis on the compilation of a fully consistent set of band offsets.

The coupled Schrödinger differential equations for a layered heterostructure may be solved using the finite-difference method,[51,52] the transfer matrix method,[53–56] or the finite element method,[57–59] which is a variational approach that may be considered a discretization of the action integral itself. Further details are available from the references cited above.

The $\mathbf{k}\cdot\mathbf{P}$ model has also been extended to include the intrinsic inversion asymmetry of the zinc blende structure,[60–63] and, more phenomenologically, to include the effects of Γ and X_z valley mixing in order to include such effects in modeling resonant double-barrier tunneling.[64–69] These parameterizations are beyond the framework of the considerations presented here.

B. Relation of k·P to other band structure models

The $\mathbf{k}\cdot\mathbf{P}$ model is the most economical in terms of assuring agreement with the observed bulk energy band gaps and effective masses at the center of the BZ. However, for a more complete picture of the energy bands throughout the BZ, it is necessary to adopt another approach that requires additional information as input.

1. Empirical tight binding model

In the empirical tight-binding model (ETBM) introduced by Slater and Koster,[70] the electronic states are considered to be linear combinations of atomic $(s,p,d,\ldots)$ orbitals. The Hamiltonian's matrix elements between the atomic orbital states are not evaluated directly, but are instead introduced as free parameters to be determined by fitting the band gaps and band curvatures (effective masses) at critical points in the BZ. Depending on the number of orbitals and nearest neighbors used to represent the states, the ETBM requires that the overlap integrals be determined in terms of the measured direct and indirect band gaps and/or effective masses in the

Downloaded 26 Aug 2001 to 128.42.12.177. Redistribution subject to AIP license or copyright, see http://ojps.aip.org/japo/japcr.jsp

bulk material.[71,72] For example, the sp^3s^* basis with the second-nearest-neighbor scheme[72] turns out to have 27 parameters for the zinc blende lattice structure, and the energies and effective masses obtained from the diagonalization of the Hamiltonian and the resulting energy bands are nonlinear functions of these parameters, which can be fitted by trial and error or using, e.g., genetic algorithms.[73] The lack of a transparent relationship between the input parameters and the experimentally determined quantities is probably the single greatest disadvantage of the tight-binding method in making complicated band structure calculations. In this review, we make no attempt to give a standardized set of tight-binding parameters. The ETBM can also be applied to superlattice band structure calculations.[17,74,75]

2. Effective bond orbital model

While the inclusion of additional bands and overlaps of higher orbitals is a possible approach to improving the tight-binding modeling of energy bands in bulk semiconductors, the effective bond orbital model[76–78] (EBOM) uses spin-doubled s,p_x,p_y,p_z orbitals to generate an 8×8 Hamiltonian. A crucial difference between the EBOM and related tight-binding formulations is that the s and p orbitals are centered on the face-centered cubic lattice sites of the zinc blende crystal rather than on both of the two real atoms per lattice site. The resulting somewhat *ad hoc* formulation offers considerable computational savings in comparison with the ETBM. However, the main significance of the EBOM approach derives from the fact that the resulting secular matrix has a small-**k** expansion that exactly reproduces the form of the eight-band **k·P** Hamiltonian. This allows the EBOM input parameters to be readily expressed in terms of the experimentally measured parameters, such as the band gap, the split-off gap, and the zone-center mass of each band, which has not been accomplished using the more involved ETBM. In fact, the EBOM can be thought of as an extension of the **k·P** method to provide an approximate representation of the energy bands over the full BZ. Since short-period superlattice bands sample wavevectors throughout the BZ, we may expect the EBOM to be more accurate than the **k·P** model for thin-layer structures. However, the EBOM is considerably less efficient computationally than **k·P**, especially for thicker superlattices. Each lattice position must be represented in the supercell technique, i.e., no envelope function approximation is made.

3. Empirical pseudopotential model

The influence of core electrons in keeping the valence electrons outside of the core may be represented by an effective repulsive potential in the core region. When this is added to the attractive ionic potential, the net "pseudopotential" nearly cancels[79,80] at short distances. The valence states are orthogonal to the core states, and the resulting band structure theory corresponds to the nearly free-electron model. In the empirical pseudopotential model, the crystal potential is represented by a linear superposition of atomic potentials, which are modified to obtain good fits to the experimental direct and indirect band gaps and effective masses. Further details are presented by Cohen and Chelikowsky[81] and in the reviews by Heine and Cohen.[82,83] *Ab initio* approaches employ calculated band parameters (e.g., from the density-functional theory) in lieu of experimental data. Combinations of *ab initio* and empirical methods have been developed to a high level of sophistication.[84] Extension of the pseudopotential method to heterostructures entails the construction of a supercell to assure the proper periodic boundary conditions. With atomic potentials as the essential input, the electronic properties of the heterostructure can be determined, although the required computational effort far exceeds the demands of the **k·P** method. The relative merits of the **k·P** and pseudopotential approaches have been assessed.[85,86]

III. BINARY COMPOUNDS

A. GaAs

GaAs is the most technologically important and the most studied compound semiconductor material.[3] Many band structure parameters for GaAs are known with a greater precision than for any other compound semiconductor. This is especially true of the fundamental energy gap with a value of 1.519 eV at 0 K.[87] The analysis by Thurmond[88] indicated $\alpha=0.5405$ meV/K and $\beta=204$ K [in Eq. (2.13)]. A more recent examination of a large number of samples by ellipsometry produced a very similar parameter set of $E_g(T=0)=1.517$ eV, $\alpha=0.55$ meV/K, and $\beta=225$ K.[89] The two results are well within the quoted experimental uncertainty of each other and several other experimental determinations,[3,90] although somewhat different parameter sets have been proposed recently on the basis of photoluminescence measurements: $E_g(T=0)=1.519$ eV, $\alpha=0.895-1.06$ meV/K, and $\beta=538-671$ K.[91,92]

The original controversy[87] about the ordering of the L and X-valley minima was resolved by Aspnes,[93] who proposed on the basis of numerous earlier experiments the following sets: $E_g^L(T=0)=1.815$ eV, $\alpha^L=0.605$ meV/K, and $E_g^X(T=0)=1.981$ eV, $\alpha^X=0.460$ meV/K with $\beta=204$ K in both cases. Schottky-barrier electroreflectance measurements yielded the widely accepted value for the split-off energy gap in GaAs: $\Delta_{so}=0.341$ eV.[94]

Electron effective masses of $m_e^*=0.0665m_0$ and $0.0636m_0$ were observed at $T=60$ and 290 K, respectively, by Stradling and Wood[95] using magnetophonon resonance experiments.[96–98] A low-temperature value of $0.065m_0$ was determined for the bare electron mass once the polaronic correction was subtracted.[99] While a somewhat larger mass of $\approx0.07m_0$ was derived theoretically in several *ab initio* and semiempirical band structure studies,[100–102] recent cyclotron resonance measurements[103] indicate a low-temperature result of $0.067m_0$ at the band edge. This is the value we adopt following the recommendation of Nakwaski in his comprehensive review,[104] which is based on reports employing a wide variety of different experimental techniques. At room temperature, the currently accepted value is $0.0635m_0$, as confirmed, for example, by photoluminescence measurements.[105] We employ the effective masses for the L and X valleys given by Adachi[3] and Levinshtein *et al.*,[11] which were compiled from a variety of measurements.

Downloaded 26 Aug 2001 to 128.42.12.177. Redistribution subject to AIP license or copyright, see http://ojps.aip.org/japo/japcr.jsp

Many different sets of Luttinger parameters are available in the literature.[99] The most popular set: $\gamma_1=6.85$, $\gamma_2=2.10$, and $\gamma_3=2.90$ (also given in Landolt–Bornstein[1]), which was derived by Lawaetz[106] on the basis of five-level (14-band) $\mathbf{k}\cdot\mathbf{P}$ calculations, is in good agreement with early cyclotron resonance,[107] magnetoreflection,[108] and magnetoexciton[109] experiments. While two-photon magnetoabsorption measurements[110] indicated very little warping in the valence band, those results are contradicted by optical spectroscopy[111] and Raman scattering[112] studies of GaAs quantum wells as well as by fits to the shallow acceptor spectra.[113,114] Here we prefer a composite data set, which is within the experimental error of all accurate determinations and reproduces well the measured hole masses and warping:[99,104] $\gamma_1=6.98$, $\gamma_2=2.06$, and $\gamma_3=2.93$.

While its value is usually less critical to the device design and band structure computations, the split-off hole mass in GaAs has also been measured and calculated using a variety of approaches.[106,111] A composite value $m_{so}^*=0.165m_0$ was derived by Adachi,[3] which is in excellent agreement with the recent calculation by Pfeffer and Zawadzki.[33] However, we will use a slightly different value, $m_{so}^*=0.172m_0$, in order to provide self-consistency with the $\mathbf{k}\cdot\mathbf{P}$ expression in Eq. (2.18).

The first electron-spin-resonance measurements of the interband matrix element in GaAs, which were reported by Chadi *et al.*[115] and Hermann and Weisbuch,[116] yielded $E_P=28.8-29.0$ eV. However, Shantharama *et al.*[96,117] suggested that those analyses overestimated the influence of remote bands outside of the 14-band $\mathbf{k}\cdot\mathbf{P}$ model and gave $E_P=25.0\pm0.5$ eV. Theoretical studies[99,118] have derived intermediate values. Since the analysis by Shantharama *et al.* appears to have internal consistency problems, we adopt the Hermann and Weisbuch value (implying $F=-1.94$), which has been used with some success in the literature to determine the optical gain in GaAs quantum-well lasers.[119]

The greatest uncertainty in the GaAs band structure parameters is associated with the deformation potentials, which are needed to calculate strain effects in pseudomorphically grown layers. In this review, we will consider only deformation potentials for the Γ valley. The total hydrostatic deformation potential a is proportional to the pressure coefficient of the direct band gap, where the constant of proportionality is approximately the bulk modulus. Some trends in the band gap pressure coefficients were noted by Wei *et al.*[42,120] The experimental hydrostatic pressure dependence of E_g for GaAs implies a total deformation potential $a=a_c+a_v\approx-8.5$ eV,[121] where the minus sign represents the fact that the band gap expands when the crystal is compressed (note that our sign convention for a_v is different from a large number of articles). The conduction-band deformation potential a_c corresponds to the shift of the conduction band edge with applied strain. Pseudopotential[122] and linear-muffin-tin-orbital[123] calculations yielded a_c as large as -18.3 eV, whereas various analyses of mobility data[3,124] using standard deformation-potential scattering models are consistent with a_c falling in the range -6.3 to -13.5 eV. A recent study of acoustic–phonon scattering in GaAs/AlGaAs quantum wells[125] produced an estimate of $a_c=-11.5\pm0.5$ eV. On the other hand, studies of the valence-band deformation potential[3,126,127] suggest a small a_v. In order to be consistent with the experimental hydrostatic pressure shift, we recommend using the values $a_c=-7.17$ eV and $a_v=-1.16$ eV, which were derived from the "model-solid" formalism by Van de Walle.[129] However, the first-principles calculations of Wei and Zunger[42] show that the energy of the valence-band maximum increases as the unit cell volume decreases for a number of III–V semiconductors including GaAs, GaP, GaSb, InP, InAs, and InSb, whereas it has the opposite sign in other materials. Whatever the direction of the valence-band maximum, it is generally agreed that the conduction band moves much faster with pressure. Heterolayer band-structure calculations are relatively insensitive to the value of a_v when it is close to zero.

The shear deformation potentials b and d have been determined both experimentally and theoretically.[3,121,126,128–131] Moreover, a ratio of the deformation potentials $d/b=2.4\pm0.1$ was recently derived from studies of acceptor-bound excitons in biaxially and uniaxially strained GaAs epilayers.[132] The various values for the deformation potential b varied between -1.66 and -3.9 eV, although recent results tend toward the lower end of that range. We propose the following composite values: $b=-2.0$ eV and $d=-4.8$ eV, which are consistent with the vast majority of measurements and several calculations.

All of the recommended parameters for GaAs are compiled in Table I.

B. AlAs

Because of its frequent incorporation into GaAs-based heterostructures, AlAs is also one of the most important electronic and optoelectronic materials.[3,6,8] Unlike GaAs, AlAs is an indirect-gap semiconductor with the $X-L-\Gamma$ ordering of the conduction valley minima. The X-valley minimum is located at a wave vector $k=(0.903,0,0)$. The exciton energies corresponding to the Γ-valley energy gap were measured by Monemar[133] to be 3.13 and 3.03 eV at 4 and 300 K, respectively. A small ($\approx$10 meV) correction for the exciton binding energy is presumably necessary.[134] Similar values were obtained by Onton,[135] Garriga *et al.*,[136] and Dumke *et al.*[137] Since direct measurements on AlAs are difficult owing to its rapid oxidation upon exposure to air, we choose parameters that are consistent with the more readily available data on the AlGaAs alloy discussed in detail below as well as with the foregoing measurements on bulk AlAs. The temperature dependence of the direct energy gap, which is similar to that for GaAs, was given in an extrapolated form by Logothetidis *et al.*,[138] although better agreement with the results of Monemar[133] can be obtained by increasing β to 530 K.

The low-temperature X-Γ indirect gap in AlAs was measured to be $\approx$2.23–2.25 eV.[133,137,139] We suggest the following temperature-dependence parameters, which are somewhat different from the empirical suggestion of Guzzi *et al.*,[139] but are more consistent with the experimental results of Monemar:[133] $\alpha=0.70$ meV/K and $\beta=530$ K. Not many data are available on the temperature variation of the $L-\Gamma$ gap, although it should be similar to that in GaAs. At

Downloaded 26 Aug 2001 to 128.42.12.177. Redistribution subject to AIP license or copyright, see http://ojps.aip.org/japo/japcr.jsp

TABLE I. Band structure parameters for GaAs.

Parameters	Recommended values	Range
a_{lc} (Å)	$5.65325+3.88\times10^{-5}(T-300)$	
E_g^Γ (eV)	1.519	1.420–1.435 (300 K)
$\alpha(\Gamma)$ (meV/K)	0.5405	0.51–1.06
$\beta(\Gamma)$ (K)	204	190–671
E_g^X (eV)	1.981	···
$\alpha(X)$ (meV/K)	0.460	···
$\beta(X)$ (K)	204	···
E_g^L (eV)	1.815	···
$\alpha(L)$ (meV/K)	0.605	···
$\beta(L)$ (K)	204	···
Δ_{so} (eV)	0.341	0.32–0.36
m_c^* (Γ)	0.067	0.065–0.07 (0 K), 0.0635–0.067 (300 K)
$m_l^*(L)$	1.9	···
$m_t^*(L)$	0.0754	···
$m_{DOS}^*(L)$	0.56	···
$m_l^*(X)$	1.3	···
$m_t^*(X)$	0.23	···
$m_{DOS}^*(X)$	0.85	···
γ_1	6.98	6.79–7.20
γ_2	2.06	1.9–2.88
γ_3	2.93	2.681–3.05
m_{so}^*	0.172	0.133–0.388
E_P (eV)	28.8	25.5–29.0
F	−1.94	0.76–(−2)
VBO (eV)	−0.80	
a_c (eV)	−7.17	−6.3–(−18.3)
a_v (eV)	−1.16	−0.2–(−2.1)
b (eV)	−2.0	−1.66–(−3.9)
d (eV)	−4.8	−2.7–(−6.0)
c_{11} (GPa)	1221	···
c_{12} (GPa)	566	···
c_{44} (GPa)	600	···

room temperature, a gap of ≈2.35 eV is generally adopted.[2,3,140,141] A split-off gap of 0.275 eV was measured by Onton,[135] although the extrapolations by Aubel *et al.*[142] and Wrobel *et al.*[143] indicated higher values.

The Γ-valley electron effective mass in AlAs is difficult to determine for the same reasons that the band gaps are uncertain, and also because, in contrast to GaAs, it is impossible to maintain a Γ-valley electron population in thermal equilibrium. Various calculations and measurements have been compiled by Adachi[3] and Nakwaski.[104] As pointed out by Adachi, the indirect determinations[144,145] employing resonant tunneling diodes with AlAs barriers give an effective mass comparable to that in GaAs, but are less trustworthy than the extrapolations from AlGaAs[146,147] and theoretical calculations[100,148] which indicate $m_e^*=0.15m_0$. A slightly lower value of $0.124m_0$ was inferred from a fit to absorption data.[137]

Electron effective masses for the X valley with an ellipsoidal constant-energy surface were calculated using the pseudopotential method,[148] and measured by Faraday rotation[149] and cyclotron resonance.[104,150] The former experiment in fact measured only the ratio between the longitudinal and transverse masses (of 5.7), and there is some evidence that the assumed value for m_l was inconsistent with other data.[104,151] For reasons that are discussed in some detail by Nakwaski,[104] it appears that the recent results by Goiran *et al.*[152] represent the most reliable values available at present. For the longitudinal and transverse effective masses of the L valley, we employ the calculated results of Hess *et al.*[148]

The band edge hole masses in AlAs are also not known with a great degree of precision. Both theoretical[106,148] and experimental[111] sets of Luttinger parameters have been published. Unfortunately, the latter was obtained from a fit to measurements on GaAs/AlGaAs quantum wells, which had only limited sensitivity to the AlAs parameters. However, the agreement between different calculations of the hole masses is rather good. We propose a composite Luttinger parameter set based on an averaging of the heavy-hole and light-hole masses from various sources and recommendations by Nakwaski:[104] $\gamma_1=3.76$, $\gamma_2=0.82$, and $\gamma_3=1.42$. These values are quite similar to the composite parameters suggested by Adachi.[3] For the split-off hole mass, we adopt a value of $0.28m_0$ for consistency with the E_P value of 21.1 eV($F=-0.48$) given by Lawaetz.[106] This mass falls midway between the recommendations by Pavesi and Guzzi[134] and Adachi.[3]

Very few determinations of the electron and hole deformation potentials in AlAs exist. Most of the experimental values are in fact extrapolations from AlGaAs (see below). As for the case of GaAs, we recommend using the values $a_c=-5.64$ eV and $a_v=-2.47$ eV derived from the model-

Downloaded 26 Aug 2001 to 128.42.12.177. Redistribution subject to AIP license or copyright, see http://ojps.aip.org/japo/japcr.jsp

TABLE II. Band structure parameters for AlAs.

Parameters	Recommended values	Range
a_{lc} (Å)	$5.6611+2.90\times10^{-5}(T-300)$	···
E_g^Γ (eV)	3.099	2.9–3.14
$\alpha(\Gamma)$ (meV/K)	0.885	···
$\beta(\Gamma)$ (K)	530	···
E_g^X (eV)	2.24	2.23–2.25
$\alpha(X)$ (meV/K)	0.70	···
$\beta(X)$ (K)	530	···
E_g^L (eV)	2.46	2.35–2.53
$\alpha(L)$ (meV/K)	0.605	···
$\beta(L)$ (K)	204	···
Δ_{so} (eV)	0.28	0.275–0.31
$m_e^*(\Gamma)$	0.15	0.06–0.15
$m_l^*(L)$	1.32	···
$m_t^*(L)$	0.15	···
$m_l^*(X)$	0.97	···
$m_t^*(X)$	0.22	···
γ_1	3.76	3.42–4.04
γ_2	0.82	0.67–1.23
γ_3	1.42	1.17–1.57
m_{so}^*	0.28	0.24–0.68
E_P (eV)	21.1	···
F	−0.48	···
VBO (eV)	−1.33	···
a_c (eV)	−5.64	0.7–(−5.64)
a_v (eV)	−2.47	−1.2–(−2.6)
b (eV)	−2.3	−1.4–(−3.9)
d (eV)	−3.4	−2.7–(−6.0)
c_{11} (GPa)	1250	···
c_{12} (GPa)	534	···
c_{44} (GPa)	542	···

TABLE III. Band structure parameters for InAs.

Parameters	Recommended values	Range
a_{lc} (Å)	$6.0583+2.74\times10^{-5}(T-300)$	···
E_g^Γ (eV)	0.417	0.410–0.450
$\alpha(\Gamma)$ (meV/K)	0.276	···
$\beta(\Gamma)$ (K)	93	···
E_g^X (eV)	1.433	···
$\alpha(X)$ (meV/K)	0.276	···
$\beta(X)$ (K)	93	···
E_g^L (eV)	1.133	1.13–1.175
$\alpha(L)$ (meV/K)	0.276	···
$\beta(L)$ (K)	93	···
Δ_{so} (eV)	0.39	0.37–0.41
$m_e^*(\Gamma)$	0.026	0.023–0.03
$m_l^*(L)$	0.64	···
$m_t^*(L)$	0.05	···
$m_{DOS}^*(L)$	0.29	···
$m_l^*(X)$	1.13	···
$m_t^*(X)$	0.16	···
$m_{DOS}^*(X)$	0.64	···
γ_1	20.0	6.79–7.20
γ_2	8.5	1.9–2.88
γ_3	9.2	2.681–3.05
m_{so}^*	0.14	0.09–0.15
E_P (eV)	21.5	21.5–22.2
F	−2.90	0–(−2.90)
VBO (eV)	−0.59	···
a_c (eV)	−5.08	−5.08–(−11.7)
a_v (eV)	−1.00	−1.00–(−5.2)
b (eV)	−1.8	−8–(−2.57)
d (eV)	−3.6	···
c_{11} (GPa)	832.9	···
c_{12} (GPa)	452.6	···
c_{44} (GPa)	395.9	···

solid formalism by Van de Walle.[129] For the shear deformation potentials, the following values are suggested: $b=-2.3$ eV[153] and $d=-3.4$ eV.[3] The former is supported by ellipsometry measurements of the heavy-light hole exciton splittings in AlGaAs epitaxial layers, whereas further experiments are necessary to confirm the latter.

All of the recommended parameters for AlAs are compiled in Table II.

C. InAs

InAs has assumed increasing importance in recent years as the electron quantum well material for InAs/GaSb/AlSb-based electronic[154] and long-wavelength optoelectronic[155] devices. The vast majority of experimental low-temperature energy gaps fall in the 0.41–0.42 eV range,[156–159] although somewhat higher values have also been reported.[160,161] We adopt the value 0.417 eV that was obtained from recent measurements on a high-purity InAs sample,[162] in which it was possible to separate shallow impurity, exciton, and band-to-band transitions. The temperature dependence of the band gap has also been reported by several authors.[2,27,163–165] Although there is considerable variation in the proposed Varshni parameters, most of the data agree reasonably well with the values given by Fang *et al.*:[164] $\alpha=0.276$ meV/K and $\beta=93$ K. Energies for the L and X conduction-band minima in InAs have not been studied experimentally. Our recommended values are based on the suggestions by Adachi[166] and Levinshtein *et al.*[11] extrapolated from room temperature to 0 K. The temperature dependences of the indirect gaps are taken to be identical to the direct gap, since no determinations appear to be available. The experimental spin-orbit splittings given in Landolt–Bornstein[1] fall in the 0.37–0.41 eV range. We take an average of 0.39 eV, which also agrees well with the more recent experiments of Zverev *et al.*[167]

The electron effective mass in InAs has been determined by magnetophonon resonance, magnetoabsorption, cyclotron resonance, and band structure calculations.[95,104,162,168–179] Owing to the strong conduction-band nonparabolicity in this narrow-gap semiconductor, considerable care must be taken to measure the mass at the band edge rather than at the Fermi level.[180] The majority of results at both low and high temperatures fall between $0.0215m_0$[174] and $0.026m_0$.[171] Although a few theoretical and experimental studies have obtained low-temperature masses as high as $0.03m_0$,[101,102,104,181] these values were most likely influenced by the strong nonparabolicity. While a value near the bottom of the reported range is usually recommended since the band edge mass represents a lower limit on the measured quantity,[104] many of the results supporting such a mass were in fact performed at room temperature. Since there are almost no credible reports of an effective mass lower than $0.0215m_0$ at any temperature,[104] our recommended low-temperature value is $0.026m_0$ which, accounting for the shift of the energy gap, implies $0.022m_0$ at 300 K. The small (1%) polaronic correction is well within the experimental uncer-

Downloaded 26 Aug 2001 to 128.42.12.177. Redistribution subject to AIP license or copyright, see http://ojps.aip.org/japo/japcr.jsp

tainty in this case. The density-of-states effective masses for the X and L valleys are taken from Levinshtein *et al.*[11] By employing typical experimental m_l/m_t ratios for related III–V materials (such as GaAs and GaSb) corresponding longitudinal and transverse masses have been estimated and listed in Table III.

Although Luttinger parameters for InAs were determined experimentally by Kanskaya *et al.*,[159] those parameters appear to disagree with the heavy-hole masses for various directions given in the same reference. The values of γ_1 and γ_3 given in that reference are very close to a previous determination of Pidgeon *et al.*[157] A number of theoretical works[104,106,182] predict a much higher degree of anisotropy in the valence band. Surveying the data available to date, Nakwaski[104] concludes that further experimental work is needed to resolve the matter. Noting the considerable uncertainty involved in this estimate, we suggest the following composite set: $\gamma_1=20$, $\gamma_2=8.5$, and $\gamma_3=9.2$. Experimental studies[183] have suggested a split-off mass of $0.14m_0$ in InAs.

The interband matrix element in InAs appears to have been determined relatively accurately owing to the large g factor in this narrow-gap semiconductor. Whereas early studies suggested a value of 22.2 eV,[106,116] more recently $E_P=21.5$ eV has gained acceptance.[159,184] We recommend this value, which leads to $F=-2.90$. This is somewhat larger than the effect predicted by other workers,[159] which also assumed a smaller low-temperature electron mass ($0.024m_0$).

The hydrostatic deformation potential in InAs was determined to be $a=-6.0$ eV.[1] We take the conduction and valence-band deformation potentials of Van de Walle,[129] who estimates that most of the energy shift occurs in the conduction band. Somewhat different values were calculated by Blacha *et al.*[122] and Wei and Zunger.[42] The shear deformation potentials adopted from Landolt–Bornstein[1] are in good agreement with the calculations of Blacha *et al.*[122] Another set of deformation potentials has been calculated by Wang *et al.*[86] Unfortunately, at present there exist little experimental data from which to judge the relative merits of the above calculations. All of the recommended parameters for InAs are compiled in Table III.

D. GaP

Nitrogen-doped GaP has for a long time been used as the active material for visible light-emitting diodes (LEDs).[185] GaP is the only indirect-gap (with X–L–Γ ordering of the conduction-band minima) binary semiconductor we will consider that does not contain Al. The band structure is somewhat similar to that of AlAs, with the X-valley minimum at $k=(0.95,0,0)$.[5] Indirect X–Γ energy gaps of 2.338–2.350 eV have been reported.[186,187] The main uncertainty in determining the various energy gaps for GaP is that excitonic rather than band-to-band absorption lines typically dominate, so that a calculated exciton binding energy (which presumably has a weak temperature dependence) must be added to the experimental results. The situation is further complicated by the camel's back structure of the X-valley conduction-band minimum.[187] The most commonly employed Varshni parameters, reported in Casey and Panish,[2] are in excellent agreement with piezomodulation spectroscopy results by Auvergne *et al.*[188] The L-valley minimum is located $\approx$0.37 eV above the X valley,[4] although its temperature dependence has not been determined. The low-temperature value for the direct excitonic band gap was found to be 2.86–2.87 eV from absorption measurements.[133,137,189] An exciton binding energy of 20 meV is added to obtain the energy for interband transitions, although the precise value is not well known. GaP has a small spin-orbit splitting of 0.08 eV.[1,189]

The electron effective mass in the Γ valley is estimated from theory to be $0.09m_0$,[11,96] although higher values have also been reported.[101,106] The diamagnetic shifts measured in magnetoluminescence experiments on $GaAs_{1-x}P_x$ alloys with $x<0.45$[190] suggest an effective mass of $\approx 0.13m_0$ for GaP, which is in good agreement with tight-binding calculations by Shen and Fan.[191]

There have been a number of experimental determinations[192] of the X-valley longitudinal and transverse masses, although the measurements are complicated by the camel's back structure that makes the longitudinal mass highly nonparabolic. This nonparabolicity must be accounted for in any treatment of the density of electron states in GaP, and is in fact more crucial than the precise value of m_l far above the camel's back. Effective masses of $5-7m_0$ have been reported for the bottom of the camel's back,[193] whereas $m_l^*\approx 2m_0$ high above.[194] Estimates for the transverse mass range from $0.19m_0$[182] to $0.275m_0$,[195] although the present consensus puts the value at $0.25m_0$.[193] We have taken longitudinal and transverse effective masses for the L-valley minimum from Levinshtein *et al.*[11]

The Luttinger parameters for GaP were first calculated by Lawaetz.[106] Subsequent cyclotron resonance experiments refined the masses along the [111][196–198] and [100][198] directions. Street and Senske also determined Luttinger parameters from acceptor binding energies.[199] Those parameters as corrected in Landolt–Bornstein[1] are in reasonably good agreement with cyclotron resonance results, and may be considered the most reliable: $\gamma_1=4.05$, $\gamma_2=0.49$, and $\gamma_3=1.25$. A split-off hole mass of $0.23-0.24m_0$ was calculated by Lawaetz[106] and by Krijn.[101] We use a slightly higher value of $0.25m_0$ in order to be consistent with the interband matrix element.

Lawaetz obtained $E_P=22.2$ eV using a rather high theoretical estimate for the Γ-valley effective mass in GaP.[106] Recently, more accurate determinations of the interband matrix element in GaAsP have been published.[190,191] By analogy with the case of GaAs discussed above, these imply a much higher E_P of 31.4 eV, which leads to $F=-2.04$. Although such an extrapolation from data on As-rich alloys is somewhat questionable, there is no *a priori* reason that an interband matrix element in GaP so much different from that in GaAs is unreasonable.

The hydrostatic deformation potential for the direct energy gap in GaP was measured by Mathieu *et al.*[200] to be $a=-9.9$ eV. Van de Walle[129] estimated that the valence-band shift is small compared with the conduction-band shift. We recommend his valence-band deformation potential, with the conduction-band contribution corrected to reproduce the result of Mathieu *et al.*[200] A number of theoretical and experi-

Downloaded 26 Aug 2001 to 128.42.12.177. Redistribution subject to AIP license or copyright, see http://ojps.aip.org/japo/japcr.jsp

TABLE IV. Band structure parameters for GaP.

Parameters	Recommended values	Range
a_{lc} (Å)	$5.4505+2.92\times10^{-5}(T-300)$	···
E_g^Γ (eV)	$2.886+0.1081$ [1-coth(164/T)]	2.86–2.895
E_g^X (eV)	2.35	2.338–2.350
$\alpha(X)$ (meV/K)	0.5771	···
$\beta(X)$ (K)	372	···
E_g^L (eV)	2.72	···
$\alpha(L)$ (meV/K)	0.5771	···
$\beta(L)$ (K)	372	···
Δ_{so} (eV)	0.08	0.08–0.13
$m_e^*(\Gamma)$	0.13	0.09–0.17
$m_l^*(X)$	2.0 (camel back)	2–7
$m_t^*(X)$	0.253 (camel back)	0.19–0.275
$m_l^*(L)$	1.2	···
$m_t^*(L)$	0.15	···
γ_1	4.05	4.04–4.20
γ_2	0.49	···
γ_3	2.93	···
m_{so}^*	0.25	0.23–0.25
E_P (eV)	31.4	22.2–31.4
F	−2.04	0–(−2.04)
VBO (eV)	−1.27	···
a_c (eV)	−8.2	−6.3–(−18.3)
a_v (eV)	−1.7	−0.2–(−2.1)
b (eV)	−1.6	−1.66–(−3.9)
d (eV)	−4.6	−2.7–(−6.0)
c_{11} (GPa)	1405	···
c_{12} (GPa)	620.3	···
c_{44} (GPa)	703.3	···

TABLE V. Band structure parameters for AlP.

Parameters	Recommended values	Range
a_{lc} (Å)	$5.4672+2.92\times10^{-5}(T-300)$	···
E_g^Γ (eV)	3.63	3.62 (77 K), 3.56 (300 K)
$\alpha(\Gamma)$ (meV/K)	0.5771	···
$\beta(\Gamma)$ (K)	372	···
E_g^X (eV)	2.52	2.49–2.53
$\alpha(X)$ (meV/K)	0.318	···
$\beta(X)$ (K)	588	···
E_g^L (eV)	3.57	···
$\alpha(L)$ (meV/K)	0.318	···
$\beta(L)$ (K)	588	···
Δ_{so} (eV)	0.07	0.06–0.07
$m_e^*(\Gamma)$	0.22	···
$m_l^*(X)$	2.68	2.68–3.67
$m_t^*(X)$	0.155	0.155–0.212
γ_1	3.35	···
γ_2	0.71	···
γ_3	1.23	···
m_{so}^*	0.30	0.29–0.34
E_P (eV)	17.7	···
F	−0.65	···
VBO (eV)	−1.74	···
a_c (eV)	−5.7	−5.54–(−5.7)
a_v (eV)	−3.0	−3.0–(−3.15)
b (eV)	−1.5	−1.4–(−4.1)
d (eV)	−4.6	···
c_{11} (GPa)	1330	···
c_{12} (GPa)	630	···
c_{44} (GPa)	615	···

mental values have been reported[130,187,200] for the shear deformation potentials, which are generally in good agreement with each other. We suggest the following composite values: $b=-1.6$ eV and $d=-4.6$ eV.

All of the recommended parameters for GaP are compiled in Table IV.

E. AlP

AlP, with the largest direct gap of the III–V compound semiconductors, is undoubtedly the most "exotic" and least studied. Nevertheless, the essential characteristics have been known for some time. It is unclear whether the conduction-band minima follow the X–Γ–L[201] or X–L–Γ[182] ordering, since no actual measurements of the L-valley position appear to have been performed. The indirect energy gap of 2.5 eV and its temperature dependence are given in Casey and Panish[2] with appropriate corrections to the original determinations. A similar value has been obtained by extrapolation from AlGaP alloys by Alferov *et al.*[202] The direct gap of AlP was measured by Monemar[133] to be 3.63 eV at 4 K and 3.62 eV at 77 K, while Bour *et al.*[203] obtained an extrapolation to 300 K of 3.56 eV. The required correction of these results due to the exciton binding energy is unclear. The spin-orbit splitting in AlP should be small, on the order of 0.06–0.07 eV,[101,204] although the actual value has apparently never been measured.

Almost no experimental data are available on the effective masses in AlP. A Γ-valley mass of $0.22m_0$ was calculated using the augmented spherical wave approach.[101] Another *ab initio* calculation[182] yielded $m_l^*=3.67m_0$ and $m_t^*=0.212m_0$ for the X valley, although Issiki *et al.*[205] obtained better agreement with photoluminescence results for AlP/GaP heterostructures using a somewhat smaller X-valley mass. We have adjusted the theoretical longitudinal and transverse masses by the same factor to conform to that fitting, although further studies are clearly needed to confirm our projections. Composite values for the Luttinger parameters and the split-off hole mass have been taken from various calculations.[101,106,182] An interband matrix element of 17.7 eV ($F=-0.65$) is given by Lawaetz.[106]

The hydrostatic deformation potentials were calculated by Van de Walle,[129] although a slight correction was found to be necessary when energy level alignments in a GaInP/AlGaInP laser structure were fit.[206] We select $b=-1.5$ eV in accordance with the calculations of O'Reilly[130] and Krijn,[101] although higher values have been computed by Blacha *et al.*[122] No values for the shear deformation potential d appear to have been reported. In the absence of other information, we recommend the value of $d=-4.6$ eV derived for GaP (see previous subsection).

All of the band structure parameters for AlP are collected in Table V.

F. InP

InP is a direct-gap semiconductor of great technological significance,[4–7,10] since it serves as the substrate for most optoelectronic devices operating at the communications wavelength of 1.55 μm. Numerous studies of the band structure parameters for InP and its alloys have been carried out.

Downloaded 26 Aug 2001 to 128.42.12.177. Redistribution subject to AIP license or copyright, see http://ojps.aip.org/japo/japcr.jsp

Rochon and Fortin[207] found the low-temperature direct band gap to be 1.423 eV, with most other reports agreeing to within a few meV.[1] Since exciton rather than interband transitions are usually observed in such absorption measurements, the binding energy of 5 meV has been added to the spectral position of the resonance.[1,207] The temperature dependence of the direct band gap has been reported by Varshni,[27] Casey and Panish,[2] Lautenschlager *et al.*,[208] Hang *et al.*,[209] and Pavesi *et al.*[210] When $T \gg \beta$, the gap decreases linearly with temperature and use of the Varshni expression is not necessary (i.e., $\beta=0$). Lautenschlager *et al.* and Pavesi *et al.* did not use the Varshni functional form, and Hang *et al.* focused primarily on fitting higher-temperature band gaps up to 870 K. We recommend using the Casey and Panish temperature dependence (with a corrected value of E_g at $T=0$) if one's interest is primarily in the temperature range from 0 K to somewhat above room temperature. However, the Lautenschlager *et al.*[211] and Hang *et al.*[212] forms are more appropriate at temperatures well above 300 K.

There are greater uncertainties in the positions of the X-valley and L-valley conduction-band minima in InP. The L-valley minimum is believed to lie 0.4–0.7 eV above the Γ-valley minimum, with the most reliable values favoring an approximately 0.6 eV separation. The temperature dependence is unclear.[1,4,11,201] The $\Gamma-X$ separation has been studied more closely,[1] and the different works have been compared in detail.[213] The inferred low-temperature value is 0.96 eV, with $dE_{\Gamma-X}/dT=-0.37$ meV/K. The spin-orbit splitting was determined as $\Delta_{so}=0.108$ eV by wavelength-modulated reflection[214] and photovoltaic effect[207] measurements.

The Γ-valley electron effective mass in InP has been investigated in great detail by cyclotron resonance, magnetophonon resonance, and magnetospectroscopy of donor transitions. While values have spanned the range $0.068-0.084m_0$.[97,98,108,173,207,215–225] if early and ambiguous determinations are excluded and the polaron correction is estimated to retrieve the bare mass,[99,218] the reasonable range for $m_e^*(T=0)$ narrows to $0.077-0.081m_0$. Averaging the results from different groups, we obtain $m_e^*(T=0)=0.0795m_0$, which is slightly smaller than the typically recommended values of $0.080-0.081m_0$.[1,10] The effective masses for the L and X valleys are taken from Pitt,[213] although there is some controversy on this point and a different set of parameters was given by Levinshtein *et al.*[11]

Luttinger parameters for InP have been measured using cyclotron resonance,[198] magnetoreflectance,[109,226] the piezo-modulated photovoltaic effect,[207] and magnetoabsorption.[227] Furthermore, the valence-band warping was accurately determined by Alekseev *et al.* using hot-carrier photoluminescence,[228,229] and theoretical calculations have also been performed.[101,106] In arriving at our composite parameters, we follow the procedure of averaging the reported values for heavy-hole and light-hole masses along the [100] and [111] directions. The resulting set of $\gamma_1=5.08$, $\gamma_2=1.60$, and $\gamma_3=2.10$ is in good agreement with all of the most reliable experimental results. The split-off hole mass was measured by Rochon and Fortin[207] to be $0.21m_0$.

TABLE VI. Band structure parameters for InP.

Parameters	Recommended values	Range
a_{lc} (Å)	$5.8697+2.79\times10^{-5}(T-300)$	···
E_g^Γ (eV)	1.4236	1.420–1.432
$\alpha(\Gamma)$ (meV/K)	0.363	0.51–1.06
$\beta(\Gamma)$ (K)	162	190–671
E_g^X (eV)	$2.384-3.7\times10^{-4}T$	1.48–2.39
E_g^L (eV)	2.014	1.82–2.12
$\alpha(L)$ (meV/K)	0.363	···
$\beta(L)$ (K)	162	···
Δ_{so} (eV)	0.108	0.108–0.13
$m_e^*(\Gamma)$	0.0795	0.068–0.084
$m_{DOS}^*(L)$	0.47	0.25–0.47
$m_{DOS}^*(X)$	0.88	0.32–0.88
γ_1	5.08	4.61–6.28
γ_2	1.60	0.94–2.08
γ_3	2.10	1.62–2.76
m_{so}^*	0.21	0.17–0.21
E_P (eV)	20.7	16.6–20.7
F	−1.31	0.–(−1.31)
VBO (eV)	−0.94	···
a_c (eV)	−6.0	−3.4–(−21)
a_v (eV)	−0.6	−0.4–(−7.1)
b (eV)	−2.0	−1.0–(−2.0)
d (eV)	−5.0	−4.2–(−5.0)
c_{11} (GPa)	1011	···
c_{12} (GPa)	561	···
c_{44} (GPa)	456	···

Lawaetz[106] and Gorczyca *et al.*[118] calculated the interband matrix element E_P in InP to be close to 20 eV. This result is in good agreement with the value of 20.7 eV proposed by Hermann and Weisbuch.[116] However, a number of other experimental determinations have favored a value close to 16.5 eV.[96,117,207,219,223] This discrepancy is easily resolved once it is realized that the majority of references did not consider remote-band effects on the electron mass. The difference between the results of Hermann and Weisbuch[116] and Shantharama *et al.*[96] has already been discussed in connection with the interband matrix element for GaAs. We adopt the former value of $E_P=20.7$ for InP, which implies $F=-1.31$ (the latter result would imply $F\approx0$), although a more detailed examination of this issue is called for in view of the large divergence between the two results.

There is a great deal of variation in the experimental and theoretical deformation potentials for InP as compiled by Adachi.[4] The most reliable values for the conduction-band deformation potential are probably those of Nolte *et al.*[127] (−7 eV) and Van de Walle[129] (−5.04 eV). In combination with the reported direct-gap deformation potential of −6.6 eV,[1] these values imply a rather small shift in the valence band. The shear deformation potentials b and d have been determined by Camassel *et al.*[214] and are in good agreement with exciton reflectance measurements.[230]

All of the band structure parameters for InP are collected in Table VI.

G. GaSb

GaSb is often referred to an intermediate-gap semiconductor, i.e., its gap of ≈0.8 eV is neither as wide as in GaAs

Downloaded 26 Aug 2001 to 128.42.12.177. Redistribution subject to AIP license or copyright, see http://ojps.aip.org/japo/japcr.jsp

and InP nor as narrow as in InAs and InSb. Since GaSb forms an increasingly important component of mid-infrared optoelectronic devices,[155] its various alloys have been investigated in some detail. Dutta *et al.* have recently published a comprehensive review of the material and structural properties of GaSb.[231]

Photoluminescence measurements on high-purity layers grown by liquid-phase epitaxy yielded a free exciton transition energy of 0.810 eV at 16 K.[232] Correcting for the exciton binding energy and extrapolating the temperature, we obtain $E_g(T=0)=0.812$ eV, which agrees to within 1 meV with earlier determinations[1] and also with the recent transmission measurements of Ghezzi *et al.*[233] Varshni parameters for the direct gap have been given by Casey and Panish,[2] Wu and Chen ($0<T<215$ K),[232] Ghezzi *et al.*,[233] Bellani *et al.*,[234] and Joullie *et al.*[235] (numerical values used in that work are given in Ref. 231). The four results that fit the data to room temperature are in excellent agreement with each other, and recommended values have been obtained by simply averaging the Varshni parameters α and β.

At low temperatures, the L valley in GaSb is only 0.063–0.100 meV higher than the Γ valley.[1,11,231,235,236,237] The values near the bottom of that range, which were obtained by electroreflectance[235] and modulation spectroscopy,[236] appear to be the most reliable. The temperature dependence of the L-valley minimum is known to be stronger than that of the Γ valley.[11,236] The position and temperature dependence of the X-valley minimum were determined by Lee and Woolley,[238] although there was some spread in the earlier reports.[1] The spin-orbit splitting was measured by a number of techniques,[1] with a value of 0.76 eV[236] being commonly accepted.

The Γ-valley band-edge electron mass in GaSb has been studied by a variety of techniques,[175,233,239–245] which produced low-temperature values in the rather narrow range of $0.039-0.042m_0$. The smallness of the spread is rather surprising in consideration of the indirect nature of many of the determinations, which are complicated by the relatively strong conduction-band nonparabolicity in GaSb. Once again, care must be taken to separate results for the polaron and bare effective masses, although as is often the case the polaron correction is no greater than the experimental uncertainty. Averaging produces a bare effective mass of $m_e^*=0.039m_0$ at 0 K. Somewhat higher values for the effective mass have been calculated theoretically.[100–106]

Owing to the small $\Gamma-L$ energy separation in GaSb and the much lower density of states at the Γ minimum, at room temperature a significant fraction of the electrons occupy L-valley states. Effective masses for those states were measured by cyclotron resonance,[11,244,245] Faraday rotation,[1] and piezoresistance.[1] On the basis of these results, we form composite values of $m_l^*=0.10m_0$ and $m_t^*=1.3m_0$. A large nonparabolicity at the L point has also been reported.[245] Effective masses for the X valley are taken from Levinshtein *et al.*[11]

The Luttinger parameters for GaSb have been determined using a number of experimental and theoretical approaches.[106,239,240,242,243,246,247] On the basis of these results, we suggest the composite values $\gamma_1=13.4$, $\gamma_2=4.7$, and $\gamma_3=6.0$, which are weighted toward the more recent experiments, but are also quite close to the ones typically used in the literature.[248] The split-off hole mass in GaSb was measured by Reine *et al.*[239]

TABLE VII. Band structure parameters for GaSb.

Parameters	Recommended values	Range
a_{lc} (Å)	$6.0959+4.72\times10^{-5}(T-300)$	···
E_g^Γ (eV)	0.812	0.811–0.813
$\alpha(\Gamma)$ (meV/K)	0.417	0.108–0.453
$\beta(\Gamma)$ (K)	140	−10–186
E_g^X (eV)	1.141	1.12–1.242
$\alpha(X)$ (meV/K)	0.475	···
$\beta(X)$ (K)	94	···
E_g^L (eV)	0.875	0.871–0.92
$\alpha(L)$ (meV/K)	0.597	···
$\beta(L)$ (K)	140	···
Δ_{so} (eV)	0.76	0.749–0.82
$m_e^*(\Gamma)$	0.039	0.039–0.042
$m_l^*(L)$	1.3	1.1–1.4
$m_t^*(L)$	0.10	0.085–0.14
$m_l^*(X)$	1.51	···
$m_t^*(X)$	0.22	···
γ_1	13.4	11–14.5
γ_2	4.7	3–5.3
γ_3	6.0	4.4–6.6
m_{so}^*	0.12	0.12–0.14
E_P (eV)	27.0	···
F	−1.63	···
VBO (eV)	−0.03	···
a_c (eV)	−7.5	···
a_v (eV)	−0.8	···
b (eV)	−2.0	···
d (eV)	−4.7	···
c_{11} (GPa)	884.2	···
c_{12} (GPa)	402.6	···
c_{44} (GPa)	432.2	···

The interband matrix element for GaSb has been estimated by several workers.[116,239–243] Here the band structure is more sensitive to the adopted value of E_P than in most materials, because the energy gap is nearly equal to the split-off gap. Therefore, instead of using the result of Hermann and Weisbuch,[116] we determine a composite value $E_P=27.0$ eV, which is within the experimental uncertainty of nearly all the reports. This composite implies $F=-1.63$, which is quite close to the results of Reine *et al.*[239] and Roth and Fortin.[243]

An average value for the direct-gap deformation potential $a=-8.3$ eV was determined for GaSb by uniaxial stress and transmission experiments.[1] We adopt the Van de Walle[129] suggestion for the valence-band potential of $a_v=-0.8$ eV, and adjust his a_c slightly to produce the consistent value of a. There is good agreement between various measurements of the shear deformation potentials in GaSb, as summarized in Landolt–Bornstein.[1]

All of the band structure parameters for GaSb are collected in Table VII.

H. AlSb

AlSb is an indirect-gap semiconductor with a lattice constant only slightly larger than that of GaSb. In recent years it

Downloaded 26 Aug 2001 to 128.42.12.177. Redistribution subject to AIP license or copyright, see http://ojps.aip.org/japo/japcr.jsp

has found considerable use as the barrier material in high-mobility electronic[154] and long-wavelength optoelectronic[155] devices. The direct gap in AlSb was measured using modulation spectroscopy by Alibert *et al.*,[236] spectroscopic ellipsometry by Zollner *et al.*,[249] and also using other methods.[1] Bulk AlSb samples were found to exhibit a gap of 2.35–2.39 eV at liquid-helium temperature, and a T dependence similar to that in GaSb. The conduction-band minima ordering is believed to be the same as in GaP and AlAs: X–L–Γ, with the L valley only 60–90 meV above the Γ valley[236] (also quite similar to GaSb). The indirect gap associated with the lowest X valley was investigated by Sirota and Lukomskii,[250] Mathieu *et al.*,[251] and Alibert *et al.*[236] It has been suggested[1] that early estimates of the band gap needed to be revised, since the exciton binding energy is 19 meV[252] instead of the assumed value of 10 meV.[250] We employ the resulting low-temperature value given in Landolt–Bornstein,[1] along with composite Varshni parameters. The spin-orbit splitting is taken from Alibert *et al.*,[236] which falls near the data compiled in Landolt–Bornstein.[1]

The electron mass in the Γ valley was measured using hot-electron luminescence.[253] While the L-valley and X-valley effective masses have been calculated,[1,254] there appear to be no definitive measurements. It is likely that the X valley in AlSb exhibits a camel's back structure by analogy with AlAs and GaP. Little information is available on the hole masses in AlSb.[253,255] We form our composite values of the Luttinger parameters on the basis of theoretical studies[101,106,182,254] in conjunction with literature values for the hole masses. The interband matrix element is taken from Lawaetz,[106] and the split-off mass is taken to be consistent with Eq. (2.18), although it could be argued that both parameters have a high degree of uncertainty.

The deformation potentials in AlSb were measured at 77 K using a wavelength modulation technique.[256] Once again, we take the valence-band hydrostatic deformation potential calculated by Van de Walle,[129] and make the rest of the results consistent with what appears to be the sole experimental determination.

All of the band structure parameters for AlSb are collected in Table VIII.

TABLE VIII. Band structure parameters for AlSb.

Parameters	Recommended values	Range
a_{lc} (Å)	$6.1355+2.60\times10^{-5}(T-300)$	···
E_g^Γ (eV)	2.386	2.35–2.39
$\alpha(\Gamma)$ (meV/K)	0.42	···
$\beta(\Gamma)$ (K)	140	···
E_g^X (eV)	1.696	1.68–1.70
$\alpha(X)$ (meV/K)	0.39	···
$\beta(X)$ (K)	140	···
E_g^L (eV)	2.329	2.327–2.329
$\alpha(L)$ (meV/K)	0.58	···
$\beta(L)$ (K)	140	···
Δ_{so} (eV)	0.676	···
$m_e^*(\Gamma)$	0.14	0.09–0.18
$m_l^*(L)$	1.64	···
$m_t^*(L)$	0.23	···
$m_l^*(X)$	1.357	···
$m_t^*(X)$	0.123	···
γ_1	5.18	4.15–5.89
γ_2	1.19	1.01–1.29
γ_3	1.97	1.75–2.25
m_{so}^*	0.22	···
E_P (eV)	18.7	···
F	−0.56	···
VBO (eV)	−0.41	···
a_c (eV)	−4.5	···
a_v (eV)	−1.4	···
b (eV)	−1.35	···
d (eV)	−4.3	···
c_{11} (GPa)	876.9	···
c_{12} (GPa)	434.1	···
c_{44} (GPa)	407.6	···

I. InSb

InSb is the III–V binary semiconductor with the smallest band gap. For many years it has been a touchstone for band structure computational methods,[257] partly because of the strong band mixing and nonparabolicity that result from the small gap. The primary technological importance of InSb arises from mid-infrared optoelectronics applications.[258]

Numerous studies of the fundamental energy gap and its temperature dependence have been conducted over the last 3 decades.[1,2,11,160,161,164,243,259–264] While there is a broad consensus that $E_g(T=0)=0.235$ eV, several different sets of Varshni parameters have been proposed.[2,164,259,264,265] Averaging parameters from the most reliable references, we obtain the composite set: $\alpha=0.32$ meV/K and $\beta=170$ K. The L- and X-valley energies are taken from Adachi.[166] The spin-orbit splitting energy was measured to be 0.81–0.82 eV.[183,260]

Experimental and theoretical studies have found band-edge electron masses for InSb in the range $0.012-0.015m_0$.[95,106,168,171,260,262,265–275] A bare effective mass of $0.0135m_0$ at 0 K is in good agreement with a majority of the investigations. On the other hand, little information on the effective masses in the indirect valleys is available. Levinshtein *et al.* quotes a density-of-states effective mass of $0.25m_0$ for the L valley.[11] We have found no explicit theoretical or experimental results for the X-valley effective masses, although in principle it should be possible to extract them from pseudopotential calculations that have already been performed for bulk InSb.

A wide variety of experimental and theoretical techniques such as magnetophonon resonance and other magneto-optical approaches have been employed to investigate the valence-band structure of InSb.[106,168,243,265,266,269,276–282] By averaging the values for γ_1, $m_{hh}^*(001)$, and $m_{hh}^*(111)$, we deduce the composite set: $\gamma_1=34.8$, $\gamma_2=15.5$, $\gamma_3=16.5$. These parameters are in good agreement with the majority of the values found in the cited references. Owing to the narrow energy gap, the light-hole effective mass in InSb is only slightly larger than the electron mass.[168,260,265,267,282,283] The split-off hole mass is estimated to be $0.10-0.11m_0$.[106,260]

Our composite interband matrix element for InSb is 23.2 eV.[106,118,263,269,284] A slightly higher value was deduced by

Downloaded 26 Aug 2001 to 128.42.12.177. Redistribution subject to AIP license or copyright, see http://ojps.aip.org/japo/japcr.jsp

TABLE IX. Band structures parameters for InSb.

Parameters	Recommended values	Range
a_{lc} (Å)	$6.4794+3.48\times10^{-5}(T-300)$	...
E_g^{Γ} (eV)	0.235	...
$\alpha(\Gamma)$ (meV/K)	0.32	0.299–0.6
$\beta(\Gamma)$ (K)	170	106–500
E_g^X (eV)	0.63	...
E_g^L (eV)	0.93	...
Δ_{so} (eV)	0.81	0.8–0.9
$m_e^*(\Gamma)$	0.0135	0.012–0.015
$m_{DOS}^*(L)$	0.25	...
γ_1	34.8	32.4–38.5
γ_2	15.5	13.4–18.1
γ_3	16.5	15.15–18
m_{so}^*	0.11	...
E_P (eV)	23.3	...
F	−0.23	...
VBO (eV)	0	...
a_c (eV)	−6.94	...
a_v (eV)	−0.36	...
b (eV)	−2.0	...
d (eV)	−4.7	...
c_{11} (GPa)	684.7	...
c_{12} (GPa)	373.5	...
c_{44} (GPa)	311.1	...

Hermann and Weisbuch,[116] possibly due to an overestimate of the effective g factor. Somewhat lower values for E_P are also encountered in the literature.[243,260] Our corresponding F parameter (−0.23) is close to other determinations.[243,284]

The deformation potentials in InSb have been studied by various optical and electrical techniques.[1,285,286] For the total hydrostatic deformation potential, we take an average value of −7.3 eV. According to the model-solid calculations of Van de Walle,[129] the valence-band deformation potential is rather small by analogy with the other III–V materials. There appears to be a consensus on values for the shear deformation potentials in InSb: $b=-2.0$ and $d=-4.7$.[1,285–287]

All of the recommended band structure parameters for InSb are given in Table IX.

J. GaN

GaN is a wide-gap semiconductor that usually crystallizes in the wurtzite lattice (also known as hexagonal or α-GaN). However, under certain conditions zinc blende GaN (sometimes referred to as cubic or β-GaN) can also be grown on zinc blende substrates under certain conditions. Under very high pressure, GaN and other nitrides experience a phase transition to the rocksalt lattice structure.[288] If the crystal structure of a nitride semiconductor is not stated in what follows, the wurtzite phase is implied, whereas the zinc blende phase is always explicitly specified. A review of the physical properties of GaN and other group-III nitride semiconductors up to 1994 was edited by Edgar.[289] The status of GaN work in the 1970's was summarized in two reviews[290,291] as well as in Landolt-Bornstein.[1] For a comprehensive recent review of the growth, characterization, and various properties of nitride materials, we refer the reader to the article by Jain *et al.*[292]

1. Wurtzite GaN

Unlike any of the non-nitride wide-gap III–V semiconductors discussed above, GaN is a direct-gap material, which has led to its successful application in blue lasers and LEDs.[293] It has been known since the early 1970's that the energy gap in wurtzite GaN is about 3.5 eV.[294,295] However, a precise determination from luminescence experiments is not straightforward, since what is usually measured at cryogenic temperatures are the energies for various pronounced exciton transitions. The identification of these closely spaced resonances is nontrivial. For example, at very low temperatures, the lowest-order A, B, and C exciton types related to the three valence bands can be resolved, as well as higher-order $A(2s,2p)$ exciton transitions.[296] The situation is further complicated by the excitons bound to various impurities, such as neutral donors.[290] All of these considerations contribute to the rather large experimental uncertainty in the bare direct energy gap at low temperatures.

Early measurements of the temperature-dependent direct gap in wurtzite GaN, which are still the most frequently quoted in the nitride device literature, were performed by Monemar.[297,298] Those experiments yielded a free-A-exciton transition energy of 3.475 eV and an estimate of 28 meV for the binding energy. Numerous other PL and absorption studies were published in the 1990s,[296,299–308] which broadened the range of reported A-exciton transition energies at 0 K to 3.474–3.507 eV. It has been suggested that this spread is due to variations of the strain conditions present in the different experiments.[309] If we average all of the available experimental values, an exciton transition energy of 3.484 eV is obtained. Experimental binding energies for the A exciton range from 18 to 28 meV.[296,298,302,303,306,310–312] An accurate theoretical determination[313] is out of reach at present owing to the large uncertainty in the reduced mass (primarily associated with the poorly known hole effective mass). We therefore average the most reliable experimental binding energies deduced from the difference between the ground-state and first-excited-state energies of the A exciton.[296,302,303,306,308,310,311] This gives 23 meV for the exciton binding energy, which implies 3.507 eV for the zero-temperature energy gap.

The temperature dependence of the GaN energy gap was first reported by Monemar,[298] who obtained $\alpha=-0.508$ meV/K and $\beta=-996$ K. While the signs of his Varshni coefficients are opposite to all of the other materials considered in this review, a large number of subsequent studies have derived less anomalous results. From optical absorption measurements on bulk and epitaxial layers grown on sapphire, Teisseyre *et al.*[314] obtained $\alpha=0.939-1.08$ meV/K and $\beta=745-772$ K. For the temperature variation of the A exciton resonance, Shan *et al.* reported $\alpha=0.832$ meV/K and $\beta=836$ K.[299] Petalas *et al.*[315] fixed $\beta=700$ K and found $\alpha=0.858$ meV/K using spectroscopic ellipsometry. Salvador *et al.*[316] obtained $\alpha=0.732$ meV/K and $\beta=700$ K based on PL results. Manasreh[304] reported $\alpha=0.566-1.156$ meV/K and $\beta=738-1187$ K from absorption measurements on samples grown by MBE and metalorganic chemical vapor deposition. The contactless electroreflectance study of Li *et al.*[307] led to $\alpha=1.28$ meV/K and $\beta=1190$ K

Downloaded 26 Aug 2001 to 128.42.12.177. Redistribution subject to AIP license or copyright, see http://ojps.aip.org/japo/japcr.jsp

for the A exciton transition energy. Finally, Zubrilov *et al.*[317] suggested $\alpha = 0.74$ meV/K and $\beta = 600$ K based on exciton luminescence spectra. It is not obvious how to reconcile these diverse parameter sets, especially since in several cases considerably different values are inferred even in the same study. Much of the difficulty stems from the fact that the resonances dominating the exciton spectra at low temperatures are not readily distinguishable at ambient temperature. Our recommended Varshni parameters represent a simple average of the various reported values except the anomalous results of Monemar.[298] This yields $\alpha = 0.909$ meV/K and $\beta = 830$ K, which are in good agreement with the parameters suggested by absorption measurements on AlGaN (a negligible composition dependence was reported).[318] It is fortunate that owing to the small relative change in the band gap energy (only 72 meV between 0 and 300 K), the precise choice of Varshni parameters has only a modest impact on the device characteristics.

The indirect energy gaps in GaN are much larger than the direct gap. Few studies have attempted to resolve them, although various estimates of the critical points are available from theory and experiment.[1,290,319–323] Considering the huge uncertainties in the indirect gaps and their lack of importance to device applications, we do not recommended values for the wurtzite forms of the nitride materials. Zinc blende indirect gaps are specified in the tables, however, because they are smaller and somewhat better known.

In contrast to most zinc blende materials, for which only the spin-orbit splitting must be specified, in wurtzite materials the crystal-field splitting is at least as important and cannot be ignored if one wishes to recover a realistic description of the valence-band states (see Sec. II for details).[324] In the following, we take $\Delta_2 = \Delta_3 = \Delta_{so}/3$ and $\Delta_1 = \Delta_{cr}$. An early study of Dingle *et al.* found $\Delta_{cr} = 22$ meV and $\Delta_{so} = 11$ meV.[294] A more recent and detailed analysis by Gil *et al.* yielded the values $\Delta_{cr} = 10$ meV and $\Delta_{so} = 18$ meV.[301] Reynolds *et al.* obtained $\Delta_{cr} = 25$ meV and $\Delta_{so} = 17$ meV from a fit of their exciton data.[311] Using a more precise description of the strain variation of the valence band-edge energies, Chuang and Chang reanalyzed the Gil *et al.* data and derived $\Delta_{cr} = 16$ meV and $\Delta_{so} = 12$ meV.[325] From a similar approach, Shikanai *et al.* obtained $\Delta_{cr} = 22$ meV and $\Delta_{so} = 15$ meV from their own data. *Ab initio* theoretical calculations[326] support a rather small value for the spin-orbit splitting ($\leqslant 10$ meV), but tend to overestimate the crystal-field splitting. To obtain our recommended set of $\Delta_{cr} = 19$ meV and $\Delta_{so} = 14$ meV, we averaged all of the reported values with the exception of those from the first-principles theory.

The bottom of the conduction band in GaN is well approximated by a parabolic dispersion relation, although a slight anisotropy (resulting from the reduced lattice symmetry) is not ruled out.[327] In early studies, Barker and Illegems[328] obtained an effective mass of $0.20m_0$ from plasma reflection measurements, Rheinlander and Neumann[329] inferred $0.27m_0$ from the Faraday rotation, and Sidorov *et al.*[330] derived values of $0.1m_0$–$0.28m_0$, depending on what primary scattering channel was assumed, from fits to the thermoelectric power. Other early values may be found in the reviews from the 1970s.[291,290] However, a considerable body of recent work has led to more precise evaluations of the effective mass. Meyer *et al.*[331] and Witowski *et al.*[332] used measurements of the shallow-donor transition energies to obtain masses of $0.236m_0$ and $0.222m_0$, respectively. The latter result has the smallest error bounds quoted in the literature (0.2%). Drechsler *et al.* pointed out the importance of the polaron correction in GaN since it is so strongly polar (10%), and derived a bare mass of $0.20m_0$ from cyclotron resonance measurements.[333] Perlin *et al.*[334] obtained similar results using infrared-reflectivity and Hall-effect measurements, and additionally found the anisotropy to be less than 1%. A slightly higher dressed mass of $0.23m_0$ was recently obtained by Wang *et al.*[335] and Knap *et al.* The former may require a slight downward revision because the electron gas was confined in a quantum well, whereas the latter report apparently corrected for that effect.[336] No appreciable correction appears to be necessary for the measurement by infrared ellipsometry on bulk n-doped GaN reported by Kasic *et al.*,[337] in which a marginally anisotropic electron effective mass with the values of $0.237 \pm 0.006m_0$ and $0.228 \pm 0.008m_0$ along the two axes was obtained. Finally, Elhamri *et al.*,[338] Saxler *et al.*,[339] Wong *et al.*,[340] and Wang *et al.*[341] determined masses ranging from $0.18m_0$ to $0.23m_0$ from Shubnikov–de Haas oscillations in the two-dimensional (2D) electron gas at a GaN/AlGaN heterojunction. It was suggested[338] that strain effects may have to some extent compromised the masses obtained by some of the other studies. Our recommendation of $0.20m_0$ for the bare mass is close to the consensus from the investigations of bulk materials, and to the average from the studies of 2D electrons.

The experimental information presently available is sufficient only to suggest an approximate band-edge effective mass for the holes. Factors contributing to this uncertainty include strong nonparabolicity near the valence-band edge and the close proximity of heavy-, light-, and crystal-hole bands [see the schematic diagram in Fig. 4(b)].[325] In order to derive the various parameters needed to characterize the valence band of a wurtzite material, one must resort to theoretical projections.[327,342] In the cubic approximation, these parameters may also be recast in terms of the Luttinger parameters familiar from the case of the zinc blende materials.[324] While early work suggested a GaN hole effective mass of $0.8m_0$.[290,343,344] consideration of the acceptor binding energies led Orton[345] to suggest a much smaller value of $0.4m_0$. An even smaller mass of $0.3m_0$ was obtained by Salvador *et al.* from a fit to the PL results.[316] On the other hand, the excess-carrier lifetime measurements of Im *et al.* indicated a very heavy hole mass of $2.2m_0$.[305] Merz *et al.* obtained an isotropically averaged heavy-hole mass of $0.54m_0$ from luminescence data.[303] Fits of the exciton binding energies yielded hole masses in the range 0.9–$1.2m_0$.[308,346] Finally, an infrared ellipsometric study by Kasic *et al.* yielded a hole mass of $1.4m_0$ for p-doped GaN.[337] It should be pointed out that most of these experimental values are somewhat lower than the theoretical masses derived by Suzuki *et al.*,[327] which are commonly used in band structure calculations, and are much lower than

Downloaded 26 Aug 2001 to 128.42.12.177. Redistribution subject to AIP license or copyright, see http://ojps.aip.org/japo/japcr.jsp

the pseudopotential results of Yeo *et al.*[323] On the other hand, first-principles calculations by Chen *et al.* produced a smaller density-of-states effective mass of $0.6m_0$.[302] An alternative set of effective-mass parameters was recently calculated from a pseudopotential model by Dugdale *et al.*[347] Their electron mass is lower than the experimental results, which may indicate lower accuracy of the A parameters. Yet another parameter set was extracted from empirical pseudopotential calculations by Ren *et al.*[38] That work succeeded in theoretically extracting the inversion parameter $A_7 = 93.7$ meV/Å from a comparison with empirical pseudopotential calculations. Our recommendation is to use the effective-mass parameters of Suzuki *et al.*,[327] which imply an average hole mass approximately equal to the free electron value (m_0). It is hoped that a theoretical band structure picture that is fully consistent with the recent experimental results will be developed in the near future.

In principle, there are two independent momentum matrix elements in wurtzite GaN. However, the assumption that the electron mass anisotropy is small implies that these are nearly equal. Insofar as no information is available on the effects of remote bands on the wurtzite GaN band structure, that interaction is neglected. If one then derives an interband matrix element directly from the electron effective mass, the result is $E_P = 14$ eV($F = 0$). While there is one report[305] of $E_P = 7.7$ eV in wurtzite GaN, that would imply a unrealistic positive F parameter.

Six distinct valence-band deformation potentials, in addition to the strain tensor and the overall hydrostatic deformation potential, are necessary to describe the band structure of GaN under strain. Using the cubic approximation, these can be re-expressed in terms of the more familiar a_v, b, and d potentials.[324] Christensen and Gorczyca[319] reported a hydrostatic deformation potential $a = -7.8$ eV, which is in good agreement with fits to the data of Gil *et al.* (−8.16 eV).[301] A somewhat lower $a = -6.9$ eV was derived from an *ab initio* calculation by Kim *et al.*[348] Shan *et al.*[349] noted that the hydrostatic deformation potential should be anisotropic due to the reduced symmetry of the wurtzite crystal, and gave the values: $a_1 = -6.5$ eV and $a_2 = -11.8$ eV for the two components. These are our recommended values. Numerous sets of valence-band deformation potentials have been derived from both first-principles calculations[325,342,350] and fits to experimental data.[301,306,349] There are considerable discrepancies between the reported data, with variations of nearly a factor of 6 in some cases. Obviously, further work is needed to resolve this controversy. We form our composite set of deformation potentials by selecting those values that seem to be most representative of the majority of results: $D_1 = -3.0$ eV,[350] $D_2 = 3.6$ eV,[350] $D_3 = 8.82$ eV,[306] $D_4 = -4.41$ eV,[306] $D_5 = -4.0$ eV,[350] and $D_6 = -5.1$ eV (derived by adopting the cubic approximation[325]).

The determination of elastic constants for wurtzite GaN has been reviewed by Wright,[351] who compared the results of a number of experiments[352–355] with two calculations.[348,351] Overall, theory agrees best with the data of Polian *et al.*,[353] who obtained the recommended values: $C_{11} = 390$ GPa, $C_{12} = 145$ GPa, $C_{13} = 106$ GPa, $C_{33} = 398$ GPa, and $C_{44} = 105$ GPa. However, there are significant disagreements between the various experimental results, so that in contrast to the zinc blende materials the elastic constants for GaN remain somewhat controversial.

Very few measurements of the piezoelectric coefficients in GaN have been reported. Guy *et al.*[356,357] performed a careful study, which pointed out the differences between the coefficients in a bulk material versus a strained thin film. Coefficients of $d_{33} = 3.7$ pm/V and $d_{13} = -1.9$ pm/V were deduced for the bulk GaN from the single-crystal thin-film value $d_{33} = 2.8$ pm/V and the relation $d_{13} = -d_{33}/2$. Another measurement by Lueng *et al.* yielded a thin-film value $d_{33} = 2.13$ pm/V.[358] The latter measurement had the inherent uncertainty of an AlN buffer layer being present. Bykhovski *et al.* attempted to derive the e_{31} and e_{33} coefficients from the e_{14} coefficient in zinc blende GaN, obtaining values of $e_{31} = -0.22$ C/m^2 and $e_{33} = 0.43$ C/m^2.[359] Bernardini *et al.* employed a first-principles calculation to derive $e_{31} = -0.49$ C/m^2 and $e_{33} = 0.73$ C/m^2.[360] A calculation of Shimada *et al.* yielded values of $e_{31} = -0.32$ C/m^2 and $e_{33} = 0.63$ C/m^2.[361] We recommend using the d coefficients from the experimental study of Guy *et al.* and use the assumed elastic constants to obtain the e coefficients: $e_{31} = -0.35$ C/m^2 and $e_{33} = 1.27$ C/m^2, which turn out to be somewhat different from those calculated in the original report.[357]

Only two first-principles calculations of the spontaneous polarization in GaN are available.[360,362] Very different values of $P_{sp} = -0.029$ C/m^2 and $P_{sp} = -0.074$ C/m^2 were reported. In one of the papers,[362] it was noted that the computed spontaneous polarization is highly sensitive to the values of the internal structure parameters such as the lengths of the atomic bonds. This consideration may prevent an accurate theoretical evaluation of the spontaneous polarization for realistic nitride structures. Since only *differences* in the spontaneous polarization are important in heterostructure band calculations, we defer a full discussion of the experimental probes of the spontaneous polarization in GaN/AlGaN quantum wells until the AlN section. The band structure parameters for wurtzite GaN are compiled in Table X.

2. Zinc blende GaN

A number of theoretical and experimental studies of the energy gap for the zinc blende phase of GaN have been reported.[315,363–371] Some works rely on an explicit comparison with the better understood case of wurtzite GaN, whereas the most accurate appear to come from low-temperature luminescence measurements[372–374] of the free-exciton peak, which is estimated to be 26.5 meV below the energy gap. Experimentally, the low-temperature energy gaps range from 3.2 to 3.5 eV, although the most reliable values fall approximately midway, between 3.29 and 3.35 eV.[365,367,368] We recommend a value of 3.299 eV obtained from averaging the results of the luminescence measurements. The temperature dependence of the energy gap was studied in detail by Ramirez-Flores *et al.*[368] and Petalas *et al.*[315] Although the two studies obtain the same $\beta = 600$ K (using the more reliable model 1 in Ref. 315), the α parameters are different, and we recommend using an average value of 0.593 meV/K. Although the indirect-gap energies have not been measured, a

Downloaded 26 Aug 2001 to 128.42.12.177. Redistribution subject to AIP license or copyright, see http://ojps.aip.org/japo/japcr.jsp

TABLE X. Recommended band structure parameters for wurtzite nitride binaries.

Parameters	GaN	AlN	InN
a_{lc} (Å) at $T=300$ K	3.189	3.112	3.545
c_{lc} (Å) at $T=300$ K	5.185	4.982	5.703
E_g (eV)	3.507	6.23	1.994
α (meV/K)	0.909	1.799	0.245
β (K)	830	1462	624
Δ_{cr} (eV)	0.019	−0.164	0.041
Δ_{so} (eV)	0.014	0.019	0.001
$m_e^{\parallel}$	0.20	0.28	0.12
$m_e^{\perp}$	0.20	0.32	0.12
A_1	−6.56	−3.95	−8.21
A_2	−0.91	−0.27	−0.68
A_3	5.65	3.68	7.57
A_4	−2.83	−1.84	−5.23
A_5	−3.13	−1.95	−5.11
A_6	−4.86	−2.91	−5.96
E_P (eV)	14.0	14.5	14.6
F	0	0	0
VBO (eV)	−2.64	−3.44	−1.59
a_1 (eV)	−6.5	−9.0	−3.5
a_2 (eV)	−11.8	−9.0	−3.5
D_1 (eV)	−3.0	−3.0	−3.0
D_2 (eV)	3.6	3.6	3.6
D_3 (eV)	8.82	9.6	8.82
D_4 (eV)	−4.41	−4.8	−4.41
D_5 (eV)	−4.0	−4.0	−4.0
D_6 (eV)	−5.1	−5.1	−5.1
c_{11} (GPa)	390	396	223
c_{12} (GPa)	145	137	115
c_{13} (GPa)	106	108	92
c_{33} (GPa)	398	373	224
c_{44} (GPa)	105	116	48
e_{13} (C/m^2)	−0.35	−0.50	−0.57
e_{33} (C/m^2)	1.27	1.79	0.97
P_{sp} (C/m^2)	−0.029	−0.081	−0.032

recent calculation of Fan *et al.* puts the X-valley and L-valley minima at 1.19 and 2.26 eV above the Γ valley, respectively.[369] Ramirez-Flores *et al.*[368] have measured the spin-orbit splitting in zinc blende GaN to be 17 meV.

Electron spin resonance measurements indicated an electron effective mass of $0.15m_0$ in zinc blende GaN.[375] Since this appears to be the only experimental result, we adopt it as our recommendation. Similar Γ-valley effective masses were derived from first-principles calculations by Chow *et al.*[376] and Fan *et al.*[369] Effective masses of $m_l^*=0.5m_0$ and $m_t^*=0.3m_0$ were recently calculated for the X valley in GaN,[370] which are similar to values obtained by Fan *et al.*[369] The convergence of results from two different studies allows us to adopt these as our recommended values.

Although the hole effective masses in zinc blende GaN have not been measured, a number of theoretical sets of Luttinger parameters are available.[369–378] In order to derive our recommended values, we average the heavy-hole and light-hole masses along [001] as well as the degree of anisotropy $\gamma_3-\gamma_2$. This results in the following parameter set: $\gamma_1=2.67$, $\gamma_2=0.75$, and $\gamma_3=1.10$. When all of the reported[369–371,379] split-off masses are averaged, we obtain $m_{so}^*=0.29m_0$.

TABLE XI. Recommended band structure parameters for zinc blende nitride binaries.

Parameters	GaN	AlN	InN
a_{lc} (Å) at $T=300$ K	4.50	4.38	4.98
E_g^{Γ} (eV)	3.299	4.9	1.94
$\alpha(\Gamma)$ (meV/K)	0.593	0.593	0.245
$\beta(\Gamma)$ (K)	600	600	624
E_g^X (eV)	4.52	6.0	2.51
$\alpha(X)$ (K)	0.593	0.593	0.245
$\beta(X)$ (meV/K)	600	600	624
E_g^L (eV)	5.59	9.3	5.82
$\alpha(L)$ (K)	0.593	0.593	0.245
$\beta(L)$ (meV/K)	600	600	624
Δ_{so} (eV)	0.017	0.019	0.006
$m_e^*(\Gamma)$	0.15	0.25	0.12
$m_l^*(X)$	0.5	0.53	0.48
$m_t^*(X)$	0.3	0.31	0.27
γ_1	2.67	1.92	3.72
γ_2	0.75	0.47	1.26
γ_3	1.10	0.85	1.63
m_{so}^*	0.29	0.47	0.3
E_P (eV)	25.0	27.1	25.0
F	−0.92	0.76	−0.92
VBO (eV)	−2.64	−3.44	−2.38
a_c (eV)	−2.2	−6.0	−1.85
a_v (eV)	−5.2	−3.4	−1.5
b (eV)	−2.2	−1.9	−1.2
d (eV)	−3.4	−10	−9.3
c_{11} (GPa)	293	304	187
c_{12} (GPa)	159	160	125
c_{44} (GPa)	155	193	86

Two theoretical values for E_P in zinc blende GaN have been reported in the literature.[371,379] An average of the two yields $E_P=25.0$ eV, which in turn implies $F=-0.92$. A note of caution is that these values have not been verified experimentally.

Various calculations put the hydrostatic deformation potential for zinc blende GaN in the range between −6.4 and −8.5 eV.[42,319,369,370,376,380] We choose an average value of $a=-7.4$ eV. The same procedure is followed in obtaining the recommended values of $a_v=-5.2$ eV (−0.69 to −13.6 eV range) and $b=-2.2$ eV (−1.6 to −3.6 eV range). The value of $d=-3.4$ eV is an average between the only published values from Ohtoshi *et al.*[380] and Van de Walle and Neugebauer.[381] No experimental confirmations of any of these deformation potentials for zinc blende GaN appear to exist. Elastic constants of $C_{11}=293$ GPa, $C_{12}=159$ GPa, and $C_{44}=155$ GPa are taken from the theoretical analysis of Wright.[351] Very similar sets were calculated by Kim *et al.*[382] and Bechstedt *et al.*[362] The band structure parameters for zinc blende GaN are compiled in Table XI.

K. AlN

Although binary AlN is rarely used in practical devices, it represents the end point for the technologically important AlGaN alloy. As in the case of GaN, both wurtzite and zinc blende forms of AlN can in principle be grown, although the growth of zinc blende AlN has not been reported. Wurtzite AlN has the distinction of being the only Al-containing III–V semiconductor compound with a direct energy gap.

Downloaded 26 Aug 2001 to 128.42.12.177. Redistribution subject to AIP license or copyright, see http://ojps.aip.org/japo/japcr.jsp

Furthermore, it is the largest-gap material that is still commonly considered to be a semiconductor. The absorption measurements of Yim *et al.*[383] and Perry and Rutz[384] indicate that the energy gap in wurtzite AlN varies from 6.28 eV at 5 K to 6.2 eV at room temperature. Varshni parameters of $\alpha = 1.799$ meV/K and $\beta = 1462$ K were reported by Guo and Yoshida, who also found the low-temperature gap to be 6.13 eV.[385] A similar energy gap was reported by Vispute *et al.*[386] With the aid of cathodoluminescence experiments, Tang *et al.*[387] resolved at 300 K what they believed to be the free or shallow-impurity-bound exciton, at an energy of 6.11 eV. We recommend an intermediate value of 6.23 eV for the low-temperature band gap, in conjunction with the Varshni parameters of Guo and Yoshida.[385] Although Brunner *et al.*[318] also reported Varshni parameters, the finding of no significant differences from GaN for the entire composition range of the AlGaN alloy may indicate that their results are somewhat less reliable.

The crystal-field splitting in AlN is believed to be negative, which implies that the topmost valence band is crystal hole-like. Suzuki *et al.*[327] calculated $\Delta_{cr} = -58$ meV, whereas Wei and Zunger[326] obtained $\Delta_{cr} = -217$ meV. Pugh *et al.*[371] cited values of -104 and -169 meV from first-principles and semiempirical pseudopotential calculations, respectively, and Kim *et al.*[388] obtained $\Delta_{cr} = -215$ meV. Averaging all of the available theoretical crystal-field splittings, we obtain our recommended value of $\Delta_{cr} = -164$ meV. Spin-orbit splittings ranging from 11[371] to 20 meV[327] have been cited in the literature. We adopt the value of 19 meV suggested by Wei and Zunger.[326] Again, it is important to emphasize that our recommendations for the crystal-field and spin-orbit splittings in AlN have only provisional status, since it appears that no experimental data exist.

A number of calculations are available for the electron effective mass in AlN.[327,371,388] A greater anisotropy than in wurtzite GaN is predicted.[327] The recommended values of $m_e^{\perp} = 0.28m_0$ and $m_e^{\parallel} = 0.32m_0$ were obtained by averaging all available theoretical masses, although it is again noted that experimental studies are needed to verify these calculations. We recommend the valence-band effective mass parameters of Suzuki *et al.*[327] An alternative set of A parameters was recently published by Dugdale *et al.*[347] The apparent disagreement in signs in various papers for A_5 and A_6 is ignored, since only absolute values of these parameters enter the Hamiltonian.[371,388]

The hydrostatic deformation potential for wurtzite AlN is believed to lie in the range between -7.1 and -9.5 eV.[319,348] We select a median value of -9.0 eV, which is consistent with the observation that the band gap pressure coefficients in AlGaN alloys have little dependence on composition.[389] Theoretical values are also available for a few of the valence-band deformation potentials ($D_3 = 9.6$ eV, $D_4 = -4.8$ eV).[348] The elastic constants in wurtzite AlN were measured by Tsubouchi *et al.*[390] and McNeil *et al.*[391] We recommend the values $C_{11} = 396$ GPa, $C_{12} = 137$ GPa, $C_{13} = 108$ GPa, $C_{33} = 373$ GPa, and $C_{44} = 116$ GPa suggested by Wright, who provides a detailed discussion of their expected accuracy.[351]

Several early measurements[392,393] of the piezoelectric coefficient in AlN were compiled in Ref. 357. That reference obtained $d_{33} = 5.6$ pm/V and $d_{13} = -2.8$ pm/V, which were rather similar to the previous determinations. The available calculations[360,361,394] are in reasonable agreement with the experimental values. Two rigorous calculations[360,362] of the spontaneous polarization in AlN have been performed with the reported results of $P_{sp} = -0.081$ C/m^2 and $P_{sp} = -0.12$ C/m^2. The effect of the spontaneous polarization on the optical properties of GaN/AlGaN quantum wells was observed by Leroux *et al.*[395,396] However, it was found that the results were consistent with a lower value for the spontaneous polarization in AlN($-0.051 < P_{sp} < -0.036$ C/m^2). A study of the charging of GaN/AlGaN field-effect transistors led to similar conclusions.[397] Hogg *et al.* were able to fit their luminescence data by assuming negligible spontaneous polarization.[398] Park and Chuang[399] required $P_{sp} = -0.040$ C/m^2 to reproduce their GaN/AlGaN quantum-well data. On the other hand, Cingolani *et al.* reported good agreement with experiment using the original Bernardini *et al.*[360] calculation.[400] The magnitude of the estimated spontaneous polarization is dependent on the assumed piezoelectric coefficients. It may be possible to explain the remaining discrepancy between the majority of the experimental investigations and the Bernardini *et al.* calculation if a linear interpolation of P_{sp} is invalid for the AlGaN alloy, due to either bowing or long-range ordering. At this juncture, we recommend the calculated value and note that the controversy will likely be resolved in future work. The recommended band structure parameters for wurtzite AlN are compiled in Table X.

Zinc blende AlN is projected to be an indirect-band gap material, with X-, Γ-, and L-valley gaps of 4.9, 6.0, and 9.3 eV, respectively.[319,369,371] The spin-orbit splitting is believed to be the same as in wurtzite AlN (19 meV).[326] Averaging the theoretical results from different sources,[369,371,378,379,388] we obtain the recommended Γ-valley effective mass of $0.25m_0$. The longitudinal and transverse masses for the X valley are predicted to be $0.53m_0$ and $0.31m_0$, respectively.[369] The same procedure employed for GaN yields the recommended Luttinger parameters:[369,371,378,379,388] $\gamma_1 = 1.92$, $\gamma_2 = 0.47$, and $\gamma_3 = 0.85$ ($m_{so} = 0.47m_0$). The momentum matrix element is taken to be an average of the reported values:[371,379] $E_P = 27.1$ eV ($F = 0.76$). Hydrostatic deformation potentials of -9.0 eV[319] and -9.8 eV[369] have been reported. Our recommended values for the deformation potentials are $a = -9.4$ eV, $a_v = -3.4$ eV,[42,369] $b = -1.9$ eV,[369,381] and $d = -10.0$ eV.[348,381] The elastic constants of $C_{11} = 304$ GPa, $C_{12} = 160$ GPa, and $C_{44} = 193$ GPa are adopted from the calculations of Wright.[351] Similar sets were quoted in other theoretical works.[362,382,401] The recommended band structure parameters for zinc blende AlN are compiled in Table XI.

L. InN

Although InN is rarely if ever used in devices in its binary form, it forms an alloy with GaN that is at the core of the blue diode laser.[293] Especially since some degree of seg-

Downloaded 26 Aug 2001 to 128.42.12.177. Redistribution subject to AIP license or copyright, see http://ojps.aip.org/japo/japcr.jsp

regation is believed to occur when that alloy is grown, it is important to understand the properties of bulk InN in its wurtzite phase. Osamura *et al.*[402] measured the energy gap at 78 K to be 2.0 eV (although for the purposes of the quadratic fit for GaInN, a different gap was stated in the abstract of that article), which became approximately 60 meV lower at room temperature. The absorption measurements of Puychevrier and Menoret[403] on polycrystalline InN indicated gaps of 2.21 and 2.09 eV at 77 and 300 K, respectively. Another set of absorption measurements by Tyagai *et al.*[404] yielded $E_g=2.05$ eV at 300 K. The result of Tansley and Foley,[405] $E_g=1.89$ eV at 300 K for high-purity InN thin films, is often quoted in the literature. It is judged more reliable than earlier experiments performed on samples with high electron densities. An even lower gap was obtained by Westra and Brett,[406] although in their case a high electron density was also present. Varshni parameters of $\alpha=0.245$ meV/K and $\beta=624$ K were reported by Guo and Yoshida[385] for wurtzite InN, along with low-temperature and room-temperature gaps of 1.994 and 1.97 eV, respectively. These values, which closely resemble a previous result from the same group,[407] represent our recommended temperature dependence. The recommended crystal-field and spin-orbit splittings of 41 and 1 meV, respectively, are taken from the calculation of Wei and Zunger.[326]

There appear to be only two measurements of the electron mass in InN, which found values of $0.11m_0$[404] and $0.12m_0$.[408] We recommend the latter, since it closely matches the theoretical projection.[321] Valence-band effective-mass parameters were calculated by Yeo *et al.*[323] using the empirical pseudopotential method, by Pugh *et al.*[371] and Dugdale *et al.*[347] using essentially the same techniques. The results of the first two studies are quite similar, and we recommend the parameters derived by Pugh *et al.*[371]

Christensen and Gorczyca predicted a hydrostatic deformation potential of -4.1 eV for wurtzite InN,[319] although a smaller value of -2.8 eV was calculated by Kim *et al.*[348] We recommend the average of $a=-3.5$ eV. Since apparently there have been no calculations of the valence-band deformation potentials, we recommend appropriating the set specified above for GaN. While elastic constants were measured by Sheleg and Savastenko,[352] we recommend the improved set of Wright:[351] $C_{11}=223$ GPa, $C_{12}=115$ GPa, $C_{13}=92$ GPa, $C_{33}=224$ GPa, and $C_{44}=48$ GPa. The piezoelectric coefficients and spontaneous polarization for InN are taken from the calculation by Bernardini *et al.*[360] The recommended band structure parameters for wurtzite InN are compiled in Table X.

Although the growth of zinc blende InN has been reported,[409] only theoretical estimates are available for any of its band parameters. It is predicted to be a direct-gap material, with Γ-, X-, and L-valley gaps of 1.94, 2.51, and 5.82 eV, respectively.[370] The spin-orbit splitting is projected to be 6 meV.[326] We recommend an electron effective mass identical to that in wurtzite InN, $0.12m_0$, which is in the middle of the range $0.10-0.14m_0$ that has been calculated.[370,371,379] The longitudinal and transverse masses for the X valley are predicted to be $0.48m_0$ and $0.27m_0$, respectively.[370] The recommended Luttinger parameter set: $\gamma_1=3.72$, $\gamma_2=1.26$, and $\gamma_3=1.63$ is from the results of Pugh *et al.*,[371] and the split-off mass is chosen to be $m_{so}^*=0.3m_0$.[370,371] For the hydrostatic deformation potential, an average of -3.35 eV from the theoretical[319,348,370] range of -2.2 to -4.85 eV is recommended. Valence-band deformation potentials are taken from a combination of the calculations of Wei and Zunger,[42] Kim *et al.*,[370] and Van de Walle and Neugebauer:[381] $a_v=-1.5$ eV, $b=-1.2$ eV, and $d=-9.3$ eV. Elastic constants of $C_{11}=187$ GPa, $C_{12}=125$ GPa, and $C_{44}=86$ GPa have been adopted from the calculations of Wright.[351] Similar sets were derived from other calculations.[362,382] The recommended band structure parameters for zinc blende InN are compiled in Table XI.

IV. TERNARY ALLOYS

For all of the ternary alloys discussed below, the dependence of the energy gap on alloy composition is assumed to fit a simple quadratic form:[410]

$$E_g(A_{1-x}B_x)=(1-x)E_g(A)+xE_g(B)-x(1-x)C, \tag{4.1}$$

where the so-called bowing parameter C accounts for the deviation from a linear interpolation (virtual-crystal approximation) between the two binaries A and B. The bowing parameter for III–V alloys is typically positive (i.e., the alloy band gap is smaller than the linear interpolation result) and can in principle be a function of temperature. The physical origin of the band gap bowing can be traced to disorder effects created by the presence of different cations (anions).[410] A rough proportionality to the lattice mismatch between the end-point binaries has also been noted.[201]

In what follows, the bowing concept has been generalized to include quadratic terms in the alloy-composition series expansions for several other band parameters as well, which in some cases may be attributable to specific physical mechanisms but in others simply represent empirical fits to the experimental data. We will employ the above functional form for all parameters and, with minor exceptions, neglect higher-order terms in the expansions. Since full self-consistency has been imposed upon all of the recommended parameter sets, we will give only bowing parameters for the alloy properties, and note that the end points may be found in the tables corresponding to the relevant binaries.

We also point out that since the Γ-valley electron mass m_e^* can be obtained from Eq. (2.15) in conjunction with the specified values for E_g, E_P, Δ_{so}, and F, it is not an independent quantity. In compiling the tables for binaries, we have assured that the values given for the mass and the other parameters are consistent with Eq. (2.15). For alloys, the suggested approach is to: (1) interpolate linearly the E_P and F parameters,[115] (2) use the bowing parameter specified for the alloy to derive $E_g(T)$ and $\Delta_{so}(T)$ from Eq. (4.1), and (3) obtain the temperature-dependent electron mass in the alloy from Eq. (2.15). While this procedure yields a complex dependence of the effective mass on composition, it assures self-consistency and in all of the cases that we are aware of it appears to be reliable. Simpler approximations are naturally

Downloaded 26 Aug 2001 to 128.42.12.177. Redistribution subject to AIP license or copyright, see http://ojps.aip.org/japo/japcr.jsp

sometimes possible. In the tables, we attempt to give electron mass bowing parameters that are consistent with the above procedure.

Linear interpolations are suggested for the electron masses in the X and L valleys, split-off hole mass, and heavy-hole and light-hole masses along the [001] direction.[146] In order to estimate the valence-band warping, the suggested procedure is to interpolate the $\gamma_3-\gamma_2$ difference. Direct interpolation of the individual Luttinger parameters is *not* recommended. Lattice constants and elastic moduli may also be linearly interpolated.

A. Arsenides

1. AlGaAs

AlGaAs is the most important and the most studied III–V semiconductor alloy. Its key role in a variety of transistor and optoelectronic devices has necessitated a precise knowledge of the fundamental energy gap as well as the alignment of the three main conduction-band valleys. Investigations are complicated by the fact that whereas GaAs is a direct-gap material with $\Gamma-L-X$ valley ordering. AlAs is an indirect material with exactly the reverse ordering. Particular attention has been devoted to the crossover point, at which the Γ and X valley minima have the same energies.

Bowing parameters from 0.14 to 0.66 eV have been proposed for the Γ-valley energy gap when Eq. (4.1) is used for all compositions of $Al_xGa_{1-x}As$.[8,92,140,142,143,411] Casey and Panish suggested a linear x dependence in the range $0<x<0.45$ (also supported by other data)[412–415] and a quadratic dependence when $0.45<x<1$.[2] Using spectroscopic ellipsometry to derive the positions of the critical points, Aspnes *et al.* obtained a composition-dependent bowing parameter: $C=(-0.127+1.310x)$ eV.[416] A small bowing parameter was favored on theoretical grounds,[410] although a more recent treatment by Magri and Zunger[417,418] gave a complex fourth-order dependence reminiscent of the Aspnes *et al.* result. Although the bowing parameters that we recommend in all other cases (with the exception of the direct gap in AlGaSb) are not a function of composition, in the present case it appears that much more accurate results can be obtained by using the cubic form of Aspnes *et al.* There is insufficient data to determine the temperature dependence of the bowing parameter, since most of the determinations were performed either at room temperature or at liquid-helium temperature. Varshni parameters for $Al_xGa_{1-x}As$ have been obtained from photoluminescence, photoreflectance, and spectroscopic ellipsometry studies.[90,138,419] These are in reasonable agreement with our recommended assumption that the bowing parameter is independent of temperature.

Bowing parameters for the X-valley and L-valley gaps in AlGaAs were determined using electrical measurements in combination with a theoretical model by Lee *et al.*[140] and Saxena[141] as well as empirically by Casey and Panish.[2] These results and photoluminescence excitation spectroscopy data[420] support a $C(E_g^L)$ almost equal to zero. We select $C(E_g^X)=0.055$ eV obtained from photoluminescence measurements,[134,139] which is near the bottom of the earlier range of values but is the most recent and seems the most reliable. This result implies a $\Gamma-X$ crossover composition of $x=0.38$ at low temperatures (and 0.39 at 300 K), which agrees with the trend in the table compiled by Adachi.[3] Composition dependences for all three of the direct and indirect gaps in $Al_xGa_{1-x}As$ are plotted in Fig. 5. Most studies find that the split-off gap can be fit quite well by linear interpolation.[101,138,143] A value of $C(\Delta_{so})=0.147$ eV derived by Aubel *et al.*[142] cannot be considered fully reliable, since it was based on data points in a rather narrow composition range.

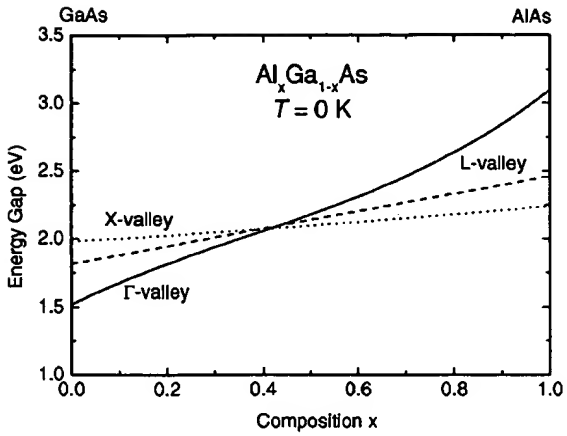

FIG. 5. Γ-, X-, and L-valley gaps for the AlGaAs alloy at $T=0$ K (solid, dotted, and dashed curves, respectively).

Several studies of the composition dependence of the Γ-valley electron mass have been reported for $x<0.33$.[146,147,421] The points have been fit to a quadratic dependence,[421] although owing to the narrow composition range and spread in the data points, it is difficult to judge the accuracy of such a scheme. From other reports, it appears that the linear approximation gives adequate results for small x.[3,104,140,146,147] Since the effective mass in AlAs was chosen to be consistent with the results in AlGaAs, a zero bowing parameter is recommended and gives good agreement with the interpolation procedures discussed at the beginning of Sec. V. The same procedures should be used to obtain the X-valley and L-valley electron masses, Luttinger parameters, and hole masses.

Qiang *et al.* have derived a hydrostatic deformation potential of $a=-10.6$ to -10.85 eV for $x=0.22$.[422] However, the same authors obtained a much smaller value of $a=-8.6$ eV for $x=0.27$. The latter result is in good agreement with a linear interpolation between the GaAs and AlAs values ($a=-8.3$ eV, in this case). A linear dependence of the shear deformation potentials on composition was suggested by the ellipsometry study of exciton splittings and

TABLE XII. Nonzero bowing parameters for AlGaAs.

Parameters (eV)	Recommended values	Range
E_g^Γ	$-0.127+1.310x$	-0.127–1.183
E_g^X	0.055	0.055–0.245
E_g^L	0	0–0.055
Δ_{so}	0	0–0.147

Downloaded 26 Aug 2001 to 128.42.12.177. Redistribution subject to AIP license or copyright, see http://ojps.aip.org/japo/japcr.jsp

shifts by Logothetidis *et al.*,[153] although their best fit was obtained for a slightly smaller value of b in GaAs than we recommend in Table I. The relative paucity of deformation-potential data for this important alloy is due in no small part to the very property that is one of its greatest attractions, namely its excellent lattice match to GaAs that renders strain effects on the band structure rather insignificant.

The recommended bowing parameters for AlGaAs are collected in Table XII. In those cases where no value is listed, linear variation should be assumed.

2. GaInAs

The GaInAs alloy is a key component in the active regions of high-speed electronic devices,[423] infrared lasers,[424] and long-wavelength quantum cascade lasers.[425] It remains a direct-gap material over its entire composition range. While bowing parameters spanning the wide range 0.32–0.6 eV have been reported,[101,166,201,410,426–434] the most recent and seemingly most reliable values lie within the more restricted vicinity of 0.45–0.5 eV. It has also been proposed that the bowing depends on temperature, being almost flat below 100 K and decreasing rapidly at higher temperatures.[434] Owing to the spread in values, we have fixed our recommended $Ga_{1-x}In_xAs$ bowing parameter by emphasizing the fit at the important $x=0.53$ alloy that is lattice matched to InP. The fundamental energy gap of $Ga_{0.47}In_{0.53}As$ has been studied extensively, e.g., by absorption,[435,436] magnetoabsorption,[437] photoluminescence,[430,438,439] and photoconductivity experiments.[440] On the basis of low-temperature results ranging from 810 to 821 meV, we choose a composite average of $E_g(T=0)=816$ meV, which in turn implies a bowing parameter $C=0.477$ eV. This is quite close to the recent determinations of Paul *et al.* (0.475 eV),[431] Karachevtseva *et al.* (0.486 eV),[434] Kim *et al.* (0.479 eV),[433] and Jensen *et al.*[441] This bowing parameter also agrees well with photoreflectance measurements on GaAs-rich GaInAs by Hang *et al.*[442] We choose to assume that the bowing is temperature independent,[431] in disagreement with Karachevtseva *et al.*,[434] because the room-temperature gap implied by that $C(T)$ is higher than nearly all experimental values.[438,439,443] The composition dependence of the Varshni parameters obtained in this manner is in good agreement with the functional form of Karachevtseva *et al.*[434]

Bowing parameters for the indirect energy gaps were calculated by Porod and Ferry[428] using a modified virtual crystal approximation. That study predicts large bowing parameters for both E_g^X(1.4 eV) and E_g^L(0.72 eV).[166] Tiwari and Frank[432] give a much different set: $C(E_g^X)=0.08$ eV and $C(E_g^L)=0.5$ eV. The only reliable experimental result appears to be a determination of E_g^L in $Ga_{0.47}In_{0.53}As$.[444] That study supports a lower value for the bowing parameter. The experimental and theoretical bowing parameters for the split-off gap have been reported by Vishnubhatla *et al.*,[426] Van Vechten *et al.*,[445] and Berolo *et al.*[446] These are in reasonably good agreement with the electroreflectance measurement of Perea *et al.*[443] for $Ga_{0.47}In_{0.53}As$, and imply $C(\Delta_{so})=0.15$ eV.

The electron effective mass in GaInAs has been studied both theoretically and experimentally.[171,172,446,447] As in the case of the energy gap, the most reliable data are for $Ga_{0.47}In_{0.53}As$ lattice matched to InP. While early studies proposed $m_e^*=0.041m_0$.[443,448–452] and even smaller values,[453] more recent experiments in strong magnetic fields have suggested that the polaron effective mass is in fact higher.[440] That agrees with modeling of the diamagnetic shift of the exciton absorption peaks in $Ga_{0.47}In_{0.53}As$/InP quantum wells.[454,455] In recent years, evidence has accumulated favoring a low-temperature value of $m_e^*=0.043m_0$.[447,456–458] This result implies the presence of bowing if the electron mass is interpolated directly using an expression similar to Eq. (4.1). Application of the more general approach using Eq. (2.15) in conjunction with interpolated values for the interband matrix element and the F parameter is discussed below. Since no reliable data on the bowing parameters for the X- and L-valley electron masses appear to exist, we suggest linear interpolation.

TABLE XIII. Nonzero bowing parameters for GaInAs.

Parameters	Recommended values	Range
E_g^Γ (eV)	0.477	0.32–0.46
E_g^X (eV)	1.4	0.08–1.4
E_g^L (eV)	0.33	0.33–0.72
Δ_{so} (eV)	0.15	0.15–0.20
$m_e^*(\Gamma)$	0.0091	···
$m_{hh}^*(001)$	−0.145	···
$m_{lh}^*(001)$	0.0202	···
$\gamma_3-\gamma_2$	0.481	···
E_P (eV)	−1.48	···
F	1.77	···
VBO (eV)	−0.38	···
a_c (eV)	2.61	···

For $Ga_{0.47}In_{0.53}As$, Alavi *et al.*[437] suggested the set of Luttinger parameters: $\gamma_1=11.01$, $\gamma_2=4.18$, $\gamma_3=4.84$. Those values are in good agreement with the light-hole masses derived from spin-polarized photoluminescence measurements by Hermann and Pearsall,[459] and with cyclotron resonance experiments.[460] On the other hand, Sugawara *et al.*[455] obtained a much larger light-hole mass, although with considerable spread in the results. We suggest that the bowing parameters for the hole effective masses should be consistent with the results of Alavi *et al.*[437] The split-off hole mass should be interpolated linearly.

Most studies have employed an interband matrix element of $E_P=25.3$ eV for $Ga_{0.47}In_{0.53}As$[437,448,453,459] although Zielinski *et al.*[436] derived a much smaller value from an analysis of absorption spectra. The former value is much more consistent with the matrix elements employed for GaAs and InAs (see above), and implies only a small E_P bowing parameter. The bowing of F is then obtained using the already-derived relations for the energy gap and the effective mass.

The hydrostatic deformation potential in $Ga_{0.47}In_{0.53}As$ was measured by People *et al.*[461] to be $a=-7.79$ eV. A reduction in a was also observed by Wilkinson *et al.*[462] in a study of GaInAs strained to a GaAs substrate. These results indicate some bowing in the hydrostatic deformation poten-

Downloaded 26 Aug 2001 to 128.42.12.177. Redistribution subject to AIP license or copyright, see http://ojps.aip.org/japo/japcr.jsp

tial, which we ascribe to a nonlinear shift of the conduction band edge.[4]

The recommended nonzero bowing parameters for GaInAs are collected in Table XIII.

3. AlInAs

AlInAs serves as the barrier layer in the important $Ga_{0.47}In_{0.53}As/Al_{0.48}In_{0.52}As$ heterostructure system that is lattice matched to InP. For this reason, the most precise band gap determinations are available for $Al_{1-x}In_xAs$ with the $x=0.52$ composition. While Matyas reported a Γ-valley bowing parameter of 0.24 eV for $x<0.7$ on the basis of absorption measurements,[463] theoretical work indicated that it should be larger.[201,418] Wakefield *et al.*[464] reported a value of 0.74 eV based on cathodoluminescence spectroscopy data. Similar results were recently obtained by Kopf *et al.*,[465] and were also recommended in several compilations of bowing parameters.[101,432] With the inclusion of strain effects, the temperature-dependent band gap of $Al_{0.46}In_{0.54}As$ on InP reported by Abraham *et al.* implies a bowing parameter of ≈ 0.66 eV.[466] We select a composite value of $C=0.70$ eV to reflect the majority of these results.

In contrast to GaInAs, the X conduction valley is lower than the Γ valley in AlAs-rich $Al_xIn_{1-x}As$. Linear interpolations are usually employed to obtain the X-valley and L-valley minima in AlInAs. That approximation implies that the X and Γ valleys should cross at a composition of $x=0.64$, which is slightly lower than the early experimental result of $x=0.68$ by Lorenz and Onton.[467] Since the larger crossover composition would require a negative bowing parameter for the X-valley gap, we recommend $C=0$. Krijn[101] gave a bowing parameter of 0.15 eV for the spin-orbit splitting, which is equal to the GaInAs value adopted in the previous subsection.

Optically detected cyclotron resonance measurements have yielded $m_e^*=0.10\pm0.01m_0$ for $Al_{0.48}In_{0.52}As$.[468] On the other hand, Cury *et al.*[457] obtained a much smaller mass of $0.069m_0$, which is only a little lower than extrapolations from GaInAs-rich AlGaInAs.[456,465] The smaller result is supported by the cyclotron-resonance measurements of Chen *et al.*[469] Calculations by Shen and Fan[470] also indicate an effective mass of $\approx 0.075m_0$. The reasonably good agreement of all but one result allows us to suggest a Γ-valley effective mass bowing parameter for AlInAs. In view of the lack of hard data, we recommend linear interpolation for the other masses in the AlInAs alloy.

In order to explain the electron effective mass in AlGaInAs quaternaries, Fan and Chen introduced a disorder-induced conduction-valence band mixing. They found that an interband matrix element of 22.5 eV was necessary to account for the experimental results. This value of E_P requires $F=-0.63$ for consistency. We have derived bowing parameters for AlInAs employing this system of values, although it should be noted that the results depend sensitively on the electron effective mass adopted for $Al_{0.48}In_{0.52}As$.[458]

The hydrostatic deformation potential for $x=0.52$ was measured by Ferguson *et al.*[471] to be $a=-6.7$ eV, which falls between the values adopted for InAs (−6.1 eV) and AlAs (−8.1 eV). On the other hand, Yeh *et al.*[472] obtained a valence-band deformation potential opposite in sign from the trend predicted by the model-solid theory of Van de Walle.[129] That result would imply a considerable bowing parameter even within the a_v theory presented by Wei and Zunger.[42] Pending further confirmation, we recommend linear interpolation.

TABLE XIV. Nonzero bowing parameters for AlInAs.

Parameters	Recommended values	Range
E_g^Γ (eV)	0.70	0.24–0.74
E_g^X (eV)	0	−0.5–0
Δ_{so} (eV)	0.15	···
$m_e^*(\Gamma)$	0.049	···
E_P (eV)	−4.81	···
F	−4.44	···
VBO (eV)	−0.64	···
a_c (eV)	−1.4	···

The recommended nonzero bowing parameters for AlInAs are collected in Table XIV.

B. Phosphides

1. GaInP

The GaInP alloy exhibits some of the largest direct gaps among the non-nitride III–V semiconductors. Furthermore, $Ga_{0.51}In_{0.49}P$ ($E_g=1.9$ eV at 300 K) is lattice matched to GaAs, which makes it an attractive material for wide-gap GaAs-based quantum well devices such as red diode lasers.[473] This application has spurred extensive studies of the band structure characteristics of GaInP, which are at present rather well known.

For the Γ-valley band gap, early photoluminescence and cathodoluminescence determinations yielded bowing parameters ranging from 0.39 to 0.76 eV.[467,474–478] Subsequent electroreflectance and modulation spectroscopy studies favored a value near the higher end of that range.[479–481] Theoretical studies have also produced a wide range of bowing parameters,[101,201,410,418,482] with the most reliable results clustered around 0.5–0.75 eV. By analogy to GaInAs and AlInAs, it is useful to consider the $Ga_{0.51}In_{0.49}P$ alloy for which the most extensive data are available. Unfortunately, a precise measurement for this lattice-matched alloy is somewhat complicated by its proximity to the indirect crossover point, and by long-range ordering of the group-III atoms which can take the form of a monolayer InP–GaP superlattice along the [111] direction.[483–486] The ordering-induced reduction of the direct energy gap can be on the order of 100 meV.[487] Low-temperature band gaps of 1.969–2.018 eV have been reported for random GaInP alloys that are nominally lattice matched to GaAs.[488–494] Using the result of Emanuelsson *et al.*,[495] corrected for the exciton binding energy of 8 meV,[493] we obtain a recommended bowing parameter of $C=0.65$ eV. That value is consistent with recent data for nonlattice-matched compositions.[496,497]

The X-valley gap energies in InP and GaP are nearly equal (2.38 and 2.35 eV, respectively, at 0 K), and the $\Gamma-X$ crossover composition in GaInP is believed to be close to $x=0.7$.[479] Although early work usually assumed a linear

Downloaded 26 Aug 2001 to 128.42.12.177. Redistribution subject to AIP license or copyright, see http://ojps.aip.org/japo/japcr.jsp

TABLE XV. Nonzero bowing parameters for GaInP.

Parameters	Recommended values	Range
E_g^Γ (eV)	0.65	0.39–0.76
E_g^X (eV)	0.20	0–0.35
E_g^L (eV)	1.03	0.23–0.86
Δ_{so} (eV)	0	−0.05–0
m_e^* (Γ)	0.051	···
F	0.78	···
d (eV)	0	0–2.4

variation of the X-valley gap, Auvergne *et al.* have more recently suggested $C(E_g^X)=0.147$ eV on the basis of piezoreflectance spectroscopy in the composition range near the crossover point. Somewhat larger bowing parameters are implied by the pressure experiments of Goni *et al.*[496] and Meney *et al.*[498] Our recommended value of $C(E_g^X)=0.2$ eV agrees with other experimental and theoretical results.[482] Early experimental and theoretical determinations of the bowing parameter for the L-valley gap were summarized by Bugajski *et al.*[482] The $\Gamma-L$ crossover most likely occurs at x slightly smaller than the $\Gamma-X$ crossover point,[480] which makes L the lowest conduction valley for x greater than ≈ 0.67. Krutogolov *et al.*[499] suggested $C(E_g^L)=0.71$ eV, although that article assumed L-valley indirect band gaps in the end-point binaries that are considerably different from the ones adopted here. Modeling of the ellipsometric and thermoreflectance data of Ozaki *et al.*[500] yielded $E_g^L=2.25$ eV in $Ga_{0.5}In_{0.5}P$ at 300 K, which favors a small L-valley bowing. In deriving our recommended bowing parameter, we employed the $\Gamma-L$ crossover point of $x=0.67$,[482,499] which was confirmed recently by Interholzinger *et al.*[501] The bowing of the spin-orbit splitting in GaInP is known to be very small,[446,476,479] with recent results[502] implying a linear interpolation to within experimental uncertainty.

The electron effective mass in a random alloy with $x=0.5$ was measured by Emanuelsson *et al.*[495] to be $m_e^*=0.092m_0$, which is somewhat lower than the linearly interpolated values quoted in other papers.[473,490] Similar results were obtained by Wong *et al.*[503] In the absence of reliable data for the other electron and hole masses, linear interpolation is advised using the scheme outlined above. With a linearly interpolated value of $E_P=26$ eV for the interband matrix element in $Ga_{0.5}In_{0.5}P$, we derive an F parameter of -1.48, and from it the corresponding bowing.

The shear deformation potential d was measured for GaInP grown on GaAs(111)B substrates.[504] While the results imply a bowing parameter of 2.4 eV, the large uncertainties in existing determinations make it difficult to conclusively prefer this value over a linear interpolation.

The recommended nonzero bowing parameters for GaInP are collected in Table XV.

2. AlInP

$Al_xIn_{1-x}P$ has a direct energy gap for $x<0.44$, and at the crossover composition the Γ-valley value of $E_g^\Gamma \approx 2.4$ eV is the largest of any non-nitride direct-gap III–V semiconductor.[2] For a precise determination of the bowing parameter, it is convenient to consider compositions close to $Al_{0.52}In_{0.48}P$, which is lattice-matched to GaAs. However, the inherent difficulty of experimentally determining E_g^Γ in close proximity to the indirect-gap transition caused underestimates by some workers. Bour *et al.*[203] obtained 0.38 eV for the direct-gap bowing parameter from relatively early electroreflectance measurements. Mowbray *et al.*[505] reported a low-temperature direct excitonic gap of 2.680 eV for the lattice-matched composition, which implies a negative C. This result was supported by the work of Dawson *et al.*[506,507] and by the ellipsometry experiments of Adachi *et al.*[502] and Schubert *et al.*[508] In fact, a direct gap of 2.69 eV for $Al_{0.52}In_{0.48}P$ at 0 K (corrected for the exciton binding energy) must be considered a better-established value than the 3.63 eV gap for AlP (see above). However, instead of extrapolating the AlInP gap to the AlP binary, we recommend using a negative bowing parameter of $C=-0.48$ eV, while noting that considerable uncertainty exists for large x.

For $Al_{0.52}In_{0.48}P$, indirect X-valley gaps of 2.34–2.36 eV have been deduced from a variety of optical measurements.[500,505,507] Taking into account the correction for the exciton binding energy (a rough estimate insofar as precise values have not been calculated), a bowing parameter $C(E_g^X)=0.38$ eV is deduced. Few data are available for the position of the L-valley minimum in AlInP, although a room-temperature value of $E_g^L=2.7$ eV is given by Ozaki *et al.*[500] Since that implies at most a very small bowing parameter, linear interpolation is recommended. The spin-orbit splitting in $Al_{0.5}In_{0.5}P$ is thought to be 135 meV,[502,509] which translates into an upward bowing of 0.19 eV. No direct experimental determinations of the effective masses in AlInP appear available, although various estimates put the Γ-valley electron mass close to $0.11m_0$.[509,510]

The recommended nonzero bowing parameters for AlInP are collected in Table XVI.

TABLE XVI. Nonzero bowing parameters for AlInP.

Parameters	Recommended values	Range
E_g^Γ (eV)	−0.48	−0.48–0.38
E_g^X (eV)	0.38	···
Δ_{so} (eV)	−0.19	···
m_e^* (Γ)	0.22	···

3. AlGaP

The "exotic" AlGaP alloy has an indirect band gap throughout its composition range.[202] The lowest-energy optical transitions are typically associated with donor or acceptor impurities. Linear interpolation of the indirect X-valley gap was found to give good agreement with photolumines-

TABLE XVII. Nonzero bowing parameters for AlGaP.

Parameters (eV)	Recommended values	Range
E_g^Γ	0	0.0–0.49
E_g^X	0.13	0–0.13

Downloaded 26 Aug 2001 to 128.42.12.177. Redistribution subject to AIP license or copyright, see http://ojps.aip.org/japo/japcr.jsp

cence spectra, once impurity and phonon band transitions were carefully separated from the interband transitions.[202,511] The direct gap in AlGaP was studied by Rodriguez *et al.*[512,513] Using a limited number of data points, the authors concluded that either a linear variation or a quadratic variation with a bowing parameter of 0.49 eV were consistent with the data. As in the case of AlInP, extrapolation to AlP gives a value for E_g^Γ that is somewhat higher than the value listed in Table V for the binary (also based on limited data). Recent cathodoluminescence experiments support a small bowing of 0.13 eV for the lowest X-valley gap in AlGaP.[514]

We recommend that a linear variation be assumed for all other band structure parameters of AlGaP (see Table XVII).

C. Antimonides

1. GaInSb

Although GaInSb cannot by itself be lattice matched to any of the readily available substrates, it serves as the hole quantum well material in type-II infrared lasers[155] and photodetectors[515] with strain-balanced active regions. A number of experimental[243,260,426] and theoretical[410,516] studies of the direct band gap in GaInSb have been published. The different reports, which are generally in excellent agreement with each other, support a bowing parameter of 0.415 eV. Negligible dependence of the bowing parameter on temperature was obtained using the photovoltaic effect,[259] whereas the pseudopotential calculations of Bouarissa and Aourag[517] suggested a slow variation from 0.43 at 0 K to 0.415 at room temperature.

Bowing parameters for the X- and L-valley gaps were estimated by Adachi[166] and Glisson *et al.*[201] The method employed by Adachi is rather indirect, in that an average of the bowing for two direct critical points is used to represent the bowing of the indirect gap. Nonetheless, in the absence of experimental data for the X-valley gap, it appears to be the best available approximation. The pseudopotential calculations of Bouarissa *et al.*[516] yielded very weak bowing of the two indirect gaps. This finding is in apparent contradiction with the limited data of Lorenz *et al.*,[518] which suggest a smaller L-valley gap for GaInSb than that for GaSb (no estimate of the L-valley gap in InSb was available at the time, so the article assumed a linear variation with composition). Also, the data presented in clear form by Zitouni *et al.*,[519] which cover only part of the composition range, indicate appreciable bowing for both the X and L valleys. We conclude that the considerable uncertainty for the indirect gaps in GaSb and especially InSb translates into a poor understanding of the indirect-gap bowing in GaInSb. We recommend using bowing parameters of 0.33 and 0.4 eV for the X-valley and L-valley gaps, respectively, which are near the top of the reported range. A small bowing parameter of 0.1 eV was found for the spin-orbit splitting in GaInSb.[243,260]

A small bowing of the electron effective mass in the Γ valley has been determined both experimentally and theoretically.[260,446] Roth and Fortin[243] compiled results from a number of references, from which Levinshtein *et al.*[11] deduced a bowing parameter of $0.0092m_0$. We assume a linear variation of the interband matrix element and determine the F bowing parameter from that assumption. Linear interpolation is also suggested for the heavy-hole and split-off hole masses. Levinshtein *et al.*[11] give a large bowing of the light-hole mass, in agreement with the band structure model of Auvergne *et al.*[260] Since the light-hole masses in InSb and GaSb are only a little larger than the electron masses, it follows that the bowing should be similar in the two cases. While considerably larger masses were reported by Barjon *et al.*[520] on the basis of a model of their galvanomagnetic measurements, the bowing parameter for light holes is chosen to be consistent with the results of Roth and Fortin.[243]

The recommended nonzero bowing parameters for GaInSb are collected in Table XVIII.

TABLE XVIII. Nonzero bowing parameters for GaInSb.

Parameters	Recommended values	Range
E_g^Γ (eV)	0.415	0.36–0.43
E_g^X (eV)	0.33	−0.14–0.33
E_g^L (eV)	0.4	0.093–0.6
Δ_{so} (eV)	0.1	0.06–0.72
m_e^* (Γ)	0.0092	...
m_{lh}^* (001)	0.011	...
F	−6.84	...

2. AlInSb

While not widely used, AlInSb provides a convenient strain-compensating barrier material for mid-IR interband cascade lasers[521] and other antimonide device structures. Early absorption measurements of Agaev and Bekmedova[522] yielded a linear variation of the direct energy gap with composition. However, that result was discounted[1,2] in favor of the electroreflectance determination of $C=0.43$ eV by Isomura *et al.*,[523] which is in good agreement with the empirical curve charting the increase of the bowing parameter with lattice mismatch between the binary constituents.[201] While Dai *et al.*[524] recently found a linear variation of the direct energy gap with alloy lattice constant (i.e., composition) for InSb-rich AlInSb, those results were confined to a relatively small range of compositions and as such were conceivably not sensitive enough to the quadratic bowing term. Since the electroreflectance measurements should have been more precise than the absorption experiments of Agaev and Bekmedova, we recommend use of the bowing parameter determined by Isomura *et al.*[523]

The only other band structure parameter whose composition dependence has been studied is the spin-orbit splitting. Isomura *et al.*[523] deduced a relatively strong bowing of $C=0.25$ eV in the split-off gap. The recommended nonzero bowing parameters for AlInSb are collected in Table XIX.

TABLE XIX. Nonzero bowing parameters for AlInSb.

Parameters (eV)	Recommended values	Range
E_g^Γ	0.43	0–0.43
Δ_{so}	0.25	...

Downloaded 26 Aug 2001 to 128.42.12.177. Redistribution subject to AIP license or copyright, see http://ojps.aip.org/japo/japcr.jsp

TABLE XX. Nonzero bowing parameters for AlGaSb.

Parameters (eV)	Recommended values	Range
E_g^Γ	$-0.044+1.22x$	−1.18–0.69
E_g^X	0	0–0.48
E_g^L	0	0.21–0.754
Δ_{so}	0.3	···

TABLE XXI. Nonzero bowing parameters for GaAsSb.

Parameters (eV)	Recommended values	Range
E_g^Γ	1.43	1.0–1.44
E_g^X	1.2	···
E_g^L	1.2	···
Δ_{so}	0.6	0.1–0.61
VBO	−1.06	···

3. AlGaSb

AlGaSb is an important material employed in high-speed electronic[525] and infrared optoelectronic[526] devices. Apart from a considerably larger lattice mismatch, the GaSb/AlGaSb heterostructure is a lower-gap analog of the GaAs/AlGaAs material system. The band structure in AlGaSb was originally studied by piezomodulation, and bowing parameters of 0.69 and 0.48 eV were proposed for the Γ-valley and X-valley gaps, respectively.[251] A much more comprehensive investigation was carried out by Alibert *et al.*,[236] who incorporated the results of many other reports. They obtained direct-gap bowing parameters of 0.48 and 0.47 eV at low temperatures and room temperature, respectively, values that have been used by many subsequent workers.[255,527] However, recently Bignazzi *et al.*[254] obtained a better fit to the absorption spectra by assuming a linear band gap variation at low Al mole fractions. Those results were confirmed by thermoreflectance spectroscopy performed by Bellani *et al.*[528] Consequently, a cubic band gap variation was proposed for the direct gap of $Al_xGa_{1-x}Sb$: $C=-0.044+1.22x$, which produces little deviation from linearity at small x but also bowing parameters in the range suggested by Mathieu *et al.*[251] and Alibert *et al.*[236] in the middle of the composition range (with the inflection point at $x=0.35$). In spite of the fact that only $x<0.5$ alloys were investigated in that article, it must be considered to be the most reliable study to date.

Although there was an early indication of appreciable X-valley bowing,[251] later reports have established that it is quite small or nonexistent.[2,236] L-valley gap bowing parameters ranging from 0.21 to 0.75 eV are encountered in the literature.[2,236,527,528] The $\Gamma-L$ crossover composition is quite sensitive to the exact choice of the bowing parameters, owing to the proximity of the two valleys in both GaSb and AlSb. Crossover compositions of $x=0.27$ and $x=0.23$ were determined on the basis of photoluminescence measurements[529] and from wavelength-modulated absorption spectra,[2] respectively. If those crossover points are to be consistent with our choice for the direct gap's dependence on composition, we must choose a very weak L-valley bowing. Therefore, we recommend $C(E_g^L)=0$ and note that with this choice the bowing in AlGaSb becomes rather similar to the case of AlGaAs covered above. A bowing parameter of 0.3 eV was deduced by Alibert *et al.*[236] for the spin-orbit splitting.

For electron effective masses in the AlGaSb alloy, it is recommended that the procedure outlined in the AlGaAs section be followed. That is, any nonlinearity in the composition dependence of the effective mass stems entirely from the bowing of the energy gap.[251,527] This is expected to give better results than using the Landolt–Bornstein bowing parameter[1] or interpolating linearly between the masses in GaSb and AlSb.

The recommended nonzero bowing parameters for AlGaSb are collected in Table XX.

D. Arsenides antimonides

1. GaAsSb

$GaAs_{1-x}Sb_x$ is most often encountered with the $x=0.5$ composition that matches the lattice constant of InP, although it should also be noted that at $x=0.91$ is lattice matched to InAs. Direct-gap bowing parameters in the range 1.0–1.2 eV have been determined by a number of workers from absorption measurements.[530–535] It was noted in the first study[536] of epitaxial $GaAs_{0.5}Sb_{0.5}$ on InP in 1984 that the apparent band gap of 0.804–0.807 eV was smaller than that implied by previously determined bowing parameters.[537–539] Recently, a low-temperature E_g^Γ of 0.813 eV was measured by Merkel *et al.*[540] and Hu *et al.*,[541] and its temperature dependence was obtained. Those results implied a bowing parameter of 1.42–1.44 eV, although it was suggested that ordering effects may have reduced the band gap.[537] A low-temperature bowing parameter of 1.3 eV was determined for $GaAs_{0.09}Sb_{0.91}$ lattice matched to InAs,[542] and quite recently a bowing parameter of 1.41 eV was obtained by Ferrini *et al.*[543] from ellipsometry and photoreflectance studies. Since different growth temperatures were employed in recent studies of $GaAs_{1-x}Sb_x$ with a rather small range of compositions near $x\approx0.5$, the evidence for ordering is inconclusive at present. We recommend a bowing parameter of 1.43 eV, although this value should be revised downward if additional investigations substantiating the partial ordering in GaAsSb with compositions close to a lattice match with InP become available.

Rough estimates of the bowing parameters for the X-valley and L-valley gaps (both 1.09 eV) have been published by Adachi.[166] We recommend slightly higher values, in order to assure consistency with both the experimental crossover points and the larger adopted direct-gap bowing parameter. L-gap and X-gap bowing parameters of 1.1–1.2 eV are consistent with the reported measurements.[11] On the basis of rather limited data, Mani *et al.*[542] suggested a bowing parameter of 0.1 eV for the spin-orbit splitting in GaAsSb. On the other hand, theoretical studies[101,166] have derived a considerably larger value of 0.6 eV, which we recommend.

The composition dependence of the GaAsSb effective mass was determined by Delvin *et al.*[544] Although they pro-

Downloaded 26 Aug 2001 to 128.42.12.177. Redistribution subject to AIP license or copyright, see http://ojps.aip.org/japo/japcr.jsp

posed a bowing parameter of $0.0252m_0$, the room-temperature GaSb mass obtained in that study was significantly higher than our recommendation based on a consensus of other data. A safer procedure is to take the mass nonlinearity to arise from the band gap bowing as outlined above.

The recommended nonzero bowing parameters for GaAsSb are collected in Table XXI.

2. InAsSb

The InAsSb alloy has the lowest band gap among all III–V semiconductors, with values as small as 0.1 eV at room temperature. For that reason, it is an important material for a variety of mid-infrared optoelectronic devices, including lasers[545] and photodetectors.[546] Initial reports put the direct-gap bowing parameter in InAsSb at 0.58–0.6 eV.[160,161,426,547] Those studies were performed at temperatures above or near 100 K, and gaps were extrapolated to lower temperatures in a linear fashion. It is now understood that this resulted in an overestimate of the low-temperature energy gap and an underestimate of the bowing parameter. Theoretical considerations led to a higher projected bowing parameter of 0.7 eV,[410] which is recommended by Rogalski and Jozwikowski.[548] This estimate was revised to $C=0.65$ eV by a more accurate pseudopotential calculation,[549] while Bouarissa *et al.*[516] computed an even smaller value. More recent photoluminescence studies on MBE-grown InAsSb obtained $C=0.67-0.69$ eV.[164,261,550] Similar results (e.g., $C=0.64$ eV) were obtained by Gong *et al.*[551,552] from measurements on a sequence of InAs-rich samples. Elies *et al.*[553] obtained Varshni parameters for $InAs_{0.91}Sb_{0.09}$, and suggested a temperature dependence of the bowing parameter based on those results. The possible importance of ordering has been discussed in several recent works (Wei and Zunger,[554] Kurtz *et al.*,[555] Marciniak *et al.*[556]). Smaller than expected band gaps were obtained for compositions close to the lattice-matching condition on GaSb ($x=0.09$).[557] On the basis of all these investigations, we recommend a composite bowing parameter of 0.67 eV. Currently, the bowing parameters for both the X-valley and L-valley gaps are both thought to be $\approx$0.6 eV.[166,201,516]

Experimental and theoretical data for the composition dependence of the spin-orbit splitting in InAsSb were collected by Berolo *et al.*,[446] who suggest a bowing parameter of 1.1–1.2 eV. The estimated[558] spin-orbit splitting of 0.325 eV in $InAs_{0.91}Sb_{0.09}$ (lattice matched to GaSb) implies a similar bowing parameter of 1.26 eV.

Plasma reflectance and other measurements of the electron effective mass in InAsSb were summarized by Thomas and Woolley.[171] The best fit to the data collected in that article favored a mass of $0.0103m_0$ for the alloy with the smallest direct gap ($InAs_{0.4}Sb_{0.6}$). That result agreed well with the theory developed by Berolo *et al.*[446] While magneto-optical measurements by Kuchar *et al.* indicated an extrapolated band edge electron mass of $0.0088m_0$ for $InAs_{0.145}Sb_{0.855}$, which corresponds to a larger mass bowing, that finding is inconsistent with a linear interpolation of the interband matrix elements and F parameters between InAs and InSb, and also disagrees with the model of Rogalski and Jozwikowski.[548] A recent report of the electron effective mass in InAsSb is from a cyclotron resonance measurement by Stradling *et al.*[184] for two alloy compositions. Their measurements appear to support a smaller mass bowing as well as negative bowing for the interband matrix element, although a great deal of uncertainty is inherent in assigning a value based on two data points. Our recommended bowing parameter for the electron effective mass is $0.035m_0$, which is near the bottom of the reported range and roughly consistent with the results of assuming the mass bowing to be caused entirely by band gap bowing.

TABLE XXII. Nonzero bowing parameters for InAsSb.

Parameters	Recommended values	Range
E_g^Γ (eV)	0.67	0.58–0.7
E_g^X (eV)	0.6	···
E_g^L (eV)	0.6	0.55–0.8
Δ_{so} (eV)	1.2	···
$m_c^*(\Gamma)$	0.035	0.03–0.055

The recommended nonzero bowing parameters for InAsSb are collected in Table XXII.

3. AlAsSb

AlAsSb is a versatile large-gap barrier material that can be lattice matched to InP, InAs, or GaSb substrates. Whereas many workers assume a linear variation of the direct energy gap in AlAsSb,[559] theoretical projections indicate a bowing parameter in the 0.72–0.84 eV range.[101,201] The little experimental information that is available on AlAsSb alloys lattice matched to GaSb[560] and InP[561] can be interpreted to support either a small ($\approx$0.25 eV)[560] or a large ($\approx$0.8 eV)[561] value. We recommend the latter, but also note that the uncertainty may not greatly affect most quantum heterostructures calculations in view of the large absolute value of the gap. Bowing parameters for the two indirect gaps are both chosen to be 0.28 eV in accordance with photoluminescence and electroreflectance measurements, the results of which have been summarized by Ait Kaci *et al.*[560] The bowing parameter for the spin-orbit splitting (0.15 eV) is taken from the theoretical estimate of Krijn.[101]

The recommended nonzero bowing parameters for AlAsSb are collected in Table XXIII.

E. Arsenides phosphides

1. GaAsP

$GaAs_{1-x}P_x$ is a wide-band gap alloy that is often employed in red LEDs.[562] The alloy becomes indirect for $x>0.45$ (at 0 K)[482] when the X valley minimum crosses below

TABLE XXIII. Nonzero bowing parameters for AlAsSb.

Parameters (eV)	Recommended values	Range
E_g^Γ	0.8	0–0.84
E_g^X	0.28	···
E_g^L	0.28	···
Δ_{so}	0.15	···
VBO	−1.71	···

Downloaded 26 Aug 2001 to 128.42.12.177. Redistribution subject to AIP license or copyright, see http://ojps.aip.org/japo/japcr.jsp

TABLE XXIV. Nonzero bowing parameters for GaAsP.

Parameters (eV)	Recommended values	Range
E_g^Γ	0.19	0.174–0.21
E_g^X	0.24	0.20–0.28
E_g^L	0.16	0.16–0.25

TABLE XXV. Nonzero bowing parameters for InAsP.

Parameters (eV)	Recommended values	Range
E_g^Γ	0.10	0.09–0.38
E_g^X	0.27	···
E_g^L	0.27	···
Δ_{so}	0.16	···

the Γ valley minimum. Most experimental results for the direct-gap bowing parameter lie within a relatively narrow range, 0.175–0.21 eV.[93,426,467,482,562–565] A small bowing parameter is also expected on theoretical grounds, for both the direct and indirect gaps.[191] However, it has been noted that the bowing parameter more than doubles if CuPt-like ordering sets in.[566] While a recent ellipsometry study of disordered GaAsP alloys produced a direct-gap bowing parameter of 0.54 eV,[567] that outlying result lacks other verification and relied on only two data points with intermediate x. We therefore assume that either it was anomalous or some ordering did occur. Since a meaningful temperature dependence cannot be extracted from the existing data, we recommend $C=0.19\,\text{eV}$ for the direct gap at all temperatures. This is somewhat higher than the value suggested by Aspnes,[93] partly because we employ a larger band gap for GaP at 77 K.

The X-valley gap bowing parameter was studied by a number of workers.[93,482,562,568,569] Again, there is not much controversy since the crossover composition is rather well established. Our recommended value ($C=0.24\,\text{eV}$) lies approximately in the middle of the reported range of 0.20–0.28 eV. Both experimental and theoretical results for the L-valley bowing parameter imply $C=0.16\,\text{eV}$.[93,482] The spin-orbit splitting was found to vary linearly with composition.[563]

A linear variation of the electron effective mass with x in GaAsP was reported by Wetzel *et al.*[190] A **k·P** calculation with explicit inclusion of the higher conduction bands and slightly different band parameters predicts a small bowing parameter of $0.0086m_0$.[191] We recommend following the general procedure tying the mass bowing to the direct-gap bowing as outlined above, which yields reasonable agreement with that theory and experiment.

The deformation potentials in GaAsP were studied by Gonzalez *et al.*[570] The shear deformation potential b found in that work lies between the recommended values for GaAs (−2.0 eV) and GaP (−1.7 eV). Although the hydrostatic deformation potentials were found to be somewhat smaller than either of the binary values, that may have been an artifact of the measurements rather than an alloy-specific property.

The recommended nonzero bowing parameters for GaAsP are collected in Table XXIV.

2. InAsP

InAsP spans an interesting IR wavelength range (0.87–3 μm), retains a direct gap throughout, and has a high electron mobility. However, it has found far less practical use than its quaternary cousin GaInAsP because except at the endpoints the $InAs_xP_{1-x}$ lattice constant does not match any of the binary III–V substrate materials.

The dependence of the energy gap on composition was originally studied by Vishnubhatla *et al.*[426] and Antypas and Yep.[571] Whereas the first group reported a bowing parameter of 0.27 eV at 300 K, the second group obtained a similar C at $T=77\,\text{K}$ but a much smaller value (0.10 eV) at 300 K. Bodnar *et al.* later reported the opposite trend for the temperature dependence of C,[158] and Nicholas *et al.* suggested similar bowing parameters of 0.32–0.36 eV throughout the entire temperature range.[572] A recent fitting of the absorption spectra of InAsP/InP strained quantum wells also yielded a weak temperature dependence, but with values between 0.10 and 0.12 eV.[573] Similar results were reported by Wada *et al.*,[574] who used a combination of PL, x-ray diffraction, and absorption measurements. We recommend a value of $C=0.10\,\text{eV}$, which is consistent with the latest experimental works and is slightly lower than the theoretical estimate of 0.23 eV.[410]

The bowing parameters for the indirect gaps were estimated by Adachi[166] and Glisson *et al.*[201] Using their projections, we recommend $C=0.27\,\text{eV}$ for both X and L valleys. A bowing parameter of 0.16 eV was determined for the spin-orbit splitting.[446]

The electron effective mass in InAsP alloys was first investigated by Kesamanly *et al.*[173] This work and also the subsequent magnetophonon experiments of Nicholas *et al.*[572,575] found a nearly linear dependence of the mass on composition. Although the authors conjectured a reduction in the interband matrix element in the alloy, their quantitative conclusions are in doubt since they overestimated the direct-gap bowing parameter as well as the interband matrix element for InAs. With these corrections, it is unclear whether a nonlinear term needs to be introduced for E_P. The effective mass for InAs-rich alloys was determined by Kruzhaev *et al.* from tunneling magnetospectroscopy[576] and for three different compositions by Sotomayor Torres and Stradling using far-IR magneto-optics.[577] Again, due to the experimental uncertainty it is difficult to determine whether the standard procedure needs to be supplemented. In fact, the most recent experimental results are in very good agreement with the assumption that both the interband matrix element and the F parameter vary linearly with composition.

TABLE XXVI. Nonzero bowing parameters for AlAsP.

Parameters (eV)	Recommended values	Range
E_g^Γ	0.22	···
E_g^X	0.22	···
E_g^L	0.22	···

Downloaded 26 Aug 2001 to 128.42.12.177. Redistribution subject to AIP license or copyright, see http://ojps.aip.org/japo/japcr.jsp

TABLE XXVII. Nonzero bowing parameters for GaPSb.

Parameters (eV)	Recommended values	Range
E_g^Γ	2.7	2.7–3.8
E_g^X	2.7	···
E_g^L	2.7	···

TABLE XXIX. Nonzero bowing parameters for AlPSb.

Parameters (eV)	Recommended values	Range
E_g^Γ	2.7	1.2–2.7
E_g^X	2.7	···
E_g^L	2.7	···

The recommended nonzero bowing parameters for InAsP are collected in Table XXV.

3. AlAsP

If the exotic AlAsP alloy has ever been grown, it was apparently not reported. Glisson *et al.* surmised that the direct-gap bowing parameter in AlAsP would be quite small (0.22 eV).[201] Using the criterion relating to the bond-length difference in the endpoint binaries, one would not expect the bowing parameter to exceed those in GaAsP (0.19 eV) and InAsP (0.22 eV) (see Table XXVI).

F. Phosphides antimonides

1. GaPSb

The growth of GaPSb was first reported by Jou *et al.*[578,579] The primary object was to determine whether the energy gap in the $GaP_{0.68}Sb_{0.32}$ alloy, which is lattice matched to GaAs, is direct or indirect. Strong PL was observed, which led the authors to conclude that the energy gap is direct. Large bowing parameters of 3.8 and 2.7 eV (lower bound) were derived for the Γ-valley and X-valley gaps, respectively. Since these greatly exceed the available theoretical estimates,[201,580] it cannot be ruled out that ordering substantially reduced the energy gaps in these and perhaps most other investigated GaPSb alloys. Subsequently, Loualiche *et al.*[581] studied $GaSb_{0.65}P_{0.35}$, which is lattice matched to an InP substrate. Since at this composition the direct nature of the energy gap is not in question, it may be argued that the analysis of their data should yield a more reliable value for the direct-gap bowing parameter ($C=2.7$ eV). The room-temperature PL measurements of Shimomura *et al.*[582] produced approximately the same result, which is our recommended value. The same C is also recommended for the X and L-valley gaps, since no studies have been reported (see Table XXVII).

2. InPSb

The energy gap in InPSb remains direct at all compositions. Bowing parameters in the 1.2–2.0 eV range have been reported for the direct gap.[101,166,201,579,580,583–586] The study by Jou *et al.*[579] of alloys with a range of compositions appears to be the most useful. A recent experiment[587] obtained an energy gap of 0.48 eV for $InP_{0.69}Sb_{0.31}$ lattice matched to an InAs substrate, which implies an even larger value of the bowing parameter. Although further work will be needed to establish complete confidence, our recommended direct-gap bowing parameter is $C=1.9$ eV. Since the indirect gaps in InPSb have not been studied, it is not unreasonable to assume the same values for their bowing. The bowing parameter for the spin-orbit splitting has been calculated to be 0.75 eV (see Table XXVIII).[101]

TABLE XXVIII. Nonzero bowing parameters for InPSb.

Parameters (eV)	Recommended values	Range
E_g^Γ	1.9	1.2–2.0
E_g^X	1.9	···
E_g^L	1.9	···
Δ_{so}	0.75	···

3. AlPSb

The successful growth of $AlP_{0.40}Sb_{0.60}$ lattice matched to InP has been reported.[582] An early projection of Glisson *et al.*[201] was $C=1.2$ eV for the direct-gap bowing parameter. However, considering the trends in the common group-III alloys, it is likely that the gaps corresponding to the three major valleys have bowing parameters that are not too different from those in GaPSb. We therefore recommend $C=2.7$ eV (see Table XXIX).

G. Nitrides

1. GaInN

GaInN quantum wells represent a key constituent in the active regions of blue diode lasers and LEDs.[293] This technological significance justifies the quest for a thorough understanding of the bulk properties of wurtzite GaInN alloys. Unfortunately, however, there is still considerable disagreement over such fundamental parameters as the bowing of the energy gap. A (partial) phase decomposition of the GaInN quantum wells employed in blue and green LEDs is believed to occur.[588] Nearly pure InN quantum dots are formed, which act as efficient radiative recombination centers. Since it is not yet clear whether this phase segregation has been com-

TABLE XXX. Energy-gap bowing parameters for nitride ternaries. For other information available for these compounds, see Table XXXI and the text.

Materials	Recommended values
Wurtzite GaInN	3.0
Zinc blende GaInN	3.0
Wurtzite AlGaN	1.0
Zinc blende AlGaN	0
Wurtzite AlInN	$16-9.1x$
Zinc blende AlInN	$16-9.1x$
Zinc blende GaAsN	$120.4-100x$
Zinc blende GaPN	3.9
Zinc blende InPN	15
Zinc blende InAsN	4.22

Downloaded 26 Aug 2001 to 128.42.12.177. Redistribution subject to AIP license or copyright, see http://ojps.aip.org/japo/japcr.jsp

TABLE XXXI. Bowing parameters for quantities other than the energy gap of nitride ternaries.

Parameters (eV)	Materials	Recommended values
E_g^X	Zinc blende GaInN	0.38
E_g^X	Zinc blende AlGaN	0.61
E_g^L	Zinc blende AlGaN	0.80
Δ_{so}	Zinc blende GaAsN	0

pletely avoided in thicker layers of GaInN, interpretation of the reported bowing parameters requires great care (see Tables XXX and XXXI).

Early studies suggested an energy-gap bowing parameter C of between 0 and 1.0 eV.[402,589,590] Wright and Nelson more recently derived $C=1$ eV for zinc blende GaInN,[591] which is relevant because of the common expectation that the zinc blende and wurtzite alloys should have approximately the same bowing parameters. Nakamura found that this bowing parameter produced a good fit to the results of PL measurements for low In compositions.[592] A slightly larger bowing parameter (1.6 eV if our values for the energy gaps of GaN and InN are employed) was found by Li *et al.*, on the basis of PL from GaInN/GaN superlattices.[593] A similar bowing parameter of 1.4 eV was reported for zinc blende GaInN; however, the results were given for relatively thin GaInN layers, the strain in which cannot be considered fully relaxed.[594] Bellaiche and Zunger[595] investigated the effects of short-range atomic ordering in GaInN, and established that a large reduction in the band gap should be expected for that scenario. Although all of these studies are consistent with a bowing parameter of ≈ 1 eV for the random GaInN alloy, several more recent investigations of GaInN layers with small In fractions arrived at significantly larger values. The experimental band gap results of McCluskey *et al.* for $Ga_{1-x}In_xN$ epilayers with $x<0.12$ were found to be consistent with bowing parameters as large as 3.5 eV.[596] Furthermore, first-principles calculations performed by those authors showed that the bowing parameter itself may be a strong function of composition, at least for small In fractions. Similarly large bowing parameters (in the range 2.4–4.5 eV) were obtained in a large number of subsequent studies by different groups.[597–602] A bowing parameter of 2.7 eV can also be inferred from a recent investigation of zinc blende GaInN.[603] Some of those works tentatively attributed the previous reports of small bowing to erroneous estimates of the alloy composition. On the other hand, Shan *et al.*[599] suggested that the more recent PL emission may have resulted from local fluctuations in the In fraction, which could lead to overestimates of the bowing parameter. Since the most important practical applications of GaInN alloys require only a small In fraction, we suggest a bowing parameter of 3 eV for both the wurtzite and zinc-blende phases, although we emphasize that at present there exists no verification that this C applies equally well to higher In compositions. There is also a strong possibility that the alloys studied in recent works are not truly random. It should be emphasized that the physical understanding of these materials is far from complete, and that the parameters recommended in this review are provisional quantities that will almost surely be revised in the course of future work. A further comment which applies to all of the nitride alloys as well as other systems affected by unknown degrees and types of segregation, is that the parameter set most relevant to a given theoretical comparison with data may not be that representing the ideal materials, but rather the nonideal properties resulting from specific growth conditions of interest.

There is very little information on the other band parameters for GaInN. Tight-binding calculations[321] provide some support for our recommended standard procedure of using the band-gap bowing parameter to derive the compositional variation of the electron effective mass and interpolating the rest of the quantities linearly. For the X-valley gap in zinc blende GaInN, a small bowing parameter of $C=0.38$ eV was estimated from first principles.[591]

2. AlGaN

AlGaN is often used as the barrier material for nitride electronic and optoelectronic devices. Initial studies of the compositional dependence of the energy gap reported downward,[604] upward,[605] and negligible[606] bowing. Subsequent early PL[607] and absorption[608] measurements found a bowing parameter of 1.0 eV, which continues to be widely used in band structure calculations even though a number of more recent investigations question the conclusions of the early work. Several studies[597,609,610] found negligible bowing, and it has been suggested that the other values resulted from an incomplete relaxation of strain in the AlGaN thin films.[609] This statement is supported to some extent by a large bowing parameter of 1.78 eV reported for highly strained layers grown on SiC.[611] Other workers quite recently calculated[612] and measured[613] smaller bowing parameters (0.25–0.6 eV depending on the measurement method and assumed binary end points). Brunner *et al.*[318] reported $C=1.3$ eV and the data of Huang and Harris[614] imply an even larger bowing parameter for AlGaN epilayers grown by pulsed laser deposition, although in both cases residual strain due to the differing lattice and thermal expansion coefficients of AlGaN and sapphire could have affected the results. Cathodoluminescence measurements for AlGaN epitaxially grown on Si(111) suggest $C=1.5$ eV.[615] We recommend continued use of the accepted bowing parameter of 1.0 eV until a broader consensus is reached on the effects of strain and other issues.

Theory projects that the Γ-valley bowing parameter in zinc blende AlGaN is small.[369,591] This is consistent with the experimental report of a linear variation of PL energies in thin films of cubic AlGaN.[616] We therefore recommend a zero bowing parameter for this case. Recommended values for the X-valley (0.61 eV) and L-valley (0.80 eV) bowing parameters are taken from the empirical pseudopotential method calculations of Fan *et al.*[369]

3. AlInN

$Al_xIn_{1-x}N$ is drawing attention because at $x=0.83$ it can be lattice matched to GaN. The first experimental study observed such a strong bowing that the band gap for the lattice-

Downloaded 26 Aug 2001 to 128.42.12.177. Redistribution subject to AIP license or copyright, see http://ojps.aip.org/japo/japcr.jsp

matched composition was found to be smaller than that of GaN.[617] Furthermore, the standard quadratic expression did not fit the compositional variation of the band gap very well. Guo *et al.*[618] and Kim *et al.*[619] subsequently presented results for InN-rich and AlN-rich AlInN, respectively, which indicated somewhat weaker bowing. Peng *et al.*[620] gave a cubic expression for the energy gap, based on results over the entire range of compositions. A similarly large bowing was observed by Yamaguchi *et al.*[621] On the theoretical side, a first-principles calculation for zinc blende AlInN yielded a bowing parameter of 2.53 eV, which was assumed to be equal to that in the wurtzite alloy.[622] Of these, the most trustworthy quantitative report appears to be that of Peng *et al.* However, the suggested expression, $E_g(300\,\mathrm{K})=1.97+1.968x-6.9x^2+9.1x^3$ eV, has been corrected to reflect our recommendations for the binary end points. In the absence of further information, we recommend that the temperature dependence be incorporated by using the recommended end points to fix the constant and linear terms at each T, and then use the Peng *et al.* quadratic and cubic terms at all temperatures. The same approach is recommended for zinc blende AlInN.

4. GaAsN

Although it has been known for a long time that small quantities of nitrogen form deep-level impurities in GaAs and GaP, growth of the GaAsN alloy with appreciable (close to 1%) N fractions has been reported only recently.[623,624] The somewhat unexpected discovery of a giant bowing parameter in this and other $AB_{1-x}N_x$ alloys in principle opens prospects for growing direct-gap III–V semiconductors with band gaps in the near-IR onto Si substrates.

As a general rule, the non-nitride constituents do not easily take the wurtzite form. It is therefore expected that GaAsN and the other analogous alloys will crystallize in a zinc blende lattice, and that a large miscibility gap will make it difficult to prepare alloys with large N fractions. Phase separation has indeed been observed in GaN-rich alloys.[625] Furthermore, the substantial differences between the properties of the light-atom constituent (e.g., GaN) and the heavy-atom constituent (e.g., GaAs) call for a close scrutiny of the usual quadratic relations for the alloy band parameters, since one expects the alloy concentration dependence to be highly nonlinear.

An early theoretical study predicted a bowing parameter of 25 eV for the direct energy gap of GaAsN.[626] $C=18$ eV was obtained from PL measurements of GaAsN with N fractions of no more than 1.5%.[627] The same result was inferred from studies of the GaAsN near the two binary limits, with the decrease in the energy gap being linear for N fractions as high as 3%.[628] A quadratic form with $C\approx 11$ eV fit the results of an ellipsometry study for $x<3.3\%$ fairly well.[629] Other studies of dilute GaAsN indicated bowing parameters as large as 22 eV.[630–632] A series of first-principles calculations examined various aspects of the band structure for GaAsN, including ordering effects.[566,633–638] Those studies found that the band-edge wave functions in GaAsN tend to be localized impurity-like states, with the conduction-band wave function strongly localized on the As sublattice and the valence-band wave function on the N sublattice. The projected bowing parameters were large and composition-dependent (varying in the range from 7 to 16 eV between $GaAs_{0.5}N_{0.5}$ and $GaAs_{0.875}N_{0.125}$) whenever the dilute alloy displayed a localized deep impurity level in the gap.[566,635] Recent experimental work on GaAsN with N fractions as large as 15% confirmed the strong composition dependence of the bowing, with values ranging from 20 eV for dilute alloys to 5 eV for concentrated alloys.[639,640] On the other hand, Uesugi *et al.*[641] found a more gradual reduction of the bowing parameter with composition, and attributed the discrepancy to different strain conditions in the different studies. On the basis of the most complete available data set,[639] a compromise cubic form for the band-gap dependence on composition (at all temperatures) can be derived with the following nonlinear terms: $20.4x^2-100x^3$ eV. This expression avoids the early semimetallic transition (predicted by using $C=20$ eV) that was not observed in the single relevant experimental study.[639] A note of caution is that this expression is expected to be valid only in the region $x<0.15$, beyond which no experimental data are available. This description may in fact be a rather crude approximation of the band-gap dependence over the entire range of compositions.

An alternative description of the energy gap in GaAs-rich GaAsN in terms of the level repulsion model has been developed recently.[642] The transformation from N acting as an isoelectronic impurity to band formation was found to occur at $x=0.2\%$. The energy gap is sublinear with composition for N fractions as small as a few percent. No upper limit on the composition, for which this description is valid, is available at this moment and the results have been verified only for $x<3\%$. Nonetheless, in view of the strong evidence for its correctness, it may be advisable to use that description rather than the nonlinear bowing approximation for low N compositions, which are of interest for most device applications. A potentially more accurate four-level repulsion model was recently introduced by Gil.[643]

The Varshni parameters measured by Malikova *et al.*[644] for two GaAsN alloys were found to lie between those of GaAs and zinc-blende GaN. The temperature dependence of the energy gap in a few GaAsN alloys was found to be much weaker (60%) than that in GaAs for N fractions as small as 1%.[645] The spin-orbit splitting obtained from electroreflectance measurements[646] was found to vary approximately linearly in GaAsN. The interband matrix element of GaAsN (and other alloys such as GaPN) is predicted[647] to be strongly reduced relative to the virtual crystal approximation. This theoretical result, which is important primarily at large N compositions, has yet to be verified experimentally. Furthermore, an abrupt increase in the effective mass in GaAsN/GaAs quantum wells with 1.2% and 2% N has been reported.[648,649] The effective mass is larger than that predicted on the basis of theoretical calculations.[638,650]

The valence-band shear deformation potential b in dilute GaAsN epilayers was studied by Zhang *et al.*[651] using electroreflectance measurements to determine the splitting between the heavy-hole and light-hole bands. The deformation

Downloaded 26 Aug 2001 to 128.42.12.177. Redistribution subject to AIP license or copyright, see http://ojps.aip.org/japo/japcr.jsp

potential did not follow a simple linear interpolation between GaAs and GaN. The cause is not quite clear, since N incorporation is expected to affect primarily the conduction band of GaAsN, and further studies over a wider composition range are required to pin down the (possibly complicated) N fraction dependence.

5. GaPN

Most of the band properties of GaPN are expected to be analogous to those of GaAsN, based on the simple observation that the N impurity behaves in a similar manner in both GaAs and GaP. The main complication is that GaP is an indirect-gap semiconductor. Both the Γ-valley and X-valley gaps in GaPN were predicted to have bowing parameters of 14 eV,[652] and subsequent experimental data agreed with those projections.[652–654] Sakai *et al.* used the same theoretical description and obtained similar results.[626] Recently, Bi and Tu were able to observe the energy-gap variation for alloys incorporating up to 16% N.[639] Their results are consistent with the predictions of another model, which yields bowing parameters of 10 and 3.9 eV for the X-valley and Γ-valley gaps, respectively. These results are quite close to the recent tight-binding calculations of Miyoshi *et al.*[655] and appear to be the best available values for interpolating between GaP and zinc blende GaN using the conventional model. Pseudopotential calculations indicate that even though both GaP and GaN have substantial matrix elements, the momentum matrix element in GaPN is very small for almost any concentrated GaPN alloy.[647] On the other hand, Xin *et al.*[656] recently observed intense PL from GaPN alloys with a N fraction larger than 0.43% and demonstrated a red LED based on $GaP_{0.989}N_{0.011}$.[657] These results are quite consistent with the picture developed by Shan *et al.*,[658] which challenges the once accepted wisdom that GaPN retains an indirect gap for very small N concentrations (≈1%). These authors formulated a model based on the interaction between highly localized nitrogen states and extended states at the Γ conduction-band minimum. According to the so-called "band anticrossing" picture, incorporation of even small amounts of N into GaP changes the nature of the fundamental optical transition from indirect to direct. The optical transition energy is smaller than the nitrogen level in GaP (2.18 eV) by a term linear in x for small x and varying as x for larger x. Another piece of the evidence supporting strong Γ–X mixing is the recent measurement of a heavy ($0.9m_0$) electron mass in $GaP_{0.975}N_{0.025}$/GaP quantum wells.[659] Provided the accuracy and validity limits of the "band anticrossing" picture are conclusively established, the theoretical approach summarized in Ref. 658 should be employed to determine the optical transition energies in GaPN. Similar considerations apply to other low-N-fraction-containing alloys (see Sec. IV G 4). In this review, we refrain from exploring the consequences of the band anticrossing model in more detail.

6. InPN

InPN with less than 1% N has been studied by Bi and Tu.[660] In spite of the low solubility of N in InP, they, found a significant band gap reduction that corresponded to a bowing parameter in the range 13–17 eV. We recommend an average value of $C=15$ eV, and refer the reader to Sec. IV G 4 for the necessary caveats.

7. InAsN

A theoretical calculation of the band structure of InAsN has been reported,[661] and one recent experimental study of the growth of this interesting ternary has been made.[662] The primary importance of InAsN is that it serves as one of the end points of the GaInAsN quaternary, which is promising for 1.55 μm semiconductor lasers on GaAs substrates. A tight-binding calculation[661] deduced a bowing parameter of 4.22 eV, which was obtained assuming a particular value (3.79 eV) for the valence-band discontinuity between InAs and InN. This is our recommended value, although it must be noted that the quadratic fit in Ref. 661 was rather poor. Another recent tight-binding study[663] showed that the band gap variation for small N fractions depends on the degree of ordering present in the material and that the maximally N-clustered alloy has a lower energy gap than the As-clustered alloy. It remains to be determined which configuration can be realized experimentally.

The recommended bowing parameters for all the nitride ternary alloys are collected in Tables XXX and XXXI.

V. QUATERNARY ALLOYS

The capabilities of III–V quantum well devices can frequently be expanded by introducing quaternary layers to the design. This increased flexibility does, however, come at the expense of a more difficult growth coupled with the need for multiple tedious calibration runs to accurately fix the composition. Furthermore, extensive miscibility gaps limit the range of stable compositions, since in thermal equilibrium the components often tend to segregate into inhomogeneous mixtures of binaries and ternaries. While the nonequilibrium MBE growth process can extend the miscibility boundaries considerably, inaccessible composition gaps remain for some of the III–V quaternary systems.

General methods for deriving quaternary alloy band parameters from those of the underlying binary and ternary materials have been summarized by a number of authors.[101,166,201] While no single approach guarantees good results in all cases, the interpolation procedure introduced by Glisson *et al.*[201] usually provides a reasonable approximation. It is applicable to the most commonly encountered quaternaries of the $A_xB_{1-x}C_yD_{1-y}$ type, that are made up of two group-III and two group-V elements. Using the notation from Eq. (4.1), a given band parameter for the ternary $A_{1-x}B_xC$ is given by

$$G'_{ABC}(x)=(1-x)G_{AC}+xG_{BC}-x(1-x)C_{ABC}, \quad (5.1)$$

where G_{AC} and G_{BC} are the values at the binary end points and C_{ABC} is the appropriate bowing. The corresponding band parameter in the quaternary $A_xB_{1-x}C_yD_{1-y}$ is then expressed as a weighted sum of the related ternary values:

Downloaded 26 Aug 2001 to 128.42.12.177. Redistribution subject to AIP license or copyright, see http://ojps.aip.org/japo/japcr.jsp

$$G''_{ABCD}(x,y)=\frac{x(1-x)[(1-y)G'_{ABD}(x)+yG'_{ABC}(x)]+y(1-y)[xG'_{ACD}(y)+(1-x)G'_{BCD}(y)]}{x(1-x)+y(1-y)}. \tag{5.2}$$

This approach can be extended to treat quaternary alloys of the $AB_xC_yD_{1-x-y}$ and $B_xC_yD_{1-x-y}A$ types[664]

$$G'_{ABCD}(x,y)=\frac{xyG'_{ABD}(u)+y(1-x-y)G'_{BCD}(v)+(1-x-y)xG'_{ACD}(w)}{xy+y(1-x-y)+(1-x-y)x}, \tag{5.3}$$

where $u\equiv(1-x-y)/2$, $v\equiv(2-x-2y)/2$, and $w\equiv(2-2x-y)/2$. The approach of Eqs. (5.2) and (5.3) tends to give better agreement with experiment than an alternative treatment of Moon *et al.*,[665] which is known to overestimate the quaternary bowing.[201,666] Krijn[101] gives polynomial expansions of $Q(x,y)$ derived from Eqs. (5.2) and (5.3) for the energy gaps and spin-orbit splittings of several III–V quaternaries.

Generally speaking, a given quaternary comprises a vast two-dimensional space of compositions, $[x,y]$. In practice, however, most experiments have focused on the one-dimensional subsets, $[x,y(x)]$ that are (approximately) lattice matched to one of the common binary substrate materials (GaAs, InP, InAs, or GaSb). The quaternary may then be represented as a combination of two lattice-matched constituents, one of which must be a ternary while the other may be either a binary or a ternary. The treatment is considerably simplified by the usual absence of any strong bowing of the band parameters for such an alloy, which is expected on theoretical grounds because the two constituents have identical lattice constants.

In the following, we will assume two lattice matched binary or ternary end points, α (e.g., $A_{1-x}B_xC$) and β (e.g., $AC_{1-y}D_y$), which are combined with arbitrary composition z to form the lattice-matched quaternary alloy $\alpha_{1-z}\beta_z$. We then employ the expression

$$G''_{\alpha\beta}(z)=(1-z)G'_\alpha+zG'_\beta-z(1-z)C_{\alpha\beta}, \tag{5.4}$$

where G'_α and G'_β are the values at the end points and $C_{\alpha\beta}$ is the additional bowing associated with combining the two end point materials to form a quaternary. For lattice-matched quaternaries, using Eq. (5.4) with the available experimental evidence to determine $C_{\alpha\beta}$ for each property should lead to a better representation than either the procedure of Eqs. (5.2) and (5.3) or simple linear interpolation.

A. Lattice matched to GaAs

1. AlGaInP

$(Al_zGa_{1-z})_{0.51}In_{0.49}P$ [or, more accurately, $(Al_{0.52}In_{0.48}P)_z/(Ga_{0.51}In_{0.49}P)_{1-z}$] lattice matched to GaAs is often employed as the barrier and cladding material in GaInP/AlGaInP red diode lasers.[473,498] Early studies of lattice-matched AlGaInP, which is a quaternary of the second type (with one group-V element), found that the band gap variation between $Ga_{0.51}In_{0.49}P$ and $Al_{0.51}In_{0.49}P$ is indeed nearly linear, as expected.[494,505,667] However, subsequent PL, PL excitation (PLE),[507] electroreflectance,[502] thermoreflectance,[500] and ellipsometry[508] measurements indicated that a small additional bowing parameter between 0.11 and 0.18 eV is needed to fully account for the data. Using $C=0.18$ eV in conjunction with the recommended expressions for the temperature-dependent direct gaps of GaInP and AlInP, Eq. (5.4) can be used to find the lattice-matched AlGaInP gaps for all z and T. For example, at $T=0$ we obtain $E_g=[2.007(1-z)+2.691z-0.18z(1-z)]$ eV.

Using linear interpolation for the X-valley energy gap in AlGaInP (supported by the PL data of Najda *et al.*[507]), we find that the direct-to-indirect crossover (at 0 K) should occur at $z=0.55$, which is in good agreement with experiment.[494,507] The composition-dependent variation of the 300 K energy gap in the lattice-matched quaternary $(Al_zGa_{1-z})_{0.51}In_{0.49}P$ is plotted by Fig. 6, in which the Γ-valley gap is given by a solid curve and the X-valley gap by a dashed curve. Linear interpolation between the lattice-matched alloys is also suggested for the L-valley gap and the spin-orbit splitting.[502] There appears to be only one cyclotron resonance study of the electron mass in $Al_{0.15}Ga_{0.35}In_{0.5}P$,[495] in which ordering and L-valley interactions could have distorted the reported electron mass of $0.14m_0$. It is therefore suggested that the standard procedure be followed, except that electron masses in the lattice-matched ternaries should be used as the end points in place of binaries. In this particular example, linear interpolation of the end point ternary masses should also give adequate results.

2. GaInAsP

Not very much is known about the band structure of GaInAsP lattice matched to GaAs [or $(GaAs)_{1-z}(Ga_{0.51}In_{0.49}P)_z$]. There has been little motivation to pursue this quaternary, since its direct band gap spans roughly the same range as direct-gap AlGaAs, which is considerably easier to grow.

However, there has been some work[668,669] on lattice-matched and strained alloys (in the vicinity of $z=0.67$), for

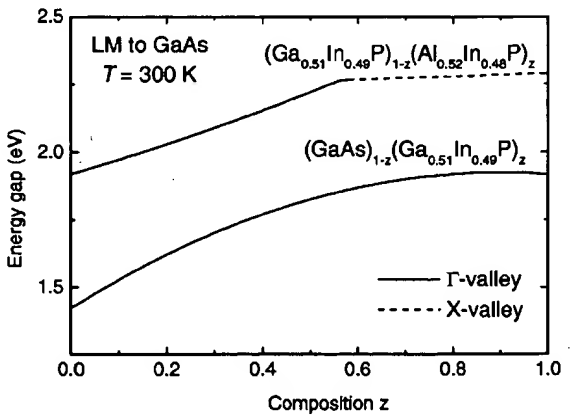

FIG. 6. Lowest energy gaps as a function of composition for $(Al_{0.52}In_{0.48}P)_z/(Ga_{0.51}In_{0.49}P)_{1-z}$ and $(Ga_{0.51}In_{0.49}P)_z/(GaAs)_{1-z}$ quaternary alloys, lattice matched to GaAs, at $T=300$ K. The region of AlGaInP for which the X-valley gap is lowest is indicated with a dashed line.

Downloaded 26 Aug 2001 to 128.42.12.177. Redistribution subject to AIP license or copyright, see http://ojps.aip.org/japo/japcr.jsp

which the quaternary constituents may be rewritten $(GaP)_x(InAs)_{1-x}$ (with $x \approx z$ for the case of lattice matching to GaAs). Absorption measurements[669] yielded $x_c = 0.73$ for the direct-to-indirect crossover point. Since the authors greatly overestimated the X valley gap in InAs, their corresponding bowing parameter cannot be considered reliable. Instead we adopt their direct-gap bowing parameter of 0.40 eV and estimate $C_X = -0.28$ eV from the crossover composition (note that these bowings are in terms of x with GaP and InAs as end points, not z with GaAs and $Ga_{0.51}In_{0.49}P$ as end points). It should be noted that results for the GaP-rich quaternary do not necessarily support upward bowing, whereas a linear variation does produce a reasonably good fit.

Using the results for $(GaP)_x(InAs)_{1-x}$ discussed above, a straightforward evaluation of the bowing parameters for the lattice-matched quaternary $(GaAs)_{1-z}(Ga_{0.51}In_{0.49}P)_z$ gives $C_X = 0.53$ eV and $C_\Gamma = -0.62$ eV. The composition-dependent variation of the 300 K energy gap in GaInAsP lattice matched to GaAs is plotted in Fig. 6. The recommended parameters imply a direct band gap at all compositions z.

3. AlGaInAs

Band gaps for strained AlGaInAs on GaAs (with low Al and In fractions) have been reported by Jensen *et al.*,[441] on the basis of PL measurements.

4. GaInAsN

The GaInAsN quaternary has drawn considerable attention recently, since the addition of a small N fraction compensates the compressive strain that limits the critical thickness of GaInAs layers grown on GaAs substrates. In terms of the band structure properties, the alloy may be thought of as $(GaAs)_{1-z}(InAs_{0.62}N_{0.38})_z$ and represents a quaternary analog of the nitrogen-containing zinc blende ternaries discussed in the previous section. Unfortunately, the properties of InAsN have not been measured, and such experiments may run into difficulty in the future owing to the expected miscibility gap. An alternative approach proposed by Chow *et al.*[670] on the basis of the experimental result of Jones *et al.*[671] is to derive the energy gap from the GaInAs alloy with the same In fraction and then *reduce* it by $(53\Delta\varepsilon)$ eV, where $\Delta\varepsilon$ is the difference between the in-plane strains computed for the In-containing ternary and quaternary (we have revised the coefficient in order to fit our band-gap scheme). The results of absorption[672] and photomodulation spectroscopy[673] are in accord with the PL measurement of Jones *et al.*[671] Pseudopotential calculations[674] are in good agreement with this approach for low N fractions. Calculations and measurements for GaInAsN lattice matched to InP have also been reported.[674,675] Recently, a large increase in the electron mass in GaInAsN with a small N fraction was observed via reflectivity measurements.[676] This result appears to invalidate any simple interpolation scheme and favor the authors' proposed model of the interaction between localized N states and the extended states of the semiconductor matrix as discussed in Sec. IV G 4.

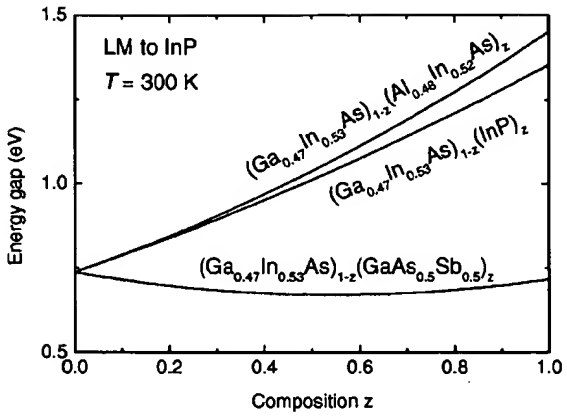

FIG. 7. Energy gaps as a function of composition for $(InP)_z(Ga_{0.47}In_{0.53}As)_{1-z}$, $(Al_{0.48}In_{0.52}As)_z(Ga_{0.47}In_{0.53}As)_{1-z}$, and $(GaAs_{0.5}Sb_{0.5})_z(Ga_{0.47}In_{0.53}As)_{1-z}$ quaternary alloys, lattice matched to InP, at $T = 300$ K.

B. Lattice matched to InP

1. GaInAsP

GaInAsP lattice matched to InP $[(InP)_{1-z}(Ga_{0.47}In_{0.53}As)_z$, which is $Ga_xIn_{1-x}As_zP_{1-z}$ with $x = 0.47z$,] is an extremely important quaternary alloy. It is currently employed in commercial optoelectronic (especially semiconductor lasers emitting at 1.3 and 1.55 μm) and electronic (especially high-electron-mobility transistor) devices. This alloy has been the subject of numerous review articles[5,6,429,666,677] and at least one book.[4]

Numerous measurements of the direct energy gap in GaInAsP have been reported.[427,443,678–680] Pearsall summarized the experimental results available by 1982 in his review,[677] and deduced a bowing parameter of 0.149 eV. For the most part, a small spread in the experimental data was found, and it was pointed out that Perea *et al.*[443] ($C = 0.25$ eV) underestimated the gaps somewhat in analyzing their electroreflectance data. Further electroreflectance experiments of Lahtinen and Tuomi[680] indicated a substantially smaller bowing parameter of 0.038 eV. An early tight-binding calculation also yielded a bowing parameter of 0.19 eV,[428] with error bounds sufficient to include almost all of the experimental data sets. We recommend using Eq. (5.4) with a bowing parameter of $C = 0.13$ at all temperatures, which is consistent with the relations currently employed to estimate device characteristics.[4] This procedure yields $E_g = [1.4236(1-z) + 0.816z + 0.13z^2]$ eV at 0 K and $E_g = [1.353(1-z) + 0.737z + 0.13z^2]$ eV at 300 K. The composition-dependent variation of the 300 K energy gap in the lattice-matched quaternary $(InP)_{1-z}(Ga_{0.47}In_{0.53}As)_z$ is plotted in Fig. 7.

Two studies have reported Varshni parameters for GaInAsP.[681,682] Although the band gaps obtained in the two studies were similar, the resulting Varshni parameters were very different. Deducing the temperature variation of the quaternary band gap from the bulk Varshni parameters given above is therefore probably a safer procedure (and gives reasonable agreement with the results of Satzke *et al.*[682]). A linear variation is usually assumed for the indirect band gaps

Downloaded 26 Aug 2001 to 128.42.12.177. Redistribution subject to AIP license or copyright, see http://ojps.aip.org/japo/japcr.jsp

between the two end point materials,[4] although that dependence has apparently not been verified experimentally.

Electroreflectance studies have concluded that the bowing parameter for the spin-orbit splitting is either close to zero[678,680] or negative.[443,679] This upward bowing was explained by considering the interband and intraband contributions to disorder-induced mixing of conduction-band and valence-band states.[683] We derive our recommended value of $C(\Delta_{so})=-0.06\,\text{eV}$, which implies $\Delta_{so}=[0.108(1-z)+0.33z-0.06z^2]\,\text{eV}$, by averaging all reported spin-orbit bowing parameters.

The electron mass in GaInAsP has been measured by a variety of approaches such as cyclotron resonance, magnetophonon resonance, Shubnikov–de Haas oscillations, and shallow donor photoconductivity.[448–451,453,684] Some studies found roughly zero bowing,[448,449,684] while others obtained appreciable downward bowing.[450,451,453] In the former case, it was claimed that the lack of effective mass bowing was due to the band gap bowing being compensated by a disorder-induced bowing of the interband matrix element.[677] However, from a consideration of all available experimental data there is no obvious reason to deviate from our standard mass-bowing procedure (e.g., see Fig. 6.7 in Ref. 4). Using our adopted band gap variation and interpolating the interband matrix element and the F parameter linearly, we find the totality of the data to be consistent with that procedure. The resulting masses are slightly lower than those in Refs. 448, 449, and 684, but not nearly as small as in Ref. 453. The light-hole effective mass in GaInAsP lattice matched to InP was measured by Hermann and Pearsall.[459] On the basis of those data, Adachi suggested a bowing parameter of $0.03m_0$.[4] However, we recommend using a slightly modified version of the Adachi expression, $m_{lh}^*=(0.1208-0.099z+0.0302z^2)$ eV, in order to assure consistency with the end point values in $Ga_{0.47}In_{0.53}As$ and InP. Using linear interpolation for the heavy-hole mass and the valence-band anisotropy, the split-off mass can be determined using Eqs. (5.4) and (2.18).

By measuring the pressure dependence of the stimulated emission in a buried heterostructure near-IR diode laser, a hydrostatic deformation potential of $a=-5.7$ eV was determined for $Ga_xIn_{1-x}As_zP_{1-z}$ with $y=0.6$.[685] This represents a smaller absolute value than in either InP (−6.6 eV) or $Ga_{0.47}In_{0.53}As$(−7.79 eV), and requires a rather large bowing parameter of $C=-6.7$ eV. While we recommend this value in the absence of other information, additional experiments are necessary to confirm this strong bowing.

2. AlGaInAs

Another important quaternary lattice matched to InP is AlGaInAs [or $(Al_{0.48}In_{0.52}As)_z(Ga_{0.47}In_{0.53}As)_{1-z}$], which combines two lattice-matched ternary alloys. Initial characterization of this quaternary was performed by Olego *et al.*,[456] who found a direct-gap bowing parameter of 0.20 eV [when cast into the form of Eq. (5.4)]. Subsequent PL measurements of Kopf *et al.*[465] and Cury *et al.*[457] implied a linear variation of the energy gap, whereas the low-temperature PL results of Bohrer *et al.*[686] suggested a large bowing parameter of 0.68 eV. Fan and Chen obtained a value of 0.225 eV between those two extremes,[458] while Shen and Fan calculated a rather small bowing using the tight-binding method with the virtual-crystal approximation.[470] Averaging the various experimental results, we obtain a composite direct-gap bowing parameter of 0.22 eV, which is close to the values of Olego *et al.*[456] and Fan and Chen.[458] The composition-dependent variation of the 300 K energy gap in the lattice-matched quaternary $(Al_{0.48}In_{0.52}As)_z(Ga_{0.47}In_{0.53}As)_{1-z}$ is plotted in Fig. 7.

The only other AlGaInAs band structure parameter with a validated nonlinear compositional variation is the electron effective mass, for which there is strong evidence for a slight upward bowing.[457,469] This can be explained by disorder-induced band mixing,[447,458] whose effect on the interband matrix element is described by expressions in Refs. 447 and 458. Whereas the evidence for a similar mechanism in GaInAsP was inconclusive, here we suggest an effective-mass bowing parameter of $-0.016m_0$. This is consistent with the other parameters if E_P is assumed to have a quadratic dependence, with $C=-5.68$ eV adjusted to provide the correct result for AlGaInAs with $x=0.5$. The F parameter is then interpolated linearly (between −2.89 in $Ga_{0.47}In_{0.53}As$ and −0.63 in $Al_{0.48}In_{0.52}As$) in that scheme.

3. GaInAsSb

Despite the presence of a miscibility gap, the growth of metastable GaInAsSb lattice matched to InP [or $(Ga_{0.47}In_{0.53}As)_z(GaAs_{0.5}Sb_{0.5})_{1-z}$] has been reported over the entire composition range.[687,688] However, the usefulness of this quaternary is limited because both end points have nearly the same energy gap, even though the cutoff wavelengths are close to the important 1.55 μm low-loss window for optical fiber communications.

The first reported growth and characterization study of this quaternary obtained little bowing,[687] whereas more recent PL measurements on bulk $Ga_{0.64}In_{0.36}As_{0.84}Sb_{0.16}$ at 8 K implied a gap of 0.7654 eV,[688] as compared to ≈0.81 eV at the two end points. Based on this data point we recommend a composition dependence of $E_g(T=0)=[0.808(1-z)+0.816z-0.22z(1-z)]$ eV. Further study is clearly desirable. The recommended composition-dependent variation of the 300 K energy gap in the lattice-matched quaternary $(Ga_{0.47}In_{0.53}As)_z(GaAs_{0.5}Sb_{0.5})_{1-z}$ is plotted in Fig. 7. The approximate location of the miscibility gap according to recent calculations[689] is indicated with the dotted line. The precise extent of the miscibility gap depends on the growth procedure and temperature, and the growth of metastable materials inside the gap is not ruled out.

C. Lattice matched to InAs

1. GaInAsSb

GAInAsSb lattice matched to InAs [or $(InAs)_{1-z}(GaAs_{0.08}Sb_{0.92})_z$] has been studied by a number of authors.[165,690,691] The growth of slightly strained GaInAsSb layers has also been reported by Shin *et al.*[692] Although data for the composition dependence of the direct band gap are somewhat sparse, the available results are consistent with the relatively large bowing parameter of ≈0.6 eV suggested by

Downloaded 26 Aug 2001 to 128.42.12.177. Redistribution subject to AIP license or copyright, see http://ojps.aip.org/japo/japcr.jsp

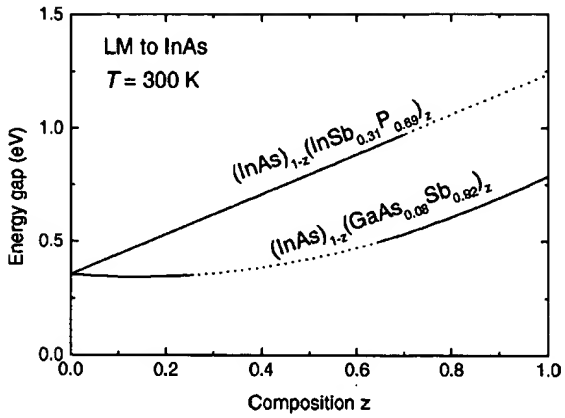

FIG. 8. Energy gaps as a function of composition for $(InAs)_{1-z}(InSb_{0.31}P_{0.69})_z$ and $(InAs)_{1-z}(GaAs_{0.08}Sb_{0.92})_z$ quaternary alloys, lattice matched to InAs, at $T=300$ K. The approximate locations of miscibility gaps are indicated by dotted lines.

Levinshtein *et al.*[11] (see also Fig. 3 of Ref. 691). This is our recommended value, which implies $E_g(T=0)=[0.412z+0.876(1-z)-0.6z(1-z)]$ eV. In the following section it will be seen that this value is similar to the recommended bowing parameter for GaInAsSb on GaSb, which is not surprising in view of the near equality of the InAs and GaSb lattice constants. The empirical relation suggested in Ref. 691 also appears to produce good agreement with the data, although it cannot be recast in the form of Eq. (5.4) with a constant bowing parameter. While in one study Varshni parameters have been deduced for GaInAsSb on InAs,[165] it is recommended that our usual procedure be followed to derive the temperature dependence of the energy gap in this quaternary. The composition-dependent variation of the 300 K energy gap in GaInAsSb lattice matched to InAs is plotted in Fig. 8. The approximate location of the miscibility gap is indicated by the dotted line. Bouarissa[693] obtains X-valley and L-valley bowing parameters of 0.15 and 0.60 eV from pseudopotential calculations accommodating the effects of alloy disorder.

2. AlGaAsSb

The direct and indirect energy gaps in AlGaAsSb lattice matched to InAs [or $(GaAs_{0.08}Sb_{0.92})_{1-z}(AlAs_{0.16}Sb_{0.84})_z$] were studied theoretically by Adachi,[166] and Anwar and Webster.[559] They respectively employed expressions suggested by Glisson *et al.*[201] and Moon *et al.*[665] (who combined the direct and indirect-gap composition dependences). Abid *et al.*[694] also treated AlGaAsSb, using the empirical pseudopotential method with the virtual crystal approximation. That little bowing was found for any of the energy gaps may be an artifact of neglecting the disorder potential. We therefore recommend using the bowing parameters specified below for AlGaAsSb on GaSb.

3. InAsSbP

$InAs_{1-x-y}Sb_xP_y$ is the only quaternary with three group-V elements that has been studied in the literature. In spite of some miscibility-gap problems, it has been successfully grown on InAs substrates $[(InAs)_{1-z}(InSb_{0.31}P_{0.69})_z$, where $z=x+y]$ by several groups.[583,695–697] Because of the large uncertainty in the $InSb_{0.31}P_{0.69}$ energy gap, the first study tried to use the quaternary data, assuming a linear variation between the InAs and $InP_{0.69}Sb_{0.31}$ end points, to deduce the bowing parameter for the ternary.[583] Subsequent studies similarly derived a vanishing bowing parameter for the quaternary.[695–697] Since with that assumption the most recent data[696,697] are consistent with our adopted band gap for $InP_{0.69}Sb_{0.31}$, we recommend $C=0$. However, Adachi[166] suggested the possibility of upward bowing based on the general quaternary relations of Glisson *et al.*,[201] and the data of Voronina *et al.*[695] can possibly be explained in that manner. The recommended composition-dependent variation of the 300 K energy gap in InAsSbP lattice matched to InAs is plotted in Fig. 8. The approximate location of the miscibility gap is indicated with a dotted line.

The spin-orbit splitting in InAsSbP has been found to be larger than in either InAs or $InP_{0.69}Sb_{0.31}$,[696] although only theoretical estimates are available for the latter. The measurements imply the form: $\Delta_{so}=0.39(1-z)+0.166z+0.75z(1-z)$, where the upward bowing parameter is larger than in Ref. 696 owing to a different value assumed for InPSb. While an electron effective mass of $0.027m_0$ determined[698] for $InAs_{0.62}Sb_{0.12}P_{0.26}$ is lower than the value of $0.0288m_0$ derived from a linear interpolation of the interband matrix element and the F parameter, the latter is nonetheless quite close to the band edge mass found from the band structure fits to the carrier density dependence performed in the same reference. We therefore recommend employing the usual procedure.

D. Lattice matched to GaSb

1. GaInAsSb

GaInAsSb lattice matched to GaSb [or $(GaSb)_{1-z}(InAs_{0.91}Sb_{0.09})_z$] is particularly well studied,[699] in part because it is an important active-region constituent of diode lasers emitting at $\lambda=2$ μm.[700] Early work[687,690,701] on the direct band gap in GaSb-rich GaInAsSb was summarized by Karouta *et al.*,[558] who suggested a bowing parameter of 0.6 eV. At the other extreme, data for $InAs_{0.91}Sb_{0.09}$-rich alloys were found to be consistent with a slightly higher bowing parameter of 0.65–0.73 eV.[695,702] Photoreflectance studies by Herrera-Perez *et al.*[703] and spectral ellipsometry results of Munoz *et al.*[704] support an even higher value for C. Similarly, recent reports of GaInAsSb grown by liquid-phase epitaxy tend toward higher bowing parameters.[705,706] Our recommended value of $C=0.75$ eV is a composite obtained by averaging all of the available results. The dependence on composition is then: $E_g=[0.812(1-z)+0.346z-0.75z(1-z)]$ eV at 0 K and $E_g=[0.727(1-z)+0.283z-0.75z(1-z)]$ eV at 300 K. The data of Karouta *et al.*[558] suggest $C=-0.26$ eV for the spin-orbit splitting, which implies: $\Delta_0=[0.76(1-z)+0.33z+0.26z(1-z)]$ eV. However, this expression is at variance with the recent ellipsometric data of Munoz *et al.*, which suggests downward bowing of the spin-orbit splitting with $C=0.25$ eV.[704] The latter result was obtained only for compositions of $z=0.14-0.15$. Both the

Downloaded 26 Aug 2001 to 128.42.12.177. Redistribution subject to AIP license or copyright, see http://ojps.aip.org/japo/japcr.jsp

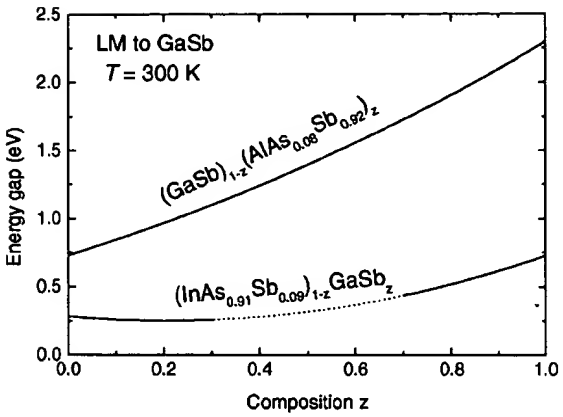

FIG. 9. Energy gaps as a function of composition for $(GaSb)_{1-z}(AlAs_{0.08}Sb_{0.92})_z$ and $(InAs_{0.91}Sb_{0.09})_{1-z}(GaSb)_z$ quaternary alloys, lattice matched to GaSb, at $T=300$ K. The approximate location of a miscibility gap for InGaAsSb is indicated by a dotted line.

downward bowing of the energy gap and the upward bowing of the spin-orbit splitting are well described[699] quantitatively by the expression of Moon *et al.*,[665] although it should be remarked that in performing such calculations some authors used different bowing parameters for the related ternary alloys.[695] Energy gaps for certain strained GaInAsSb compositions have also been reported.[707–709] The composition-dependent variation of the 300 K energy gap in GaInAsSb lattice matched to GaSb is plotted in Fig. 9. The approximate location of the miscibility gap is indicated by the dotted line.

Pseudopotential results of Bouarissa[710] predict bowing parameters of 0.85 and 0.43 eV for the L-valley and X-valley gaps, respectively. The direct-gap bowing parameter quoted in that reference is in reasonably good agreement with the experimental results.

2. AlGaAsSb

AlGaAsSb lattice matched to GaSb [or $(GaSb)_{1-z}(AlAs_{0.08}Sb_{0.92})_z$] is a natural barrier and cladding material for mid-infrared semiconductor lasers. Relations for the direct and indirect energy gaps were calculated by Adachi,[166] and the experimental results have been summarized by Ait Kaci *et al.*[560] The quoted direct-gap bowing parameter of 0.47 eV agreed well with the pseudopotential calculation of Abid *et al.*[694] and the photoreflectance measurements of Herrera-Perez *et al.*[703] Based on all of these data points, we recommend a composite result of $C=0.48$ eV. The band gap at 300 K is then: $E_g=[0.727(1-z)+2.297z-0.48z(1-z)]$ eV. This composition-dependent variation of the direct energy gap in AlGaAsSb lattice matched to GaSb is plotted in Fig. 9.

Although general considerations imply that the bowing of the L-valley gap should be similar while the X-valley gap should display little bowing,[166] pseudopotential calculations[694] have suggested bowing parameters of 0.807 and 1.454 eV, respectively. A consequence of the large X-valley bowing would be a decrease of the predicted direct-to-indirect crossover composition to $z=0.14$.

E. Other substrates

1. AlGaAsP

AlGaAsP has been grown on commercially available $GaAs_{0.61}P_{0.39}$ substrates.[711–713] It can be considered as a combination of GaAsP and AlAsP alloys with phosphorus fractions similar to the substrate. A careful investigation of the pump intensity dependence of the PL peaks revealed both impurity and band-to-band transitions.[711] Those results imply a surprisingly large direct-gap bowing parameter of 1.3 eV for the quaternary. However, that value would be reduced considerably if it turns out that the theoretical projection of 0.22 eV for the bowing parameter in AlAsP (see above) is too small.

F. Nitride quaternaries

The growth of AlGaInN has been reported,[602,621] although little is known about its band structure properties. Recent results indicate a nearly linear band gap reduction for small In compositions (<2%).[714] The cutoff wavelengths of AlGaInN (lattice matched to GaN) ultraviolet photodetectors were also generally consistent with a linear interpolation.[715] Improved crystal quality in comparison with AlGaN has also been noted.[716] Until more precise data become available, we suggest employing the usual quaternary expressions in order to estimate the parameters of this poorly explored material.

VI. HETEROSTRUCTURE BAND OFFSETS

The preceding sections have discussed the bulk properties of III–V semiconductors and their alloys in isolation. In this section, we turn to a consideration of the conduction and valence band alignments that result when the materials are joined to form heterojunctions in various combinations. Fortunately, it is usually a good approximation to view the valence band position as a bulk parameter for each individual material, which can then be subtracted to determine the relative band alignment at a given heterojunction. The interface dipole contribution, that is particular to each material combination tends to be small, since it is largely screened even when the interface bonding configurations are vastly different. However, it will be seen below that at least for the case of an InAs/GaSb interface, which has no common anion or cation, there is reliable experimental evidence for a small dependence of the offset on the interface bond type.

Our discussion will build upon the previous summary of Yu *et al.*[717] who comprehensively reviewed the understanding of band offsets as of 1991. That work, which may be considered an update of earlier reviews by Kroemer,[718,719] also provided an excellent overview of the methods commonly used in experimental band offset determinations.

Some of the existing theories, such as the model solid theory of Van de Walle,[129] assert that very little bowing of the valence band offset should be expected (although some bowing may arise if there is a strong nonlinearity in the spin-orbit splitting). However, if we are to maintain consistency with the most reliable experimental results for a variety of heterojunctions (e.g., GaAs/AlAs and lattice-matched $Ga_{0.47}In_{0.53}As/Al_{0.48}In_{0.52}As$), a bowing parameter must be assigned to some of the ternary alloys. Since there are almost

Downloaded 26 Aug 2001 to 128.42.12.177. Redistribution subject to AIP license or copyright, see http://ojps.aip.org/japo/japcr.jsp

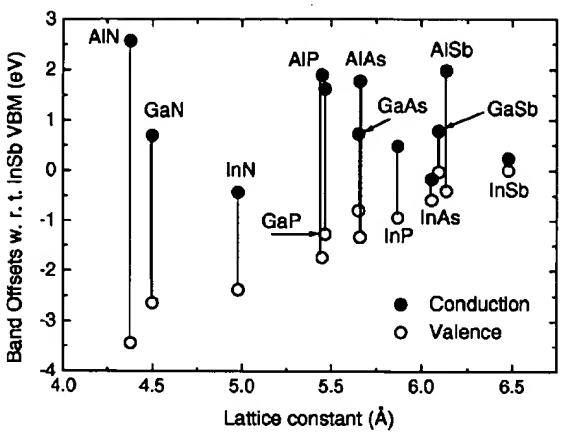

FIG. 10. Conduction (filled) and valence (open) band offsets for the 12 binaries. The Γ-valley energy gap for a given binary corresponds to the difference between the conduction and valence band positions, i.e., the length of the vertical line connecting the filled and open points. Similarly, the conduction (valence) band offset between two distinct binaries corresponds to the energy difference between their respective conduction or valence band positions on the absolute energy scale of the figure.

no reports of temperature variations that exceed the experimental uncertainties, in all cases we will take the valence band offsets to be independent of T.

Recommended valence band offsets (VBOs) (open points) and conduction band offsets (CBOs) (filled points) for all 12 of the binaries are summarized in Fig. 10. The extent of the energy gap for each material is indicated by the vertical line. Relative positions of the CBOs and VBOs in this figure may be compared to determine the offset for any given heterojunction combination.

The recommended VBOs for materials lattice matched to the common substrate materials of GaAs, InP, InAs, and GaSb are shown in Fig. 11. The points indicate offsets for binary and ternary compounds, while the vertical lines signify VBO ranges that are available using lattice-matched quaternaries. Since a linear variation with composition is assumed for all quaternaries, simple interpolation between the

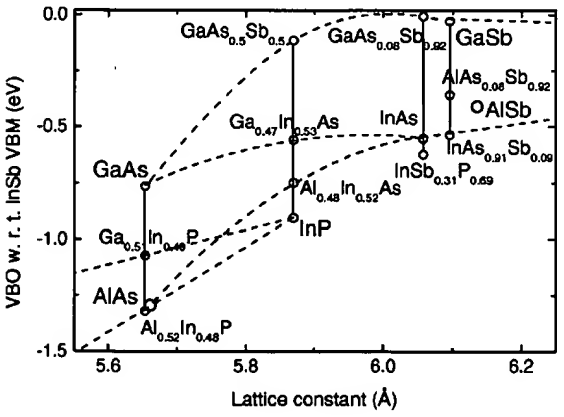

FIG. 11. Valence band offset as a function of lattice constant. The offsets for binaries and lattice-matched ternaries are indicated by points, offset variations with composition for lattice-mismatched ternaries (not including strain effects) are given by dashed curves, and the VBO ranges for quaternary alloys lattice matched to a particular substrate material (GaAs, InP, InAs, or GaSb) are given by the vertical solid lines.

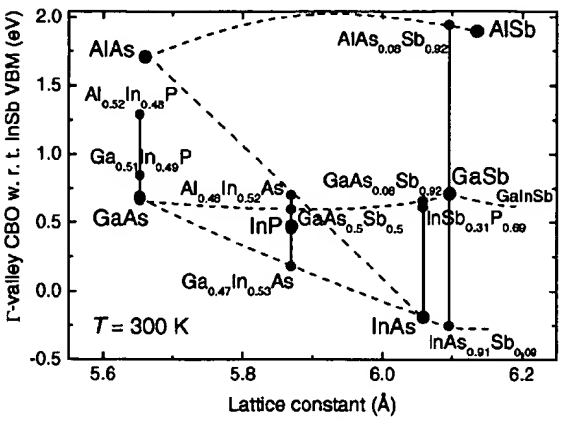

FIG. 12. Conduction band offsets corresponding to the VBOs in Fig. 11. The various points and curves have the same meaning as in that figure.

end point offsets yields the VBO for any desired quaternary alloy. The dashed lines illustrate VBO variations in a number of important lattice-mismatched ternary alloys. Corresponding conduction-band offsets are given in Fig. 12. Although strain effects are neglected in these plots, they are relatively strong and must be included to determine the correct CBO. Note also that since the band gap variation with composition is in general nonlinear (and sometimes double valued), a given point on one of the vertical lines in Fig. 12 does not necessarily map to a single, distinct quaternary alloy composition.

A. GaAs/AlAs

The GaAs/AlAs heterojunction, which is unique among the III–V semiconductors in terms of growth quality and lattice match, is also the one that has received the most intensive investigation over the years. Although the early work by Dingle *et al.*[720,721] suggested that nearly all of the discontinuity was in the conduction band, later measurements established the well-known 65:35 split between the conduction and valence bands, respectively.[717] Batey and Wright examined the full range of AlGaAs compositions and found that a linear variation of the band offset with Al fraction fitted the results quite well.[722] Although other reports have implied a slight deviation from linearity,[723] we will take the small bowing to occur entirely in the CBO. With this assumption, we average the results obtained for GaAs/AlGaAs by various measurement methods[717,724–743] to obtain the relative VBO between GaAs and AlAs. The result is $\Delta E_v = 0.53\,\text{eV} = 0.34\Delta E_g$, which is the best known value for all of the III–V semiconductors and is well within the uncertainty limits of most experiments.

Ref. 717 presented a compilation of early theoretical results for the GaAs/AlAs band offset. While our composite experimental value agrees quite well with the predictions of first-principles calculations by Christensen,[744] Lambrecht *et al.*,[745] and Wei and Zunger,[746] the model-solid theory of Van de Walle[129] obtained a slightly larger offset of $\Delta E_v = 0.59\,\text{eV}$ and the transition-metal impurity theory of Langer *et al.* yielded a smaller value of 0.453 eV.[747] Similarly small values were also predicted by the dielectric midgap energy models of Cardona and Christensen[748] and Lambrecht and

Downloaded 26 Aug 2001 to 128.42.12.177. Redistribution subject to AIP license or copyright, see http://ojps.aip.org/japo/japcr.jsp

Segall.[749] Offsets ranging from 0.36 to 0.54 eV were obtained by Wang *et al.* from the alignment of the average bonding–antibonding energy on the two sides of the heterojunction.[750] The interface dipole theory of Ohler *et al.* yielded the lowest of the recently reported values, $\Delta E_v = 0.38$ eV.[751] Considering the uncertainties involved in reliably calculating band offsets, it must be concluded that the bulk of the theoretical work agrees reasonably well with the experiments.

B. GaInAs/AlInAs/InP

The other well-studied group of heterojunctions is $Ga_{0.47}In_{0.53}As/Al_{0.48}In_{0.52}As/InP$. This system is especially interesting in that it provides a direct test of the degree of offset bowing, since the lattice-matched GaInAs and AlInAs alloys have nearly identical InAs fractions. In light of the well-established GaAs/AlAs result, the expected VBO in the absence of any bowing would be $\Delta E_v = 0.25$ eV (with $\Delta E_c = 0.46-0.465$ eV). However, both the early evidence summarized by Yu *et al.*[717] and subsequent data have consistently favored a CBO in the 0.50–0.53 eV range. For example, CBO determinations include 0.52 eV by Welch *et al.* from low-temperature PL studies,[752] 0.505 eV by Satzke *et al.* from electroabsorption data,[753] 0.53 eV by Morris *et al.* from Schottky diode transport,[754] 0.51–0.52 eV by Baltagi *et al.* from photoreflectance data on single quantum wells,[755,756] 0.49 eV by Huang and Chang from an admittance spectroscopy technique,[757] and 0.5 eV by Lugand *et al.* from photocurrent spectroscopy.[758] By carefully modeling the results of PL measurements, Bohrer *et al.* suggested $\Delta E_c = 0.504$ eV,[759] and a similar result was reported by Huang and Chang on the basis of capacitance–voltage ($C-V$) and current–voltage–temperature data.[760] From an XPS study of the $Ga_{0.47}In_{0.53}As/Al_{0.48}In_{0.52}As$ junction, Waldrop *et al.* obtained 0.22 eV for the VBO,[761] while Tanaka *et al.* measured the same result using photocurrent spectroscopy.[762] Hybertsen derived a VBO of 0.17 eV from first-principles calculations,[763] which was in good agreement with earlier theoretical determinations (0.14–0.21 eV).[129,748] A CBO of 0.516 eV was determined from tight-binding calculations of Shen and Fan.[470] While Seidel *et al.* observed nontransitivity for the GaInAs/AlInAs CBO using a combination of internal photoemission, current–voltage ($I-V$) measurements, and PLE spectroscopy (values of 0.5 and 0.64 eV were obtained for the two possible growth sequences[764]), further investigations of that effect are called for.

Based on this broad and remarkably consistent variety of experimental and theoretical determinations, we recommend a composite result of 0.52 eV (0.19 eV) for the CBO (VBO) at the $Ga_{0.47}In_{0.53}As/Al_{0.48}In_{0.52}As$ heterojunction. Making use of the already determined GaAs/AlAs VBO, we can also derive the *difference* between the offset bowing parameters for the two alloys, which is found to be 0.26 eV. This is higher than the value of 0.048 eV suggested by the average-bond-theory results of Zheng *et al.*[765] It will be seen below that by correlating with the data for other heterojunctions, we can further determine how this bowing is distributed between the two alloys.

Using the $Ga_{0.47}In_{0.53}As/Al_{0.48}In_{0.52}As$ results, we can also extract reliable band offsets for the $Ga_{0.47}In_{0.53}As/InP$ and $Al_{0.48}In_{0.52}As/InP$ heterojunctions. On the basis of experimental reports up to 1991, Yu *et al.*[717] suggested that the CBO for $Ga_{0.47}In_{0.53}As/InP$ constituted approximately 40% of the total band gap discontinuity of 0.608–0.616 eV. This assignment is in excellent agreement with the later work of Bohrer *et al.*[686,759] Slightly smaller CBOs of 0.22 and 0.2 eV were obtained by Lee and Forrest[766] and Guillot *et al.*,[767] respectively, using $C-V$ techniques. A much larger CBO of 0.41 eV was reported from the results of absorption spectroscopy by Koteles,[732] and the XPS measurements of Waldrop *et al.* yielded a VBO of 0.34 eV (corresponding to $\Delta E_c = 0.27$ eV).[761] Theoretical work by Van de Walle[129] and Hybertsen[763] indicated CBOs in the 0.2–0.26 eV range.

A number of works have reported nontransitivity of the $Ga_{0.47}In_{0.53}As/InP$ band offset. Landesman *et al.* used ultraviolet transmission spectroscopy to study the junction and found a considerable (180 meV) difference between the offsets resulting from the two possible growth sequences (with different interface bond types).[768] The average VBO of 0.35 eV obtained in that study is in good agreement with the results given in other reports. A smaller noncommutativity of 86 meV was also reported by Seidel *et al.*,[764] whose average CBO of 0.23 eV once again agreed reasonably well with the experiments that did not find transitivity violations. The issue of noncommutativity at heterojunctions with no common anion across the interface is controversial from the theoretical point of view as well.[763,769,770] A first-principles pseudopotential calculation by Hybertsen[763] found the GaInAs/InP offset to be transitive to within 10 meV, whereas the self-consistent tight-binding model of Foulon and Priester[769] yielded a 60 meV difference, depending on whether the growth sequence employed InAs-like or GaInP-like interface bonds. Since the evidence for appreciable noncommutativity is inconclusive at this point, we do not specify an interface-bond-type dependence of the band offset in this review. If future work confirms noncommutativity for a particular heterojunction, our recommended offset values can still be used as long as they are considered to be an average for the two bond-type combinations.

Our recommended composite VBO for the $Ga_{0.47}In_{0.53}As/InP$ heterojunction is 0.345 eV, irrespective of the growth sequence, which corresponds to a CBO of 0.263 eV. With the assumption of transitivity, we also recommend a VBO of 0.155 eV for the staggered $Al_{0.48}In_{0.52}As/InP$ interface. This value is near the lower end of the 0.11–0.31 eV range of values reported in the literature.[466,472,748,763,759,769–774] One group reported noncommutativity with a 53 meV band-offset difference for that heterojunction.[764,775]

C. Strained InAs/GaAs/InP and related ternaries

In(Ga)As/GaAs is another important heterojunction that is used in a wide variety of electronic and optoelectronic devices. However, direct measurement of its band offset is considerably complicated by the high degree of strain that was not present in the more straightforward GaAs/AlAs and

Downloaded 26 Aug 2001 to 128.42.12.177. Redistribution subject to AIP license or copyright, see http://ojps.aip.org/japo/japcr.jsp

$Ga_{0.47}In_{0.53}As/Al_{0.48}In_{0.52}As/InP$ cases. One approach is to measure the offset for the lattice-matched $Ga_{0.47}In_{0.53}As/InP$ (or $Al_{0.48}In_{0.52}As/InP$) heterojunction and then make some assumption regarding the GaAs/InP band alignment. (Note that determination of the $Ga_{0.47}In_{0.53}As/Al_{0.48}In_{0.52}As$ offset is not helpful, insofar as InAs is present in both alloys in almost equal amounts.) Measurements of the offsets for heterojunctions with varying degrees of strain should be useful, as long as a consistent set of deformation potentials is used to eliminate the strain contributions.

The x-ray photoemission spectroscopy measurements of Hwang *et al.*[776] and Kowalczyk *et al.*[777] predicted VBOs of 0.11 ± 0.05 and 0.17 ± 0.07 eV, respectively, for the bulk, unstrained InAs/GaAs junction. Similar measurements by Waldrop *et al.*[778,779] implied a consistent offset value of 0.12 eV, although it is somewhat questionable whether strain was completely relieved by dislocations in all of those studies.[777] Correlating the results of Hirakawa *et al.*[780] for strained InAs/GaAs heterojunctions with our assumed deformation potentials, we obtain an average VBO of 0.365 eV. A similar study by Ohler *et al.*[781] claimed good agreement with the model-solid theory of Van de Walle,[129] yielding an offset of 0.28 eV.

Early results for strained InGaAs/GaAs were summarized by Yu *et al.*[717] Although an explicit value for the band offset was not derived in most works, Menendez *et al.* extrapolated $\Delta E_v=0.49$ eV for the InAs/GaAs junction.[782] More recently, Hrivnak pointed out the consistency of several experiments with an unstrained conduction (valence) band offset of 0.69 (0.38) eV.[783] Numerous reports of band offsets in InGaAs/GaAs quantum wells have been published.[732,784–801] Since many of those values were found not to be a constant fraction of the band gap, extrapolating to InAs/GaAs is of doubtful validity. Relative CBOs (with respect to the gap difference) tended to be in the 0.57–0.90 range. Variation of the offset with growth direction was also reported.[802]

InAs/GaAs band offsets have also been determined from optical measurements on very thin InAs layers imbedded in GaAs, although strain effects must again be subtracted from the offsets that were actually measured for heavy and light holes.[803] The recent results of Brubach *et al.* are consistent with an unstrained VBO of approximately 0.22 eV,[804] and a theoretical fit of PL data indicated an even smaller value of 0.08 eV.[805] A combination of $C-V$ and deep level transient spectroscopy (DLTS) measurements yielded 0.69 eV for the strained CBO.[806] On the other hand, another DLTS study of InAs/GaAs self-organized quantum dots found a CBO of 0.341 eV.[807] A study of InAs/AlAs superlattices produced an unstrained VBO of 0.5 eV (implying a nearly null VBO for InAs/GaAs), although the error bounds were rather large for that result.[808] $I-V$ measurements on relaxed InAs/GaAs interfaces yielded 0.34 eV for the VBO.[809]

Considering the wide spread in the experimental offsets for In(Ga)As/GaAs, it is useful to compare with theoretical findings. The Schottky-barrier arguments of Tersoff led to an offset of 0.2 eV,[810] while the transition-metal impurity theory of Langer *et al.* yielded $\Delta E_v=0.33$ eV.[747] Using midgap energy levels as a point of reference, Menendez[811] predicted a VBO of 0.13 eV. The model-solid theory of Van de Walle[129] predicted $\Delta E_v=0.28$ eV, and Ohler *et al.* obtained a slightly larger result of 0.33 eV.[751] The common-anion rule,[717] as reformulated by Wei and Zunger for the Ga/In cation pair, predicts a much smaller VBO of 0.06 eV.[746]

Weighing the large number of experimental and theoretical findings together, we conclude that the VBO for the unstrained InAs/GaAs heterojunction is most likely in the 0.1–0.35 eV range. We recommend a composite value of 0.21 eV.

X-ray photoemission spectroscopy has yielded 0.31 eV for the VBO at the InAs/InP heterojunction.[779] A somewhat smaller offset of 0.27 eV was reported on the basis of optical data.[812] Similar offsets were deduced from InAsP/InP quantum well measurements,[573,813–816] although a considerably larger VBO was found in one study.[817] An unstrained VBO of 0.39 eV was determined from PL measurements by Disseix *et al.*,[818] and 0.41 eV was obtained from fits to the PL data for very thin InAs/InP quantum wells.[819] The model-solid theory of Van de Walle[129] predicted a VBO of 0.44 eV, whereas Ohler *et al.*[751] and Tersoft[810] calculated smaller values of 0.26–0.27 eV. In order to be consistent with the majority of investigations, an intermediate VBO value of 0.35 eV is recommended for the unstrained InAs/InP heterojunction.

Assuming transitivity, the discussion above implies that the VBO for the unstrained GaAs/InP heterojunction should be 0.14 eV, which is roughly consistent with the result of x-ray photoemission spectroscopy (0.19 eV).[779] With these results in hand, we can calculate VBO bowing parameters for the GaInAs and AlInAs alloys, and find -0.38 and -0.64 eV, respectively. Note that the negative sign for the VBO bowing parameter is consistent with the reduction of the energy gap below the virtual-crystal approximation in alloys.

Accurate measurements of the VBO at heterojunctions combining GaAsSb with GaInAs and AlInAs have also been performed.[537,541,820–822] In Ref. 823, the CBO appears reliable, but the VBO was determined incorrectly, the accurate result being 0.48 eV. These data are reasonably well converged for the case of GaAsSb lattice matched to InP, and imply a large VBO bowing parameter of -1.06 eV. GaPSb lattice matched to InP has also been studied and tentatively found to exhibit a VBO of 0.5 eV, which is roughly consistent with a linear variation of the VBO in this alloy (no bowing).[581] A VBO of 0.28 eV has been reported for the InAlAs/AlAsSb heterojunction lattice matched to InP (with a type-II staggered alignment).[561] On the basis of this result, we tentatively assign a large bowing parameter of -1.71 eV to the AlAsSb alloy.

D. GaInP/AlInP/GaAs

The band gap for the lattice-matched alloy $Ga_{0.51}In_{0.49}P$ is 0.49 eV higher than that of GaAs in the temperature range up to 300 K. An early Shubnikov–de Haas experiment yielded a CBO of 0.39 eV.[824] Watanabe and Ohba measured a smaller CBO of 0.19 eV using the conduction–voltage profiling technique,[825] which is in good agreement with similar studies by Rao *et al.*,[826] Lee *et al.*,[827] and Feng *et al.*,[828] and

Downloaded 26 Aug 2001 to 128.42.12.177. Redistribution subject to AIP license or copyright, see http://ojps.aip.org/japo/japcr.jsp

with the DLTS measurements of Biswas *et al.*[829] Other experiments found that the VBO consitutes an even larger fraction of the band gap discontinuity ($\Delta E_v = 0.32-0.46$ eV).[830–837] One study obtained a small CBO for the GaInP/AlGaAs heterojunction in the low-Al-fraction limit,[838] while other recent reports have found values intermediate between the two limits.[839–841] Considering the persisting disagreement, we have averaged all of the available data points to obtain a composite recommended VBO of 0.31 eV for $Ga_{0.51}In_{0.49}P$. This value is near the median of the reported range, and is consistent with the latest studies. Foulon *et al.* predicted noncommutativity for the band offset at the GaInP/GaAs interface.[842]

The important GaInP/Al(Ga)InP heterojunction for which both constituent materials are lattice matched to GaAs has also been investigated extensively. The earliest PL study[843] assigned 57% of the total GaInP/AlInP band-gap discontinuity of 0.68 eV to the VBO. Subsequent PL and PLE studies[489,844] found the offset to be 35% and 25%, respectively. The smaller values were confirmed by the widely cited report of Dawson and Duggan who found a VBO of 33%,[493] as well as Kowalski *et al.* (35%),[845] Interholzinger *et al.* (31%),[501] and Zhang *et al.* (32%).[846] Whereas all of those authors considered a quaternary on one side of the heterojunction, the GaInP/AlInP junction was also investigated and found to exhibit[506,847] $\Delta E_v = 0.24$ eV in good agreement with the other reports. Two studies[498,848] considered the full composition range of the quaternary and found an offset of 0.22 eV in the AlInP limit, with evidence for a VBO bowing parameter of 0.157 eV. On the other hand, photoemission measurements at a considerably larger number of compositions yielded $\Delta E_v = 0.305$ eV and no substantial deviation from linearity.[849] The VBO obtained from DLTS (0.36 eV)[850] was 53% of the total band gap discontinuity. On the other hand, the combined PL, PLE, and photoreflectance (PR) investigations of Ishitani *et al.*[851] gave only 25% (0.17 eV). It is unclear why these latter studies appear to disagree with the converging PL data on which we base our recommended value of $\Delta E_v = 0.24$ eV (35% of ΔE_g). Two available studies of the GaAs/AlInP heterojunction put the VBO at 0.62–0.63 eV.[825,839] Transitivity implies a GaInP/AlInP VBO of 0.31–0.32 eV, although the disagreement with the smaller recommended result is nearly within the stated error bounds. We recommend that the unconfirmed VBO bowing for the AlGaInP quaternary be disregarded.

E. GaP and AlP

Both experimental and theoretical VBOs have been reported for the nearly lattice-matched GaP/AlP heterojunction. $C-V$ profiling,[852] x-ray photoemission spectroscopy,[853] and PL[854] indicated $\Delta E_v = 0.41$, 0.43, and 0.55 eV, respectively. A wide variety of theoretical calculations[129,746,748–750,770,855,856] produced results falling mostly in the 0.34–0.69 eV range. These values can be compared directly with the GaInP/AlInP VBO, since the InP fraction in the latter does not change across the interface. Linear extrapolation yields an offset of 0.47 eV for the GaP/AlP interface. In view of the experimental uncertainty and the small strain correction, we recommend this value. Further inference is that the VBO bowing parameters for GaInP and AlInP are nominally equal (the simplest assumption is that they both vanish). A linear variation of the VBO may be taken for the AlGaP alloy.[852,855]

Experimental and theoretical studies of the GaAs/GaP band alignment are also available. Some extrapolated from the GaAsP alloy with the assumption that there is no offset bowing. Katnani and Margaritondo used photoemission to determine an unstrained VBO of 0.63 eV,[857] while Gourley and Biefeld obtained 0.6 eV from PL/PLE measurements.[858] The assumption by Pistol *et al.*[859,860] that nearly all of the low-temperature band gap discontinuity of 0.54 eV is in the valence band, while the X-valley conduction minima line up in the two unstrained materials, was corroborated by PL measurements. Another recent optical study[861] obtained $\Delta E_v = 0.6$ eV. On the other hand, optical experiments on GaAs/GaAsP quantum wells found a much smaller VBO of 0.38–0.39 eV.[862,863] Large CBOs were derived by many of the same authors for GaAsP/GaP quantum wells.[864] A small extrapolated VBO of 0.28 eV was also proposed by Shan *et al.* on the basis of pressure-optical measurements.[865] Pseudopotential calculations in conjunction with PL measurements performed by Neff *et al.*[866] imply a VBO of 0.41 eV, which is similar to the value calculated by Di Ventra *et al.*[867] Experimental and calculated band offsets for the GaAsP/AlGaAs heterojunction with small P and Al fractions have also been reported,[868,869] although extrapolation to GaP may be problematic in that case. Various theories[129,746,870–873] found values in the 0.19–0.63 eV range. Averaging the reported experimental values we obtain a recommended GaAs/GaP VBO of 0.47 eV, which is also in the middle of the theoretical range and equal to recent first-principles calculations.[746] This value is also fully consistent with an independent report of 0.6 eV for the VBO at the GaP/InP heterojunction.[874] In view of the GaAs/InAs, InAs/InP, and GaAs/GaInP offsets derived above, it is apparent that the VBO bowing for GaInP (and by implication AlInP) can be assumed to vanish.

F. GaSb/InAs/AlSb

Since the InAs/GaAs band offset was already established above, we can use the alignment for the nearly lattice-matched InAs/GaSb and InAs/AlSb heterojunctions to forge a link between the antimonides and the GaAs-based and InP-based systems.

We first focus on the GaSb/AlSb heterojunction, which has a type-I band alignment. Early results suggesting a small VBO were reviewed by Yu *et al.*[717] However, Tejedor *et al.*[875] deduced $\Delta E_v > 0.27$ eV from a comparison of resonant Raman scattering experiments with tight-binding theory. Using x-ray photoemission spectroscopy, Gualtieri *et al.*[876] reported $\Delta E_v = 0.40$ eV with relatively large (38%) error bounds. While that finding was later disputed by Ley,[877] who suggested a revision to 0.27 eV, the former authors responded by insisting on the accuracy of their result.[878] Menendez *et al.* obtained $\Delta E_v = 0.45$ eV using a light-scattering method.[879] Cebulla *et al.* found 0.35 eV from

Downloaded 26 Aug 2001 to 128.42.12.177. Redistribution subject to AIP license or copyright, see http://ojps.aip.org/japo/japcr.jsp

absorption and excitation spectroscopy,[880] Yu *et al.* measured 0.39 eV using x-ray photoelectron spectroscopy,[881] and Shen *et al.* obtained 0.23 eV from PR measurements on GaSb/AlSb quantum wells.[882] Chen *et al.* deduced a VBO of 0.48 eV from a comparison of band structure calculations with tunneling measurements on InAs/AlSb/GaSb single-barrier interband diodes.[883] Leroux and Massies[884] derived an unstrained offset of 0.3 ± 0.075 eV from fits to the PL spectra for GaSb/AlGaSb quantum wells. Yu *et al.* noted previously[717] that most of the later experimental studies converge on an average value of 0.38 eV, which is our recommendation as well. More recent theoretical studies have also produced results in the 0.30–0.49 eV range.[129,745,746,749,750,770,870,885,886] Theory predicts a linear variation of the offset in the AlGaSb ternary.[887]

The InAs/GaSb junction has a type-II broken-gap lineup, with the bottom of the conduction band in InAs being lower than the top of the valence band in GaSb. This unusual band alignment has stimulated numerous investigations of type-II superlattices and quantum wells. For example, the junction exhibits semimetallic properties as long as quantum confinement and field-induced energy shifts are not too strong.

There have been many theoretical calculations of the valence band offset at the InAs/GaSb interface,[129,717,744–746,748–750,769,770,810,888,889] the most reliable tending to yield results in the 0.43–0.59 eV range. Several models predicted that the VBO should be larger for the InSb-like interface bond type than for GaAs-like interfaces. Foulon *et al.*,[769] Dandrea *et al.*,[890] and Montanari *et al.*[888] reported an average difference of 35 meV. *Ab initio* molecular dynamics calculations of Hemstreet *et al.* yielded a difference as large as 150 meV due to varying interface charge distributions,[891] later refinements in the calculation reduced this difference to 40 meV.[892]

Experimentally, energy gaps were measured to be 25–90 meV lower in InAs/GaSb superlattices with InSb-like interface bonds than in structures with nominally identical layer thicknesses and GaAs-like bonds.[893–895] Based on a magnetotransport study the Naval Research Laboratory (NRL) concluded that the valence band offset is 14 meV larger for InSb-like bonds.[896] The Oxford University group obtained 40 meV[897] and 30 meV[898] differences in two studies, whereas Wang *et al.* did not observe any variation of the VBO with bond type.[899] It is possible that the offset may depend on details of the interface structure produced by particular growth conditions. Since most of the experimental and theoretical studies have found a small but real dependence on bond type, we recommend that the "average" InAs/GaSb VBO specified below should be applied only to cases where no particular bond type was forced in the growth. For InSb-like bonds 15 meV should be added to that result, while for GaAs-like bonds 15 meV should be subtracted.

Experimental band offset determinations for this material system fall into two main classes: (1) direct determinations, and (2) fits to the measured optical transitions in semiconducting superlattices and quantum wells (i.e., in which there is enough quantum confinement to induce an energy gap). Among the former class of results, Gualtieri *et al.* obtained a VBO of 0.51 ± 0.1 eV using x-ray photoemission spectroscopy.[900] Whereas Srivastava *et al.*[901] measured $\Delta E_v = 0.67$ eV from $C-V$ profiling of a GaSb/$InAs_{0.95}Sb_{0.05}$ heterojunction, Mebarki *et al.*[902] obtained 0.36 eV for a GaSb/$InAs_{0.89}Sb_{0.11}$ interface using essentially the same technique. X-ray photoelectron spectroscopy yielded 0.62 eV.[903] For an InAs/GaSb long-period superlattice at 4 K, the Oxford group measured band overlap energies of 100–140 meV, depending on the interface bond type.[897] That those values increased by 30 meV at room temperature implies an average VBO of 0.52 eV, with little temperature variation (<8 meV). Another study by the same group produced an average offset of 0.54 eV.[898] Wang *et al.* found a 90 meV variation of the VBO based on growth sequence (InAs on GaSb versus GaSb on InAs).[899]

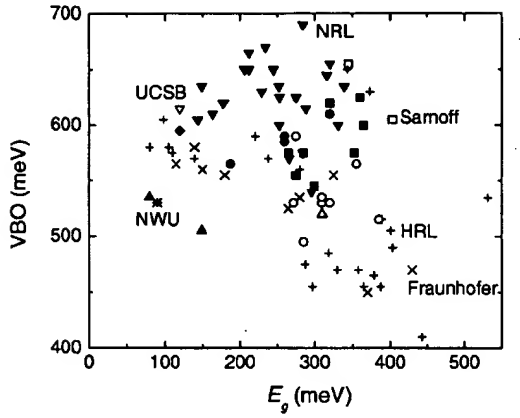

FIG. 13. InAs/GaSb valence-band offsets derived from fits to energy gaps measured for various type-II quantum well and superlattice structures. An 8-band **k·p** finite-element algorithm was used to calculate the offset corresponding to each energy gap when all other band structure parameters assumed their recommended values. The data are taken from Refs. 904 (solid squares), 905 (solid circles), 906 (solid upright triangles), 911, 912, 931, 933 (solid inverted triangles), 907, 908, 910, 913, 914, 916, 918, 920, 922, 923, 926 (crosses), 915, 921 (multiplication signs), 909 (diamond), 917 (open inverted triangle), 924, 925, 927, 929 (open circles), 930 (open upright triangles), 932 (open squares), and 919 (star).

Next, we discuss a previously unpublished application of the second approach. Experimental optical transition energies for a variety of semiconducting type-II superlattices and quantum wells[893,904–934] have been fit to theory, in this case an eight-band finite-element method **k·P** algorithm.[57] The important strain effects are included and the recommended band structure parameters in Tables III, VII, and XVIII are employed, with the only fitting parameter being the InAs/Ga(In)Sb interface VBO that is taken to be consistent with the recommended GaSb/InSb VBO discussed below. Most of the data are from PL and mid-IR laser experiments at temperatures in the 4.2–300 K range, and energies on the order of kT have been subtracted from the PL emission peaks.

Results for the fitted VBO, plotted as a function of energy gap for the given structure, are presented in Fig. 13. The various types of points correspond to data for structures grown by different groups, which are identified in the caption. The range of fitted VBO values is surprisingly large, spanning more than 200 meV. Especially noticeable are the substantial systematic differences between the offsets derived using data from different groups (or sometimes within

Downloaded 26 Aug 2001 to 128.42.12.177. Redistribution subject to AIP license or copyright, see http://ojps.aip.org/japo/japcr.jsp

the same group for different types of structures or for structures grown during different time intervals). Possible implications include: (1) the growth conditions actually influence the offset, (2) the growth-dependent nonideality of the structure, e.g., related to interface roughness or anion cross contamination, has a larger-than-expected effect on the energy gap, or (3) the layer-thickness calibrations have large uncertainties. For example, while the energy gaps corresponding to growths at the Fraunhofer Institute[915,921] and HRL Laboratories[907,908,910,913,914,916,918,920,922] yield an average VBO of 0.53 eV and structures grown at the University of Houston[924,925,927,929] yield 0.54 eV (all with fluctuations of at least 100 meV), the band gaps corresponding to NRL growths[911,912,933] imply a much larger average VBO of 0.62 eV. In some cases the differences are as large as 100 meV for structures that are nominally quite similar. Such differences are well outside the usual bounds of experimental uncertainties in the spectral data and layer thicknesses. A relatively strong dependence of the energy gap on growth temperature for nominally identical structures has also been reported.[935] Although the primary mechanism has not been isolated, subsequent TEM measurements showed that threading dislocations are present in the samples grown above the optimal growth temperature, and cross-sectional STM indicated greater interface roughness.[936]

Averaging all of the band offsets displayed in Fig. 13, along with the direct determinations summarized above, we obtain a composite InAs/GaSb VBO of 0.56 eV. This value is somewhat larger than the earlier suggestion of 0.51 eV,[717] and is at the high end of the 0.51–0.56 eV range that is usually employed in modeling antimonide materials. Since the fluctuations in reported values are so large for this system at its current level of understanding, it is advisable to account for the source and type of the structure in deciding which offset to use. Again, the recommended 0.56 eV represents an "average" value that should be corrected for the interface bond type.

The transitivity rule, applied in conjunction with the recommended InAs/GaSb and GaSb/AlSb band offsets, implies an "average" VBO of 0.18 eV for the staggered InAs/AlSb heterojunction. Bearing in mind that the transitivity assumption may be of questionable validity when applied to systems with more than one anion,[769] we can examine whether that value is consistent with the direct experimental and theoretical evidence for this interface. Nakagawa *et al.*[937] employed $C-V$ profiling to obtain a CBO of 1.35 eV between the Γ-valley minimum in InAs and the X-valley minimum in AlSb. Using our recommended band gap parameters, this corresponds to a VBO of 0.09 eV. More recently, that work was extended to AlAsSb barriers.[938] The findings are in reasonable agreement with the previously assumed large VBO (~2 eV) in AlAsSb. A PL study by Yang *et al.* found that the band alignment between $InAs_{1-x}Sb_x/AlSb$ quantum wells becomes type I when $x>0.15$.[939] In that study, InAsSb was realized as a digital superlattice. If all the offsets are referenced to the InSb valence band maximum, this implies that the AlSb VBO is no more than 85% of the InAs VBO. Using x-ray photoemission spectroscopy to study interfaces with InSb-like and AlAs-like bonds, Waldrop *et al.* obtained an average VBO of 0.18–0.19 eV and derived a difference of 60 meV between the two bond types.[940] However, a first-principles calculation by Dandrea and Duke[941] found no dependence of the VBO on bond type, and suggested that Waldrop *et al.*[940] misinterpreted their data by discarding the smaller offset obtained for an AlAs-like bond in one experiment. Other calculations[129,717,745,746,749,750,770,810,871,873,889] have found ΔE_v spanning the wide range between 0 and 0.54 eV, with the most reliable values clustered around 0.05–0.27 eV. The combined experimental and theoretical evidence appear to offer no compelling reason to reject the transitivity rule when applied to the antimonide heterojunctions. We also recommend neglecting any dependence of the InAs/AlSb VBO on interface bond type.

G. GaSb/InSb and InAs/InSb

The corrected common-anion rule predicts a negligible band offset for the unstrained GaSb/InSb heterojunction.[746] Other theories have produced values in the range -0.08 to 0.16 eV[129,810,872,873,889,942,943] (where we take the sign to be positive if the valence band maximum is higher in InSb). In experimental practice, this offset must be derived from measurements on heterojunctions such as $GaSb/Ga_{1-x}In_xSb$ and $InAs_{1-y}Sb_y/InAs_{1-x}Sb_x$ due to the large lattice mismatch between the two binaries. For an $InAs_{1-y}Sb_y/InAs_{1-x}Sb_x$ junction in the Sb-rich limit (large x and $y=1$), initial optical measurements supported an unstrained VBO of $(0.36-0.41)(1-x)$ eV.[944,945] In the As-rich limit (small x and $y=0$), on the other hand, Li *et al.* concluded from fits to magneto-optical spectra that the top of the InAsSb valence band appeared lower than that in InAs ($-0.84x$ eV).[946,947] That result implied a substantial CBO and negative VBO for small x.[948,949] Wei and Zunger pointed out that a negative VBO for InAs/InSb directly contradicts other theoretical and experimental evidence.[549] Other experiments[950–952] are in much better agreement with the usual theoretical finding of an essentially null CBO, which yields a type-I or type-II staggered alignment depending on details of the strain and ordering conditions. All of the above works found that the unstrained VBO in $InAs_{1-x}Sb_x$ depends almost linearly on composition x. While an unstrained VBO of 1.1 eV was derived for ultrathin InSb embedded in InP,[953] one cannot place high confidence in that result owing to the difficulty of precisely accounting for the very large strain effects.

A few groups[954–956] have used PL, electroluminescence, and photoconductivity to measure VBOs for GaInSb/GaSb quantum wells. Those studies assumed a linear variation of the $Ga_{1-x}In_xSb$ VBO with alloy composition, although in one study[957] the PL peak energies could not be fit using a reasonable dependence. Finally, a recent study of exciton transitions in InSb/AlInSb strained quantum wells produced heavy-hole offsets that were 38% of the total band gap discontinuity for Al fractions below 12%.[958] Unfortunately, extrapolation to the InSb/AlSb VBO from the results of this work may not be justified.

Accounting for the effects of strain and averaging the various results, we recommend a GaSb/InSb VBO of 0.03 eV.

Downloaded 26 Aug 2001 to 128.42.12.177. Redistribution subject to AIP license or copyright, see http://ojps.aip.org/japo/japcr.jsp

H. Quaternaries

Band offsets involving lattice-matched quaternaries have also been studied both experimentally and theoretically.[959] See Sec. V A 1 for a discussion of the AlGaInP/GaAs heterojunction.

Cho *et al.* considered the GaInP/GaInAsP interface lattice matched to GaAs, and suggested a linear variation of the CBO with quaternary composition.[960] Since the direct GaInAsP band gap appears to be nearly independent of composition, this implies a linear variation of the VBO as well. However, note that the value employed for the absolute gap was somewhat different from our recommendation. The same authors also investigated the band offset transitivity in AlGaAs/GaInP/GaInAsP heterostructures lattice matched to GaAs.[961] The results are in good agreement with our suggested offsets, provided a linear variation is assumed for each constituent. The small direct-gap bowing parameter and the results discussed above also imply that any bowing in the VBO for the AlGaInP alloy should be small.

Sugawara has theoretically predicted a slight bowing in the position of the valence-band maximum for GaInAsP on InP.[962] Experimentally, a VBO of 0.08 eV was measured for $Ga_{0.13}In_{0.87}As_{0.29}P_{0.71}$/InP, as compared to 0.10 eV from linear interpolation.[963] Although error bounds were not cited, this discrepancy is probably within the experimental uncertainty. Forrest *et al.*[964] found evidence that the CBO bowing is at most small, which, in combination with the small band gap bowing, implies a negligible VBO bowing. Soucail *et al.* found a small bowing parameter of 0.09 eV, which is barely larger than the estimated experimental uncertainty.[965]

The band offsets for AlGaInAs on InP have also been studied both experimentally and theoretically.[470,686,966–968] There is no clear agreement as to whether most of the band gap bowing, which is rather small in any event, should be assigned to the CBO or the VBO. We recommend a linear interpolation between the dependence for GaInAs and AlInAs, both of which exhibit appreciable VBO bowing.

Recently, a series of three articles reported determinations of the offsets for GaInAsSb and AlInAsSb, lattice matched to InP, from fits to low-temperature PL measurements.[688,969,970] All of the results agree with linear interpolations of our recommended values (with appropriate VBO bowing parameters) to within the cited experimental uncertainty.

Calculations of the band offsets for AlGaAsSb quaternaries lattice matched to various substrates have been reported.[559] In particular, Polyakov *et al.* obtained a VBO of 0.15 eV for AlGaAsSb on GaSb.[971] Rather than using this value to derive the bowing parameter for AlGaAsSb, we interpret it as reflecting the uncertainty in the bowing parameter for AlAsSb. The study on the quaternary implies a bowing parameter of 2.4 eV, which is slightly larger than the assumed value of 1.7 eV. We recommend the VBOs for AlGaAsSb obtained by linear interpolation between the ternary relations.

Mikhailova and Titkov have reviewed band offset results for the GaInAsSb quaternary on InAs and GaSb (up to 1994).[699] A theoretical work by Nakao *et al.* predicted some bowing in the VBO.[959] Results of the direct experimental study of GaInAsSb/GaSb by Mebarki *et al.*[972] are in good agreement with a linear interpolation of our recommended offsets for InAsSb and GaSb. $C-V$ measurements of Polyakov *et al.* are also consistent with that procedure.[973] The linear interpolation approach differed appreciably only with the findings of Baranov *et al.*[974] and Afrailov *et al.*,[702] for which the discrepancies are opposite in sign. Considering all of the reported experimental results, we see no compelling reason to introduce bowing. The VBOs have also been reported for the GaInAsSb/AlGaAsSb heterojunctions lattice matched to GaSb.[975] The results for both In-rich and In-poor junctions indicated reasonably good agreement with a linear interpolation. Band offset measurements have also been reported for the strained GaInAsSb/AlGaAsSb system.[976,977] Except for the case of GaInAsSb, a tight-binding calculation[959] supports our conclusion that the bowing in these quaternaries is negligible.

I. GaN, InN, and AlN

We emphasize at the outset that the band offsets recommended below for the nitride system should be understood to have large uncertainties. This is primarily because the reported results have rarely included the full effects of residual strain, spontaneous polarization, and piezoelectric fields in a completely satisfying manner. In particular, the presence of macroscopic polarization can render the notion of reference bulk energy levels somewhat ambiguous. The most significant future advancements in the understanding of nitride offsets will probably be connected with that issue.

Since the nitride materials typically crystallize in the wurtzite form, an obvious question is how the valence band edge of that phase lines up with the zinc blende phase of the same compounds. The issue was addressed by Murayama and Nakayama using a first-principles pseudopotential calculation,[978] which projected VBOs for the two phases that differed by only 34 meV in GaN and 56 meV in AlN (no results were quoted for InN). Those VBOs are much smaller than the error bounds for current experimental determinations of the nitride offsets. Wei and Zunger[326] calculated a similar difference of 30 meV between the wurtzite and zinc blende forms of the GaN/AlN interface, and also a difference on the order of 0.2 eV for GaN/InN and AlN/InN heterojunctions. While the effects of macroscopic polarization were not included, these results provisionally allow us to align the wurtzite and zinc blende materials on an absolute energy scale. Furthermore, study of the GaAs/GaN (zinc blende) heterojunction has provided a tentative connection with the other III–V materials. X-ray photoemission spectroscopy yielded a VBO of 1.84 ± 0.1 eV,[979] which is the only available direct measurement and our recommended value. The implication of a staggered alignment with $\Delta E_c = 0.03$ eV strongly disagrees with the finding of $\Delta E_v = 0.5$ eV and a large positive CBO by Martin *et al.*[980] and Huang *et al.*[981] from electrical measurements. The discrepancy may be related to strain and other uncertainties in the electrical studies. The investigations of the VBO in the GaAsN/GaN heterojunctions yielded a range of different results, and the N frac-

Downloaded 26 Aug 2001 to 128.42.12.177. Redistribution subject to AIP license or copyright, see http://ojps.aip.org/japo/japcr.jsp

tion was too low to extrapolate the GaAs/GaN VBO with any confidence.[982–984] The observed VBO was found to be quite small, with the question of type-I versus type-II alignment remaining somewhat controversial.

Theoretically, the GaAs/GaN VBO was first estimated by Harrison and Tersoff.[985] Their result of 2.21 eV is quite similar to the value of 2.18–2.28 eV recently suggested by Bellaiche *et al.*[636,746] A first-principles linear-muffin-tin-orbital calculation by Agrawal *et al.* yielded 1.86 eV for the free-standing (i.e., strain-free) GaAs/GaN superlattice.[986] Those authors also predicted a strong dependence on the interface properties. In view of the present uncertainties, the agreement between experiment and theory should be considered quite good (apart from the electrical studies).

The valence-band discontinuity at the (zinc blende) GaN/AlN interface was first probed experimentally by Sitar *et al.*,[365] who obtained 1.4 eV from fits to optical measurements on GaN/AlN superlattices. Subsequently, Baur *et al.* found a VBO of 0.5 eV by measuring the difference between the acceptor levels of iron in each material.[987] X-ray photoemission spectroscopy yielded a VBO of 0.8 eV at the wurtzite GaN/AlN junction,[988] which was revised to 0.70 eV in a later article by the same authors.[989] Using the same approach, Waldrop and Grant found a considerably different value of 1.36 eV.[990] Those authors also reported a nearly linear VBO variation in the AlGaN alloy, with a positive bowing parameter of 0.59 eV.[991] Using x-ray and ultraviolet photoelectron spectroscopy, King *et al.* found that the GaN/AlN VBO ranged from 0.5 to 0.8 eV, depending on the growth temperature.[992] They surmised that the differences arose from strain, defects, and film stoichiometry effects. A VBO in the 0.15–0.4 eV range was reported by Rizzi *et al.*,[993] who pointed out that the Ga $3d$ core level, which has been used as a reference in GaN, is in fact hybridized with other valence bands.

On the theoretical front, calculations were performed by Albanesi *et al.*[994] and Chen *et al.*[995] for the zinc blende AlN/GaN interface, and by Satta *et al.*,[996] Ke *et al.*,[997] and Wei and Zunger[746] for the corresponding wurtzite junction. All of these works obtained VBOs in a rather narrow range from 0.7 to 0.85 eV. The last two articles found almost no difference between offsets for the cubic and hexagonal versions of the junction. A slightly lower value of 0.6 eV was calculated by Monch.[998] The importance of strain was studied by Binggeli *et al.* and Nardelli *et al.* The former found $\Delta E_v = 0.94$ eV for the relaxed zinc blende interface,[999] while the latter obtained 0.44–0.73 eV for the strained zinc blende interface (depending on the substrate lattice constant) and 0.57 eV for the strained wurtzite interface.[1000] Recently, Bernardini and Fiorentini[1001] studied macroscopic bulk polarization effects on the interface-charge contribution to the offset at the wurtzite heterojunction. They found VBO values of 0.20 and 0.85 eV corresponding to the underlying GaN and AlN lattice constants. However, most of the reported difference was from band-edge shifts in the bulk band structure, with only 0.18 eV due to the interface-charge contribution. We recommend using an unstrained band offset of 0.8 eV for both wurtzite and zinc blende interfaces. This represents the median of the reported values, and is also closest to the largest number of experimental and theoretical results. However, we caution again that the effects of spontaneous polarization and piezoelectric fields must be very carefully accounted for when applying this recommendation to the modeling of real GaN/AlN interfaces.

In comparison with GaN/AlN, the GaN/InN and AlN/InN junctions have strongly mismatched lattice constants. Theoretical values for the unstrained GaN/InN VBO are 0.3 eV[381] and 0.26 eV[326] for the zinc blende phase and 0.48 eV for the wurtzite phase.[326] The valence band in the technologically important GaInN alloy may be obtained from a linear interpolation. VBOs of 0.70 and 1.37 eV were calculated, respectively, for the wurtzite GaN/InN and AlN/InN junctions strained to AlN.[1000] Strain-induced piezoelectric fields, which can depend on the growth sequence, significantly complicate any experimental determination of the GaN/InN and AlN/InN band offsets. Only one experimental study of these two interfaces has been reported to date.[989] The VBO results of 1.05 and 1.81 eV were roughly corrected for piezoelectric fields due to residual strains, and it was concluded that transitivity for the GaN/AlN/InN system is obeyed to within experimental precision. Provisionally, we adopt a VBO of 1.05 eV for wurtzite GaN/InN. The large disagreement with the intuitive expectation of a small offset for this common-anion heterojunction remains to be resolved. Using transitivity, we derive 1.85 eV for the VBO of the wurtzite AlN/InN junction. For the zinc blende GaN/InN and AlN/InN interfaces, we recommend using the results of Wei and Zunger[326] (slightly modified to ensure transitivity): 0.26 eV and 1.06 eV, respectively.

VII. SUMMARY

We have reviewed the available information about band structure parameters for 12 technologically important III–V semiconductors and their ternary and quaternary alloys at the close of the 20th century. Whereas numerous reports of such parameters may be found in the literature, no *complete* and *fully consistent* set has been published previously. Earlier reviews were either restricted to particular material systems, did not address all parameters of interest, or were biased to the results of a specific group of investigators. On the other hand, our goal has been to provide a comprehensive and even-handed reference source, as free of internal contradictions and significant omissions as is practically possible in a work of this scope. We have also illustrated how the proposed parameters fit into the band structure computations.

The semiconductor band parameter knowledge base continues to expand as new reports are published daily. While the most fundamental parameters such as the energy gaps and effective masses are by now fairly well established for most of the III–V materials, we anticipate many new advances, particularly concerning band offsets and other parameters for the less mature systems such as the nitrides and antimonides. Furthermore, novel ternary, quaternary, and even quinternary alloys continue to be introduced and improved with an eye toward achieving greater flexibility in the design of quantum heterostructure devices. In view of the rapid ongoing progress on a broad front, this review should

Downloaded 26 Aug 2001 to 128.42.12.177. Redistribution subject to AIP license or copyright, see http://ojps.aip.org/japo/japcr.jsp

be regarded as a snapshot of the status at a given moment in time rather than the final word on III–V semiconductor band parameters. The goal has been to provide a one-stop summary of the present understanding, which will be revised, refined, and augmented by future experimental and theoretical investigations.

ACKNOWLEDGMENTS

The authors wish to thank Quantum Semiconductor Algorithms for the use of their finite element band structure software that was employed to test many of the input numbers. One of the authors (L.R.R.) wishes to thank Dr. Tom Reinecke and Dr. Ben Shanabrook at the Naval Research Laboratory, Washington, DC, and Dr. John Loehr and Dr. Tom Nelson at the Air Force Research Laboratory, Dayton, Ohio, for their hospitality during his sabbatical visits there.

[1] *Landolt-Bornstein Numerical Data and Functional Relationships in Science and Technology*, edited by O. Madelung, M. Schultz, and H. Weiss, New series, Vol. 17 (1982); reprinted in O. Madelung, editor, *Semiconductors-Basic Data*, 2nd ed. (Springer, New York, 1996).
[2] H. C. Casey, Jr. and M. B. Panish, *Heterostructure Lasers, Part A: Fundamental Principles* (Academic, New York, 1978), Chaps. 4 and 5.
[3] S. Adachi, *GaAs and Related Materials: Bulk Semiconducting and Superlattice Properties* (World Scientific, Singapore, 1994).
[4] S. Adachi, *Physical Properties of III–V Semiconductor Compounds: InP, InAs, GaAs, GaP, InGaAs, and InGaAsP* (Wiley, New York, 1992).
[5] V. Swaminathan, in *Indium Phosphide and Related Materials: Processing, Technology, and Devices*, edited by A. Katz (Artech House, Boston, 1992), Chap. 1.
[6] V. Swaminathan and A. T. Macrander, *Materials Aspects of GaAs and InP Based Structures* (Prentice Hall, Englewood Cliffs, NJ, 1991), Chap. 1.
[7] *Properties of Lattice-Matched and Strained Indium Gallium Arsenide*, edited by P. Bhattacharya (INSPEC, London, 1993).
[8] *Properties of Aluminum Gallium Arsenide*, edited by S. Adachi (INSPEC, Stevenage, Herts., UK, 1993).
[9] *Properties of Gallium Arsenide*, 2nd ed. (INSPEC, New York, 1990), EMIS datareviews series, No. 2.
[10] *Properties of Indium Phosphide* (INSPEC, New York, 1991), EMIS datareviews series, No. 6.
[11] *Handbook Series on Semiconductor Parameters*, edited by M. Levinshtein, S. Rumyantsev, and M. Shur (World Scientific, Singapore, 1996), Vols. 1 and 2.
[12] H. Jones, *The Theory of Brillouin Zones and Electronic States in Crystals* (North-Holland, Amsterdam, 1960).
[13] F. Bassani and G. Pastori Parravicini, *Electronic States and Optical Transitions in Solids* (Pergamon, New York, 1975).
[14] G. L. Bir and G. Pikus, *Symmetry and Strain-Induced Effects in Semiconductors* (Wiley, New York, 1974).
[15] P. Y. Yu and M. Cardona, *Fundamentals of Semiconductors* (Springer, Berlin, 1996).
[16] G. Bastard, *Wave Mechanics Applied to Semiconductor Heterostructures* (Editions de Physique, Les Ulis, France, 1988).
[17] D. L. Smith and C. Mailhiot, Rev. Mod. Phys. **62**, 173 (1990).
[18] E. L. Ivchenko and P. E. Pikus, *Superlattices and Other Heterostructures: Symmetry and Optical Phenomena* (Springer, Berlin, 1995).
[19] M. G. Burt, Semicond. Sci. Technol. **2**, 460 (1987); **2**, 701(E) (1987).
[20] M. G. Burt, J. Phys.: Condens. Matter **4**, 6651 (1992).
[21] J. M. Luttinger and W. Kohn, Phys. Rev. **97**, 869 (1955).
[22] P. O. Lowdin, J. Chem. Phys. **19**, 1396 (1951).
[23] E. O. Kane, J. Phys. Chem. Solids **6**, 236 (1958).
[24] E. O. Kane, in *Semiconductors and Semimetals*, edited by R. K. Willardson and A. C. Beer (Academic, New York, 1966), Vol. 1.
[25] E. O. Kane, in *Handbook on Semiconductors*, edited by W. Paul (North-Holland, Amsterdam, 1982), Vol. 1, p. 193.
[26] J. R. Chelikowsky and M. L. Cohen, Phys. Rev. B **14**, 556 (1976).
[27] Y. P. Varshni, Physica (Amsterdam) **34**, 149 (1967).
[28] L. Vina, S. Logothetidis, and M. Cardona, Phys. Rev. B **30**, 1979 (1984).
[29] R. Pässler, Phys. Status Solidi B **216**, 975 (1999).
[30] K. H. Yoo, L. R. Ram-Mohan, and D. F. Nelson, Phys. Rev. B **39**, 12808 (1989).
[31] P. Pfeffer and W. Zawadzki, Phys. Rev. B **37**, 2695 (1988).
[32] U. Rössler, Solid State Commun. **49**, 943 (1984).
[33] P. Pfeffer and W. Zawadzki, Phys. Rev. B **41**, 1561 (1990).
[34] S. L. Chuang and C. S. Chang, Appl. Phys. Lett. **68**, 1657 (1996).
[35] S. L. Chuang and C. S. Chang, Phys. Rev. B **54**, 2491 (1996).
[36] S. L. Chuang, *Physics of Optoelectronic Devices* (Wiley, New York, 1995).
[37] Yu. M. Sirenko, J. B. Jeon, K. W. Kim, M. A. Littlejohn, and M. A. Stroscio, Phys. Rev. B **53**, 1997 (1996).
[38] G. B. Ren, Y. M. Liu, and P. Blood, Appl. Phys. Lett. **74**, 1117 (1999).
[39] J. W. Mathews and A. E. Blakeslee, J. Cryst. Growth **32**, 265 (1976).
[40] R. People and S. A. Jackson, *Structurally Induced States from Strain and Confinement*, in Semiconductors and Semimetals, Vol. 32, edited by T. P. Pearsall, R. K. Willardson, and A. C. Beer (Academic, New York, 1990), p. 119.
[41] T. B. Bahder, Phys. Rev. B **41**, 11992 (1990); **46**, 9913(E) (1992).
[42] S.-H. Wei and A. Zunger, Phys. Rev. B **60**, 5404 (1999).
[43] S. L. Chuang, *Physics of Optoelectronic Devices* (Wiley, New York, 1995).
[44] W. F. Cady, *Piezoelectricity* (McGraw-Hill, New York, 1946), p. 192.
[45] J. F. Nye, *Physical Properties of Crystals* (Oxford University Press, Oxford, UK, 1985).
[46] I. P. Smorchkova *et al.*, J. Appl. Phys. **86**, 4520 (1990).
[47] O. Ambacher *et al.*, J. Appl. Phys. **85**, 3222 (1999).
[48] H. Morkoc, *Nitride Semiconductors and Devices* (Springer, Berlin, 1999).
[49] *Group III Nitride Semiconductor Compounds, Physics and Applications*, edited by B. Gil (Clarendon, Oxford, 1998).
[50] E. T. Yu, J. O. McCaldin, and T. C. McGill, *Solid State Physics*, edited by H. Ehrenreich and D. Turnbull (Academic, New York, 1992), Vol. 46, p. 2.
[51] J. P. Loehr and J. Singh, IEEE J. Quantum Electron. **27**, 708 (1991).
[52] J. C. Strikwerda, *Finite-Difference Schemes and Partial Differential Equations* (Wadsworth and Brooks, Pacific Grove, CA, 1989).
[53] L. R. Ram-Mohan, K. H. Yoo, and R. L. Aggarwal, Phys. Rev. B **38**, 6151 (1988).
[54] K. H. Yoo, R. L. Aggarwal, and L. R. Ram-Mohan, J. Vac. Sci. Technol. A **7**, 415 (1989).
[55] B. Chen, M. Lazzouni, and L. R. Ram-Mohan, Phys. Rev. B **45**, 1204 (1992).
[56] F. Szmulowicz, Phys. Rev. B **57**, 9081 (1998), and references therein.
[57] L. R. Ram-Mohan and J. R. Meyer, J. Nonlinear Opt. Phys. Mater. **4**, 191 (1995).
[58] K. Nakamura, A. Shimizu, M. Koshiba, and K. Hayata, Electron. Commun. Jpn., Part 2: Electron. **72**, 29 (1989); IEEE J. Quantum Electron. **25**, 889 (1989); **27**, 2035 (1991); **28**, 1670 (1992).
[59] T. Li and K. J. Kuhn, J. Comput. Phys. **115**, 288 (1994).
[60] G. C. La Rocca, S. Rodriguez, and F. Bassani, Phys. Rev. B **38**, 9819 (1988).
[61] M. Cardona, N. E. Christensen, and G. Fasol, *18th International Conference on Physics of Semiconductors* (World Scientific, Singapore, 1987), Vol. 2, p. 1133.
[62] W. Zawadzki, P. Pfeffer, and H. Sigg, Solid State Commun. **53**, 777 (1985).
[63] N. Kim, G. C. La Rocca, S. Rodriguez, and F. Bassani, Riv. Nuovo Cimento **12**, 1 (1989).
[64] H. C. Liu, Appl. Phys. Lett. **51**, 1019 (1987).
[65] H. C. Liu, Superlattices Microstruct. **7**, 35 (1990).
[66] J. P. Sun, R. K. Mains, K. Yang, and G. I. Haddad, J. Appl. Phys. **74**, 5053 (1993).
[67] Y. Fu, M. Willander, E. L. Ivchenko, and A. A. Kiselev, Phys. Rev. B **47**, 13498 (1993).
[68] M. U. Erdogan, K. W. Kim, M. A. Stroscio, and M. Dutta, J. Appl. Phys. **74**, 4777 (1993).
[69] J. P. Cuypers and W. van Haeringen, Phys. Rev. B **48**, 11469 (1993).
[70] J. C. Slater and G. F. Koster, Phys. Rev. **94**, 1498 (1954).
[71] D. J. Chadi and M. L. Cohen, Phys. Status Solidi B **68**, 405 (1975).
[72] P. Vogl, H. P. Hjalmarson, and J. D. Dow, J. Phys. Chem. Solids **44**, 365 (1983).
[73] G. Klimeck, R. C. Bowen, T. B. Boykin, and T. A. Cwik, Superlattices Microstruct. **27**, 520 (2000).

Downloaded 26 Aug 2001 to 128.42.12.177. Redistribution subject to AIP license or copyright, see http://ojps.aip.org/japo/japcr.jsp

[74] J. N. Schulman and Y.-C. Chang, Phys. Rev. B **31**, 2056 (1985).
[75] J. N. Schulman and Y.-C. Chang, Phys. Rev. B **33**, 2594 (1986).
[76] Y. C. Chang, Phys. Rev. B **37**, 8215 (1988).
[77] J. P. Loehr, Phys. Rev. B **50**, 5429 (1994).
[78] J. P. Loehr, *Physics of Strained Quantum Well Lasers* (Kluwer Academic, New York, 1997).
[79] J. C. Phillips and L. Kleinman, Phys. Rev. **116**, 287 (1959).
[80] M. H. Cohen and V. Heine, Phys. Rev. **122**, 1821 (1961).
[81] M. L. Cohen and J. R. Chelikowsky, *Electronic Structure and Optical Properties of Semiconductors*, Springer Series in Solid-State Sciences, edited by M. Cardona (Springer, Berlin, 1988), Vol. 75.
[82] V. Heine, *The Pseudopotential Concept*, in Solid State Physics, edited by H. Ehrenreich, F. Seitz, and D. Turnbull, Vol. 24 (Academic, New York, 1970), p. 1.
[83] M. L. Cohen and V. Heine, *The Fitting of Pseudopotentials to Experimental Data and their Subsequent Application*, in Solid State Physics, edited by H. Ehrenreich, F. Seitz, and D. Turnbull, Vol. 24 (Academic, New York, 1970), p. 38.
[84] L.-W. Wang and A. Zunger, in *Semiconductor Nanoclusters*, Studies in Surface Science and Catalysis, Vol. 103, edited by P. V. Kamat and D. Meisel (Elsevier Science, New York, 1996), p. 161.
[85] D. M. Wood and A. Zunger, Phys. Rev. B **53**, 7949 (1996).
[86] L.-W. Wang, S.-H. Wei, T. Mattila, A. Zunger, I. Vurgaftman, and J. R. Meyer, Phys. Rev. B **60**, 5590 (1999).
[87] J. S. Blakemore, J. Appl. Phys. **53**, R123 (1983) and references therein.
[88] C. D. Thurmond, J. Electrochem. Soc. **122**, 1133 (1975).
[89] P. Lautenschlager, M. Garriga, S. Logothetidis, and M. Cardona, Phys. Rev. B **35**, 9174 (1987).
[90] H. Shen, S. H. Pan, Z. Hang, J. Leng, F. H. Pollak, J. M. Woodall, and R. N. Sacks, Appl. Phys. Lett. **53**, 1080 (1988).
[91] E. Grilli, M. Guzzi, R. Zamboni, and L. Pavesi, Phys. Rev. B **45**, 1638 (1992).
[92] M. El Allali, C. B. Sorensen, E. Veje, and P. Tidemand-Petersson, Phys. Rev. B **48**, 4398 (1993).
[93] D. E. Aspnes, Phys. Rev. B **14**, 5331 (1976).
[94] D. E. Aspnes and A. A. Studna, Phys. Rev. B **7**, 4605 (1973).
[95] R. A. Stradling and R. A. Wood, J. Phys. C **3**, L94 (1970).
[96] L. G. Shantharama, A. R. Adams, C. N. Ahmad, and R. J. Nicholas, J. Phys. C **17**, 4429 (1984).
[97] H. Hazama, T. Sugimasa, T. Imachi, and C. Hamaguchi, J. Phys. Soc. Jpn. **54**, 3488 (1985).
[98] H. Hazama, T. Sugimasa, T. Imachi, and C. Hamaguchi, J. Phys. Soc. Jpn. **55**, 1282 (1986).
[99] P. Pfeffer and W. Zawadzki, Phys. Rev. B **53**, 12813 (1996) and references therein.
[100] A. C. Sharma, N. M. Ravindra, S. Auluck, and V. K. Srivastava, Phys. Status Solidi B **120**, 715 (1983).
[101] M. P. C. M. Krijn, Semicond. Sci. Technol. **6**, 27 (1991), and references therein.
[102] N. Bouarissa and H. Aourag, Infrared Phys. Technol. **40**, 343 (1999).
[103] N. Ahmed *et al.*, Semicond. Sci. Technol. **7**, 357 (1992).
[104] W. Nakwaski, Physica B **210**, 1 (1995) and references therein.
[105] D. M. Szmyd, P. Porro, A. Majerfeld, and S. Lagomarsino, J. Appl. Phys. **68**, 2367 (1990).
[106] P. Lawaetz, Phys. Rev. B **4**, 3460 (1971).
[107] M. S. Skolnick, A. K. Jain, R. A. Stradling, J. Leotin, J. C. Ousset, and S. Askenazy, J. Phys. C **9**, 2809 (1976).
[108] D. Bimberg, Festkoerperprobleme **XVII**, 195 (1977).
[109] W. Ekardt, K. Loesch, and D. Bimberg, Phys. Rev. B **20**, 3303 (1979).
[110] Ch. Neumann, A. Noethe, and N. O. Lipari, Phys. Rev. B **37**, 922 (1988).
[111] L. W. Molenkamp, R. Eppenga, G. W. 't Hooft, P. Dawson, C. T. Foxon, and K. J. Moore, Phys. Rev. B **38**, 4314 (1988).
[112] B. V. Shanabrook, O. J. Glembocki, D. A. Broido, and W. I. Wang, Phys. Rev. B **39**, 3411 (1989).
[113] M. Said and M. A. Kanehisa, Phys. Status Solidi B **157**, 311 (1990).
[114] N. Binggeli and A. Baldereschi, Phys. Rev. B **43**, 14734 (1991).
[115] D. J. Chadi, A. H. Clark, and R. D. Burnham, Phys. Rev. B **13**, 4466 (1976).
[116] C. Hermann and C. Weisbuch, Phys. Rev. B **15**, 823 (1977).
[117] A. R. Adams, L. G. Shantharama, R. J. Nicholas, and C. K. Sarkar, Physica B **139–140**, 401 (1986).
[118] I. Gorczyca, P. Pfeffer, and W. Zawadzki, Semicond. Sci. Technol. **6**, 963 (1991).
[119] R. H. Yan, S. W. Corzine, L. A. Coldren, and I. Suemune, IEEE J. Quantum Electron. **26**, 213 (1990).
[120] S.-H. Wei, A. Zunger, I.-H. Choi, and P. Y. Yu, Phys. Rev. B **58**, R1710 (1998).
[121] P. Pfeffer, I. Gorczyca, and W. Zawadzki, Solid State Commun. **51**, 179 (1984) and references therein.
[122] A. Blacha, H. Presting, and M. Cardona, Phys. Status Solidi B **126**, 11 (1984) and references therein.
[123] N. E. Christensen, Phys. Rev. B **30**, 5753 (1984).
[124] W. Walukiewicz, H. E. Ruda, J. Lagowski, and H. C. Gatos, Phys. Rev. B **30**, 4571 (1984).
[125] I. Gorczyca, T. Suski, E. Litwin-Staszewska, L. Dmowski, J. Krupski, and B. Etienne, Phys. Rev. B **46**, 4328 (1992).
[126] W. Walukiewicz, J. Appl. Phys. **59**, 3577 (1986).
[127] D. D. Nolte, W. Walukiewicz, and E. E. Haller, Phys. Rev. Lett. **59**, 501 (1987).
[128] S. Zollner, U. Schmid, N. E. Christensen, C. H. Grein, M. Cardona, and L. Ley, in *Proceedings of 20th International Conference On Physics of Semiconductors*, edited by E. M. Anastassakis and J. D. Joannopoulos (World Scientific, Singapore, 1990), Vol. 3, p. 1735.
[129] C. G. Van de Walle, Phys. Rev. B **39**, 1871 (1989).
[130] E. P. O'Reilly, Semicond. Sci. Technol. **1**, 128 (1986).
[131] S. P. Watkins, R. Ares, and C. A. Tran, in *Proceedings of 22nd International Conference On Physics of Semiconductors*, edited by D. J. Lockwood (World Scientific, Singapore, 1994), Vol. 1, p. 257.
[132] V. A. Karasyuk, M. L. W. Thewalt, and A. J. SpringThorpe, Phys. Status Solidi B **210**, 353 (1998).
[133] B. Monemar, Phys. Rev. B **8**, 5711 (1973).
[134] L. Pavesi and M. Guzzi, J. Appl. Phys. **75**, 4779 (1994).
[135] A. Onton, in *10th International Conference on Semiconductor Physics*, edited by S. P. Keller, J. C. Hensen, and F. Stern (U.S. Atomic Energy Commission, Washington, DC, 1970), p. 107.
[136] M. Garriga, P. Lautenschlager, M. Cardona, and K. Ploog, Solid State Commun. **61**, 157 (1987).
[137] W. P. Dumke, M. R. Lorenz, and G. D. Pettit, Phys. Rev. B **5**, 2978 (1972).
[138] S. Logothetidis, M. Cardona, and M. Garriga, Phys. Rev. B **43**, 11950 (1991).
[139] M. Guzzi, E. Grilli, S. Oggioni, J. L. Staehli, C. Bosio, and L. Pavesi, Phys. Rev. B **45**, 10951 (1992).
[140] H. J. Lee, L. Y. Juravel, J. C. Woolley, and A. J. SpringThorpe, Phys. Rev. B **21**, 659 (1980).
[141] A. K. Saxena, Phys. Status Solidi B **105**, 777 (1981).
[142] J. L. Aubel, U. K. Reddy, S. Sundaram, W. T. Beard, and J. Comas, J. Appl. Phys. **58**, 495 (1985).
[143] J. M. Wrobel, L. C. Bassett, J. L. Aubel, S. Sundaram, J. L. Davis, and J. Comas, J. Vac. Sci. Technol. **5**, 1464 (1987).
[144] T. P. E. Broekaert and C. G. Fonstad, J. Appl. Phys. **68**, 4310 (1990).
[145] D. Landheer, G. C. Aers, and Z. R. Wasilewski, Superlattices Microstruct. **11**, 55 (1992).
[146] R. V. Emlin, L. P. Zverev, and O. E. Rut, Sov. Phys. Semicond. **22**, 163 (1988) [Fiz. Tekh. Poluprovodn. (S.-Peterburg) **22**, 269 (1988)].
[147] M. Zachau, F. Koch, G. Weimann, and W. Schlapp, Phys. Rev. B **33**, 8564 (1986).
[148] E. Hess, I. Topol, K.-R. Schulze, H. Neumann, and K. Unger, Phys. Status Solidi B **55**, 187 (1973).
[149] B. Rheinlaender, H. Neumann, P. Fischer, and G. Kuehn, Phys. Status Solidi B **49**, K167 (1972).
[150] N. Miura, H. Yokoi, J. Kono, and S. Sasaki, Solid State Commun. **79**, 1039 (1991).
[151] W. R. Tribe, P. C. Klipstein, R. Gray, J. S. Roberts, and G. W. Smith, J. Phys. Chem. Solids **56**, 429 (1995).
[152] M. Goiran, J. L. Martin, J. Leotin, R. Planel, and S. Askenazy, Physica B **177**, 465 (1992).
[153] S. Logothetidis, M. Cardona, L. Tapfer, and E. Bauser, J. Appl. Phys. **66**, 2108 (1989).
[154] D. H. Chow, H. L. Dunlap, W. Williamson, III, S. Enquist, B. K. Gilbert, S. Subramaniam, P.-M. Lei, and G. H. Bernstein, IEEE Electron Device Lett. **17**, 69 (1996).
[155] J. R. Meyer *et al.*, IEE Proc.: Optoelectron. **145**, 275 (1998).
[156] F. Matossi and F. Stern, Phys. Rev. **111**, 472 (1958).
[157] C. R. Pidgeon, D. L. Mitchell, and R. N. Brown, Phys. Rev. **154**, 737 (1967).

Downloaded 26 Aug 2001 to 128.42.12.177. Redistribution subject to AIP license or copyright, see http://ojps.aip.org/japo/japcr.jsp

[158] I. V. Bodnar, A. I. Lukomskii, and G. F. Smirnova, Phys. Status Solidi A **37**, K173 (1976).
[159] L. M. Kanskaya, S. I. Kokhanovskii, R. P. Seisyan, Al. L. Efros, and V. A. Yukish, Sov. Phys. Semicond. **17**, 449 (1983) [Fiz. Tekh. Poluprovodn. (S.-Peterburg) **17**, 718 (1983)].
[160] J. C. Woolley and J. Warner, Can. J. Phys. **42**, 1879 (1964).
[161] W. M. Coderre and J. C. Woolley, Can. J. Phys. **46**, 1207 (1968).
[162] Y. Lacroix, C. A. Tran, S. P. Watkins, and M. L. W. Thewalt, J. Appl. Phys. **80**, 6416 (1996).
[163] E. Adachi, J. Phys. Soc. Jpn. **24**, 1178 (1968).
[164] Z. M. Fang, K. Y. Ma, D. H. Jaw, R. M. Cohen, and G. B. Stringfellow, J. Appl. Phys. **67**, 7034 (1990).
[165] X. Gong, H. Kan, T. Yamaguchi, I. Suzuki, M. Aoyama, M. Kumagawa, N. L. Rowell, A. Wang, and R. Rinfret, Jpn. J. Appl. Phys., Part 1 **33**, 1740 (1994).
[166] S. Adachi, J. Appl. Phys. **61**, 4869 (1987).
[167] L. V. Zverev, V. V. Kruzhaev, G. M. Min'kov, and O. E. Rut, JETP Lett. **31**, 154 (1980) [Pis'ma Zh. Eksp. Teor. Fiz. **31**, 169 (1980)].
[168] J. Kolodziejczak and S. Zukotynski, Phys. Status Solidi **16**, K55 (1966).
[169] U. K. Mishra and A. K. Walton, Phys. Status Solidi **24**, K87 (1967).
[170] N. K. S. Gaur, Physica B **48**, 112 (1970).
[171] M. B. Thomas and J. C. Woolley, Can. J. Phys. **49**, 2052 (1971).
[172] Yu. M. Burdukov, Yu. V. Mal'tsev, G. J. Pichakhchi, Yu. I. Ukhanov, and Kh. A. Khalilov, Sov. Phys. Semicond. **4**, 1184 (1971) [Fiz. Tekh. Poluprovodn. (S.-Peterburg) **4**, 1390 (1970)].
[173] F. P. Kesamanly, Yu. V. Mal'tsev, A. Ya. Nashel'skii, G. I. Pichakhchi, Y. A. Skripkin, and Yu. I. Ukhanov, Sov. Phys. Semicond. **6**, 1568 (1973) [Fiz. Tekh. Poluprovodn. (S.-Peterburg) **6**, 1816 (1973)].
[174] D. C. Tsui, Phys. Rev. B **12**, 5739 (1975).
[175] A. E. Stephens, R. E. Miller, J. R. Sybert, and D. G. Seiler, Phys. Rev. B **18**, 4394 (1978).
[176] J. Takayama, K. Shimomae, and C. Hamaguchi, Jpn. J. Appl. Phys., Part 1 **20**, 1265 (1981).
[177] P. D. Wang, S. N. Holmes, T. Le, R. A. Stradling, I. T. Ferguson, and A. G. de Oliveira, Semicond. Sci. Technol. **7**, 767 (1992).
[178] D. Schneider, C. Brink, G. Irmer, and P. Verma, Physica B **256–258**, 625 (1998).
[179] M. Morgenstern, R. Dombrowski, Chr. Wittneven, and R. Wiesendanger, Phys. Status Solidi B **210**, 845 (1998).
[180] H. A. Washburn, J. R. Sites, and H. H. Wieder, J. Appl. Phys. **50**, 4872 (1979).
[181] L. A. Kazakova, V. V. Kostsova, R. K. Karymshakov, Yu. I. Ukhanov, and V. P. Yagup'ev, Sov. Phys. Semicond. **5**, 1495 (1972) [Fiz. Tekh. Poluprovodn. (S.-Peterburg) **5**, 1710 (1971)].
[182] M.-Z. Huang and W. Y. Ching, J. Phys. Chem. Solids **46**, 977 (1985).
[183] C. R. Pidgeon, S. H. Groves, and J. Feinleib, Solid State Commun. **5**, 677 (1967).
[184] R. A. Stradling, T. A. Malik, J. Plumridge, S. J. Chung, W. T. Yuen, N. Miura, H. Arimoto, and Y. Imanaka, in *Proceedings of 23rd International Conference On Physics of Semiconductors*, edited by M. Scheffler and R. Zimmerman (World Scientific, Singapore, 1996), Vol. 3, p. 2223.
[185] S. M. Sze, *Physics of Semiconductor Devices*, 2nd ed. (Wiley, New York, 1981), Chap. 12.3.
[186] M. R. Lorenz, G. D. Pettit, and R. C. Taylor, Phys. Rev. **171**, 876 (1968).
[187] R. G. Humphreys, U. Rössler, and M. Cardona, Phys. Rev. B **18**, 5590 (1978).
[188] D. Auvergne, P. Merle, and H. Mathieu, Phys. Rev. B **12**, 1371 (1975).
[189] T. Takizawa, J. Phys. Soc. Jpn. **52**, 1057 (1983).
[190] C. Wetzel, B. K. Meyer, and P. Omling, Phys. Rev. B **47**, 15588 (1993).
[191] S.-G. Shen and X.-Q. Fan, J. Phys.: Condens. Matter **8**, 4369 (1996).
[192] L. A. Kazakova, M. V. Rapaport, B. E. Samorukov, and Yu. I. Ukhanov, Sov. Phys. Semicond. **9**, 54 (1975) [Fiz. Tekh. Poluprovodn. (S.-Peterburg) **9**, 85 (1975)].
[193] N. Miura, G. Kido, M. Suekane, and S. Chikazumi, J. Phys. Soc. Jpn. **52**, 2838 (1983).
[194] D. Bimberg, M. S. Skolnick, and L. M. Sander, Phys. Rev. B **19**, 2231 (1979).
[195] A. C. Carter, P. J. Dean, M. S. Skolnick, and R. A. Stradling, J. Phys. C **10**, 5111 (1977).
[196] C. F. Schwerdtfeger, Solid State Commun. **11**, 779 (1972).
[197] C. C. Bradley, P. E. Simmonds, J. R. Stockton, and R. A. Stradling, Solid State Commun. **12**, 413 (1973).
[198] J. Leotin, R. Barbaste, S. Askenazy, M. S. Skolnick, R. A. Stradling, and J. Tuchendler, Solid State Commun. **15**, 693 (1974).
[199] R. A. Street and W. Senske, Phys. Rev. Lett. **37**, 1292 (1976).
[200] H. Mathieu, P. Merle, E. L. Ameziane, B. Archilla, J. Camassel, and G. Poiblaud, Phys. Rev. B **19**, 2209 (1979).
[201] T. H. Glisson, J. R. Hauser, M. A. Littlejohn, and C. K. Williams, J. Electron. Mater. **7**, 1 (1978).
[202] Zh. I. Alferov, D. Z. Garbuzov, S. G. Konnikov, P. S. Kop'ev, and V. A. Mishurnyi, Sov. Phys. Semicond. **7**, 1449 (1974) [Fiz. Tekh. Poluprovodn. (S.-Peterburg) **7**, 2175 (1973)].
[203] D. P. Bour, J. R. Shealy, G. W. Wicks, and W. J. Schaff, Appl. Phys. Lett. **50**, 615 (1987).
[204] S. Tiwari, *Compound Semiconductor Device Physics* (Academic, New York, 1992).
[205] F. Issiki, S. Fukatsu, and Y. Shiraki, Appl. Phys. Lett. **67**, 1048 (1995).
[206] T. M. Ritter, B. A. Weinstein, R. E. Viturro, and D. P. Bour, Phys. Status Solidi B **211**, 869 (1999).
[207] P. Rochon and E. Fortin, Phys. Rev. B **12**, 5803 (1975).
[208] P. Lautenschlager, M. Garriga, and M. Cardona, Phys. Rev. B **36**, 4813 (1987).
[209] Z. Hang, H. Shen, and F. H. Pollak, Solid State Commun. **73**, 15 (1990).
[210] L. Pavesi, F. Piazza, A. Rudra, J. F. Carlin, and M. Ilegems, Phys. Rev. B **44**, 9052 (1991).
[211] P. Lautenschlager, M. Garriga, and M. Cardona, Phys. Rev. B **36**, 4813 (1987).
[212] Z. Hang, H. Shen, and F. H. Pollak, Solid State Commun. **73**, 15 (1990).
[213] G. D. Pitt, J. Phys. C **6**, 1586 (1973) and references therein.
[214] J. Camassel, P. Merle, L. Bayo, and H. Mathieu, Phys. Rev. B **22**, 2020 (1980).
[215] T. Ohyama, E. Otsuka, S. Yamada, T. Fukui, and N. Kobayashi, Jpn. J. Appl. Phys., Part 2 **22**, L742 (1983).
[216] K. M. Lau and W. L. Wilson, Jr., Infrared Phys. **23**, 311 (1983).
[217] T. Nakashima, C. Hamaguchi, J. Komeno, and M. Ozeki, Jpn. J. Appl. Phys., Suppl. **23**, 69 (1983).
[218] Y. Maeda, H. Taki, M. Sakata, E. Ohta, S. Yamada, T. Fukui, and N. Miura, J. Phys. Soc. Jpn. **53**, 3553 (1984).
[219] T. Nakashima, C. Hamaguchi, J. Komeno, and M. Ozeki, J. Phys. Soc. Jpn. **54**, 725 (1985).
[220] M. Helm, W. Knap, W. Seidenbuch, R. Lassnig, E. Gornik, R. Triboulet, and L. L. Taylor, Solid State Commun. **53**, 547 (1985).
[221] M. A. Hopkins, R. J. Nicholas, P. Pfeffer, W. Zawadzki, D. Gauthier, J. C. Portal, and M. A. DiForte-Poisson, Semicond. Sci. Technol. **2**, 568 (1987).
[222] D. Schneider, D. Ruerup, A. Plichta, H.-U. Grubert, A. Schlachetzki, and K. Hansen, Z. Phys. B: Condens. Matter **95**, 281 (1994).
[223] D. Schneider, D. Ruerup, B. Schoenfelder, and A. Schlachetzki, Z. Phys. B: Condens. Matter **100**, 33 (1996).
[224] X. H. Shi, P. L. Liu, S. C. Shen, J. X. Chen, H. P. Xin, and A. Z. Li, J. Appl. Phys. **80**, 4491 (1996).
[225] I. Kobori, T. Nomura, and T. Ohyama, *Proceedings of 1998 International Conference on Microwave and Millimeter Wave Technology* (Publishing House of Electronics Industry, Beijing, China, 1998), p. 269.
[226] D. Bimberg, K. Hess, N. O. Lipari, J. U. Fischbach, and M. Altarelli, Physica B **89**, 139 (1977).
[227] R. V. Emlin, L. P. Zverev, O. E. Rut, and N. V. Korovina, Sov. Phys. Semicond. **12**, 1243 (1978) [Fiz. Tekh. Poluprovodn. (S.-Peterburg) **12**, 2081 (1978)].
[228] M. A. Alekseev, I. Ya. Karlik, D. N. Mirlin, and V. F. Sapega, Sov. Phys. Semicond. **22**, 355 (1988) [Fiz. Tekh. Poluprovodn. (S.-Peterburg) **22**, 569 (1988)].
[229] M. A. Alekseev, I. Ya. Karlik, I. A. Merkulov, D. N. Mirlin, and V. F. Sapega, Phys. Lett. A **127**, 373 (1988).
[230] G. Weber and W. Rühle, Phys. Status Solidi B **92**, 425 (1979).
[231] P. S. Dutta, Appl. Phys. Rev. **81**, 5821 (1997).
[232] M.-C. Wu and C.-C. Chen, J. Appl. Phys. **72**, 4275 (1992).
[233] C. Ghezzi, R. Magnanini, A. Parisini, B. Rotelli, L. Tarricone, A. Bosacchi, and S. Franchi, Phys. Rev. B **52**, 1463 (1995).
[234] V. Bellani, S. DiLernia, M. Geddo, G. Guizzetti, A. Bosacchi, S. Franchi, and R. Magnanini, Solid State Commun. **104**, 81 (1997).
[235] A. Joullie, A. Zein Eddin, and B. Girault, Phys. Rev. B **23**, 928 (1981).
[236] C. Alibert, A. Joullie, A. M. Joullie, and C. Ance, Phys. Rev. B **27**, 4946 (1983).
[237] C. D. Kourkoutas, P. D. Bekris, G. J. Papioannou, and P. C. Euthymiou, Solid State Commun. **49**, 1071 (1984) and references therein.
[238] H. J. Lee and J. C. Woolley, Can. J. Phys. **59**, 1844 (1981).
[239] M. Reine, R. L. Aggarwal, and B. Lax, Phys. Rev. B **5**, 3033 (1972).

Downloaded 26 Aug 2001 to 128.42.12.177. Redistribution subject to AIP license or copyright, see http://ojps.aip.org/japo/japcr.jsp

[240] A. Filion and E. Fortin, Phys. Rev. B **8**, 3852 (1973).
[241] D. A. Hill and C. F. Schwerdtfeger, J. Phys. Chem. Solids **35**, 1533 (1974).
[242] A. V. Varfolomeev, A. Ya. Ryskin, and R. P. Seisyan, Sov. Phys. Semicond. **10**, 1234 (1977) [Fiz. Tekh. Poluprovodn. (S.-Peterburg) **10**, 2072 (1976)].
[243] A. P. Roth and E. Fortin, Can. J. Phys. **56**, 1468 (1978).
[244] H. Arimoto, N. Miura, R. J. Nicholas, and C. Hamaguchi, *Proceedings of the 8th International Conference on Narrow-Gap Semiconductors* (World Scientific, London, 1998), p. 279.
[245] H. Arimoto, N. Miura, R. J. Nicholas, N. J. Mason, and P. J. Walker, Phys. Rev. B **58**, 4560 (1998).
[246] R. A. Stradling, Phys. Lett. **20**, 217 (1966).
[247] H. I. Zhang, Phys. Rev. B **1**, 3450 (1970).
[248] M. Cardona, N. E. Christensen, and G. Fasol, Phys. Rev. B **38**, 1806 (1988).
[249] S. Zollner, C. Lin, E. Schönherr, A. Böhringer, and M. Cardona, J. Appl. Phys. **66**, 383 (1989).
[250] N. N. Sirota and A. I. Lukomskii, Sov. Phys. Semicond. **7**, 140 (1973) [Fiz. Tekh. Poluprovodn. (S.-Peterburg) **7**, 196 (1973)].
[251] H. Mathieu, D. Auvergne, P. Merle, and K. C. Rustagi, Phys. Rev. B **12**, 5846 (1975).
[252] G. F. Glinskii, A. A. Kopylov, and A. N. Pikhtin, Solid State Commun. **30**, 631 (1979).
[253] M. Maaref, F. F. Charfi, M. Zouaghi, C. Benoit à la Guillaume, and A. Joullie, Phys. Rev. B **34**, 8650 (1986).
[254] A. Bignazzi, E. Grilli, M. Guzzi, C. Bocchi, A. Bosacchi, S. Franchi, and R. Magnanini, Phys. Rev. B **57**, 2295 (1998).
[255] F. W. O. Da Silva, C. Raisin, S. Gaillard, C. Alibert, and A. Rocher, Thin Solid Films **190**, 21 (1990).
[256] L. L. Laude, M. Cardona, and F. H. Pollack, Phys. Rev. B **1**, 1436 (1970).
[257] E. O. Kane, J. Phys. Chem. Solids **1**, 249 (1957).
[258] M. Razeghi, Opto-Electron. Rev. **6**, 155 (1998).
[259] A. P. Roth, W. J. Keeler, and E. Fortin, Can. J. Phys. **58**, 560 (1980).
[260] D. Auvergne, J. Camassel, H. Mathieu, and A. Joullie, J. Phys. Chem. Solids **35**, 133 (1974).
[261] M. Y. Yen, R. People, K. W. Wecht, and A. Y. Cho, Appl. Phys. Lett. **52**, 489 (1988).
[262] O. M. Leshko and E. M. Sheregii, Sov. Phys. Semicond. **21**, 424 (1987) [Fiz. Tekh. Poluprovodn. (S.-Peterburg) **21**, 694 (1987)].
[263] C. L. Littler and D. G. Seiler, Appl. Phys. Lett. **46**, 986 (1985).
[264] Y. J. Jung, M. K. Park, S. I. Tae, K. H. Lee, and H. J. Lee, J. Appl. Phys. **69**, 3109 (1991).
[265] S. Zwerdling, W. H. Kleiner, and J. P. Theriault, J. Appl. Phys. **32**, 2118 (1961).
[266] C. R. Pidgeon and R. N. Brown, Phys. Rev. **146**, 575 (1966).
[267] N. A. Belov, K. G. De, O. V. Kosogov, and M. A. Maramzina, Sov. Phys. Semicond. **7**, 1451 (1974) [Fiz. Tekh. Poluprovodn. (S.-Peterburg) **7**, 2179 (1973)].
[268] H. Kahlert, Phys. Rev. B **18**, 5667 (1978).
[269] M. H. Weiler, J. Magn. Magn. Mater. **11**, 131 (1979).
[270] V. V. Monakhov, A. M. Yafyasov, and O. V. Romanov, Sov. Phys. Semicond. **20**, 603 (1986) [Fiz. Tekh. Poluprovodn. (S.-Peterburg) **20**, 954 (1986)].
[271] X. Qijiang, C. Chenjia, W. Xuezhong, S. Shouxu, Z. Yinkang, W. Weili, C. Shushi, L. Jizhou, and L. Caixia, Chin. J. Semicond. **4**, 549 (1983).
[272] F. Rouli, Z. Guozhen, and T. Dinqyuan, Chin. J. Semicond. **4**, 230 (1983).
[273] B. Kessler, R. Paul, and R. Nies, Phys. Status Solidi B **167**, 349 (1991).
[274] T. Morimoto, M. Chiba, G. Kido, and A. Tanaka, Semicond. Sci. Technol. **8**, S417 (1993).
[275] P. Y. Liu and J. C. Maan, Phys. Rev. B **47**, 16274 (1993); **47**, 16274 (1993).
[276] I. M. Tsidil'kovskii and M. V. Yakunin, Sov. Phys. Semicond. **13**, 178 (1979) [Fiz. Tekh. Poluprovodn. (S.-Peterburg) **13**, 311 (1979)].
[277] C. R. Pidgeon and S. H. Groves, Phys. Rev. **186**, 824 (1969).
[278] E. Otsuka, T. Ohyama, and K. Fujii, J. Phys. Colloq. **42**, C7-393 (1981).
[279] R. Meisels and F. Kuchar, Phys. Status Solidi B **116**, 557 (1983).
[280] M. V. Yakunin, Sov. Phys. Semicond. **21**, 859 (1987) [Fiz. Tekh. Poluprovodn. (S.-Peterburg) **21**, 1413 (1987)].
[281] E. M. Sheregii and Yu. O. Ugrin, Sov. Phys. Semicond. **24**, 660 (1990) [Fiz. Tekh. Poluprovodn. (S.-Peterburg) **24**, 1047 (1990)].
[282] K. Shimomae, K. Senda, K. Kasai, and C. Hamaguchi, J. Phys. Soc. Jpn. **49**, 1060 (1980).
[283] A. S. Filipchenko and L. N. Radaikina, Phys. Status Solidi B **55**, K139 (1973).
[284] S. Huant, L. Dmowski, M. Baj, and L. C. Brunel, Phys. Status Solidi B **135**, K129 (1986).
[285] D. G. Seiler, B. D. Bajaj, and A. E. Stephens, Phys. Rev. B **16**, 2822 (1977) and references therein.
[286] A. P. Menushenkov and E. A. Protasov, Sov. Phys. Semicond. **13**, 773 (1979) [Fiz. Tekh. Poluprovodn. (S.-Peterburg) **13**, 1319 (1979)].
[287] D. G. Seiler and K. L. Hathcox, Phys. Rev. Lett. **29**, 647 (1972).
[288] P. E. Van Camp, V. E. Van Doren, and J. T. Devreese, Phys. Rev. B **44**, 9056 (1991).
[289] *Properties of Group-III Nitrides*, edited by J. H. Edgar (INSPEC, IEE, London, 1994), EMIS Datareviews Series No. 11.
[290] J. I. Pankove, S. Bloom, and G. Harbeke, RCA Rev. **36**, 163 (1975).
[291] F. P. Kesamanly, Sov. Phys. Semicond. **8**, 147 (1974) [Fiz. Tekh. Poluprovodn. (S.-Peterburg) **8**, 225 (1974)].
[292] S. C. Jain, M. Willander, J. Narayan, and R. Van Overstraeten, J. Appl. Phys. **87**, 965 (2000).
[293] *The Blue Laser Diode*, edited by S. Nakamura and G. Fasol (Springer, Berlin, 1997).
[294] R. Dingle, D. D. Sell, S. E. Stokowski, and M. Ilegems, Phys. Rev. B **4**, 1211 (1971).
[295] M. Ilegems, R. Dingle, and R. A. Logan, J. Appl. Phys. **43**, 3797 (1972).
[296] See, e.g., C. Guenaud, E. Deleporte, M. Voos, C. Delalande, B. Beaumont, M. Leroux, P. Gibart, and J. P. Faurie, MRS Internet J. Nitride Semicond. Res. **2**, 10 (1997).
[297] O. Lagerstedt and B. Monemar, J. Appl. Phys. **45**, 2266 (1974).
[298] B. Monemar, Phys. Rev. B **10**, 676 (1974).
[299] W. Shan, T. J. Schmidt, X. H. Yang, S. J. Hwang, J. J. Song, and B. Goldenberg, Appl. Phys. Lett. **66**, 985 (1995).
[300] W. Shan, X. C. Xie, J. J. Song, and B. Goldenberg, Appl. Phys. Lett. **67**, 2512 (1995).
[301] B. Gil, O. Briot, and R.-L. Aulombard, Phys. Rev. B **52**, R17028 (1995).
[302] G. D. Chen, M. Smith, J. Y. Lin, H. X. Jiang, S.-H. Wei, M. A. Khan, and C. J. Sun, Appl. Phys. Lett. **68**, 2784 (1996).
[303] C. Merz, M. Kunzer, U. Kaufmann, I. Akasaki, and H. Amano, Semicond. Sci. Technol. **11**, 712 (1996).
[304] M. O. Manasreh, Phys. Rev. B **53**, 16425 (1996).
[305] J. S. Im, A. Moritz, F. Steuber, V. Haerle, F. Scholz, and A. Hangleiter, Appl. Phys. Lett. **70**, 631 (1997).
[306] A. Shikanai, T. Azuhata, T. Sota, S. Chichibu, A. Kuramata, K. Horino, and S. Nakamura, J. Appl. Phys. **81**, 417 (1997).
[307] C. F. Li, Y. S. Huang, L. Malikova, and F. H. Pollak, Phys. Rev. B **55**, 9251 (1997).
[308] K. Reimann, M. Steube, D. Froelich, and S. J. Clarke, J. Cryst. Growth **189/190**, 652 (1998).
[309] B. Monemar, J. P. Bergman, I. A. Buyanova, W. Li, H. Amano, and I. Akasaki, MRS Internet J. Nitride Semicond. Res. **1**, 2 (1996).
[310] M. Smith, G. D. Chen, J. Y. Lin, H. X. Jiang, M. Asif Khan, C. J. Sun, Q. Chen, and J. W. Yang, J. Appl. Phys. **79**, 7001 (1996).
[311] D. C. Reynolds, D. C. Look, W. Kim, O. Aktas, A. Botchkarev, A. Salvador, H. Morkoc, and D. N. Talwar, J. Appl. Phys. **80**, 594 (1996).
[312] J. F. Muth, J. H. Lee, I. K. Shmagin, R. M. Kolbas, H. C. Casey, Jr., B. P. Keller, U. K. Mishra, and S. P. DenBaars, Appl. Phys. Lett. **71**, 2572 (1997).
[313] S. Chichibu, T. Azuhata, T. Sota, and S. Nakamura, J. Appl. Phys. **79**, 2784 (1996).
[314] H. Teisseyre, P. Perlin, T. Suski, I. Grzegory, S. Porowski, J. Jun, A. Pietraszko, and T. D. Moustakas, J. Appl. Phys. **76**, 2429 (1994).
[315] J. Petalas, S. Logothetidis, S. Boultadakis, M. Alouani, and J. M. Wills, Phys. Rev. B **52**, 8082 (1995).
[316] A. Salvador, G. Liu, W. Kim, O. Aktas, A. Botchkarev, and H. Morkoc, Appl. Phys. Lett. **67**, 3322 (1995).
[317] A. S. Zubrilov, Yu. V. Melnik, A. E. Nikolaev, M. A. Jacobson, D. K. Nelson, and V. A. Dmitriev, Sov. Phys. Semicond. **33**, 1067 (1999) [Fiz. Tekh. Poluprovodn. (S.-Peterburg) **33**, 1173 (1999)].
[318] D. Brunner, H. Angerer, E. Bustarret, F. Freudenberg, R. Hoepler, R. Dimitrov, O. Ambacher, and M. Stutzmann, J. Appl. Phys. **82**, 5090 (1997).
[319] N. E. Christensen and I. Gorczyca, Phys. Rev. B **50**, 4397 (1994).
[320] S. Logothetidis, J. Petalas, M. Cardona, and T. D. Moustakas, Phys. Rev. B **50**, 18017 (1994).

Downloaded 26 Aug 2001 to 128.42.12.177. Redistribution subject to AIP license or copyright, see http://ojps.aip.org/japo/japcr.jsp

[321] T. Yang, S. Nakajima, and S. Sakai, Jpn. J. Appl. Phys., Part 1 **34**, 5912 (1995).
[322] Z. Yang and Z. Xu, Phys. Rev. B **54**, 17577 (1996).
[323] Y. C. Yeo, T. C. Chong, and M. F. Li, J. Appl. Phys. **83**, 1429 (1998).
[324] Yu. M. Sirenko, J. B. Jeon, B. C. Lee, K. W. Kim, M. A. Littlejohn, M. A. Stroscio, and G. J. Iafrate, Phys. Rev. B **55**, 4360 (1997).
[325] S. L. Chuang and C. S. Chang, Phys. Rev. B **54**, 2491 (1996).
[326] S.-H. Wei and A. Zunger, Appl. Phys. Lett. **69**, 2719 (1996).
[327] M. Suzuki, T. Uenoyama, and A. Yanase, Phys. Rev. B **52**, 8132 (1995).
[328] A. S. Barker, Jr. and M. Ilegems, Phys. Rev. B **7**, 743 (1973).
[329] B. Rheinlander and H. Neumann, Phys. Status Solidi B **64**, K123 (1974).
[330] V. G. Sidorov, L. S. Sveshkova, M. D. Shagalov, and Yu. K. Shalabutov, Sov. Phys. Semicond. **10**, 1309 (1976) [Fiz. Tekh. Poluprovodn. (S.-Peterburg) **10**, 2200 (1976)].
[331] B. K. Meyer, D. Volm, A. Graber, H. C. Alt, T. Detchprohm, A. Amano, and I. Akasaki, Solid State Commun. **95**, 597 (1995).
[332] A. M. Witowski, K. Pakula, J. M. Baranowski, M. L. Sadowski, and P. Wyder, Appl. Phys. Lett. **75**, 4154 (1999).
[333] M. Drechsler, D. M. Hoffman, B. K. Meyer, T. Detchprohm, H. Amano, and I. Akasaki, Jpn. J. Appl. Phys., Part 2 **34**, L1178 (1995).
[334] P. Perlin *et al.*, Appl. Phys. Lett. **68**, 1114 (1996).
[335] Y. J. Wang, R. Kaplan, H. K. Ng, K. Doverspike, D. K. Gaskill, T. Ikedo, I. Akasaki, and H. Amono, J. Appl. Phys. **79**, 8007 (1996).
[336] W. Knap *et al.*, Appl. Phys. Lett. **70**, 2123 (1997).
[337] A. Kasic, M. Schubert, S. Einfeldt, D. Hommel, and T. E. Tiwald, Phys. Rev. B **62**, 7365 (2000).
[338] S. Elhamri, R. S. Newrock, D. B. Mast, M. Ahoujja, W. C. Mitchel, J. M. Redwing, M. A. Tischler, and J. S. Flynn, Phys. Rev. B **57**, 1374 (1998).
[339] A. Saxler *et al.*, J. Appl. Phys. **87**, 369 (2000).
[340] L. W. Wong, S. J. Cai, R. Li, K. Wang, H. W. Jiang, and M. Chen, Appl. Phys. Lett. **73**, 1391 (1998).
[341] T. Wang, J. Bai, S. Sakai, Y. Ohno, and H. Ohno, Appl. Phys. Lett. **76**, 2737 (2000).
[342] S. Kamiyama, K. Ohnaka, M. Suzuki, and T. Uenoyama, Jpn. J. Appl. Phys., Part 2 **34**, L822 (1995).
[343] B. B. Kosicki, R. J. Powell, and J. C. Burgiel, Phys. Rev. Lett. **24**, 1421 (1970).
[344] R. D. Cunningham, R. W. Brander, N. D. Knee, and D. K. Wickenden, J. Lumin. **5**, 21 (1972).
[345] J. W. Orton, Semicond. Sci. Technol. **10**, 101 (1995).
[346] M. Steube, K. Reimann, D. Froelich, and S. J. Clarke, Appl. Phys. Lett. **71**, 948 (1997).
[347] D. J. Dugdale, S. Brand, and R. A. Abram, Phys. Rev. B **61**, 12933 (2000).
[348] K. Kim, W. R. L. Lambrecht, and B. Segall, Phys. Rev. B **53**, 16310 (1996).
[349] W. Shan, R. J. Hauenstein, A. J. Fischer, J. J. Song, W. G. Perry, M. D. Bremser, R. F. Davis, and B. Goldenberg, Phys. Rev. B **54**, 13460 (1996).
[350] T. Ohtoshi, A. Niwa, and T. Kuroda, J. Appl. Phys. **82**, 1518 (1997).
[351] A. F. Wright, J. Appl. Phys. **82**, 2833 (1997).
[352] A. U. Sheleg and A. V. Savastenko, Izv. Akad. Nauk SSSR, Neorg. Mater. **15**, 1598 (1979) [Inorg. Mater. **15**, 1257 (1979)].
[353] A. Polian, M. Grimsditch, and I. Grzegory, J. Appl. Phys. **79**, 3343 (1996).
[354] Y. Takagi, M. Ahart, T. Azuhata, T. Sota, K. Suzuki, and S. Nakamura, Physica B **219–220**, 547 (1996).
[355] R. B. Schwarz, K. Khachaturyan, and E. R. Weber, Appl. Phys. Lett. **70**, 1122 (1997).
[356] S. Muensit and I. L. Guy, Appl. Phys. Lett. **72**, 1896 (1998).
[357] I. L. Guy, S. Muensit, and E. M. Goldys, Appl. Phys. Lett. **75**, 4133 (1999).
[358] C. M. Lueng, H. L. W. Chan, C. Surya, W. K. Fong, C. L. Choy, P. Chow, and M. Rosamond, J. Non-Cryst. Solids **254**, 123 (1999).
[359] A. D. Bykhovski, V. V. Kaminski, M. S. Shur, Q. C. Chen, and M. A. Khan, Appl. Phys. Lett. **68**, 818 (1996).
[360] F. Bernardini, V. Fiorentini, and D. Vanderbilt, Phys. Rev. B **56**, R10024 (1997).
[361] K. Shimada, T. Sota, and K. Suzuki, J. Appl. Phys. **84**, 4951 (1998).
[362] F. Bechstedt, U. Grossner, and J. Furthmüller, Phys. Rev. B **62**, 8003 (2000).
[363] S. Bloom, G. Harbeke, E. Meier, and I. B. Ortenburger, Phys. Status Solidi B **66**, 161 (1974).
[364] S. Strite, J. Ran, Z. Li, A. Salvador, H. Chen, D. J. Smith, W. J. Choyke, and H. Morkoc, J. Vac. Sci. Technol. B **9**, 1924 (1991).
[365] Z. Sitar, M. J. Paisley, J. Ruan, J. W. Choyke, and R. F. Davis, J. Mater. Sci. Lett. **11**, 261 (1992).
[366] R. C. Powell, N.-E. Lee, Y.-W. Kim, and J. E. Greene, J. Appl. Phys. **73**, 189 (1993).
[367] H. Okumura, S. Yoshida, and T. Okahisa, Appl. Phys. Lett. **64**, 2997 (1994).
[368] G. Ramirez-Flores, H. Navarro-Contreras, A. Lastras-Martinez, R. C. Powell, and J. E. Greene, Phys. Rev. B **50**, 8433 (1994).
[369] W. J. Fan, M. F. Li, T. C. Chong, and J. B. Xia, J. Appl. Phys. **79**, 188 (1996).
[370] A. Tadjer, B. Abbar, M. Rezki, H. Aourag, and M. Certier, J. Phys. Chem. Solids **60**, 419 (1999).
[371] S. K. Pugh, D. J. Dugdale, S. Brand, and R. A. Abram, Semicond. Sci. Technol. **14**, 23 (1999).
[372] J. Menniger, U. Jahn, O. Brandt, H. Yang, and K. Ploog, Phys. Rev. B **53**, 1881 (1996).
[373] J. Wu, H. Yaguchi, K. Onable, and R. Ito, Appl. Phys. Lett. **71**, 2067 (1997).
[374] D. Xu, H. Yang, J. B. Li, D. G. Zhao, S. F. Li, S. M. Zhuang, R. H. Wu, Y. Chen, and G. H. Li, Appl. Phys. Lett. **76**, 3025 (2000).
[375] M. Fanciulli, T. Lei, and T. D. Moustakas, Phys. Rev. B **48**, 15144 (1993).
[376] W. W. Chow, A. F. Wright, and J. S. Nelson, Appl. Phys. Lett. **68**, 296 (1996).
[377] D. Ahn, J. Appl. Phys. **79**, 7731 (1996).
[378] M. Suzuki and T. Uenoyama, Appl. Phys. Lett. **69**, 3378 (1996).
[379] A. T. Meney, E. P. O'Reilly, and A. R. Adams, Semicond. Sci. Technol. **11**, 897 (1996).
[380] T. Ohtoshi, A. Niwa, and T. Kuroda, IEEE J. Sel. Top. Quantum Electron. **4**, 527 (1998).
[381] C. G. Van de Walle and J. Neugebauer, Appl. Phys. Lett. **70**, 2577 (1997).
[382] K. Kim, W. R. L. Lambrecht, and B. Segall, Phys. Rev. B **56**, 7018 (1997).
[383] W. M. Yim, E. J. Stofko, P. J. Zanzucchi, J. I. Pankove, M. Ettenberg, and S. L. Gilbert, J. Appl. Phys. **44**, 292 (1973).
[384] P. B. Perry and R. F. Rutz, Appl. Phys. Lett. **33**, 319 (1978).
[385] Q. Guo and A. Yoshida, Jpn. J. Appl. Phys., Part 1 **33**, 2454 (1994).
[386] R. D. Vispute, H. Wu, and J. Narayan, Appl. Phys. Lett. **67**, 1549 (1995).
[387] X. Tang, F. Hossain, K. Wongchotigul, and M. G. Spencer, Appl. Phys. Lett. **72**, 1501 (1998).
[388] K. Kim, W. R. L. Lambrecht, B. Segall, and M. van Schilfgaarde, Phys. Rev. B **56**, 7363 (1997).
[389] W. Shan *et al.*, Appl. Phys. Lett. **72**, 2274 (1998).
[390] K. Tsubouchi, K. Sugai, and N. Mikoshiba, in *1981 Ultrasonics Symposium*, edited by B. R. McAvoy (IEEE, New York, 1981), Vol. 1, p. 375.
[391] L. E. McNeil, M. Grimditch, and R. H. French, J. Am. Ceram. Soc. **76**, 1132 (1993).
[392] A. R. Hutson, U.S. Patent No. 3,090,876 (May 21, 1963).
[393] K. Tsubouchi, K. Sugai, and N. Mikoshiba, *Proceedings of the IEEE Ultrasonic Symposium* (IEEE, New York, 1982), p. 340.
[394] T. Kamiya, Jpn. J. Appl. Phys., Part 1 **35**, 4421 (1996).
[395] M. Leroux, N. Grandjean, J. Massies, B. Gil, P. Lefebvre, and P. Bigenwald, Phys. Rev. B **60**, 1496 (1999).
[396] N. Grandjean, B. Damilano, S. Dalmasso, M. Leroux, M. Laugt, and J. Massies, J. Appl. Phys. **86**, 3714 (1999).
[397] J. A. Garrido, J. L. Sanchez-Rojas, A. Jimenez, E. Munoz, F. Omnes, and P. Gibart, Appl. Phys. Lett. **75**, 2407 (1999).
[398] R. A. Hogg, C. E. Norman, A. J. Shields, M. Pepper, and M. Iizuka, Appl. Phys. Lett. **76**, 1428 (2000).
[399] S.-H. Park and S.-L. Chuang, Appl. Phys. Lett. **76**, 1981 (2000).
[400] R. Cingolani *et al.*, Phys. Rev. B **61**, 2711 (2000).
[401] K. Karch and F. Bechstedt, Phys. Rev. B **56**, 7404 (1997).
[402] K. Osamura, S. Naka, and Y. Murakami, J. Appl. Phys. **46**, 3432 (1975).
[403] N. Puychevrier and M. Menoret, Thin Solid Films **36**, 141 (1976).
[404] V. A. Tyagai, A. M. Evstigneev, A. N. Krasiko, A. F. Andreeva, and V. Ya. Malakhov, Sov. Phys. Semicond. **11**, 1257 (1977) [Fiz. Tekh. Poluprovodn. (S.-Peterburg) **11**, 2142 (1977)].
[405] T. L. Tansley and C. P. Foley, J. Appl. Phys. **59**, 3241 (1986).
[406] K. L. Westra and M. J. Brett, Thin Solid Films **192**, 227 (1990).
[407] A. Wakahara, T. Tsuchiya, and A. Yoshida, Vacuum **41**, 1071 (1990).
[408] T. Inushima, T. Yaguchi, A. Nagase, A. Iso, T. Shiraishi, and S. Ooya,

Downloaded 26 Aug 2001 to 128.42.12.177. Redistribution subject to AIP license or copyright, see http://ojps.aip.org/japo/japcr.jsp

Proceedings of 7th International Conference on InP and Related Materials, 1995, p. 187.
[409] S. Strite and H. Morkoc, J. Vac. Sci. Technol. B **10**, 1237 (1992).
[410] J. A. Van Vechten and T. K. Bergstresser, Phys. Rev. B **1**, 3351 (1970).
[411] C. Bosio, J. L. Staehli, M. Guzzi, G. Burri, and R. A. Logan, Phys. Rev. B **38**, 3263 (1988).
[412] T. F. Kuech, D. J. Wolford, R. Potemski, J. A. Bradley, K. H. Kelleher, D. Yan, J. P. Farrell, P. M. S. Lesser, and F. H. Pollak, Appl. Phys. Lett. **51**, 505 (1987).
[413] G. Oelgart, R. Schwabe, M. Heider, and B. Jacobs, Semicond. Sci. Technol. **2**, 468 (1987).
[414] D. Huang, G. Ji, U. K. Reddy, H. Morkoc, F. Xiong, and T. A. Tombrello, J. Appl. Phys. **63**, 5447 (1988).
[415] A small negative bowing parameter was determined by N. C. Miller, S. Zemon, G. P. Werber, and W. Powazinik, J. Appl. Phys. **57**, 512 (1985).
[416] D. E. Aspnes, S. M. Kelso, R. A. Logan, and R. Bhat, J. Appl. Phys. **60**, 754 (1986).
[417] R. Magri and A. Zunger, Phys. Rev. B **44**, 8672 (1991).
[418] K. A. Maeder and A. Zunger, Phys. Rev. B **51**, 10462 (1995).
[419] R. G. Waters, J. Appl. Phys. **52**, 3586 (1981).
[420] J. C. M. Henning, J. P. M. Ansems, and P. J. Roksnoer, J. Phys. C **19**, L335 (1986).
[421] P. El Jani, P. Gibart, J. C. Portal, and R. L. Aulombard, J. Appl. Phys. **58**, 3481 (1985).
[422] H. Qiang, F. H. Pollak, and G. Hickman, Solid State Commun. **76**, 1087 (1990).
[423] R. Driad, Z. H. Lu, S. Charbonneau, W. R. McKinnon, S. Laframboise, P. J. Poole, and S. P. McAlister, Appl. Phys. Lett. **73**, 665 (1998).
[424] Y. Lam, J. P. Loehr, and J. Singh, IEEE J. Quantum Electron. **28**, 1248 (1992).
[425] F. Capasso, J. Faist, C. Sirtori, and A. Y. Cho, Solid State Commun. **102**, 231 (1997).
[426] S. S. Vishnubhatla, B. Eyglunent, and J. C. Woolley, Can. J. Phys. **47**, 1661 (1969).
[427] R. E. Nahory, M. A. Pollack, W. D. Johnston, Jr., and R. L. Barns, Appl. Phys. Lett. **33**, 659 (1978).
[428] W. Porod and D. K. Ferry, Phys. Rev. B **27**, 2587 (1983).
[429] S. Adachi, J. Appl. Phys. **53**, 8775 (1982).
[430] K.-H. Goetz, D. Bimberg, H. Jürgensen, J. Selders, A. V. Solomonov, G. F. Glinskii, and M. Razeghi, J. Appl. Phys. **54**, 4543 (1983).
[431] S. Paul, J. B. Roy, and P. K. Basu, J. Appl. Phys. **69**, 827 (1991).
[432] S. Tiwari and D. J. Frank, Appl. Phys. Lett. **60**, 630 (1992).
[433] D.-S. Kim, S. R. Forrest, M. J. Lange, M. J. Cohen, G. H. Olsen, R. J. Menna, and R. J. Paff, J. Appl. Phys. **80**, 6229 (1996).
[434] M. V. Karachevtseva, A. S. Ignat'ev, V. G. Mokerov, G. Z. Nemtsev, V. A. Strakhov, and N. G. Yaremenko, Sov. Phys. Semicond. **28**, 691 (1994) [Fiz. Tekh. Poluprovodn. (S.-Peterburg) **28**, 1211 (1994)].
[435] Y. Takeda, A. Sasaki, Y. Imamura, and T. Takagi, J. Appl. Phys. **47**, 5405 (1976).
[436] E. Zielinski, H. Schweizer, K. Streubel, H. Eisele, and G. Weimann, J. Appl. Phys. **59**, 2196 (1986).
[437] K. Alavi, R. L. Aggarwal, and S. H. Groves, Phys. Rev. B **21**, 1311 (1980).
[438] E. Towe, J. Appl. Phys. **53**, 5136 (1982).
[439] P. W. Yu and E. Kuphal, Solid State Commun. **49**, 907 (1984).
[440] J. Beerens, G. Bernier, S. Lasserre, D. Pelenc, N. Puetz, and C. J. Miner, Can. J. Phys. **69**, 441 (1991).
[441] J. R. Jensen, J. M. Hvam, and W. Langbein, J. Appl. Phys. **86**, 2584 (1999).
[442] Z. Hang, D. Yan, F. H. Pollak, G. D. Pettit, and J. M. Woodall, Phys. Rev. B **44**, 10546 (1991).
[443] E. H. Perea, E. E. Mendez, and C. G. Fonstad, Appl. Phys. Lett. **36**, 978 (1980).
[444] K. Y. Cheng, A. Y. Cho, S. B. Christman, T. P. Pearsall, and J. E. Rowe, Appl. Phys. Lett. **40**, 423 (1982).
[445] J. A. Van Vechten, O. Berolo, and J. C. Woolley, Phys. Rev. Lett. **29**, 1400 (1972).
[446] O. Berolo, J. C. Woolley, and J. A. Van Vechten, Phys. Rev. B **8**, 3794 (1973).
[447] J. C. Fan and Y. F. Chen, J. Appl. Phys. **80**, 6761 (1996).
[448] R. J. Nicholas, J. C. Portal, C. Houlbert, P. Perrier, and T. P. Pearsall, Appl. Phys. Lett. **34**, 492 (1979).
[449] R. J. Nicholas, S. J. Sessions, and J. C. Portal, Appl. Phys. Lett. **37**, 178 (1980).
[450] E. H. Perea, E. Mendez, and C. G. Fonstad, J. Electron. Mater. **9**, 459 (1980).
[451] J. B. Restorrf, B. Houston, R. S. Allgaier, M. A. Littlejohn, and S. B. Phatak, J. Appl. Phys. **51**, 2277 (1980).
[452] C. K. Sarkar, R. J. Nicholas, J. C. Portal, M. Razeghi, J. Chevrier, and J. Massies, J. Phys. C **18**, 2667 (1985).
[453] H. Brendecke, H. L. Stormer, and R. J. Nelson, Appl. Phys. Lett. **35**, 772 (1979).
[454] M. Sugawara, N. Okazaki, T. Fujii, and S. Yamazaki, Phys. Rev. B **48**, 8102 (1993).
[455] M. Sugawara, N. Okazaki, T. Fujii, and S. Yamazaki, Phys. Rev. B **48**, 8848 (1993).
[456] D. Olego, T. Y. Chang, E. Silberg, E. A. Caridi, and A. Pinczuk, Appl. Phys. Lett. **41**, 476 (1982).
[457] L. A. Cury, J. Beerens, and J. P. Praseuth, Appl. Phys. Lett. **63**, 1804 (1993).
[458] J. C. Fan and Y. F. Chen, J. Appl. Phys. **80**, 1239 (1996).
[459] C. Hermann and T. P. Pearsall, Appl. Phys. Lett. **38**, 450 (1981).
[460] K. Tanaka, N. Kotera, and H. Nakamura, J. Appl. Phys. **85**, 4071 (1999).
[461] R. People, A. Jayaraman, K. W. Wecht, D. L. Sivco, and A. Y. Cho, Appl. Phys. Lett. **52**, 2124 (1988).
[462] V. A. Wilkinson, A. D. Prins, J. D. Lambkin, E. P. O'Reilly, D. J. Dunstan, L. K. Howard, and M. T. Emeny, Phys. Rev. B **42**, 3113 (1990).
[463] E. E. Matyas, Sov. Phys. Semicond. **13**, 1194 (1979) [Fiz. Tekh. Poluprovodn. (S.-Peterburg) **13**, 2046 (1979)].
[464] B. Wakefield, M. A. G. Halliwell, T. Kerr, D. A. Andrews, G. J. Davies, and D. R. Wood, Appl. Phys. Lett. **44**, 341 (1984).
[465] R. F. Kopf, H. P. Wei, A. P. Perley, and G. Livescu, Appl. Phys. Lett. **60**, 2386 (1992).
[466] P. Abraham, M. A. Garcia-Perez, T. Benyattou, G. Guillot, M. Sacilotti, and X. Letartre, Semicond. Sci. Technol. **10**, 1585 (1995).
[467] M. A. Lorenz and A. Onton, *Proceedings of the 10th International Conference on Physics of Semiconductors* (Cambridge University Press, Cambridge, 1970), p. 444.
[468] M. G. Wright, A. Kana'ah, B. C. Cavenett, G. R. Johnson, and S. T. Davey, Semicond. Sci. Technol. **4**, 590 (1989).
[469] Y. F. Chen, Y. T. Dai, J. C. Fan, T. L. Lee, and H. H. Lin, Appl. Phys. Lett. **67**, 1256 (1995).
[470] S.-G. Shen and X.-Q. Fan, J. Phys. Condens. Matter **9**, 3151 (1997).
[471] I. T. Ferguson, T. P. Beales, T. S. Cheng, C. M. Sotomayor-Torres, and E. G. Scott, Semicond. Sci. Technol. **4**, 243 (1989).
[472] C. N. Yeh, L. E. McNeil, R. E. Nahory, and R. Bhat, Phys. Rev. B **52**, 14682 (1995).
[473] D. P. Bour, in *Quantum Well Lasers*, edited by P. S. Zory (Academic, New York, 1993), p. 415.
[474] A. Onton, M. R. Lorenz, and W. Reuter, J. Appl. Phys. **42**, 3420 (1971).
[475] A. W. Mabbitt, Solid State Commun. **9**, 245 (1971).
[476] C. Alibert, G. Bordure, A. Laugier, and J. Chevallier, Phys. Rev. B **6**, 1301 (1972).
[477] G. B. Stringfellow, P. F. Lindquist, and R. A. Burmeister, J. Electron. Mater. **1**, 437 (1972).
[478] A. Laugier and J. Chevallier, Solid State Commun. **10**, 353 (1972).
[479] H. Lange, J. Donecker, and H. Friedrich, Phys. Status Solidi B **73**, 633 (1976).
[480] D. Auvergne, P. Merle, and H. Mathieu, Solid State Commun. **21**, 437 (1977).
[481] P. Merle, D. Auvergne, H. Mathieu, and J. Chevallier, Phys. Rev. B **15**, 2032 (1977).
[482] M. Bugajski, A. M. Kontkiewicz, and H. Mariette, Phys. Rev. B **28**, 7105 (1983) and references therein.
[483] C. Nozaki, Y. Ohba, H. Sugawara, S. Yasuami, and T. Nakanisi, J. Cryst. Growth **93**, 406 (1988).
[484] N. El-Masry and S. M. Bedair, Opt. Quantum Electron. **23**, S909 (1991).
[485] R. G. Alonso, A. Mascarenhas, G. S. Horner, K. A. Bertness, S. R. Kurtz, and J. M. Olson, Phys. Rev. B **48**, 11833 (1993).
[486] T. Sass, I. Pietzonka, and H. Schmidt, J. Appl. Phys. **85**, 3561 (1999).
[487] L. C. Su, S. T. Pu, G. B. Stringfellow, J. Christen, H. Selber, and D. Bimberg, J. Electron. Mater. **23**, 125 (1994).
[488] T. Hayakawa, K. Takahashi, M. Hosoda, S. Yamamoto, and T. Hijikata, Jpn. J. Appl. Phys., Part 2 **27**, L1553 (1988).
[489] C. T. H. F. Liedenbaum, A. Valster, A. L. G. J. Steverens, and G. W. 't Hooft, Appl. Phys. Lett. **57**, 2698 (1990).
[490] F. Omnes and M. Razeghi, Appl. Phys. Lett. **59**, 1034 (1991).

Downloaded 26 Aug 2001 to 128.42.12.177. Redistribution subject to AIP license or copyright, see http://ojps.aip.org/japo/japcr.jsp

[491] J. Chen, J. R. Sites, I. L. Spain, M. J. Hafich, and G. Y. Robinson, Appl. Phys. Lett. **58**, 744 (1991).
[492] G. W. 't Hooft, C. J. B. Riviere, M. P. C. M. Krijn, C. T. H. F. Liedenbaum, and A. Valster, Appl. Phys. Lett. **61**, 3169 (1992).
[493] M. D. Dawson and G. Duggan, Phys. Rev. B **47**, 12598 (1993).
[494] A. D. Prins, J. L. Sly, A. T. Meney, D. J. Dunstan, E. P. O'Reilly, A. R. Adams, and A. Valster, J. Phys. Chem. Solids **56**, 349 (1995).
[495] P. Emanuelsson, M. Drechsler, D. M. Hoffman, and B. K. Meyer, Appl. Phys. Lett. **64**, 2849 (1994).
[496] A. R. Goni, K. Syassen, K. Stroessner, and M. Cardona, Phys. Rev. B **39**, 3178 (1989).
[497] T. P. Chin, J. C. P. Chang, K. L. Kavanagh, C. W. Tu, P. D. Kirchner, and J. M. Woodall, Appl. Phys. Lett. **62**, 2369 (1993).
[498] A. T. Meney, A. D. Prins, A. F. Phillips, J. L. Sly, E. P. O'Reilly, D. J. Dunstan, A. R. Adams, and A. Valster, IEEE J. Sel. Top. Quantum Electron. **1**, 697 (1995).
[499] Yu. K. Krutogolov, S. V. Dovzhenko, S. A. Diordiev, L. I. Krutogolova, Yu. I. Kunakin, and S. S. Ryzhikh, Sov. Phys. Semicond. **23**, 557 (1989) [Fiz. Tekh. Poluprovodn. (S.-Peterburg) **23**, 887 (1989)].
[500] S. Ozaki, S. Adachi, M. Sato, and K. Ohtsuka, J. Appl. Phys. **79**, 439 (1996).
[501] K. Interholzinger, D. Patel, C. S. Menoni, P. Thiagarajan, G. Y. Robinson, and J. E. Fouquet, IEEE J. Quantum Electron. **34**, 93 (1998).
[502] S. Adachi, S. Ozaki, M. Sato, and K. Ohtsuka, J. Appl. Phys. **35**, 537 (1996).
[503] S. L. Wong, D. Kinder, J. G. Michels, R. J. Nicholas, G. Duggan, M. D. Dawson, and A. H. Kean, *Proceedings of the 22nd Conference on Physics of Semiconductors* (World Scientific, Singapore, 1995), Vol. 2, p. 1272.
[504] Yu. B. Bolkhovityanov, A. S. Jaroshevich, M. A. Revenko, H. E. Scheibler, and A. S. Terekhov, Semicond. Sci. Technol. **11**, 1847 (1996).
[505] D. J. Mowbray, O. P. Kowalski, M. Hopkinson, M. S. Skolnick, and J. P. R. David, Appl. Phys. Lett. **65**, 213 (1994).
[506] M. D. Dawson, S. P. Najda, A. H. Kean, G. Duggan, D. J. Mowbray, O. P. Kowalski, M. S. Skolnick, and M. Hopkinson, Phys. Rev. B **50**, 11190 (1994).
[507] S. P. Najda, A. H. Kean, M. D. Dawson, and G. Duggan, J. Appl. Phys. **77**, 3412 (1995).
[508] M. Schubert, J. A. Woollam, G. Leibiger, B. Rheinländer, I. Pietzonka, T. Sass, and V. Gottschalch, J. Appl. Phys. **86**, 2025 (1999).
[509] H. C. Kuo, J. M. Kuo, Y. C. Wang, C. H. Lin, H. Chen, and G. E. Stillman, J. Electron. Mater. **26**, 944 (1997).
[510] L. Hrivnak, Phys. Status Solidi A **128**, K89 (1991).
[511] H. Sonomura, T. Naumori, and T. Miyauchi, Appl. Phys. Lett. **24**, 77 (1974).
[512] J. M. Rodriguez, G. Armelles, and P. Salvador, J. Appl. Phys. **66**, 3929 (1989).
[513] J. M. Rodriguez and G. Armelles, J. Appl. Phys. **69**, 965 (1991).
[514] L. K. Vodop'yanov, V. I. Kozlovskii, and N. N. Mel'nik, Sov. Phys. Semicond. **34**, 405 (2000) [Fiz. Tekh. Poluprovodn. (S.-Peterburg) **34**, 418 (2000)].
[515] F. Fuchs, U. Weimer, W. Pletschen, J. Schmitz, E. Ahlswede, M. Walther, J. Wagner, and P. Koidl, Appl. Phys. Lett. **71**, 3251 (1997).
[516] N. Bouarissa, N. Amrane, and H. Aourag, Infrared Phys. Technol. **36**, 755 (1995).
[517] N. Bouarissa and H. Aourag, Phys. Status Solidi B **199**, 403 (1997).
[518] M. R. Lorenz, J. C. McGroddy, T. S. Plaskett, and S. Porowski, IBM J. Res. Dev. **13**, 583 (1969).
[519] K. Zitouni, A. Kadri, and R. L. Aulombard, Phys. Rev. B **34**, 2638 (1986).
[520] D. Barjon, A. Raymond, A. Joullie, and J. L. Robert, Phys. Status Solidi B **68**, K81 (1975).
[521] I. Vurgaftman, J. R. Meyer, and L. R. Ram-Mohan, IEEE Photonics Technol. Lett. **9**, 170 (1997).
[522] Ya. Agaev and N. G. Bekmedova, Sov. Phys. Semicond. **5**, 1330 (1972) [Fiz. Tekh. Poluprovodn. (S.-Peterburg) **5**, 1523 (1971)].
[523] S. Isomura, F. G. D. Prat, and J. C. Woolley, Phys. Status Solidi B **65**, 213 (1974).
[524] N. Dai, F. Brown, R. E. Doezema, S. J. Chung, K. J. Goldammer, and M. B. Santos, Appl. Phys. Lett. **73**, 3132 (1998).
[525] A. Furukawa and M. Mizuta, Electron. Lett. **24**, 1378 (1988).
[526] H. Xie and W. I. Wang, Appl. Phys. Lett. **63**, 776 (1993).
[527] J. Massies, M. Leroux, Y. Martinez, P. Vennegues, and S. Laugt, J. Cryst. Growth **160**, 211 (1996).
[528] V. Bellani, M. Geddo, G. Guizzetti, S. Franchi, and R. Magnanini, Phys. Rev. B **59**, 12272 (1999).
[529] Yu. F. Biryulin, S. P. Vul', T. T. Dedegkaev, I. I. Kryukov, T. A. Polyanskaya, and Yu. V. Shmartsev, Sov. Phys. Semicond. **11**, 913 (1977) [Fiz. Tekh. Poluprovodn. (S.-Peterburg) **11**, 1555 (1977)].
[530] G. A. Antypas and L. W. James, J. Appl. Phys. **41**, 2165 (1970).
[531] M. B. Thomas, W. M. Coderre, and J. C. Woolley, Phys. Status Solidi A **2**, K141 (1970).
[532] N. N. Sirota and E. E. Matyas, Phys. Status Solidi A **4**, K143 (1971).
[533] A. Filion and E. Fortin, Can. J. Phys. **52**, 743 (1974).
[534] R. E. Nahory, M. A. Pollack, J. C. DeWinter, and K. M. Williams, J. Appl. Phys. **48**, 1607 (1977).
[535] M. Yano, Y. Suzuki, T. Ishii, Y. Matsushima, and M. Kimata, Jpn. J. Appl. Phys., Part 1 **17**, 2091 (1978).
[536] W. T. Tsang, T. H. Chiu, S. N. G. Chu, and J. A. Ditzenberger, Appl. Phys. Lett. **46**, 659 (1985).
[537] J. Klem, D. Huang, H. Morkoc, Y. E. Ihm, and N. Otsuka, Appl. Phys. Lett. **50**, 1364 (1987).
[538] D. Huang, J. Chyi, J. Klem, and H. Morkoc, J. Appl. Phys. **63**, 5859 (1988).
[539] P. W. Yu, C. E. Stutz, M. O. Manasreh, R. Kaspi, and M. A. Capano, J. Appl. Phys. **76**, 504 (1994).
[540] K. G. Merkel, V. M. Bright, M. A. Marciniak, C. L. A. Cerny, and M. O. Manasreh, Appl. Phys. Lett. **65**, 2442 (1994).
[541] J. Hu, X. G. Xu, J. A. H. Stotz, S. P. Watkins, A. E. Curzon, M. L. W. Thewalt, N. Matine, and C. R. Bolognesi, Appl. Phys. Lett. **73**, 2799 (1998).
[542] H. Mani, A. Joullie, A. M. Joullie, B. Girault, and C. Alibert, J. Appl. Phys. **61**, 2101 (1987).
[543] R. Ferrini, M. Geddo, G. Guizzetti, M. Patrini, S. Franchi, C. Bocchi, F. Germini, A. Baraldi, and R. Magnanini, J. Appl. Phys. **86**, 4706 (1999).
[544] P. Delvin, H. M. Heravi, and J. C. Woolley, Can. J. Phys. **52**, 743 (1981).
[545] P. J. P. Tang, M. J. Pullin, S. J. Chung, C. C. Phillips, R. A. Stradling, A. G. Norman, Y. B. Li, and L. Hart, Semicond. Sci. Technol. **10**, 1177 (1995).
[546] W. Dobbelaere, J. Deboeck, P. Heremans, R. Mertens, G. Borghs, W. Luyten, and J. van Landuyt, Appl. Phys. Lett. **60**, 3256 (1992).
[547] G. B. Stringfellow and P. E. Greene, J. Electrochem. Soc. **118**, 805 (1971).
[548] A. Rogalski and K. Jozwikowski, Infrared Phys. **29**, 35 (1989).
[549] S.-H. Wei and A. Zunger, Phys. Rev. B **52**, 12039 (1995).
[550] M. Y. Yen, B. F. Levine, C. G. Bethea, K. K. Choi, and A. Y. Cho, Appl. Phys. Lett. **50**, 927 (1987).
[551] X. Y. Gong, H. Kan, T. Makino, T. Yamaguchi, T. Nakatsasa, M. Kumagawa, N. L. Rowell, A. Wang, and R. Rinfret, Cryst. Res. Technol. **30**, 603 (1995).
[552] X. Y. Gong, T. Yamaguchi, H. Kan, T. Makino, N. L. Rowell, Y. Lacroix, A. Mangyou, M. Aoyama, and M. Kumagawa, Jpn. J. Appl. Phys., Part 1 **36**, 738 (1997).
[553] S. Elies, A. Krier, I. R. Cleverley, and K. Singer, J. Phys. D **26**, 159 (1993).
[554] S.-H. Wei and A. Zunger, Appl. Phys. Lett. **58**, 2684 (1991).
[555] S. R. Kurtz, L. R. Dawson, R. M. Biefeld, D. M. Follstaedt, and B. L. Doyle, Phys. Rev. B **46**, 1909 (1992).
[556] M. A. Marciniak, R. L. Hengehold, Y. K. Yeo, and G. W. Turner, J. Appl. Phys. **84**, 480 (1998).
[557] A. Rakovska, V. Berger, X. Marcadet, B. Vinter, K. Bouzehouane, and D. Kaplan, Semicond. Sci. Technol. **15**, 34 (2000).
[558] F. Karouta, H. Mani, J. Bhan, F. J. Hua, and A. Joullie, Rev. Phys. Appl. **22**, 1459 (1987).
[559] A. F. M. Anwar and R. T. Webster, Solid-State Electron. **42**, 2101 (1998).
[560] H. Ait Kaci, D. Boukredimi, and M. Mebarki, Phys. Status Solidi A **163**, 101 (1997).
[561] Y. Kawamura, H. Kurisu, K. Yoshimatsu, A. Kamada, Y. Naito, and N. Inoue, Jpn. J. Appl. Phys., Part 2 **36**, L757 (1997).
[562] M. G. Craford, R. W. Shaw, A. H. Herzog, and W. O. Groves, J. Appl. Phys. **43**, 4075 (1972).
[563] A. G. Thompson, M. Cardona, K. L. Shaklee, and J. C. Woolley, Phys. Rev. **146**, 601 (1966).
[564] R. J. Nelson, N. Holonyak, and W. O. Groves, Phys. Rev. B **13**, 5415 (1976).
[565] M. Oueslatti, C. Hirlimann, and M. Balkanski, J. Phys. (Paris) **42**, 1151 (1981).

Downloaded 26 Aug 2001 to 128.42.12.177. Redistribution subject to AIP license or copyright, see http://ojps.aip.org/japo/japcr.jsp

[566] S.-H. Wei and A. Zunger, Phys. Rev. Lett. **76**, 664 (1996).
[567] K. J. Kim, M. H. Lee, J. H. Bahng, K. Shim, and B. D. Choe, J. Appl. Phys. **84**, 3696 (1998).
[568] A. Onton and L. M. Foster, J. Appl. Phys. **43**, 5084 (1972).
[569] H. Mathieu, P. Merle, and E. L. Ameziane, Phys. Rev. B **15**, 2048 (1977).
[570] Y. Gonzalez, G. Armelles, and L. Gonzalez, J. Appl. Phys. **76**, 1951 (1994).
[571] G. A. Antypas and T. O. Yep, J. Appl. Phys. **42**, 3201 (1971).
[572] R. J. Nicholas, R. A. Stradling, and J. C. Ramage, J. Phys. C **12**, 1641 (1979).
[573] M. Beaudoin, A. Bensaada, R. Leonelli, P. Desjardins, R. A. Masut, L. Isnard, A. Chennouf, and G. L'Esperance, Phys. Rev. B **53**, 1990 (1996).
[574] M. Wada, S. Araki, T. Kudou, T. Umezawa, S. Nakajima, and T. Ueda, Appl. Phys. Lett. **76**, 2722 (2000).
[575] R. J. Nicholas, R. A. Stradling, J. C. Portal, and S. Askenazy, J. Phys. C **12**, 1653 (1979).
[576] V. V. Kruzhaev, G. M. Min'kov, and O. E. Rut, Sov. Phys. Semicond. **16**, 596 (1982) [Fiz. Tekh. Poluprovodn. (S.-Peterburg) **16**, 928 (1982)].
[577] C. M. Sotomayor Torres and R. A. Stradling, Semicond. Sci. Technol. **2**, 323 (1987).
[578] M. J. Jou, Y. T. Cherng, H. R. Jen, and G. B. Stringfellow, Appl. Phys. Lett. **52**, 549 (1988).
[579] M. J. Jou, Y. T. Cherng, H. R. Jen, and G. B. Stringfellow, J. Cryst. Growth **93**, 62 (1988).
[580] G. B. Stringfellow, J. Electron. Mater. **10**, 919 (1981).
[581] S. Loualiche, A. Le Corre, S. Salaun, J. Caulet, B. Lambert, M. Gauneau, D. Lecrosnier, and B. Deveaud, Appl. Phys. Lett. **59**, 423 (1991).
[582] H. Shimomura, T. Anan, and S. Sugou, J. Cryst. Growth **162**, 121 (1996).
[583] T. Fukui and Y. Horikoshi, Jpn. J. Appl. Phys. **20**, 587 (1981).
[584] V. M. Amus'ya, Yu. F. Biryulin, V. V. Vorob'eva, L. V. Golubev, S. V. Novikov, V. V. Chaldyshev, and Yu. V. Shmartsev, Sov. Phys. Semicond. **22**, 211 (1988) [Fiz. Tekh. Poluprovodn. (S.-Peterburg) **22**, 342 (1988)].
[585] E. H. Reihlen, M. J. Jou, Z. M. Fang, and G. B. Stringfellow, J. Appl. Phys. **68**, 4604 (1990).
[586] R. M. Biefeld, K. C. Baucom, S. R. Kurtz, and D. M. Follstaedt, J. Cryst. Growth **133**, 38 (1993).
[587] D. Drews, A. Schneider, T. Werninghaus, A. Behres, M. Heuken, K. Heime, and D. R. T. Zahn, Appl. Surf. Sci. **123/124**, 746 (1998).
[588] K. P. O'Donnell, R. W. Martin, and P. G. Middleton, Phys. Rev. Lett. **82**, 237 (1999).
[589] T. Nagatomo, T. Kuboyama, H. Minamino, and O. Omoto, Jpn. J. Appl. Phys., Part 2 **28**, L1334 (1989).
[590] N. Yoshimoto, T. Matsuoka, and A. Katsui, Appl. Phys. Lett. **59**, 2251 (1991).
[591] A. F. Wright and J. S. Nelson, Appl. Phys. Lett. **66**, 3051 (1995).
[592] S. Nakamura, J. Vac. Sci. Technol. A **13**, 705 (1995).
[593] W. Li, P. Bergman, I. Ivanov, W.-X. Ni, H. Amano, and I. Akasa, Appl. Phys. Lett. **69**, 3390 (1996).
[594] R. Goldhahn, J. Scheiner, S. Shokhovets, T. Frey, U. Kohler, D. J. As, and K. Lischka, Appl. Phys. Lett. **76**, 291 (2000).
[595] L. Bellaiche and A. Zunger, Phys. Rev. B **57**, 4425 (1998).
[596] M. D. McCluskey, C. G. Van de Walle, C. P. Master, L. T. Romano, and N. M. Johnson, Appl. Phys. Lett. **72**, 2725 (1998).
[597] T. Takeuchi, H. Takeuchi, S. Sota, H. Sakai, H. Amano, and I. Akasaki, Jpn. J. Appl. Phys., Part 2 **36**, L177 (1997).
[598] C. Wetzel, T. Takeuchi, S. Yamaguchi, H. Katoh, H. Amano, and I. Akasaki, Appl. Phys. Lett. **73**, 1994 (1998).
[599] W. Shan *et al.*, J. Appl. Phys. **84**, 4452 (1998).
[600] C. A. Parker, J. C. Roberts, S. M. Bedair, M. J. Reed, S. X. Liu, N. A. El-Masry, and L. H. Robins, Appl. Phys. Lett. **75**, 2566 (1999).
[601] H. P. D. Schrenk, P. de Mierry, M. Laugt, F. Omnes, M. Leroux, B. Beaumont, and P. Gibart, Appl. Phys. Lett. **75**, 2587 (1999).
[602] M. E. Aumer, S. F. LeBoeuf, F. G. McIntosh, and S. M. Bedair, Appl. Phys. Lett. **75**, 3315 (1999).
[603] J.-Chr. Holst *et al.*, Appl. Phys. Lett. **76**, 2832 (2000).
[604] J. Hagen, R. D. Metcalfe, D. Wickenden, and W. Clark, J. Phys. C **11**, L143 (1978).
[605] S. Yoshida, S. Misawa, and S. Gonda, J. Appl. Phys. **53**, 6844 (1982).
[606] M. A. Khan, R. A. Skogman, R. G. Schulze, and M. Gershenzon, Appl. Phys. Lett. **43**, 492 (1983).
[607] M. R. H. Khan, Y. Koide, H. Itoh, N. Sawaki, and I. Akasaki, Solid State Commun. **60**, 509 (1986).
[608] Y. Koide, H. Itoh, M. R. H. Khan, K. Hiramatu, and I. Akasaki, J. Appl. Phys. **61**, 4540 (1987).
[609] D. K. Wickenden, C. B. Bargeron, W. A. Bryden, J. Miragliotta, and T. J. Kistenmacher, Appl. Phys. Lett. **65**, 2024 (1994).
[610] L.-C. Duda, C. B. Stagarescu, J. Downes, K. E. Smith, D. Korakakis, T. D. Moustakas, J. Guo, and J. Nordgren, Phys. Rev. B **58**, 1928 (1998).
[611] M. D. Bremser, W. G. Perry, T. Zheleva, N. V. Edwards, O. H. Nam, N. Parikh, D. E. Aspnes, and R. F. Davis, MRS Internet J. Nitride Semicond. Res. **1**, 8 (1996).
[612] V. G. Deibuk, A. V. Voznyi, and M. M. Sletov, Sov. Phys. Semicond. **34**, 35 (2000) [Fiz. Tekh. Poluprovodn. (S.-Peterburg) **34**, 36 (2000)].
[613] G. Steude, D. M. Hofmann, B. K. Meyer, H. Amano, and I. Akasaki, Phys. Status Solidi B **205**, R7 (1998).
[614] T. Huang and J. S. Harris, Jr., Appl. Phys. Lett. **72**, 1158 (1998).
[615] S. A. Nikishin, N. N. Faleev, A. S. Zubrilov, V. G. Antipov, and H. Temkin, Appl. Phys. Lett. **76**, 3028 (2000).
[616] A. Nakadaira and H. Tanaka, Appl. Phys. Lett. **70**, 2720 (1997).
[617] K. Kubota, Y. Kobayashi, and K. Fujimoto, J. Appl. Phys. **66**, 2984 (1989).
[618] Q. Guo, H. Ogawa, and A. Yoshida, J. Cryst. Growth **146**, 462 (1995).
[619] K. S. Kim, A. Saxler, P. Kung, M. Razeghi, and K. Y. Lim, Appl. Phys. Lett. **71**, 800 (1997).
[620] T. Peng, J. Piprek, G. Qiu, J. O. Olowolafe, K. M. Unruh, C. P. Swann, and E. F. Schubert, Appl. Phys. Lett. **71**, 2439 (1997).
[621] S. Yamaguchi, M. Kariya, S. Nitta, H. Kato, T. Takeuchi, C. Wetzel, H. Amano, and I. Akasaki, J. Cryst. Growth **195**, 309 (1998).
[622] A. F. Wright and J. S. Nelson, Appl. Phys. Lett. **66**, 3465 (1995).
[623] M. Weyers, M. Sato, and H. Ando, Jpn. J. Appl. Phys., Part 2 **31**, L853 (1992).
[624] M. Weyers and M. Sato, Appl. Phys. Lett. **62**, 1396 (1993).
[625] R. Kuroiwa, H. Asahi, K. Asami, S.-J. Kim, K. Iwata, and S. Gonda, Appl. Phys. Lett. **73**, 2630 (1998).
[626] S. Sakai, Y. Ueta, and Y. Terauchi, Jpn. J. Appl. Phys., Part 1 **32**, 4413 (1993).
[627] M. Kondow, K. Uomi, K. Hosomi, and T. Mozume, Jpn. J. Appl. Phys., Part 2 **33**, L1056 (1994).
[628] G. Pozina, I. Ivanov, B. Monemar, J. V. Thordson, and T. G. Andersson, J. Appl. Phys. **84**, 3830 (1998).
[629] J. Sik, M. Schubert, G. Leibiger, V. Gottschalch, G. Kirpal, and J. Humlicek, Appl. Phys. Lett. **76**, 2859 (2000).
[630] A. Ougazzaden, Y. Le Bellego, E. V. K. Rao, M. Juhel, L. Leprince, and G. Patriarche, Appl. Phys. Lett. **70**, 2861 (1997).
[631] T. Makimoto, H. Saito, T. Nishida, and N. Kobayashi, Appl. Phys. Lett. **70**, 2984 (1997).
[632] M. Kozhevnikov, V. Narayanamurti, C. V. Reddy, H. P. Xin, C. W. Tu, A. Mascarenhas, and Y. Zhang, Phys. Rev. B **61**, R7861 (2000).
[633] J. Neugebauer and C. G. Van de Walle, Phys. Rev. B **51**, 10568 (1995).
[634] A. Rubio and M. L. Cohen, Phys. Rev. B **51**, 4343 (1995).
[635] L. Bellaiche, S.-H. Wei, and A. Zunger, Phys. Rev. B **54**, 17568 (1996).
[636] L. Bellaiche, S.-H. Wei, and A. Zunger, Appl. Phys. Lett. **70**, 3558 (1997).
[637] T. Mattila, S.-H. Wei, and A. Zunger, Phys. Rev. B **60**, R11245 (1999).
[638] A. Lindsay and E. P. O'Reilly, Solid State Commun. **112**, 443 (1999).
[639] W. G. Bi and C. W. Tu, Appl. Phys. Lett. **70**, 1608 (1997).
[640] J. Salzman and H. Temkin, Mater. Sci. Eng., B **50**, 148 (1997).
[641] K. Uesugi, N. Morooka, and I. Suemune, Appl. Phys. Lett. **74**, 1254 (1999).
[642] P. J. Klar, H. Gruning, W. Heimbrodt, J. Koch, F. Hohnsdorf, W. Stolz, P. M. A. Vicente, and J. Camassel, Appl. Phys. Lett. **76**, 3439 (2000).
[643] B. Gil, Solid State Commun. **114**, 623 (2000).
[644] L. Malikova, F. H. Pollak, and R. Bhat, J. Electron. Mater. **27**, 484 (1998).
[645] K. Uesugi, I. Suemune, K. Hasegawa, T. Akutagawa, and T. Nakamura, Appl. Phys. Lett. **76**, 1285 (2000).
[646] J. D. Perkins, A. Mascarenhas, Y. Zhang, J. F. Geisz, D. J. Friedman, J. M. Olson, and S. R. Kurtz, Phys. Rev. Lett. **82**, 3312 (1999).
[647] L. Bellaiche, S.-H. Wei, and A. Zunger, Phys. Rev. B **56**, 10233 (1997).
[648] Y. Zhang, A. Mascarenhas, H. P. Xin, and C. W. Tu, Phys. Rev. B **61**, 7479 (2000).
[649] P. N. Hai, W. M. Chen, I. A. Buyanova, H. P. Xin, and C. W. Tu, Appl. Phys. Lett. **77**, 1843 (2000).
[650] C. Skiebriszewski *et al.*, Phys. Status Solidi B **216**, 135 (1999).
[651] Y. Zhang, A. Mascarenhas, H. P. Xin, and C. W. Tu, Phys. Rev. B **61**, 4433 (2000).

Downloaded 26 Aug 2001 to 128.42.12.177. Redistribution subject to AIP license or copyright, see http://ojps.aip.org/japo/japcr.jsp

[652] J. N. Baillargeon, K. Y. Cheng, G. E. Hofler, P. J. Pearah, and K. C. Hsieh, Appl. Phys. Lett. **60**, 2540 (1992).
[653] X. Liu, S. G. Bishop, J. N. Baillargeon, and K. Y. Cheng, Appl. Phys. Lett. **63**, 208 (1993).
[654] S. Miyoshi, H. Yaguchi, K. Onabe, R. Ito, and Y. Shiraki, J. Cryst. Growth **145**, 87 (1994).
[655] S. Miyoshi and K. Onabe, Jpn. J. Appl. Phys., Part 1 **37**, 4680 (1998).
[656] H. P. Xin, C. W. Tu, Y. Zhang, and A. Mascarenhas, Appl. Phys. Lett. **76**, 1267 (2000).
[657] H. P. Xin, R. J. Welty, and C. W. Tu, Appl. Phys. Lett. **77**, 1946 (2000).
[658] W. Shan, W. Walukiewicz, K. M. Yu, J. Wu, J. W. Ager III, E. E. Haller, H. P. Xin, and C. W. Tu, Appl. Phys. Lett. **76**, 3251 (2000).
[659] H. P. Xin and C. W. Tu, Appl. Phys. Lett. **77**, 2180 (2000).
[660] W. G. Bi and C. W. Tu, J. Appl. Phys. **80**, 1934 (1996).
[661] T. Yang, S. Nakajima, and S. Sakai, Jpn. J. Appl. Phys., Part 2 **36**, L320 (1997).
[662] R. Beresford, K. S. Stevens, and A. F. Schwatzman, J. Vac. Sci. Technol. B **16**, 1293 (1998).
[663] N. Tit and M. W. C. Dharma-wardana, Appl. Phys. Lett. **76**, 3576 (2000).
[664] C. K. Williams, T. H. Glisson, J. R. Hauser, and M. A. Littlejohn, J. Electron. Mater. **7**, 639 (1978).
[665] R. L. Moon, G. A. Antypas, and L. W. James, J. Electron. Mater. **3**, 635 (1974).
[666] P. A. Houston, J. Mater. Sci. **16**, 2935 (1981).
[667] K. Asami, H. Asahi, S. Gonda, Y. Kawamura, and H. Tanaka, Solid State Commun. **70**, 33 (1989).
[668] N. N. Sirota, I. V. Bodnar, A. I. Lukomskii, G. F. Smirnova, and L. M. Finkelstein, Phys. Status Solidi B **73**, K135 (1976).
[669] G. F. Smirnova, Sov. Phys. Semicond. **11**, 910 (1977) [Fiz. Tekh. Poluprovodn. (S.-Peterburg) **11**, 1550 (1977)].
[670] W. W. Chow, E. D. Jones, N. A. Modine, A. A. Allerman, and S. R. Kurtz, Appl. Phys. Lett. **75**, 2891 (1999).
[671] E. D. Jones, N. A. Modine, A. A. Allerman, S. R. Kurtz, A. F. Wright, S. T. Tozer, and X. Wei, Phys. Rev. B **60**, 4430 (1999).
[672] P. Perlin, S. G. Subramanya, D. E. Mars, J. Kruger, N. A. Shapiro, H. Siegle, and E. R. Weber, Appl. Phys. Lett. **73**, 3703 (1998).
[673] W. Shan, W. Walukiewicz, J. W. Ager III, E. E. Haller, J. F. Geisz, D. J. Friedman, J. M. Olson, and S. R. Kurtz, Phys. Rev. Lett. **82**, 1221 (1999).
[674] L. Bellaiche, Appl. Phys. Lett. **75**, 2578 (1999).
[675] M. R. Gokhale, J. Wei, H. Wang, and S. R. Forrest, Appl. Phys. Lett. **74**, 1287 (1999).
[676] C. Skierbiszewski *et al.*, Appl. Phys. Lett. **76**, 2409 (2000).
[677] T. P. Pearsall, in *GaInAsP Alloy Semiconductors*, edited by T. P. Pearsall, Chap. 12, p. 295 and references therein.
[678] P. M. Laufer, F. H. Pollack, R. E. Nahory, and M. A. Pollack, Solid State Commun. **36**, 419 (1980).
[679] Y. Yamazoe, T. Nishino, and Y. Hamarakawa, IEEE J. Quantum Electron. **17**, 139 (1981).
[680] J. A. Lahtinen and T. Tuomi, Phys. Status Solidi B **130**, 637 (1985).
[681] R. Madelon and M. Dore, Solid State Commun. **39**, 639 (1981).
[682] K. Satzke, G. Weiser, R. Hoger, and W. Thulke, J. Appl. Phys. **63**, 5485 (1988).
[683] P. Parayanthal and F. H. Pollack, Phys. Rev. B **28**, 3632 (1983).
[684] J. M. Chamberlain, A. A. Reeder, R. J. Turner, E. Kuphal, and J. L. Benchimol, Solid-State Electron. **30**, 217 (1987).
[685] D. Patel, C. S. Menoni, H. Temkin, C. Tome, R. A. Logan, and D. Coblentz, J. Appl. Phys. **74**, 737 (1993).
[686] J. Bohrer, A. Krost, and D. Bimberg, Appl. Phys. Lett. **63**, 1918 (1993).
[687] M. J. Cherng, G. B. Stringfellow, D. W. Kisker, A. K. Srivastava, and J. L. Zyskind, Appl. Phys. Lett. **48**, 419 (1986).
[688] J. R. Chang, Y. K. Su, C. L. Lin, K. M. Wu, W. C. Huang, Y. T. Lu, D. H. Jaw, W. L. Li, and S. M. Chen, Appl. Phys. Lett. **75**, 238 (1999).
[689] V. S. Sorokin, S. V. Sorokin, A. N. Semenov, B. Ya. Meltser, and S. V. Ivanov, J. Cryst. Growth **216**, 97 (2000).
[690] M. Astles, H. Hill, A. J. Williams, P. J. Wright, and M. L. Young, J. Electron. Mater. **15**, 41 (1986).
[691] T. I. Voronina, T. S. Lagunova, M. P. Mikhailova, M. A. Sipovskaya, V. V. Sherstnev, and Yu. P. Yakovlev, Sov. Phys. Semicond. **25**, 167 (1991) [Fiz. Tekh. Poluprovodn. (S.-Peterburg) **25**, 276 (1991)].
[692] J. Shin, T. C. Hsu, Y. Hsu, and G. B. Stringfellow, J. Cryst. Growth **179**, 1 (1997).
[693] N. Bouarissa, Infrared Phys. Technol. **40**, 423 (1999).
[694] H. Abid, M. Rezki, and H. Aourag, Mater. Sci. Eng., B **41**, 314 (1996).
[695] T. I. Voronina, T. S. Lagunova, K. D. Moiseev, N. A. Prokof'eva, T. B. Popova, M. A. Sipovskaya, V. V. Sherstnev, and Yu. P. Yakovlev, Sov. Phys. Semicond. **25**, 989 (1991) [Fiz. Tekh. Poluprovodn. (S.-Peterburg) **25**, 1639 (1991)].
[696] H. Mani, E. Tournie, J. L. Lazzari, C. Alibert, A. Joullie, and B. Lambert, J. Cryst. Growth **121**, 463 (1992).
[697] L.-C. Chen, W.-J. Ho, and M.-C. Wu, Jpn. J. Appl. Phys., Part 1 **38**, 1314 (1999).
[698] T. I. Voronina, T. S. Lagunova, K. D. Moiseev, M. A. Sipovskaya, I. N. Timchenko, and Yu. P. Yakovlev, Sov. Phys. Semicond. **27**, 978 (1993) [Fiz. Tekh. Poluprovodn. (S.-Peterburg) **27**, 1777 (1993)].
[699] M. P. Mikhailova and A. N. Titkov, Semicond. Sci. Technol. **9**, 1279 (1994).
[700] D. Z. Garbuzov *et al.*, Appl. Phys. Lett. **70**, 2931 (1997).
[701] J. C. DeWinter, M. A. Pollack, A. K. Srivastava, and J. L. Zyskind, J. Electron. Mater. **14**, 729 (1985).
[702] M. A. Afrailov, A. N. Baranov, A. P. Dmitriev, M. P. Mikhailova, Yu. P. Smorchkova, I. N. Timchenko, V. V. Sherstnev, Yu. P. Yakovlev, and I. N. Yassievich, Sov. Phys. Semicond. **24**, 876 (1990) [Fiz. Tekh. Poluprovodn. (S.-Peterburg) **24**, 1397 (1990)].
[703] J. H. Herrera-Perez, M. B. Z. Morosini, and N. B. Patel, in *Proceedings of the 5th Brazilian School on Semiconductor Physics*, edited by J. R. Leite, A. Fazzio, and A. S. Chaves (World Scientific, Singapore, 1991), p. 395.
[704] M. Munoz, K. Wei, F. H. Pollack, J. L. Freeouf, C. A. Wang, and G. W. Charache, J. Appl. Phys. **87**, 1780 (2000).
[705] M.-C. Wu and C.-W. Chen, J. Appl. Phys. **71**, 6116 (1992).
[706] S. Iyer, S. Hegde, K. K. Bajaj, A. Abul-Fadl, and W. Mitchel, J. Appl. Phys. **73**, 3958 (1993).
[707] K. E. Avdzyan, A. G. Aleksanyan, R. K. Kazaryan, L. A. Matevosyan, and G. E. Mirzabekyan, Sov. J. Quantum Electron. **18**, 117 (1988).
[708] W. Bi and A. Li, Chin. Phys. Lett. **9**, 53 (1992).
[709] P. G. Snyder, T. E. Tiwald, D. W. Thompson, N. J. Ianno, J. A. Woollam, M. G. Mauk, and Z. A. Shellenberger, Thin Solid Films **313–314**, 667 (1998).
[710] N. Bouarissa, Superlattices Microstruct. **26**, 279 (1999).
[711] R. D. Burnham, N. Holonyak, Jr., H. W. Korb, H. M. Macksey, D. R. Scifres, J. B. Woodhouse, and Zh. I. Alferov, Sov. Phys. Semicond. **6**, 77 (1972) [Fiz. Tekh. Poluprovodn. (S.-Peterburg) **6**, 97 (1972)].
[712] C.-W. Chen, M.-C. Wu, and L.-K. Kuo, Jpn. J. Appl. Phys., Part 1 **31**, 2514 (1992).
[713] M.-C. Wu and C.-W. Chen, J. Electron. Mater. **21**, 977 (1992).
[714] M. Asif Khan *et al.*, Appl. Phys. Lett. **76**, 1161 (2000).
[715] T. N. Oder, J. Li, J. Y. Lin, and H. X. Jiang, Appl. Phys. Lett. **77**, 791 (2000).
[716] G. Tamulaitis *et al.*, Appl. Phys. Lett. **77**, 2136 (2000).
[717] E. T. Yu, J. O. McCaldin, and T. C. McGill, Solid State Phys. **46**, 1 (1992), and references therein.
[718] H. Kroemer, Surf. Sci. **132**, 543 (1983).
[719] H. Kroemer, Surf. Sci. **174**, 299 (1986).
[720] R. Dingle, W. Wiegmann, and C. H. Henry, Phys. Rev. Lett. **33**, 827 (1974).
[721] R. Dingle, A. C. Gossard, and W. Wiegmann, Phys. Rev. Lett. **34**, 1327 (1975).
[722] J. Batey and S. L. Wright, J. Appl. Phys. **59**, 200 (1986).
[723] D. Arnold, A. Ketterson, T. Henderson, J. Klem, and H. Morkoc, Appl. Phys. Lett. **45**, 1237 (1984).
[724] P. Dawson, B. A. Wilson, C. W. Tu, and R. C. Miller, Appl. Phys. Lett. **48**, 541 (1986).
[725] J. Menendez, A. Pinczuk, D. J. Werder, A. C. Gossard, and J. H. English, Phys. Rev. B **33**, 8863 (1986).
[726] M. A. Haase, M. A. Emanuel, S. C. Smith, J. J. Coleman, and G. E. Stillman, Appl. Phys. Lett. **50**, 404 (1987).
[727] C. N. Yeh, L. E. McNeil, L. J. Blue, and T. Daniels-Race, J. Appl. Phys. **77**, 4541 (1995).
[728] M. O. Watanabe, J. Yoshida, M. Mashita, T. Nakanisi, and A. Hojo, J. Appl. Phys. **57**, 5340 (1985).
[729] S. Ababou, G. Guillot, and A. Regreny, J. Appl. Phys. **72**, 4134 (1992).
[730] Q. S. Zhu, S. M. Mou, X. C. Zhou, and Z. T. Zhong, Superlattices Microstruct. **12**, 163 (1992).
[731] S. A. Lyon and C. L. Petersen, Semicond. Sci. Technol. **7**, B21 (1992).
[732] E. S. Koteles, J. Appl. Phys. **73**, 8480 (1993).
[733] Q. S. Zhu, S. M. Mou, X. C. Zhou, and Z. T. Zhong, Appl. Phys. Lett. **62**, 2813 (1993).

Downloaded 26 Aug 2001 to 128.42.12.177. Redistribution subject to AIP license or copyright, see http://ojps.aip.org/japo/japcr.jsp

[734] S. R. Smith, F. Szmulowicz, and G. J. Brown, J. Appl. Phys. **75**, 1010 (1994).
[735] H. M. Cheong, J. H. Burnett, W. Paul, P. F. Hopkins, and A. C. Gossard, Phys. Rev. B **49**, 10444 (1994).
[736] K. Muraki, S. Fukatsu, Y. Shiraki, and Y. Takahashi, J. Cryst. Growth **150**, 49 (1995).
[737] T. Forchhammer, E. Veje, and P. Tidemand-Petersson, Phys. Rev. B **52**, 14693 (1995).
[738] A. Leuther, A. Forster, H. Luth, H. Holzbrecher, and U. Breuer, Semicond. Sci. Technol. **11**, 766 (1996).
[739] D. K. Guthrie, P. N. First, T. K. Gaylord, E. N. Glytsis, and R. E. Leibenguth, Appl. Phys. Lett. **71**, 2292 (1997).
[740] J. J. O'Shea, E. G. Brazel, M. E. Rubin, S. Bhargava, M. A. Chin, and V. Narayanamurti, Phys. Rev. B **56**, 2026 (1997).
[741] V. I. Zubkov, M. A. Mel'nik, A. V. Solomonov, and A. N. Pikhtin, Sov. Phys. Semicond. **33**, 858 (1999) [Fiz. Tekh. Poluprovodn. (S.-Peterburg) **33**, 940 (1999)].
[742] M. A. Melnik, A. N. Pikhtin, A. V. Solomonov, V. I. Zubkov, and F. Bugge, *Proceedings of the 23rd Symposium on Compound Semiconductors* (IOP, Bristol, UK, 1997), p. 977.
[743] A. K. Saxena, Solid State Commun. **113**, 201 (2000).
[744] N. E. Christensen, Phys. Rev. B **37**, 4528 (1988).
[745] W. R. L. Lambrecht, B. Segall, and O. K. Andersen, Phys. Rev. B **41**, 2813 (1990).
[746] S.-H. Wei and A. Zunger, Appl. Phys. Lett. **72**, 2011 (1998).
[747] J. M. Langer, C. Delerue, M. Lannoo, and H. Heinrich, Phys. Rev. B **38**, 7723 (1988).
[748] M. Cardona and N. E. Christensen, Phys. Rev. B **35**, 6182 (1987).
[749] W. R. L. Lambrecht and B. Segall, Phys. Rev. B **41**, 2832 (1990).
[750] R.-Z. Wang, S.-H. Ke, and M.-C. Huang, J. Phys.: Condens. Matter **4**, 8083 (1992).
[751] C. Ohler, C. Daniels, A. Forster, and H. Luth, Phys. Rev. B **58**, 7864 (1998).
[752] D. F. Welch, G. W. Wicks, and L. F. Eastman, J. Appl. Phys. **55**, 3176 (1984).
[753] K. Satzke, G. Weiser, W. Stolz, and K. Ploog, Phys. Rev. B **43**, 2263 (1991).
[754] I. L. Morris, R. H. Williams, J. I. Davies, and G. J. Clarke, Appl. Phys. Lett. **62**, 291 (1993).
[755] Y. Baltagi, S. Moneger, A. Tabata, T. Benyattou, C. Bru, A. Georgakilas, K. Zekentes, and G. Halkias, Appl. Surf. Sci. **63**, 172 (1993).
[756] S. Moneger, Y. Baltagi, T. Benyattou, A. Tabata, B. Ragot, G. Guillot, A. Georgakilas, K. Zekentes, and G. Halkias, J. Appl. Phys. **74**, 1437 (1993).
[757] L. F. Marsal, J. M. Lopez-Villegas, J. Bosh, and J. R. Morante, J. Appl. Phys. **76**, 1077 (1994).
[758] C. Lugand, T. Benyattou, G. Guillot, T. Venet, M. Gendry, and G. Hollinger, Superlattices Microstruct. **23**, 253 (1998).
[759] J. Bohrer, A. Krost, T. Wolf, and D. Bimberg, Phys. Rev. B **47**, 6439 (1993).
[760] J.-H. Huang and T. Y. Chang, J. Appl. Phys. **76**, 2893 (1994).
[761] J. R. Waldrop, E. A. Kraut, C. W. Farley, and R. W. Grant, J. Appl. Phys. **69**, 372 (1991).
[762] K. Tanaka, N. Kotera, and H. Nakamura, J. Appl. Phys. **85**, 4071 (1999).
[763] M. S. Hybertsen, Appl. Phys. Lett. **58**, 1759 (1991).
[764] W. Seidel, O. Krebs, P. Voisin, J. C. Harmand, F. Aristone, and J. F. Palmier, Phys. Rev. B **55**, 2274 (1997).
[765] J.-C. Zheng, Y.-M. Zheng, and R.-Z. Wang, J. Phys.: Condens. Matter **9**, 439 (1997).
[766] C. D. Lee and S. R. Forrest, J. Appl. Phys. **69**, 342 (1991).
[767] C. Guillot, M. Dugay, F. Barbarin, V. Souliere, P. Abraham, and Y. Monteil, J. Electron. Mater. **26**, L6 (1996).
[768] J. P. Landesman, J. C. Garcia, J. Massies, P. Maurel, G. Jezequel, J. P. Hirtz, and P. Alnot, Appl. Phys. Lett. **60**, 1241 (1992).
[769] Y. Foulon and C. Priester, Phys. Rev. B **45**, 6259 (1992).
[770] C. G. Van de Walle and R. M. Martin, Phys. Rev. B **35**, 8154 (1987).
[771] J. R. Waldrop, E. A. Kraut, C. W. Farley, and R. W. Grant, J. Vac. Sci. Technol. B **8**, 768 (1990).
[772] L. Aina, M. Mattingly, and L. Stecker, Appl. Phys. Lett. **53**, 1620 (1988).
[773] E. Lugagne-Delpon, P. Voisin, J. P. Vieren, M. Voos, J. P. Andre, and J. N. Patillon, Semicond. Sci. Technol. **7**, 524 (1992).
[774] E. Laureto, I. F. L. Dias, J. L. Duarte, E. Di Mauro, H. Iwamoto, M. T. P. Freitas, S. A. Lourenco, and D. O. Toginho Filho, J. Appl. Phys. **85**, 4184 (1999).
[775] E. Lugagne-Delpon, J. P. Andre, and P. Voisin, Solid State Commun. **86**, 1 (1993).
[776] J. Hwang, P. Pianetta, C. K. Shih, W. E. Spicer, Y.-C. Pao, and J. S. Harris, Jr., Appl. Phys. Lett. **51**, 1632 (1987).
[777] S. P. Kowalczyk, W. J. Schaffer, E. A. Kraut, and R. W. Grant, J. Vac. Sci. Technol. **20**, 705 (1982).
[778] J. R. Waldrop, R. W. Grant, and E. A. Kraut, Appl. Phys. Lett. **54**, 1878 (1989).
[779] J. R. Waldrop, R. W. Grant, and E. A. Kraut, J. Vac. Sci. Technol. B **7**, 815 (1989).
[780] K. Hirakawa, Y. Hashimoto, K. Harada, and T. Ikoma, Phys. Rev. B **44**, 1734 (1991).
[781] C. Ohler, J. Moers, A. Forster, and H. Luth, J. Vac. Sci. Technol. B **13**, 1728 (1995).
[782] J. Menendez, A. Pinczuk, D. J. Werder, S. K. Sputz, R. C. Miller, D. L. Sivco, and A. Y. Cho, Phys. Rev. B **36**, 8165 (1987).
[783] L. Hrivnak, Phys. Status Solidi A **124**, K111 (1991).
[784] X. Letartre, D. Stievenard, and E. Barbier, Appl. Phys. Lett. **58**, 1047 (1991).
[785] B. Jogai, Appl. Phys. Lett. **59**, 1329 (1991).
[786] M. J. Joyce, Z. Y. Xu, and M. Gal, Phys. Rev. B **44**, 3144 (1991).
[787] S. Marcinkevicius, G. Ambrazevicius, T. Lideikis, and K. Naudzius, Solid State Commun. **79**, 889 (1991).
[788] Y. S. Huang, H. Qiang, F. H. Pollak, G. D. Pettit, P. D. Kirchner, J. M. Woodall, H. Stragier, and L. B. Sorensen, J. Appl. Phys. **70**, 7537 (1991).
[789] V. D. Kulakovskii, T. G. Andersson, and L. V. Butov, Semicond. Sci. Technol. **8**, 477 (1993).
[790] W. Z. Shen, W. G. Tang, S. C. Shen, S. M. Wang, and T. Andersson, Appl. Phys. Lett. **65**, 2728 (1994).
[791] J. R. Botha and A. W. R. Leitch, Phys. Rev. B **50**, 18147 (1994).
[792] W. S. Chi and Y. S. Huang, Semicond. Sci. Technol. **10**, 127 (1995).
[793] J. Leymarie, C. Monier, A. Vasson, A.-M. Vasson, M. Leroux, B. Courboules, N. Grandjean, C. Deparis, and J. Massies, Phys. Rev. B **51**, 13274 (1995).
[794] J. Barnes, J. Nelson, K. W. J. Barnham, J. S. Roberts, M. A. Pate, R. Gray, S. S. Dosanjh, M. Mazzer, and F. Ghiraldo, J. Appl. Phys. **79**, 7775 (1996).
[795] G. Karunasiri, J. Appl. Phys. **79**, 8121 (1996).
[796] G. H. Li, A. R. Goni, K. Syassen, H. Q. Hou, W. Feng, and J. M. Zhou, Phys. Rev. B **54**, 13820 (1996).
[797] P. Disseix, J. Leymarie, A. Vasson, A.-M. Vasson, C. Monier, N. Grandjean, M. Leroux, and J. Massies, Phys. Rev. B **55**, 2406 (1997).
[798] J. Leymarie, P. Disseix, M. Rezki, C. Monier, A. Vasson, and A.-M. Vasson, Mater. Sci. Eng., B **44**, 147 (1997).
[799] E. M. Goldys, H. Y. Zuo, M. R. Phillips, C. M. Contessa, M. R. Vaughan, and T. L. Tansley, J. Electron. Mater. **26**, 922 (1997).
[800] L. Lu, J. Wang, Y. Wang, W. Ge, G. Yang, and Z. Wang, J. Appl. Phys. **83**, 2093 (1998).
[801] J. Arias, I. Esquivias, E. C. Larkins, S. Burkner, S. Weisser, and J. Rosenzweig, Appl. Phys. Lett. **77**, 776 (2000).
[802] T. Sauncy, M. Holtz, O. Brafman, D. Fekete, and Y. Finkelstein, Phys. Rev. B **59**, 5056 (1999).
[803] M.-I. Alonso, M. Ilg, and K. H. Ploog, Phys. Rev. B **50**, 1628 (1994).
[804] J. Brubach, A. Yu. Silov, J. E. M. Haverkort, W. v. d. Vleuten, and J. H. Wolter, Phys. Rev. B **59**, 10315 (1999).
[805] N. Tit, J. Vac. Sci. Technol. A **16**, 805 (1998).
[806] R. Colombelli, V. Piazza, A. Badolato, M. Lazzarino, and F. Beltram, Appl. Phys. Lett. **76**, 1146 (2000).
[807] S. Ghosh, B. Kochman, J. Singh, and P. Bhattacharya, Appl. Phys. Lett. **76**, 2571 (2000).
[808] J. Arriaga, G. Armelles, M. C. Munoz, J. M. Rodriguez, P. Castrillo, M. Recio, V. R. Velasco, F. Briones, and F. Garcia-Moliner, Phys. Rev. B **43**, 2050 (1991).
[809] T.-H. Shen, M. Elliott, R. H. Williams, and D. Westwood, Appl. Phys. Lett. **58**, 842 (1991).
[810] J. Tersoff, Phys. Rev. B **32**, 6968 (1985).
[811] J. Menendez, Phys. Rev. B **38**, 6305 (1988).
[812] R. P. Schneider, Jr. and B. W. Wessels, J. Appl. Phys. **70**, 405 (1991).
[813] R. P. Schneider, Jr. and B. W. Wessels, J. Electron. Mater. **20**, 1117 (1991).
[814] H. W. Hou and C. W. Tu, J. Appl. Phys. **75**, 4673 (1994).
[815] P. Desjardins, M. Beaudoin, R. Leonelli, G. L'Esperance, and R. A. Masut, J. Appl. Phys. **80**, 846 (1996).

Downloaded 26 Aug 2001 to 128.42.12.177. Redistribution subject to AIP license or copyright, see http://ojps.aip.org/japo/japcr.jsp

[816] C. Monier, M. F. Vilela, I. Serdiukova, and A. Freundlich, J. Cryst. Growth **188**, 332 (1998).
[817] T. Anan, K. Nishi, A. Tomita, K. Tokutome, and S. Sugou, Jpn. J. Appl. Phys., Part 1 **37**, 3915 (1998).
[818] P. Disseix, J. Leymarie, A. Vasson, A.-M. Vasson, H. Banvillet, E. Gil, N. Piffault, and R. Cadoret, Semicond. Sci. Technol. **8**, 1666 (1993).
[819] A. Bitz, C. Jordan, M. Di Ventra, K. A. Mader, L. C. Andreani, J. F. Carlin, A. Rudra, and J. L. Staehli, Nuovo Cimento D **17**, 1367 (1995).
[820] P. W. Yu, D. C. Reynolds, B. Jogai, J. Loehr, and C. E. Stutz, Appl. Phys. Lett. **61**, 2317 (1992).
[821] M. Peter, N. Herres, F. Fuchs, K. Winkler, K.-H. Bachem, and J. Wagner, Appl. Phys. Lett. **74**, 410 (1999).
[822] T. Katayama, Y. Kwamura, H. Takasaki, A. Yamamoto, and N. Inoue, J. Cryst. Growth **209**, 540 (2000).
[823] Y. Sugiyama, T. Fujii, Y. Nakata, S. Muto, and E. Miyauchi, J. Cryst. Growth **95**, 363 (1989).
[824] K. Kodama, M. Hoshino, K. Kilahara, M. Takikawa, and M. Ozeki, Jpn. J. Appl. Phys., Part 2 **25**, L127 (1986).
[825] M. O. Watanabe and Y. Ohba, Appl. Phys. Lett. **50**, 906 (1987).
[826] M. A. Rao, E. J. Caine, M. Kroemer, S. I. Long, and D. I. Babic, J. Appl. Phys. **61**, 643 (1987).
[827] T. W. Lee, P. A. Houston, R. Kumar, X. F. Yang, G. Hill, M. Hopkinson, and P. A. Claxton, Appl. Phys. Lett. **60**, 474 (1992).
[828] S. L. Feng, J. Krynicki, V. Donchev, J. C. Bourgoin, M. Di Forte-Poisson, C. Brylinski, S. Delage, H. Blanck, and S. Alaya, Semicond. Sci. Technol. **8**, 2092 (1993).
[829] D. Biswas, N. Debbas, P. Bhattacharya, M. Razeghi, M. Defour, and F. Omnes, Appl. Phys. Lett. **56**, 833 (1990).
[830] T. Kobayashi, K. Taira, F. Nakamura, and M. Kawai, J. Appl. Phys. **65**, 4898 (1989).
[831] J. Chen, J. R. Sites, I. L. Spain, M. J. Hafich, and G. Y. Robinson, Appl. Phys. Lett. **58**, 744 (1991).
[832] G. Arnaud, P. Boring, B. Gil, J.-C. Garcia, J.-P. Landesman, and M. Leroux, Phys. Rev. B **46**, 1886 (1992).
[833] M. A. Haase, M. J. Hafich, and G. Y. Robinson, Appl. Phys. Lett. **58**, 616 (1991).
[834] M. Leroux, M. L. Fille, B. Gil, J. P. Landesman, and J. C. Garcia, Phys. Rev. B **47**, 6465 (1993).
[835] S. Lan, C.-Q. Yang, W.-J. Xu, and H.-D. Liu, J. Appl. Phys. **79**, 2162 (1996).
[836] M. S. Faleh, J. Tasselli, J. P. Bailbe, and A. Marty, Appl. Phys. Lett. **69**, 1288 (1996).
[837] J. J. O'Shea, C. M. Reaves, S. P. DenBaars, M. A. Chin, and V. Narayanamurti, Appl. Phys. Lett. **69**, 3022 (1996).
[838] K.-S. Kim, Y.-H. Cho, B.-D. Choe, W. G. Jeong, and H. Lim, Appl. Phys. Lett. **67**, 1718 (1995).
[839] H. C. Kuo, J. M. Kuo, Y. C. Wang, C. H. Lin, H. Chen, and G. E. Stillman, J. Electron. Mater. **26**, 944 (1997).
[840] A. Lindell, M. Pessa, A. Salokatve, F. Bernardini, R. M. Nieminen, and M. Paalanen, J. Appl. Phys. **82**, 3374 (1997).
[841] O. Dehaese, X. Wallart, O. Schuler, and F. Mollot, J. Appl. Phys. **84**, 2127 (1998).
[842] Y. Foulon, C. Priester, G. Allan, J.-C. Garcia, and J.-P. Landesman, J. Vac. Sci. Technol. B **10**, 1754 (1992).
[843] H. Tanaka, Y. Kawamura, S. Nojima, K. Wakita, and H. Asahi, J. Appl. Phys. **61**, 1713 (1987).
[844] R. P. Schneider, Jr., R. P. Bryan, E. D. Jones, and J. A. Lott, Appl. Phys. Lett. **63**, 1240 (1993).
[845] O. P. Kowalski, J. W. Cockburn, D. J. Mowbray, M. S. Skolnick, R. Teissier, and M. Hopkinson, Appl. Phys. Lett. **66**, 619 (1995).
[846] X. H. Zhang, S. J. Chua, and W. J. Fan, Appl. Phys. Lett. **73**, 1098 (1998).
[847] D. Patel, M. J. Hafich, G. Y. Robinson, and C. S. Menoni, Phys. Rev. B **48**, 18031 (1993).
[848] A. D. Prins, J. L. Sly, A. T. Meney, D. J. Dunstan, E. P. O'Reilly, A. R. Adams, and A. Valster, J. Phys. Chem. Solids **56**, 423 (1995).
[849] H. K. Yow, P. A. Houston, and M. Hopkinson, Appl. Phys. Lett. **66**, 2852 (1995).
[850] A. Y. Polyakov, N. B. Smirnov, A. V. Govorkov, A. A. Chelnyi, A. G. Milnes, X. Li, B. M. Leiferov, and A. N. Aluev, Mater. Sci. Eng., B **39**, 79 (1996).
[851] Y. Ishitani, S. Minagawa, T. Kita, T. Nishino, H. Yaguchi, and Y. Shiraki, J. Appl. Phys. **80**, 4592 (1996).
[852] A. Morii, H. Okagawa, K. Hara, J. Yoshino, and H. Kukimoto, Jpn. J. Appl. Phys., Part 2 **31**, L1161 (1992).
[853] J. R. Waldrop, R. W. Grant, and E. A. Kraut, J. Vac. Sci. Technol. B **11**, 1617 (1993).
[854] S. Nagao, T. Fujimoto, H. Gotoh, H. Fukushima, T. Takano, H. Ito, S. Koshihara, and F. Minami, J. Appl. Phys. **81**, 1417 (1997).
[855] S. J. Chua, X. H. Zhang, S. J. Xu, and X. Gu, J. Phys.: Condens. Matter **9**, L279 (1997).
[856] S.-H. Ke, R.-Z. Wang, and M.-C. Huang, Z. Phys. B: Condens. Matter **102**, 61 (1997).
[857] A. D. Katnani and G. Margaritondo, Phys. Rev. B **28**, 1944 (1983).
[858] P. L. Gourley and R. M. Biefeld, Appl. Phys. Lett. **45**, 749 (1984).
[859] M.-E. Pistol, M. R. Leys, and L. Samuelson, Phys. Rev. B **37**, 4664 (1988).
[860] M.-E. Pistol and X. Liu, Phys. Rev. B **45**, 4312 (1992).
[861] J. A. Prieto, G. Armelles, M.-E. Pistol, P. Castrillo, J. P. Silveira, and F. Briones, Appl. Phys. Lett. **70**, 3449 (1997).
[862] X. Zhang, K. Onabe, Y. Nitta, B. Zhang, S. Fukatsu, Y. Shiraki, and R. Ito, Jpn. J. Appl. Phys., Part 2 **30**, L1631 (1991).
[863] H. Yaguchi, X. Zhang, K. Ota, M. Nagahara, K. Onabe, Y. Shiraki, and R. Ito, Jpn. J. Appl. Phys., Part 1 **32**, 544 (1993).
[864] Y. Hara, H. Yaguchi, K. Onabe, Y. Shiraki, and R. Ito, Proceedings International Symposium On GaAs and Related Compounds, Freiburg, Germany, 1993, p. 361.
[865] W. Shan, S. J. Hwang, J. J. Song, H. Q. Hou, and C. W. Tu, Appl. Phys. Lett. **62**, 2078 (1993).
[866] J. G. Neff, M. R. Islam, R. V. Chelakara, K. G. Fertitta, F. J. Ciuba, and R. D. Dupuis, J. Cryst. Growth **145**, 746 (1994).
[867] M. Di Ventra, M. Peressi, and A. Baldereschi, Phys. Rev. B **54**, 5691 (1996).
[868] X. Zhang, M. Ishikawa, H. Yaguchi, and K. Onabe, Surf. Sci. **387**, 371 (1997).
[869] X. H. Zhang, S. J. Chua, S. J. Xu, and W. J. Fan, J. Phys.: Condens. Matter **10**, 577 (1998).
[870] J. Tersoff, Phys. Rev. B **30**, 4874 (1984).
[871] W. A. Harrison, J. Vac. Sci. Technol. **14**, 1016 (1977).
[872] A. D. Katnani and G. Margaritondo, J. Appl. Phys. **54**, 2522 (1983).
[873] A. Ichii, Y. Tsou, and E. Garmire, J. Appl. Phys. **74**, 2112 (1993).
[874] G. Armelles, M. C. Munoz, and M. I. Alonso, Phys. Rev. B **47**, 16299 (1993).
[875] C. Tejedor, J. M. Calleja, F. Meseguer, E. E. Mendez, C.-A. Chang, and L. Esaki, Phys. Rev. B **32**, 5303 (1985).
[876] G. J. Gualtieri, G. P. Schwarz, R. G. Nuzzo, and W. A. Sunder, Appl. Phys. Lett. **49**, 1037 (1986).
[877] L. Ley, Appl. Phys. Lett. **50**, 1763 (1987).
[878] G. J. Gualtieri, G. P. Schwarz, R. G. Nuzzo, and W. A. Sunder, Appl. Phys. Lett. **50**, 1763 (1987).
[879] J. Menendez, A. Pinczuk, D. J. Werder, J. P. Valladares, T. H. Chiu, and W. T. Tsang, Solid State Commun. **61**, 703 (1987).
[880] U. Cebulla, G. Trankle, U. Ziem, A. Forchel, G. Griffiths, H. Kroemer, and S. Subbanna, Phys. Rev. B **37**, 6278 (1988).
[881] E. T. Yu, M. C. Phillips, D. H. Chow, D. A. Collins, M. W. Wang, J. O. McCaldin, and T. C. McGill, Phys. Rev. B **46**, 13379 (1992).
[882] H. Shen, Z. Hang, J. Leng, F. H. Pollack, L. L. Chang, W. I. Wang, and L. Esaki, Superlattices Microstruct. **5**, 591 (1989).
[883] J. F. Chen, L. Yang, M. C. Wu, S. N. G. Chu, and A. Y. Cho, J. Appl. Phys. **68**, 3451 (1990).
[884] M. Leroux and J. Massies, Appl. Phys. Lett. **68**, 54 (1996).
[885] W. Pollard, J. Appl. Phys. **69**, 3154 (1991).
[886] A. Mujica and A. Munoz, Solid State Commun. **81**, 961 (1992).
[887] N. G. Anderson and S. D. Jones, J. Appl. Phys. **70**, 4342 (1991).
[888] B. Montanari, M. Peressi, S. Baroni, and E. Molinari, Appl. Phys. Lett. **69**, 3218 (1996).
[889] A. Qteish and R. J. Needs, Phys. Rev. B **45**, 1317 (1992).
[890] R. G. Dandrea and C. B. Duke, J. Vac. Sci. Technol. B **10**, 1744 (1992).
[891] L. A. Hemstreet, C. Y. Fong, and J. S. Nelson, J. Vac. Sci. Technol. B **11**, 1693 (1993).
[892] L. A. Hemstreet (unpublished).
[893] J. R. Waterman, B. V. Shanabrook, R. J. Wagner, M. J. Yang, J. L. Davis, and J. P. Omaggio, Semicond. Sci. Technol. **8**, S106 (1993).
[894] M. Inoue, M. Yano, H. Furuse, N. Nasu, and Y. Iwai, Semicond. Sci. Technol. **8**, S121 (1993).
[895] R. H. Miles, J. N. Schulman, D. H. Chow, and T. C. McGill, Semicond. Sci. Technol. **8**, S102 (1993).

Downloaded 26 Aug 2001 to 128.42.12.177. Redistribution subject to AIP license or copyright, see http://ojps.aip.org/japo/japcr.jsp

[896] J. R. Meyer, C. A. Hoffman, B. V. Shanabrook, B. R. Bennett, R. J. Wagner, J. R. Waterman, and E. R. Youngdale, Proceedings of the 22nd International Conference on Physics of Semiconductors, Vancouver, 1994, p. 783.
[897] D. M. Symons, M. Lakrimi, M. van der Burgt, T. A. Vaughan, R. J. Nicholas, N. J. Mason, and P. J. Walker, Proceedings of the 22nd International Conference on Physics of Semiconductors, Vancouver, 1994, p. 891; Phys. Rev. B **51**, 1729 (1995).
[898] M. S. Daly, D. M. Symons, M. Lakrimi, R. J. Nicholas, N. J. Mason, and P. J. Walker, Semicond. Sci. Technol. **11**, 823 (1996).
[899] M. W. Wang, D. A. Collins, T. C. McGill, R. W. Grant, and R. M. Feenstra, Appl. Phys. Lett. **66**, 2981 (1995).
[900] G. J. Gualtieri, G. P. Schwarz, R. G. Nuzzo, R. J. Malik, and J. F. Walker, J. Appl. Phys. **61**, 5337 (1987).
[901] A. K. Srivastava, J. L. Zyskind, R. M. Lum, B. V. Dutt, and J. K. Klingert, Appl. Phys. Lett. **49**, 41 (1986).
[902] M. Mebarki, A. Kadri, and H. Mani, Solid State Commun. **72**, 795 (1989).
[903] J. T. Zborowski, A. Vigliante, S. C. Moss, and T. D. Golding, J. Appl. Phys. **79**, 8379 (1996).
[904] G. A. Sai-Halasz, L. L. Chang, J.-M. Welter, C.-A. Chang, and L. Esaki, Solid State Commun. **27**, 935 (1978).
[905] L. L. Chang, G. A. Sai-Halasz, L. Esaki, and R. L. Aggarwal, J. Vac. Sci. Technol. **19**, 589 (1981).
[906] D. A. Arch, G. Wicks, T. Tonaue, and J.-L. Staudenmann, J. Appl. Phys. **58**, 3933 (1985).
[907] D. H. Chow, R. H. Miles, J. R. Soderstrom, and T. C. McGill, Appl. Phys. Lett. **56**, 1418 (1990).
[908] R. H. Miles, D. H. Chow, J. N. Schulman, and T. C. McGill, Appl. Phys. Lett. **57**, 801 (1990).
[909] I. H. Campbell, I. Sela, B. K. Laurich, D. L. Smith, C. R. Bolognesi, L. A. Samoska, A. C. Gossard, and H. Kroemer, Appl. Phys. Lett. **59**, 846 (1991).
[910] J. P. Omaggio, J. R. Meyer, R. J. Wagner, C. A. Hoffman, M. J. Yang, D. H. Chow, and R. H. Miles, Appl. Phys. Lett. **61**, 207 (1992).
[911] J. R. Waterman, B. V. Shanabrook, R. J. Wagner, M. J. Yang, J. L. Davis, and J. P. Omaggio, Semicond. Sci. Technol. **8**, S106 (1993).
[912] B. R. Bennett, B. V. Shanabrook, R. J. Wagner, J. L. Davis, J. R. Waterman, and M. E. Twigg, Solid-State Electron. **37**, 733 (1994).
[913] R. H. Miles, D. H. Chow, Y.-H. Zhang, P. D. Brewer, and R. G. Wilson, Appl. Phys. Lett. **66**, 1921 (1995).
[914] D. H. Chow, R. H. Miles, T. C. Hasenberg, A. R. Kost, Y.-H. Zhang, H. L. Dunlap, and L. West, Appl. Phys. Lett. **67**, 3700 (1995).
[915] F. Fuchs, J. Schmitz, N. Herres, J. Wagner, J. D. Ralston, and P. Koidl, Inst. Phys. Conf. Ser. **144**, 219 (1995).
[916] T. C. Hasenberg, D. H. Chow, A. R. Kost, R. H. Miles, and L. West, Electron. Lett. **31**, 275 (1995).
[917] L. Johnson, L. A. Samoska, A. C. Gossard, J. L. Merz, M. C. Jack, G. R. Chapman, B. A. Baumgratz, K. Kosai, and S. M. Johnson, J. Appl. Phys. **80**, 1116 (1996).
[918] S. W. McCahon, S. A. Anson, D.-J. Jang, M. E. Flatté, T. F. Boggess, D. H. Chow, T. C. Hasenberg, and C. H. Grein, Appl. Phys. Lett. **68**, 2135 (1996).
[919] H. Mohseni, E. Michel, J. Sandoen, M. Razeghi, W. Mitchel, and G. Brown, Appl. Phys. Lett. **71**, 1403 (1997).
[920] H. M. Cheong, W. Paul, M. E. Flatté, and R. H. Miles, Phys. Rev. B **55**, 4477 (1997).
[921] F. Fuchs, U. Weimer, W. Pletschen, J. Schmitz, E. Ahlswede, M. Walther, J. Wagner, and P. Koidl, Appl. Phys. Lett. **71**, 3251 (1997).
[922] T. C. Hasenberg, R. H. Miles, A. R. Kost, and L. West, IEEE J. Quantum Electron. **33**, 1403 (1997).
[923] D.-J. Jang, J. T. Olesberg, M. E. Flatté, T. F. Boggess, and T. C. Hasenberg, Appl. Phys. Lett. **70**, 1125 (1997).
[924] C.-H. Lin, R. Q. Yang, S. J. Murry, S. S. Pei, C. Yan, D. L. McDaniel, Jr., and M. Falcon, IEEE Photonics Technol. Lett. **9**, 1573 (1997).
[925] C.-H. Lin, S. S. Pei, H. Q. Le, J. R. Meyer, and C. L. Felix, Appl. Phys. Lett. **71**, 3281 (1997).
[926] M. E. Flatté, T. C. Hasenberg, J. T. Olesberg, S. A. Anson, T. F. Boggess, C. Yan, and D. L. McDaniel, Jr., Appl. Phys. Lett. **71**, 3764 (1997).
[927] C. L. Felix, J. R. Meyer, I. Vurgaftman, C.-H. Lin, S. J. Murry, D. Zhang, and S.-S. Pei, IEEE Photonics Technol. Lett. **9**, 735 (1997).
[928] C. L. Felix, W. W. Bewley, I. Vurgaftman, J. R. Meyer, L. Goldberg, D. H. Chow, and E. Selvig, Appl. Phys. Lett. **71**, 3483 (1997).
[929] H. Q. Le, C. H. Lin, and S. S. Pei, Appl. Phys. Lett. **72**, 3434 (1998).
[930] M. E. Flatté, C. H. Grein, T. C. Hasenberg, S. A. Anson, D.-J. Jang, J. T. Olesberg, and T. F. Boggess, Phys. Rev. B **59**, 5745 (1999).
[931] M. J. Yang, W. J. Moore, B. R. Bennett, B. V. Shanabrook, J. O. Cross, W. W. Bewley, C. L. Felix, I. Vurgaftman, and J. R. Meyer, J. Appl. Phys. **86**, 1796 (1999).
[932] W. W. Bewley *et al.*, Appl. Phys. Lett. **73**, 3833 (1998).
[933] W. W. Bewley *et al.*, Appl. Phys. Lett. **74**, 1075 (1999).
[934] H. Lee *et al.*, Electron. Lett. **35**, 1743 (1999).
[935] M. J. Yang, W. J. Moore, B. R. Bennett, and B. V. Shanabrook, Electron. Lett. **34**, 270 (1998).
[936] W. Barvosa-Carter, M. Twigg, M. J. Yang, and L. J. Whitman (unpublished).
[937] A. Nakagawa, H. Kroemer, and J. H. English, Appl. Phys. Lett. **54**, 1893 (1989).
[938] S. Bhargava, H.-R. Blank, E. Hall, M. A. Chin, H. Kroemer, and V. Narayanamurti, Appl. Phys. Lett. **74**, 1135 (1999).
[939] M. J. Yang, B. R. Bennett, M. Fatemi, P. J. Lin-Chung, W. J. Moore, and C. H. Yang, J. Appl. Phys. **87**, 8192 (2000).
[940] J. R. Waldrop, G. J. Sullivan, R. W. Grant, E. A. Kraut, and W. A. Harrison, J. Vac. Sci. Technol. B **10**, 1773 (1992).
[941] R. G. Dandrea and C. B. Duke, Appl. Phys. Lett. **63**, 1795 (1993).
[942] S. Picozzi, A. Continenza, and A. J. Freeman, Phys. Rev. B **53**, 10852 (1996).
[943] S. Picozzi, A. Continenza, and A. J. Freeman, Phys. Rev. B **55**, 13080 (1997).
[944] S. R. Kurtz, G. C. Osbourn, R. M. Biefeld, and S. R. Lee, Appl. Phys. Lett. **53**, 216 (1988).
[945] S. R. Kurtz and R. M. Biefeld, Phys. Rev. B **44**, 1143 (1991).
[946] Y. B. Li, R. A. Stradling, A. G. Norman, P. J. P. Tang, S. J. Chung, and C. C. Phillips, Proceedings of the 22nd International Conference on Physics of Semiconductors, Vancouver, 1994, p. 1496.
[947] P. J. P. Tang *et al.*, Appl. Phys. Lett. **69**, 2501 (1996).
[948] Y. B. Li *et al.*, Phys. Rev. B **55**, 4589 (1997).
[949] P. J. P. Tang, H. Hardaway, J. Heber, C. C. Phillips, M. J. Pullin, R. A. Stradling, W. T. Yuen, and L. Hart, Appl. Phys. Lett. **72**, 3473 (1998).
[950] S. R. Kurtz, R. M. Biefeld, L. R. Dawson, K. C. Baucom, and A. J. Howard, Appl. Phys. Lett. **64**, 812 (1994).
[951] S. R. Kurtz and R. M. Biefeld, Appl. Phys. Lett. **66**, 364 (1995).
[952] Y. H. Zhang, Appl. Phys. Lett. **66**, 118 (1995).
[953] T. Utzmeier, G. Armelles, P. A. Postigo, and F. Briones, Phys. Rev. B **56**, 3621 (1997).
[954] S. L. Wong, R. J. Warburton, R. J. Nicholas, N. J. Mason, and P. J. Walker, Physica B **184**, 106 (1993).
[955] L. Q. Qian and B. W. Wessels, J. Vac. Sci. Technol. B **11**, 1652 (1993).
[956] A. N. Baranov, Y. Cuminal, G. Boissier, J. C. Nicolas, J. L. Lazzari, C. Alibert, and A. Joullie, Semicond. Sci. Technol. **11**, 1185 (1996).
[957] N. Bertru, R. Klann, A. Mazuelas, O. Brandt, and K. H. Ploog, Appl. Phys. Lett. **69**, 2237 (1996).
[958] N. Dai, G. A. Khodaparast, F. Brown, R. E. Doezema, S. J. Chung, and M. B. Santos, Appl. Phys. Lett. **76**, 3905 (2000).
[959] M. Nakao, S. Yoshida, and S. Gonda, Solid State Commun. **49**, 663 (1984).
[960] Y. H. Cho, K. S. Kim, S. Y. Ryu, S. K. Kim, B. D. Choe, and H. Lim, Appl. Phys. Lett. **66**, 1785 (1995).
[961] Y.-H. Cho, B.-D. Choe, and H. Lim, Appl. Phys. Lett. **69**, 3740 (1996).
[962] M. Sugawara, Phys. Rev. B **47**, 7588 (1993).
[963] R. Chin, N. Holonyak, Jr., S. W. Kirchoefer, R. M. Kolbas, and E. A. Rezek, Appl. Phys. Lett. **34**, 862 (1979).
[964] S. R. Forrest, P. H. Schmidt, R. B. Wilson, and M. L. Kaplan, Appl. Phys. Lett. **45**, 1199 (1984).
[965] B. Soucail, P. Voisin, M. Voos, D. Rondi, J. Nagle, and B. de Cremoux, Semicond. Sci. Technol. **5**, 918 (1990).
[966] F. Ducroquet, G. Jacovetti, K. Rezzoug, S. Ababou, G. Guillot, J. P. Praseuth, F. Olivier-Martin, and L. Giraudet, Mater. Sci. Technol. **13**, 971 (1997).
[967] X. H. Zhang, S. J. Chua, S. J. Xu, and W. J. Fan, J. Appl. Phys. **83**, 5852 (1998).
[968] C. Jelen, S. Slivken, V. Guzman, M. Razeghi, and G. J. Brown, IEEE J. Quantum Electron. **34**, 1873 (1998).
[969] J. R. Chang, Y. K. Su, Y. T. Lu, D. H. Jaw, H. P. Shiao, and W. Lin, Appl. Phys. Lett. **74**, 717 (1999).
[970] J. R. Chang, Y. K. Su, C. L. Lin, K. M. Wu, Y. T. Lu, D. H. Jaw, H. P. Shiao, and W. Lin, Appl. Phys. Lett. **74**, 3495 (1999).

Downloaded 26 Aug 2001 to 128.42.12.177. Redistribution subject to AIP license or copyright, see http://ojps.aip.org/japo/japcr.jsp

[971] A. Y. Polyakov, A. G. Milnes, S. J. Eglash, M. Ye, and A. E. Bochkarev, Solid-State Electron. **36**, 649 (1993).
[972] M. Mebarki, D. Boukredimi, S. Sadik, and J. L. Lazzari, J. Appl. Phys. **73**, 2360 (1993).
[973] A. Y. Polyakov, A. G. Milnes, N. B. Smirnov, L. V. Druzhinina, and I. V. Tunitskaya, Solid-State Electron. **36**, 1371 (1993).
[974] A. N. Baranov, A. N. Imenkov, M. P. Mikhailova, A. A. Rogachev, and Yu. P. Yakovlev, Superlattices Microstruct. **8**, 375 (1990).
[975] A. Y. Polyakov, A. G. Milnes, A. V. Govorkov, L. V. Druzhinina, I. V. Tunitskaya, and N. B. Smirnov, Solid-State Electron. **38**, 525 (1995).
[976] W. Z. Shen, S. C. Shen, W. G. Tang, Y. Zhao, and A. Z. Li, Appl. Phys. Lett. **67**, 3432 (1995).
[977] W. Z. Shen, S. C. Shen, W. G. Tang, Y. Chang, Y. Zhao, and A. Z. Li, J. Phys.: Condens. Matter **8**, 4751 (1996).
[978] M. Murayama and T. Nakayama, Phys. Rev. B **49**, 4710 (1994).
[979] S. A. Ding, S. R. Barman, K. Horn, H. Yang, B. Yang, O. Brandt, and K. Ploog, Appl. Phys. Lett. **70**, 2407 (1997).
[980] G. Martin, S. Strite, J. Thornton, and H. Morkoc, Appl. Phys. Lett. **58**, 2375 (1991).
[981] X. Huang *et al.*, J. Vac. Sci. Technol. B **13**, 1582 (1995).
[982] T. Kitatani, M. Kondow, T. Kikawa, Y. Yazawa, M. Okai, and K. Uomi, Jpn. J. Appl. Phys., Part 1 **38**, 5003 (1999).
[983] B. Q. Sun, D. S. Jiang, X. D. Luo, Z. Y. Xu, Z. Pan, L. H. Li, and R. H. Wu, Appl. Phys. Lett. **76**, 2862 (2000).
[984] P. Krispin, S. G. Spruytte, J. S. Harris, and K. H. Ploog, J. Appl. Phys. **88**, 4153 (2000).
[985] W. A. Harrison and J. Tersoff, J. Vac. Sci. Technol. B **4**, 1068 (1986).
[986] B. K. Agrawal, S. Agrawal, and R. Srivastava, Surf. Sci. **424**, 232 (1999).
[987] J. Baur, K. Maier, M. Kunzer, U. Kaufmann, and J. Schneider, Appl. Phys. Lett. **65**, 2211 (1994).
[988] G. A. Martin, S. C. Strite, A. Botchkarev, A. Agarwal, A. Rockett, W. R. L. Lambrecht, B. Segall, and H. Morkoc, Appl. Phys. Lett. **67**, 3322 (1995).
[989] G. A. Martin, A. Botchkarev, A. Rockett, and H. Morkoc, Appl. Phys. Lett. **68**, 2541 (1996).
[990] J. R. Waldrop and R. W. Grant, Appl. Phys. Lett. **68**, 2879 (1996).
[991] R. A. Beach, E. C. Piquette, R. W. Grant, and T. C. McGill, Mater. Res. Soc. Symp. Proc. **482**, 775 (1998).
[992] S. W. King, C. Ronning, R. F. Davis, M. C. Benjamin, and R. J. Nemanich, J. Appl. Phys. **84**, 2086 (1998).
[993] A. Rizzi, R. Lantier, F. Monti, H. Luth, F. Della Sala, A. Di Carlo, and P. Lugli, J. Vac. Sci. Technol. B **17**, 1674 (1999).
[994] E. A. Albanesi, W. R. L. Lambrecht, and B. Segall, J. Vac. Sci. Technol. B **12**, 2470 (1994).
[995] X. Chen, X. Hua, J. Hu, J.-M. Langlois, and W. A. Goddard III, Phys. Rev. B **53**, 1377 (1996).
[996] A. Satta, V. Fiorentini, A. Bosin, and F. Meloni, Mater. Res. Soc. Symp. Proc. **395**, 515 (1996).
[997] S.-H. Ke, K.-M. Zhang, and X.-D. Xie, J. Appl. Phys. **80**, 2918 (1996).
[998] W. Monch, J. Appl. Phys. **80**, 5076 (1996).
[999] N. Binggeli, P. Ferrara, and A. Baldereschi, Mater. Res. Soc. Symp. Proc. **482**, 911 (1998).
[1000] M. B. Nardelli, K. Rapcewicz, and J. Bernholc, Phys. Rev. B **55**, R7323 (1997).
[1001] F. Bernardini and V. Fiorentini, Phys. Rev. B **57**, R9427 (1998).

Downloaded 26 Aug 2001 to 128.42.12.177. Redistribution subject to AIP license or copyright, see http://ojps.aip.org/japo/japcr.jsp